/NASA CR-159,473

Quiet Clean Short-Haul Experimental Engine

(QCSEE)

Final Report

by

William S. Willis

GENERAL ELECTRIC COMPANY

August 1979

Prepared For

LANGLEY RESEARCH CENTER
LIBRARY, NASA
HAMPTON, VIRGINIA

NATIONAL AERONAUTICS AND SPACE ADMINISTRATION

FEDD REMOVED PER AUTH.
OF GENERAL RELEASE DATE
PRINTED ON REPORT.

5-1-80

NASA-Lewis Research Center
Contract NAS3-18021

1. Report No. CR159473	2. Government Accession No.	3. Recipient's Catalog No.
4. Title and Subtitle Quiet Clean Short-haul Experimental Engine (QCSEE) Final Report		5. Report Date August 1979
		6. Performing Organization Code
7. Author(s) William S. Willis, Manager, QCSEE Systems		8. Performing Organization Report No. R79AEG478
9. Performing Organization Name and Address General Electric Company Aircraft Engine Group Cincinnati, Ohio 45215		10. Work Unit No.
		11. Contract or Grant No. NAS3-18021
12. Sponsoring Agency Name and Address National Aeronautics and Space Administration Washington, D. C. 20546		13. Type of Report and Period Covered Contractor Report
		14. Sponsoring Agency Code

15. Supplementary Notes

Program Final Report
Project Manager: C.C. Ciepluch, QCSEE Project Office
Technical Advisor: N.E. Samanich, NASA-Lewis Research Center, Cleveland, Ohio 44135

16. Abstract

The QCSEE Program included the design, fabrication, and testing of two experimental propulsion systems for powered-lift transport aircraft. The Under-the-Wing (UTW) engine was intended for installation in an externally blown-flap configuration and the Over-the-wing (OTW) engine for use in an upper-surface-blowing aircraft. The UTW engine included variable-pitch composite fan blades, main reduction gear, composite fan frame and nacelle, and a digital control system. The OTW engine included a fixed-pitch fan, composite fan frame, boilerplate nacelle, and a full-authority digital control. Many acoustic, pollution, performance, and weight goals were demonstrated; all planned testing was satisfactorily completed prior to delivery of the engines to NASA for further testing.

17. Key Words (Suggested by Author(s)) Aircraft Propulsion Powered-Lift Systems Engine Acoustics Combustor Emissions Engine Testing	18. Distribution Statement Foreign Distribution Excluded		
19. Security Classif. (of this report) Unclassified	20. Security Classif. (of this page) Unclassified	21. No. of Pages 293	22. Price*

*For sale by the National Technical Information Service, Springfield, Virginia 22151
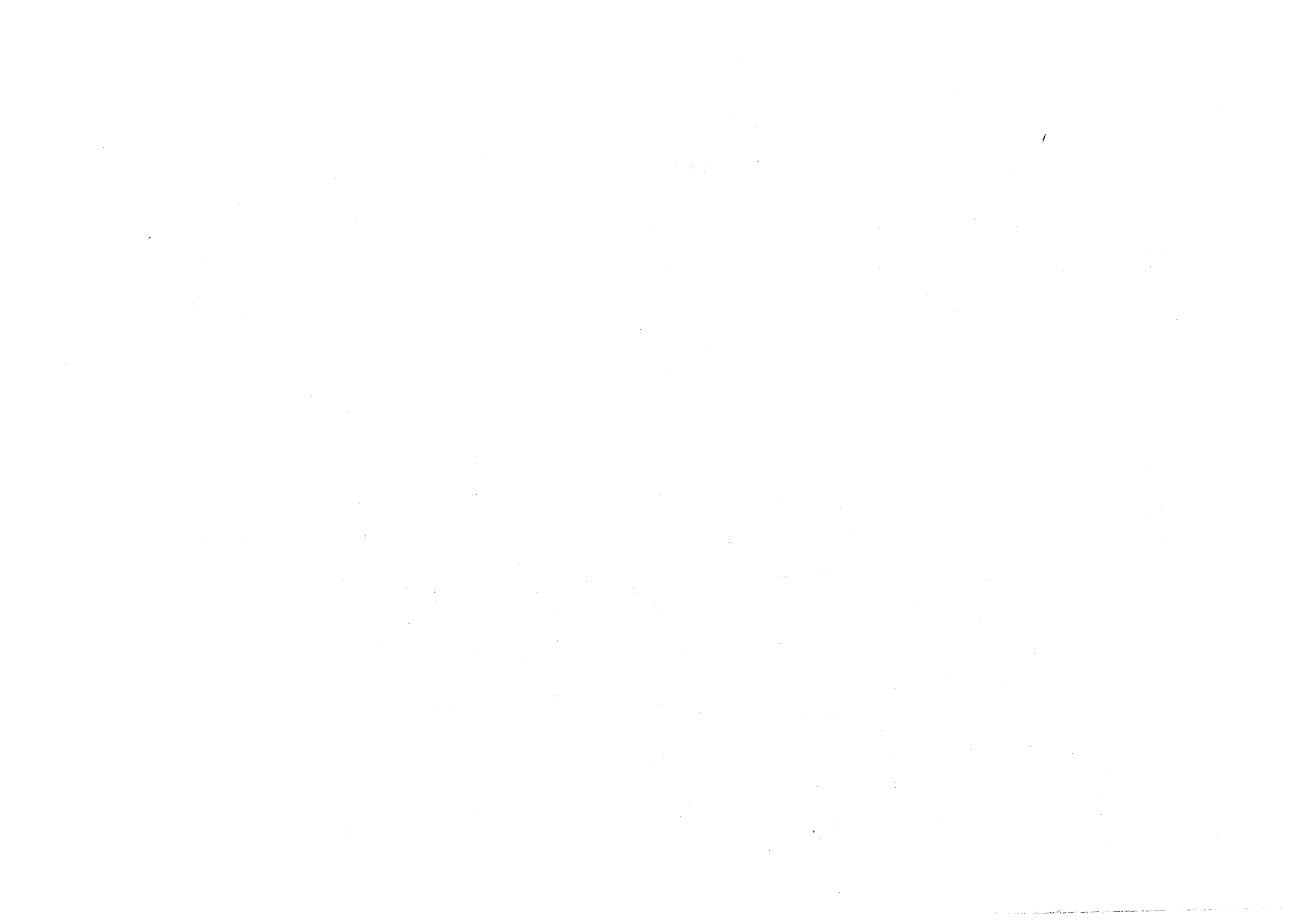
NASA-C-168 (Rev. 6-71)

N80-15120

TABLE OF CONTENTS

TABLE OF CONTENTS (Concluded)

LIST OF ILLUSTRATIONS

LIST OF ILLUSTRATIONS (Continued)

LIST OF ILLUSTRATIONS (Continued)

LIST OF ILLUSTRATIONS (Continued)

LIST OF ILLUSTRATIONS (Continued)

LIST OF ILLUSTRATIONS (Concluded)

LIST OF TABLES

1.0 SUMMARY

The Quiet Clean Short-haul Experimental Engine (QCSEE) program was conducted by General Electric Advanced Engineering and Technology Program Department under contract from NASA Lewis Research Center. The program included the design, fabrication, and testing of turbofan propulsion systems for two short-haul transport aircraft and delivery of these systems to NASA for further testing. One propulsion system was designed for an Under-the-Wing (UTW), externally blown flap application; the other was configured for Over-the-Wing (OTW) upper-surface blowing.

Major objectives of the program were to develop the technology needed to meet the stringent noise, exhaust emissions, performance, weight, and transient thrust-response requirements of future short-haul aircraft. Specific program goals are as listed in Table I.

Table I.   QCSEE Program Goals.

Parameter	UTW	OTW

Noise at 152.4 m (500 ft) Sideline
    Takeoff and Approach, EPNdB
    Maximum Reverse Thrust, PNdB
	95
	100
		95
		100

Exhaust Emissions	1979 EPA Standards for Carbon Monoxide, Unburned Hydrocarbons, and Oxides of Nitrogen	

Performance
    Uninstalled Thrust, kN (lbf)
    Installed Thrust, kN (lbf)
    Uninstalled sfc, g/sec/N (lbm/hr/lbf)
    Max Reverse Thrust, % of Max Forward
	81.4 (18,300)
	77.4 (17,400)
	0.0096 (0.34)
	35
		93.4 (21,000)
		90.3 (20,300)
		0.0102 (0.36)
		35

Thrust to Weight Ratio, N/kg (lbf/lbm)
    Uninstalled
    Installed
	60.8 (6.2)
	42.2 (4.3)
		72.6 (7.4)
		46.1 (4.7)

Thrust Transient, seconds
    Approach to Takeoff
    Approach to Max Reverse
	1
	1.5
		1
		1.5

Major design features selected for the engines include: low tip-speed fans, composite fan frames, high throat Mach number inlets, main reduction gears, and digital electronic control systems. In addition the UTW propulsion system contains a variable-pitch fan with composite blades, a variable-area fan-exhaust nozzle, and a complete composite nacelle with integral acoustic treatment. The OTW propulsion system includes a fixed-pitch fan with titanium blades, a "D" shaped exhaust nozzle, a target-type thrust reverser, and a boilerplate nacelle with interchangeable acoustic treatment. Figure 1 shows the test configuration of the UTW propulsion system with the composite nacelle, and Figure 2 shows the OTW propulsion system with the boilerplate nacelle.

The UTW propulsion system completed a total of 153 hours of testing at General Electric's Peebles, Ohio outdoor acoustic test side 4D and was delivered to NASA in August 1978. The OTW propulsion system completed 58 hours of testing at the same site and was delivered in July 1977. Major results of the test program are as listed in Table II.

Table II. QCSEE Test Results.

Parameter	UTW	OTW

Demonstrated Sideline Noise Levels
  Approach, EPNdB
  Takeoff, EPNdB
  Max Reverse, PNdB
	95.7
	97.2
	105*
		94.5
		97.2
		107

Exhaust Emissions	Met 1979 EPA Standards in Combustor Rig Test	

Performance
  Uninstalled Thrust
  Installed Thrust
  Uninstalled sfc
  Max Reverse Thrust
	Met Goal
	Met Goal
	Met Goal
	27%
		Met Goal
		Met Goal
		3% Better Than Goal
		Exceeded Goal

Thrust Transients
  Approach to Takeoff
  Approach to Max Reverse
	Not Demonstrated
	Not Demonstrated
		Met Goal
		Not Demonstrated

*at 27% Reverse Thrust
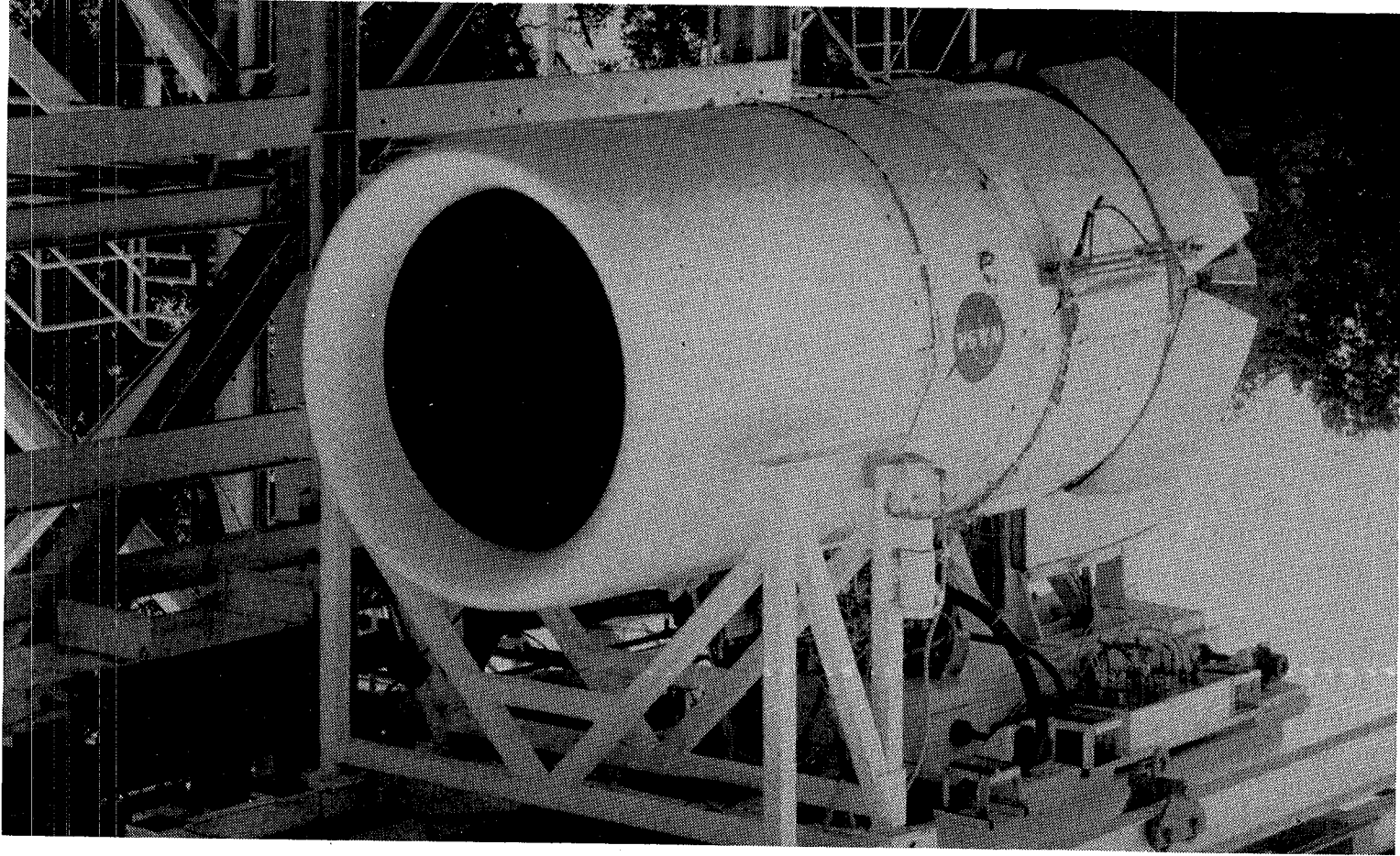
Figure 1.   UTW QCSEE.
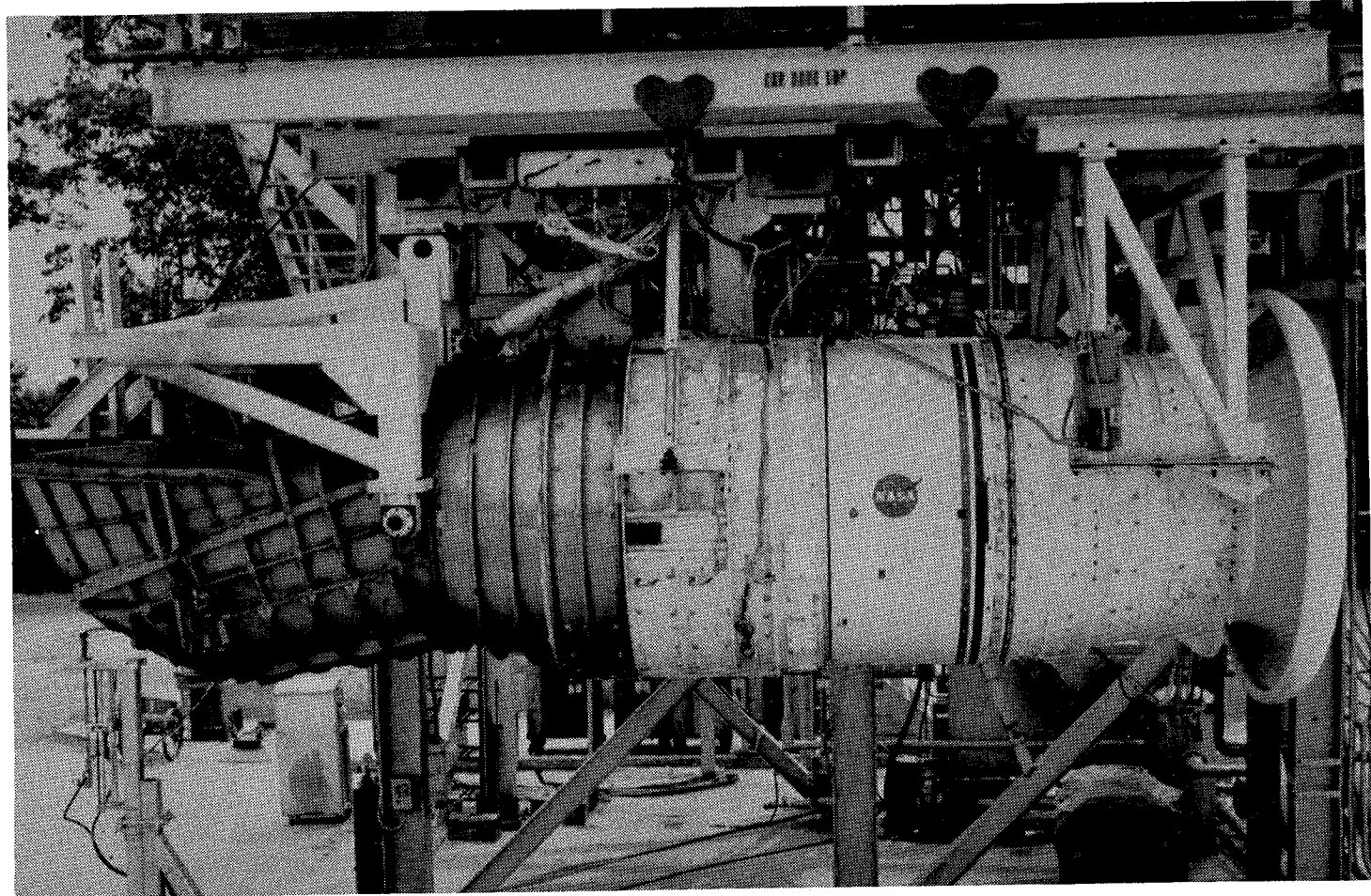
Figure 2. OTW QCSEE.

From an overall standpoint, both engines either met or closely approached all significant program objectives. The following advanced-technology components performed very successfully:

- Low Pressure-Ratio Fans

- Main Reduction Gearing

- Variable-Pitch Actuation Systems

- Composite Frame

- Composite Nacelle

- Digital Control

- Low-Emissions Combustor

As a general conclusion, the QCSEE program demonstrated that propulsion systems can be produced to meet the demanding short-haul requirements, including those for noise and pollution, without seriously compromising the economics of the transport system.

2.0 INTRODUCTION

The General Electric Company has recently completed the QCSEE program under Contract NAS3-18021. This program included the design, fabrication, and testing of two advanced turbofan propulsion systems intended to develop the technology that will be needed by powered-lift, short-haul-transport aircraft in the future.

2.1 BACKGROUND

The major problems facing the air transport industry in the early 1970's were noise and airport congestion. Noise had forced the closing of certain runways, the imposition of curfews at some airports, and the use of special flight restrictions such as reduced-throttle climb and low-altitude turns that were generally considered to be undesirable procedures. The congestion problem was manifested by traffic and parking problems, baggage-handling delays, and (especially in bad weather) long delays in departures and arrivals due to congested air space. Furthermore, air passenger traffic was increasing at a 7% annual rate, threatening to make these problems worse.

A solution to these problems was envisioned in the introduction of a separate, short-haul-transport system to cover the routes of 800 km (500 miles) or less. This system would utilize a fleet of new aircraft that would operate from smaller airports close to city centers and from auxiliary runways at the larger airports. A 610-m (2000-ft) runway capability was set as an objective, requiring that the aircraft incorporate some form of powered lift. Of the various suggested powered-lift concepts, two emerged as potentially attractive. These were the externally blown flap system used by Douglas in the YC-15 and the upper-surface-blowing concept used by Boeing in the YC-14.

Pre-QCSEE contracted studies were conducted to explore engine cycles and concepts. These studies resulted in the recommendation for very low fan pressure ratios and correspondingly high bypass ratios. They also indicated that a variable-pitch fan might be a practical means of providing reverse thrust, with less weight penalty than a conventional reverser, for a high-bypass engine. On the basis of these study results and other NASA test programs, the broad objectives and specific goals for the QCSEE program were established.

2.2 DESIGN APPROACH

Jet/flap interaction noise is a major contributor to the total noise signature of powered-lift aircraft. The under-the-wing installation results in direct impingement of the exhaust jet on the wing flap; the over-the-wing installation provides some noise shielding for the sideline observer. As shown in Figure 3, jet velocities were selected for each of the engines to keep this noise source about 3 dB below the total system noise for a balanced acoustic

6
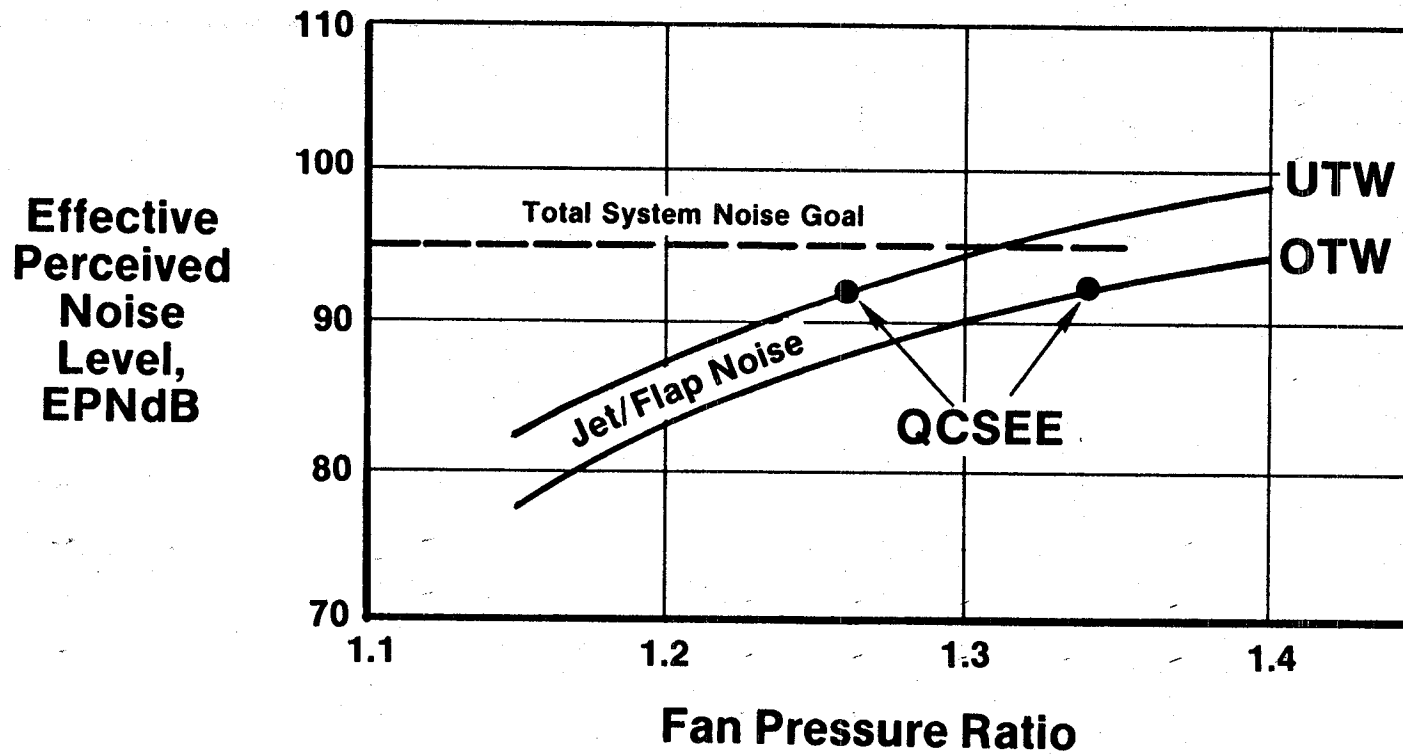
Figure 3. Effect of Jet Flap Noise on Fan Pressure Ratio Selection.

design. A very low jet velocity (and very low fan pressure ratio) was re-
quired for the UTW engine. The low noise goal also dictated a low-tip-speed
fan having reduced blade-passing frequency as well as careful selection of the
numbers of fan blades and vanes and adequate spacing between them.

Forward-radiated noise was reduced by the use of a high throat Mach num-
ber inlet - shown in the drawing of the UTW propulsion system, Figure 4. Fur-
ther suppression was added as needed by structural acoustic panels and by an
acoustic splitter in the fan discharge duct.

Both QCSEE's incorporated the YF101 core to take advantage of its ad-
vanced state of development. The combustor used in this core was already
smoke-free, but it did not meet the pollution objectives. A new double-
annular combustor was conceived to fit into the same envelope and to reduce
emissions. This design was a spin-off from the NASA Lewis Experimental Clean
Combustor Program.

The need for a high thrust-to-weight ratio was addressed by the extensive
use of graphite and Kevlar composites in the fan blades, frame, and nacelle.
This permitted the nacelle wall to be made integral with the engine, combining
two structures into one. For example, the outer casing of the fan frame func-
tions as the engine outer flowpath as well as a portion of the external nacelle.

Short-haul aircraft tend to require fairly high thrust-lapse rates so
that the engines can operate near the bottom of the sfc bucket at moderate
cruise altitude. Low-pressure-ratio fans inherently have this character-
istic. The best efficiency for low-pressure-ratio fans occurs at relatively
low fan-tip speeds. A variable-area fan-exhaust nozzle was necessary to keep
the fan pressure ratio from dropping too low at cruise, with detrimental
effects on sfc, and to provide sufficient altitude thrust. Though high lapse
rate is needed for STOL aircraft, the very low pressure ratio fans used for
low noise have an even higher lapse rate than desired.

Another characteristic needed to achieve low sfc levels is a high cycle
pressure ratio. Selection of the YF101 core was made for reasons of program
cost and risk and the appropriately advanced technology level. The use of a
low-pressure-ratio fan with this core resulted in an overall cycle pressure
ratio lower than desired. A more optimum cycle could have been produced by
adding booster stages to the fan or by increasing the pressure ratio of the
core, but this technology is already well in hand and was not considered to
be worth the added program cost.

The short-takeoff requirement implies a short landing and an effective
thrust reverser. The low-pressure-ratio UTW cycle lends itself to a reverse-
pitch fan that can provide reverse thrust without heavy, variable-geometry,
nacelle components.

A digital control was required to permit optimum coordinated control of
the variable-pitch fan, the variable nozzle, and the core engine with accept-
able pilot work load. Numerous other functions were also provided such as

8
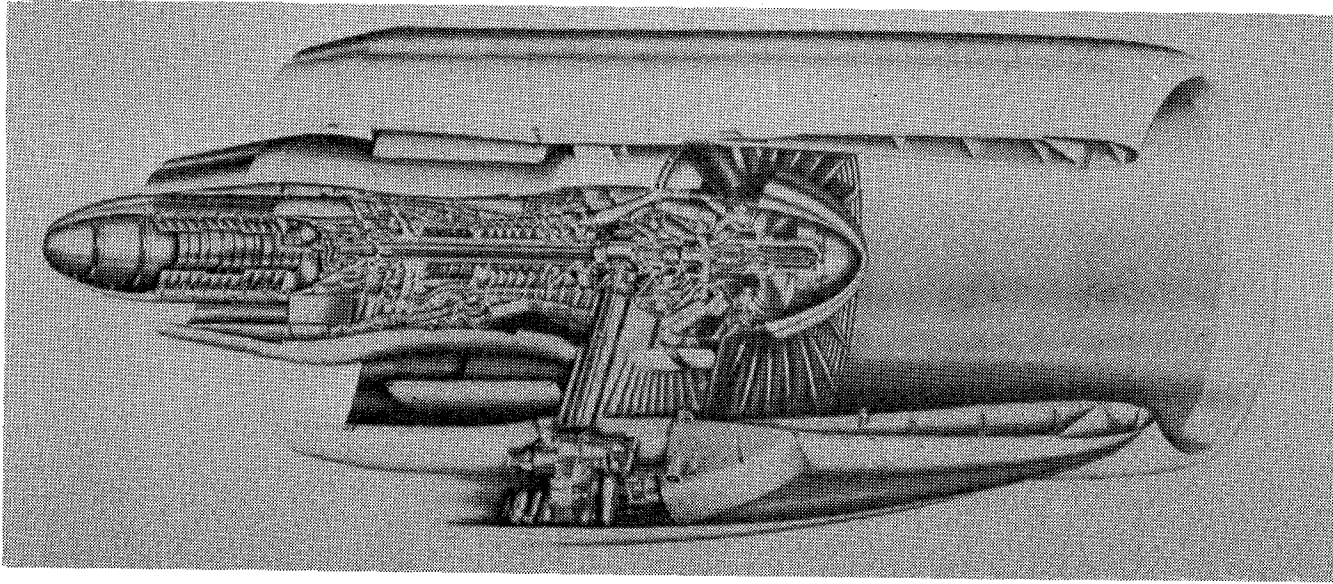
maintenance of safety limits and condition-monitoring functions. Top-mounted accessories were used on the UTW engine to permit lower weight, better maintainability, and low drag.

The OTW engine is shown in Figure 5. It required a "D" shaped exhaust nozzle to turn the flow downward and spread it over the wing and flap. Area control was provided by variable side doors. Since this engine has a fixed-pitch fan, thrust reversal is provided by pivoting the roof of the nozzle to form a target-type reverser blocker.

System studies conducted by McDonnell-Douglas and Boeing helped direct the engine-design activity. Baseline UTW and OTW aircraft designs were established to identify propulsion and installation requirements. Economic studies were conducted to assess the payoff of the new engine technologies. American Airlines contributed requirements for the aircraft and an operational scenario for the short-route structure. They were also consulted on maintenance features, mechanical design, and reliability.

Figure 6 shows the baseline aircraft projected by Douglas using the UTW engine. It would employ four QCSEE's mounted under the wing and is based on the Douglas YC-15 technology. The major characteristics are listed on the figure.

Figure 7 shows the baseline aircraft projected by Boeing using the OTW engine. It is somewhat larger, taking advantage of the greater thrust of four OTW engines, and is based on technology developed for the YC-14. The two aircraft were shown to be very competitive for short-haul operation.

These studies reached the conclusion that the 610-m (2000-ft) runway requirement was too stringent; 915 m (3000 feet) is more realistic based on projected airport availability. Another significant result was recognition that, in both installations, the engines would be mounted so high that a work stand would be required for all maintenance operations regardless of accessory location. This fact permitted the engine and aircraft accessories to be mounted in the pylon area to reduce nacelle drag for both installations and allow shorter, more direct, service lines from the wing.

The above approach resulted in the specific engine designs described in the next section of this report.
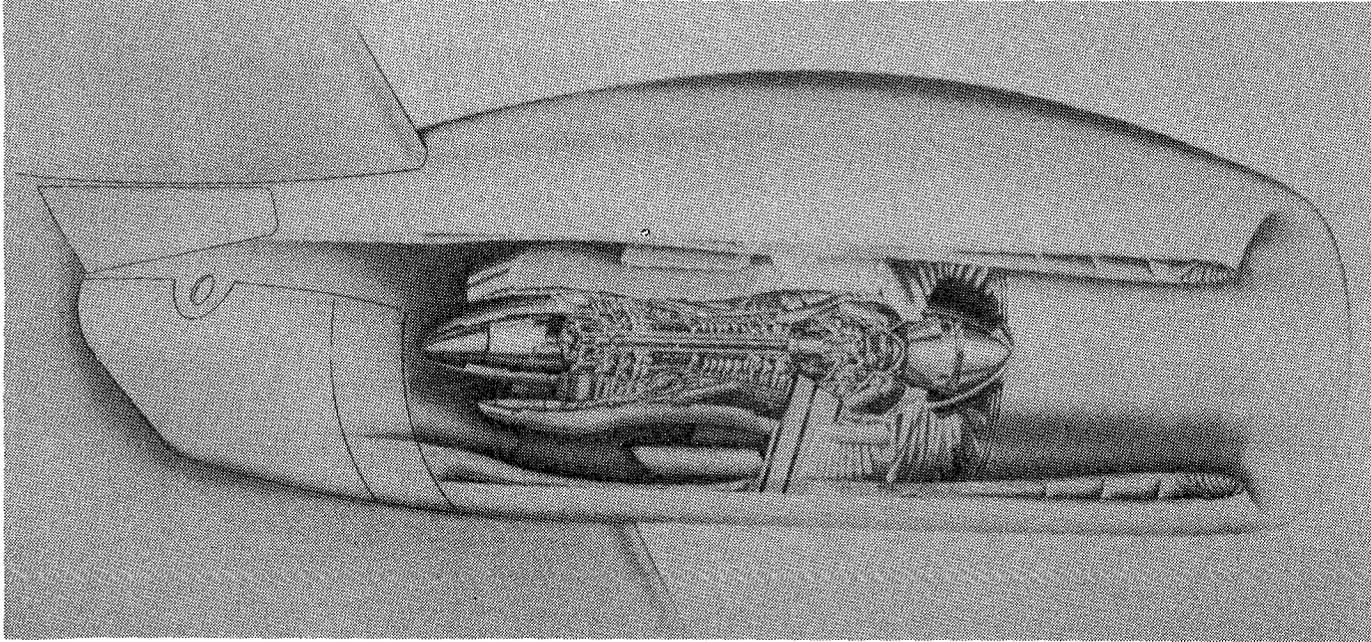
Figure 5.   OTW Propulsion System.

70,620 kg (155,700 lb) TOGW

926 km (500 n.mi.) Range

162 Passengers

914.4 m (3000 ft) Runway

4 Engines @ 81,400N (18,300 lb) Thrust

40.5m
(133 ft)

12.5m
(41 ft)

35.9m
(118 ft)
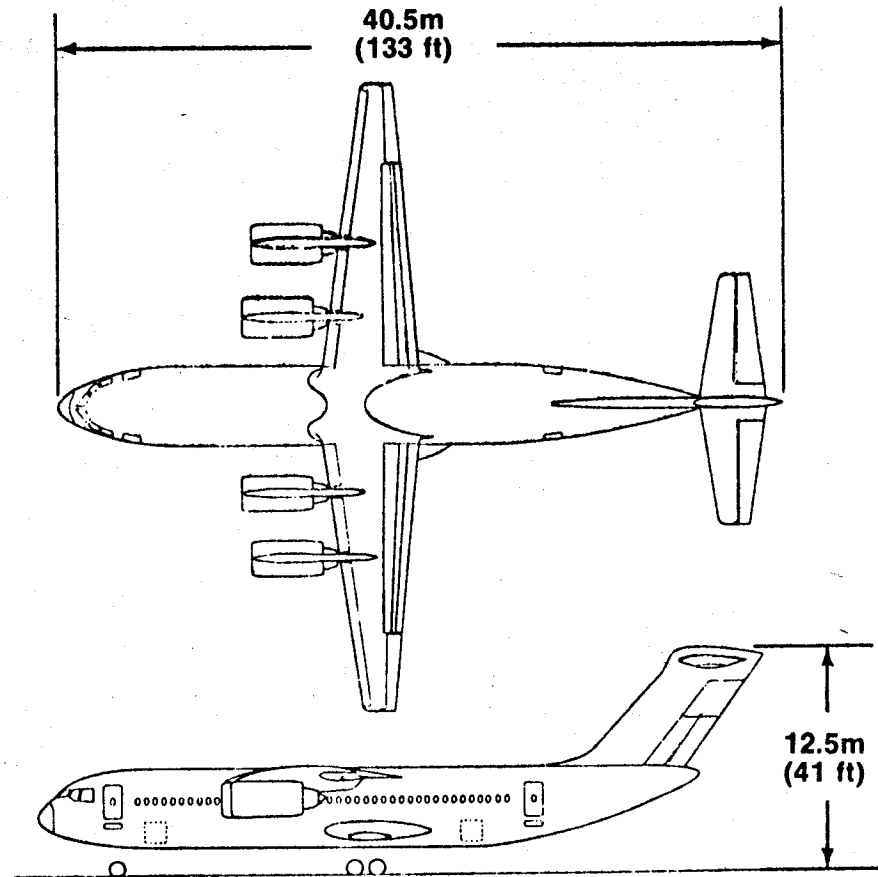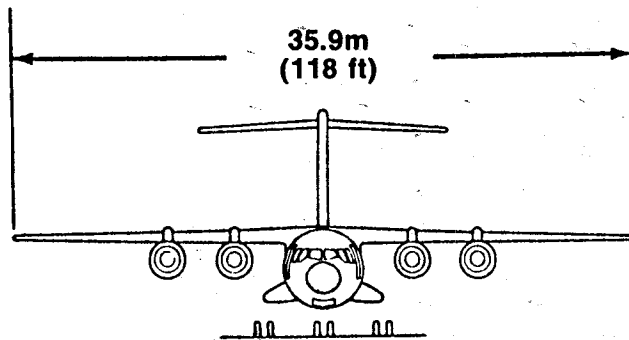
Figure 6. Baseline UTW Aircraft.

90,040 kg (198,500 lb) TOGW

926 km (500 n.mi.) Range

197 Passengers

914.4 m (3000 ft) Runway

4 Engines @ 93,408 N (21,000 lb) Thrust

46.86m
(153.75 ft)

37.75m
(123.86 ft)

13.72m
(45.00 ft)
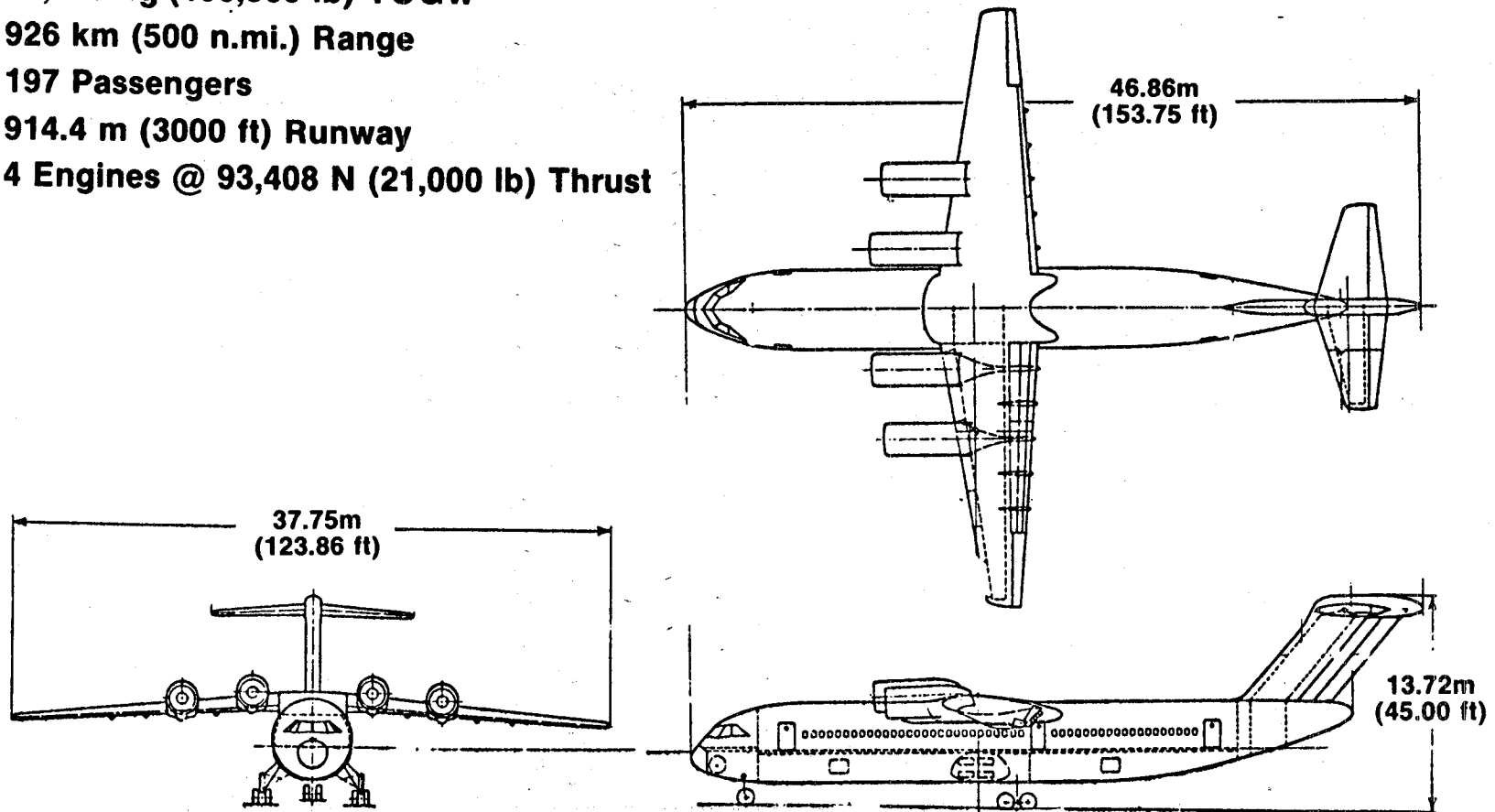
Figure 7. Baseline OTW Aircraft.

3.0 ENGINE DESIGN

This section will describe overall design of the UTW and OTW engines with particular emphasis on the advanced-technology components. Results of component testing are also included where they contributed to the final engine design.

3.1 OVERALL ENGINE DESCRIPTION

Details of the UTW engine can be seen in Figure 8. The inlet, fan blades, fan frame, fan outer duct, and fan variable nozzle are all made of graphite or Kevlar with an epoxy matrix. The fan inner duct is made of graphite with NASA-developed PMR polyimide resin for higher temperature operation. Acoustic treatment is used in the inlet, fan frame, core inlet duct, fan exhaust duct and splitter, and core exhaust nozzle. The latter includes a two-level acoustic absorber for high and low frequencies. A two-stage F101 power turbine drives a star-type, epicyclic, main reduction gear. The reduction gear was designed and developed by Curtiss-Wright Corporation. The fan nozzle is shown in the cruise position. It opens part way for takeoff and approach and further for reverse, where it functions as an inlet.

Recognizing the critical nature of the blade pitch-control system, many concepts were studied, and two variable-pitch systems were built and tested. A cam/harmonic-drive design was supplied by Hamilton Standard, and a ball spline system by General Electric. Both systems were whirl tested prior to use in a QCSEE to verify the ability to position the blades under centrifugal loading.

The major design parameters of the UTW engine are listed in Table III. The low fan-tip speed, used in conjunction with a 2.5-reduction gear ratio, permitted the use of a conventional high-speed, low-pressure turbine. The low fan pressure ratio resulted in a very low jet velocity and helped meet the acoustic requirement discussed earlier. Note the high bypass ratio made possible by the energetic core and the low-pressure-ratio fan.

A cross section of the OTW engine is shown in Figure 9. All nacelle components were of boilerplate construction for reasons of cost and to allow the evaluation of interchangeable acoustic panels. The fan uses fixed-pitch, titanium blades; the geometry would allow substitution of composite materials. The "D" shaped exhaust nozzle was tested in an inverted position so that the exhaust was directed downward in reverse-thrust mode, away from the test facility and instrumentation lines.

Major design parameters of the OTW engine are listed in Table IV. The tip diameter and airflow are identical to those of the UTW engine to permit the same inlets and fan frames to be used. A somewhat higher fan-tip speed is used to achieve the higher allowable exhaust velocity and fan pressure ratio with resultant higher overall pressure ratio and lower bypass ratio.

Digital Control

F101 Core & LPT

Variable Area Composite Fan Nozzle

High Throat Mach No. Inlet

Variable Pitch Composite Blades

Main Reduction Gear

Composite Fan Frame

Composite Fan Duct

Acoustic Splitter

Composite Core Cowl
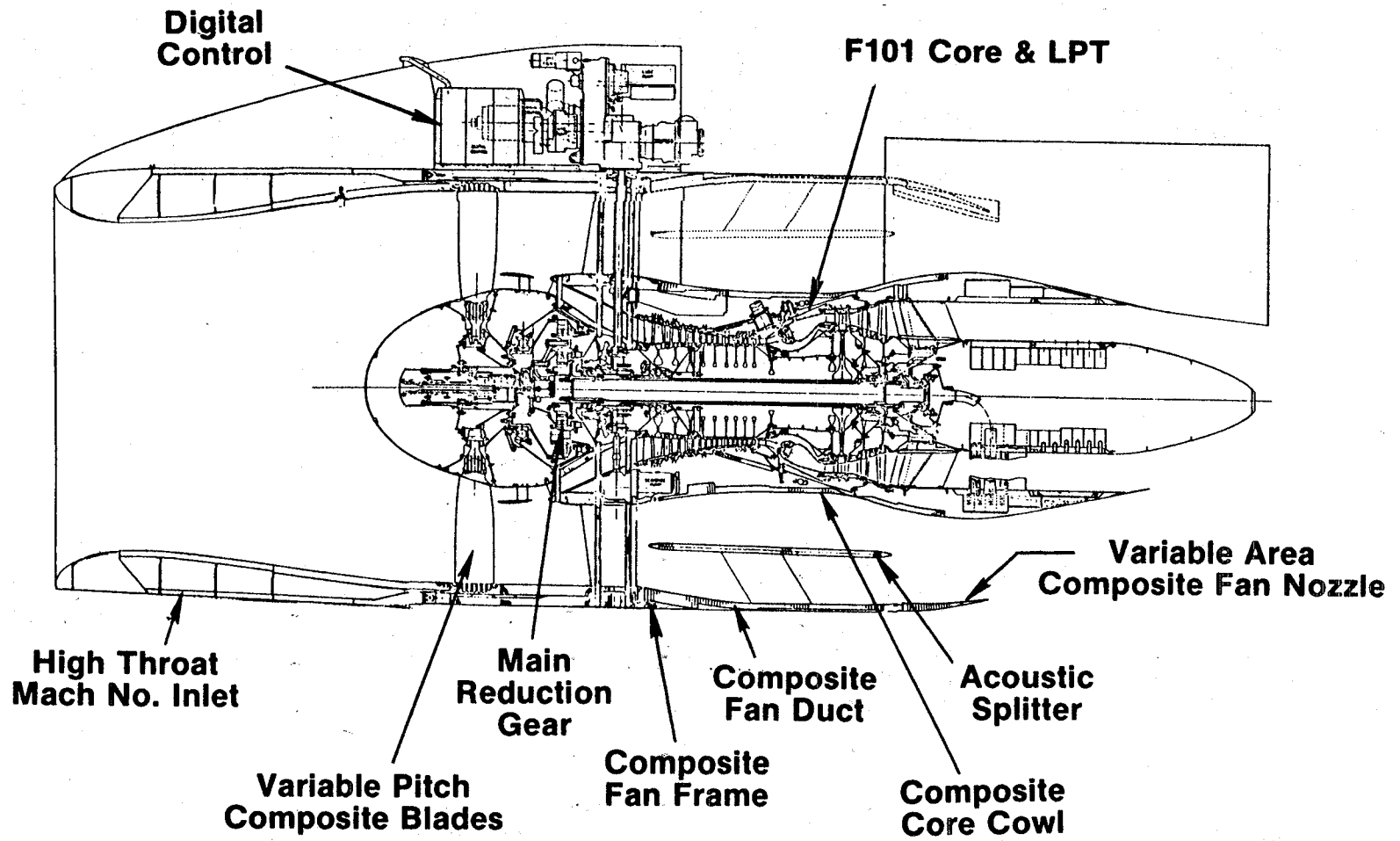
Figure 8.   UTW Engine Cross Section.

Table III. UTW Design Parameters.

Total Airflow, kg/s (lb/sec) _____ 405.5 (894))

Fan Tip Diameter, cm (in.) _____ 180.3 (71)

Fan Tip Speed, m/s (ft/sec) _____ 289.6 (950)

Bypass Ratio _____ 11.8

Fan Pressure Ratio _____ 1.27

Overall Pressure Ratio _____ 13.7

Jet Velocity (Core), m/s (ft/sec) _____ 244.7 (803)

Jet Velocity (Bypass), m/s _____ 204.2 (670)

Gear Ratio _____ 2.5

Table IV. OTW Design Parameters.

Total Airflow, kg/s (lb/sec) _____ 405.5 (894)

Fan Tip Diameter, cm (in.) _____ 180.3 (71)

Fan Tip Speed, m/s (ft/sec) _____ 350.5 (1150)

Bypass Ratio _____ 10.2

Fan Pressure Ratio _____ 1.34

Overall Pressure Ratio _____ 17.0

Jet Velocity (Core), m/s (ft/sec) _____ ⎫
                                          ⎬ Mixed 239.9 (787)
Jet Velocity (Bypass)   _____ ⎭

Gear Ratio _____ 2.1

16

Full Authority Digital Control

F101 Core & LPT

Fixed Pitch Titanium Blades

Main Reduction Gear

Composite Fan Frame

"D" Shaped Exhaust Nozzle/Thrust Reverser
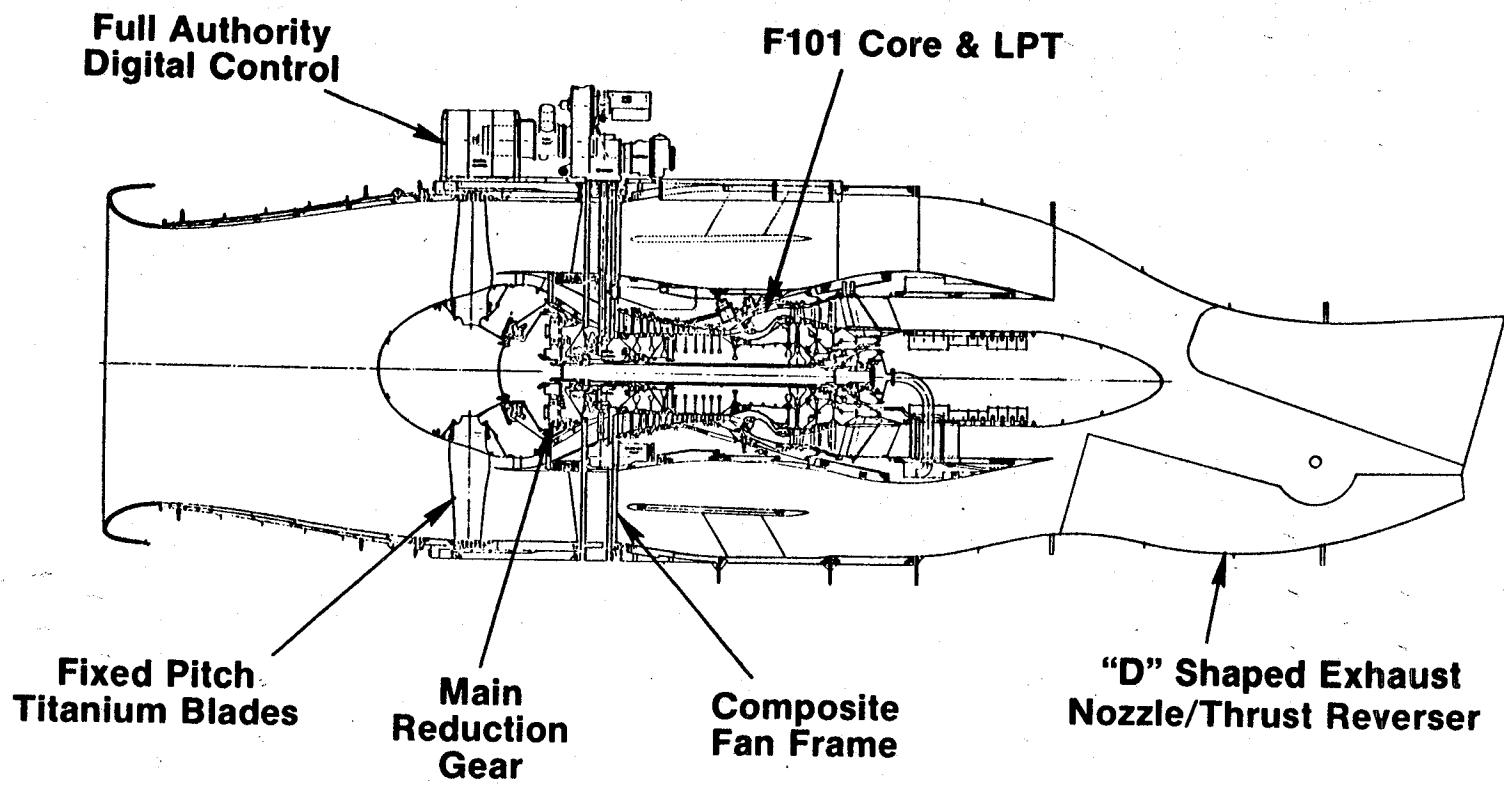
Figure 9. OTW Engine Cross Section.

Hub pressure rise is higher than outer panel pressure rise to permit better supercharging.

An electronic control system was designed, for both engines, to provide a digital interface with an aircraft on-board computer. The control accepts a percent-rated-thrust command. Several safety limits are automatically maintained including a calculated maximum temperature. Numerous provisions in the control are included to reduce the pilot work load. Inlet Mach number is automatically maintained at 0.8 consistent with acoustic requirements. Rapid thrust response is achieved via automatic blade and nozzle-area variations with minimum required fan- and core-speed variations. In the OTW engine, fuel flow and compressor stator vane angles are automatically adjusted to provide maximum rate of thrust change with minimum required core speed change. Automatic restructuring of the control computer is provided via Kalman-Bucy filtering techniques to permit operation with failed sensors.

Forty-eight items of condition-monitoring information are provided to the aircraft computer by a digital data bus. The control is engine mounted, cooled by fan-inlet-induced airflow, and designed to be compatible with the engine environment.

3.2 FAN AERODYNAMICS

Two different fans were designed for the QCSEE program; each was tailored to a particular engine cycle and operational requirements. The reversible-pitch fan for the under-the-wing engine is described first; aerodynamic design and scale-model test results are presented. The design of the fixed-pitch fan for the over-the-wing engine is described in the second subsection.

3.2.1 UTW Fan Aerodynamics

Aerodynamic Design – A cross section of the fan for the UTW engine is shown Figure 10. One of the notable features of this fan is the low-aspect-ratio, unshrouded, composite rotor. The low tip-speed rotor blades are attached to a variable-pitch mechanism and are fully reversible through either flat pitch or stall pitch. The flowpath over the rotor tip is a portion of a sphere to avoid changes in tip clearance as the rotor pitch varies. Circumferential-groove casing treatment is used over the rotor tip to increase stall margin at cruise with little or no efficiency penalty.

Another notable feature of the design is the unusual arrangement of the fan stators. The inner stator vane is placed under a ring-shaped island, closely coupled to the fan rotor, which serves as the primary splitter dividing the bypass flow from flow to the core engine. An annular slot is left open aft of this assembly, and a second flow splitter is provided at the rear of the slot for use during reverse operation. The split-stator arrangement was chosen over more conventional alternatives, such as a full-span stator, because it reduces the length required from fan rotor to core compressor inlet, and because it allows the full loading potential of the rotor hub to be

18
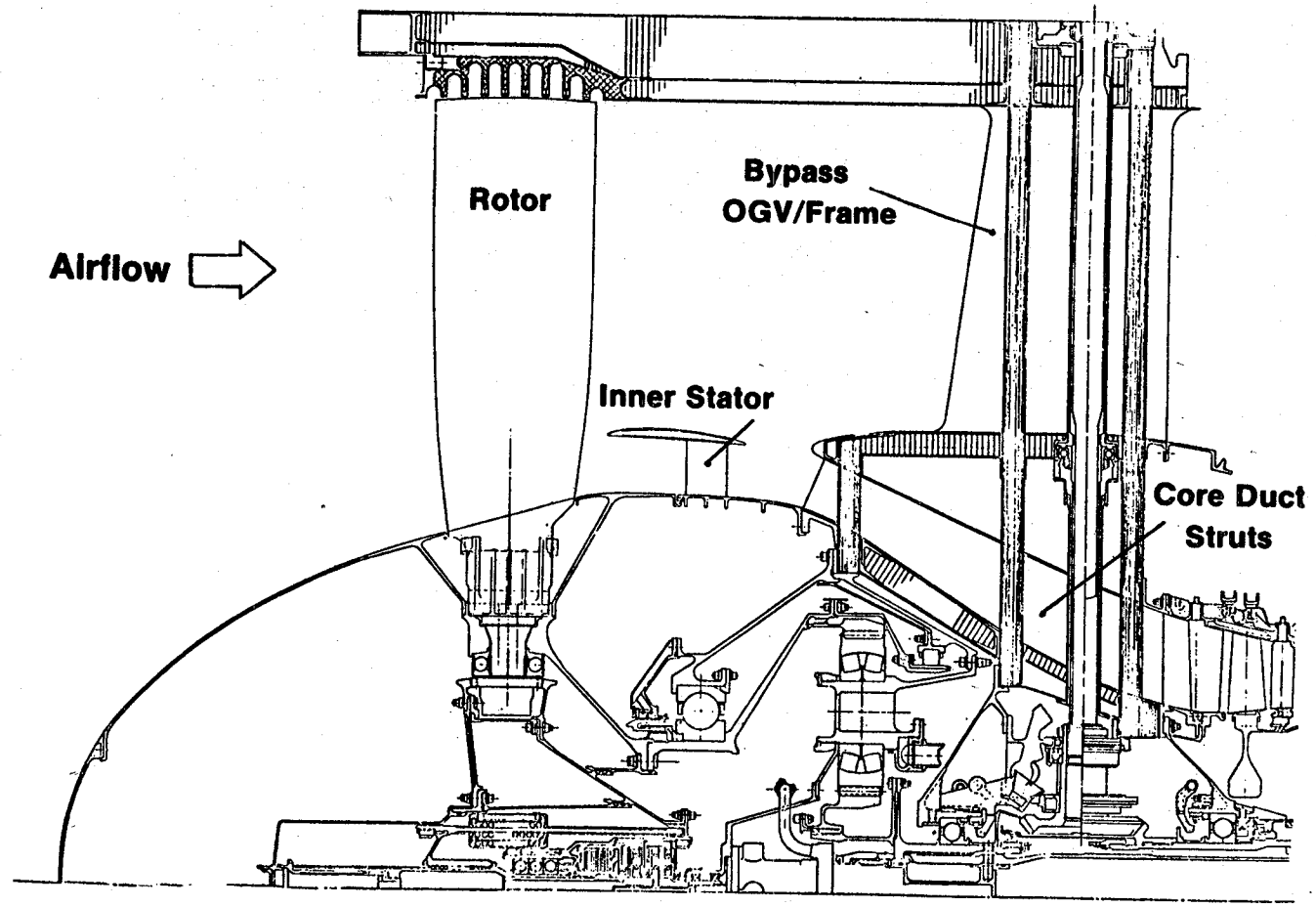
Figure 10.   UTW Fan Cross Section.

used without incurring high stator hub Mach numbers or loadings. The close-coupled splitter and inner stator arrangement by itself is unsatisfactory for reverse operation because flow drawn backwards through the bypass outlet guide vanes and entering the core engine would impinge upon the highly cambered inner stators at incidence angles of perhaps minus 70°. The annular slot is provided to allow air to be drawn directly into the core engine in reverse operation - significantly improving the pressure recovery of the core flow.

The bypass outlet guide vanes serve as structural elements in the fan frame. The pylon nose is integrated into the vane/frame, and circumferentially varying airfoil geometry is used to guide the flow smoothly around the pylon. A wide spacing between the fan rotor and the bypass vane/frame is used to reduce noise.

Key operating points for the UTW fan are indicated on the portion of the predicted-performance map shown in Figure 11. The takeoff point was selected to be on a low operating line, at a bypass stream pressure ratio of 1.27, to keep jet velocity low for reduced noise. The engine inlet was sized at this point to have a high throat Mach number of 0.79 to reduce forward-radiated fan noise. The maximum cruise point pressure ratio of 1.38 is on a higher operating line, reached by closing the variable exhaust nozzle, to increase thrust at altitude. The corrected airflow at cruise was limited to the takeoff value because inlet losses would become unacceptable if the inlet-throat Mach number increased. The aerodynamic design point of the fan was chosen to be on an intermediate operating line.

Some advantages of the variable-pitch rotor for forward-mode operation are shown in Figure 12. The dashed speedlines indicate how fan flow at a given speed could be varied by changing rotor pitch. At the takeoff condition it was estimated that the fan speed required to achieve the objective flow and pressure ratio could be reduced approximately 3% by opening the rotor pitch 2°. This could result in a worthwhile reduction in noise. At cruise, the speed could be increased several percent by closing the rotor pitch 2° to increase fan stall margin and also to reduce the low pressure turbine loading - thereby increasing its efficiency. Variable pitch could thus allow the trends of fan efficiency versus speed and pitch angle, and of turbine efficiency versus speed and loading, to be exploited to seek a minimum level of fuel consumption at cruise.

A summary of fan aerodynamic design parameters is given in Table V. The low tip speed, 306 m/sec (1005 ft/sec), and the high bypass ratio, 11.3, are notable features. Also notable is the low solidity of the fan rotor; the solidity was less than 1.0 across the full span of the blade to permit the blades to be reversed.

A photograph of the full-scale UTW fan rotor is shown in Figure 13. The black color of the blades is a result of the graphite-epoxy material used; the metal strip on the leading edge is for erosion resistance. The low aspect ratio and low solidity of the blades are apparent in this photo. Part of the the variable-pitch mechanism can be seen in the hub of the fan.

20
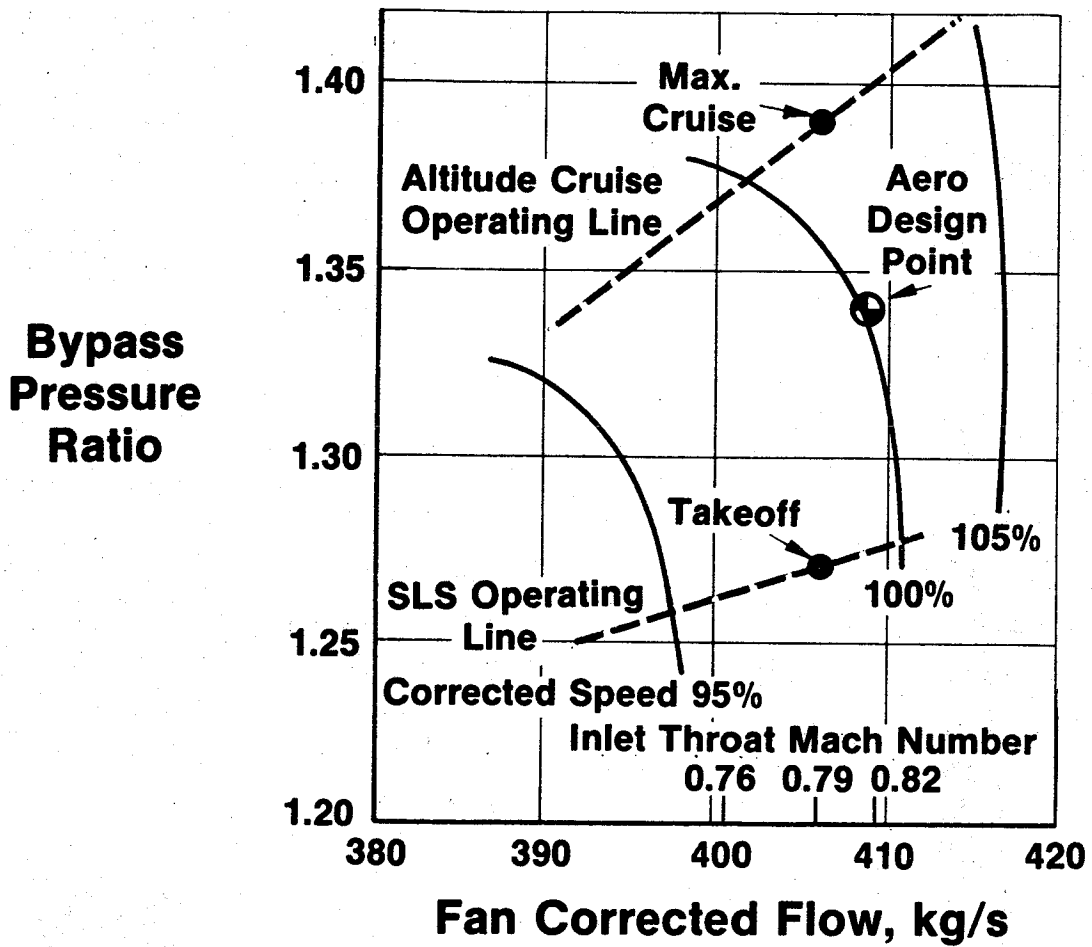
Figure 11. UTW Variable-Pitch Fan Design Map.
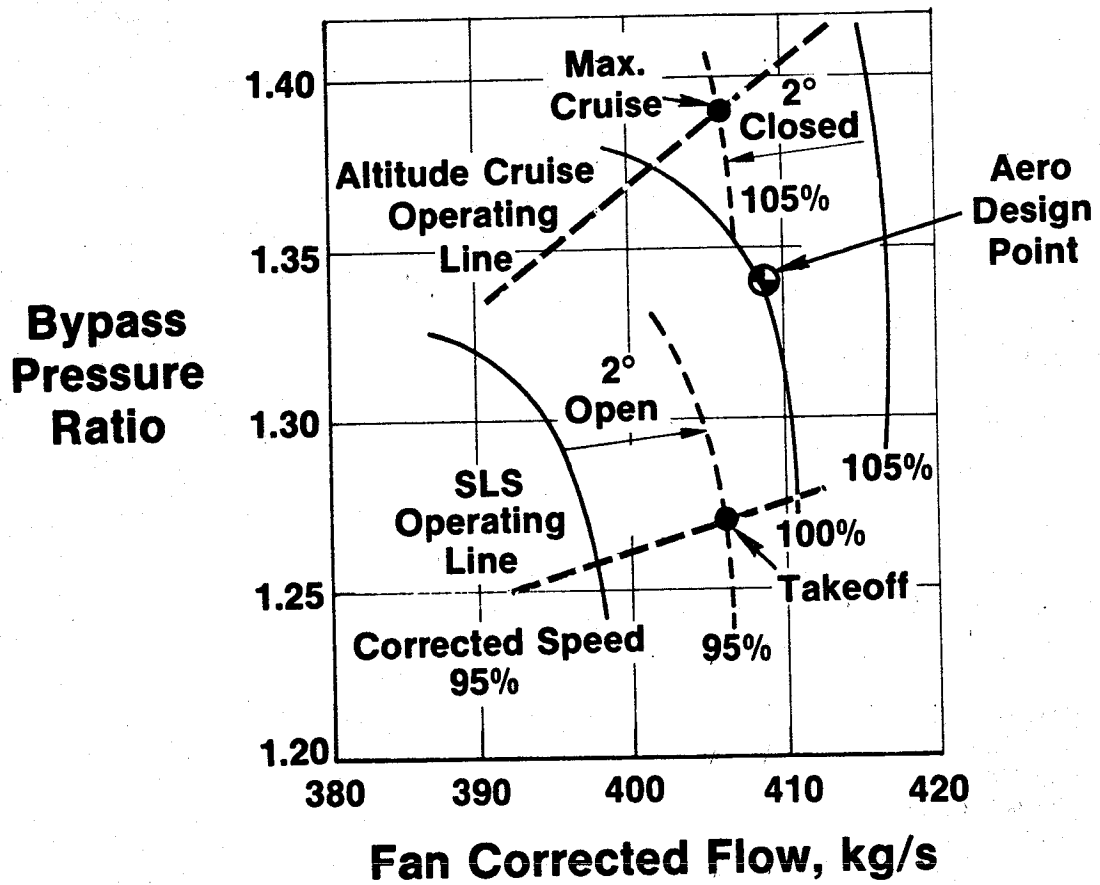
Figure 12. UTW Variable-Picth Fan Design Map.

Table V. UTW Fan Aerodynamic Design Features.

Tip Speed	306 m/s (1005 ft/sec)
Radius Ratio	0.44
Specific Flow	199 kg/sec-m^2 (40.8 lbm/sec-ft^2)
Bypass Pressure Ratio	1.34
Core Pressure Ratio	1.23
Bypass Ratio	11.3
Inlet Tip Relative Mach No.	1.13
Rotor Tip Solidity	0.95
Rotor Hub Solidity	0.98
Rotor Aspect Ratio	2.1
Number of Blades	18
Number of OGV's/Inner Stators	33/96
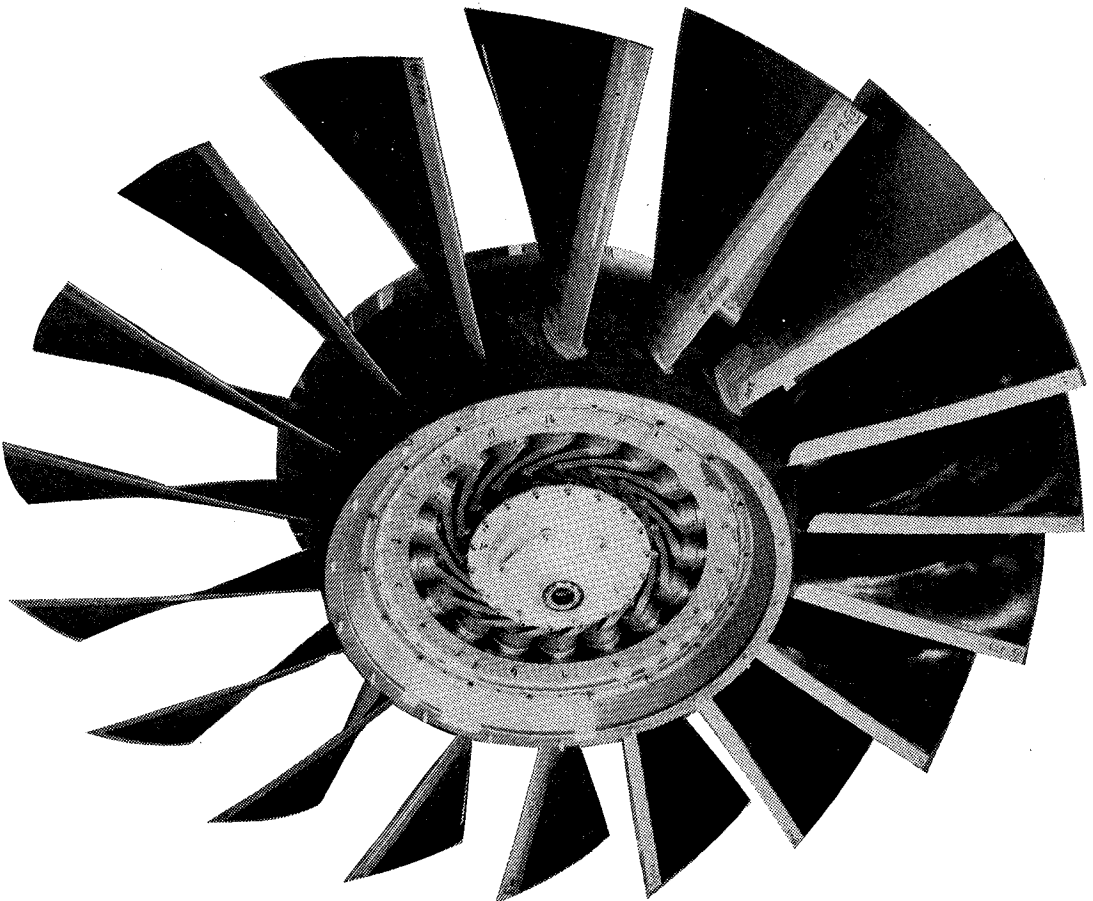
Figure 13. UTW Fan Rotor.

A section through the bypass vane/frame is shown in Figure 14. Each of the 33 low-aspect-ratio vanes is a structural member made of composite material. The pylon extends forward to the leading edge of the vane row and contains the accessory drive shaft. The leading edge of the pylon nose is a cambered airfoil shaped to properly align with the approaching flow. Five different types of airfoils, each with its own unique camber and stagger, are used to divert the flow smoothly around the pylon. Two of the five types of airfoils are shown. A nonstandard vane spacing is used on the left side, or suction surface, of the pylon nose to help reduce a local high-back-pressure region to avoid potential performance losses or noise sources.

The generation of reverse thrust by changing the rotor pitch is illustrated in the next series of figures. A top view of the rotor at nominal design pitch angle in forward-mode operation is shown in Figure 15 for reference. Airflow approaches the rotor axially because there are no inlet guide vanes to impart swirl. Hub, pitch-line, and tip blade sections are shown to illustrate the twist required to keep the blade aligned with the relative flow direction.

As shown in Figure 16, when the blade is reversed through flat pitch the blade is closed some 70° to 90°. During closure, the normal forward flow drops smoothly to zero, then reverse flow is gradually established. In reverse, flow is drawn backward through the bypass vane/frame, and the absolute flow vector is given swirl opposite to the direction of rotor rotation. The twist of the blade is in the wrong sense in reverse mode; flow through the hub is blocked off by the rotor, and only the tip section pumps air out the inlet duct. It can also be seen that blade camber is in the wrong sense when the blade is reversed through flat pitch since the flow is deflected away from the axial direction. In order to pump air despite the reverse camber, the blade must operate at a high incidence angle; therefore, it is expected that the pumping ability and the efficiency of the fan will be relatively low when reversed through flat pitch.

Blade orientation when reversed through stall is shown in Figure 17. In this case the blade is opened 95° to 105°. Initially a stall takes place; after further opening, normal airflow ceases and reverse flow becomes established. The trailing edge of the rotor becomes the effective leading edge during reverse-through-stall-pitch operation. Although rotor twist is still in the wrong sense, and the flow is still blocked at the hub, the camber is now in the proper direction for a compressor blade. It is thus expected that pumping and efficiency will be highest when the rotor is reversed through stall.

Scale Model Test Results - A 50.8-cm (20-in.) diameter model, 0.282 linear scale factor, of the UTW fan was built for aeroperformance and acoustic testing. A photograph of the scale-model fan is shown in Figure 18. Adjustable metal blades were used for the test rig. These could be fixed at any pitch angle but could not be varied while running. Tests were conducted both in forward and in reverse operating modes at several pitch angles in each mode.
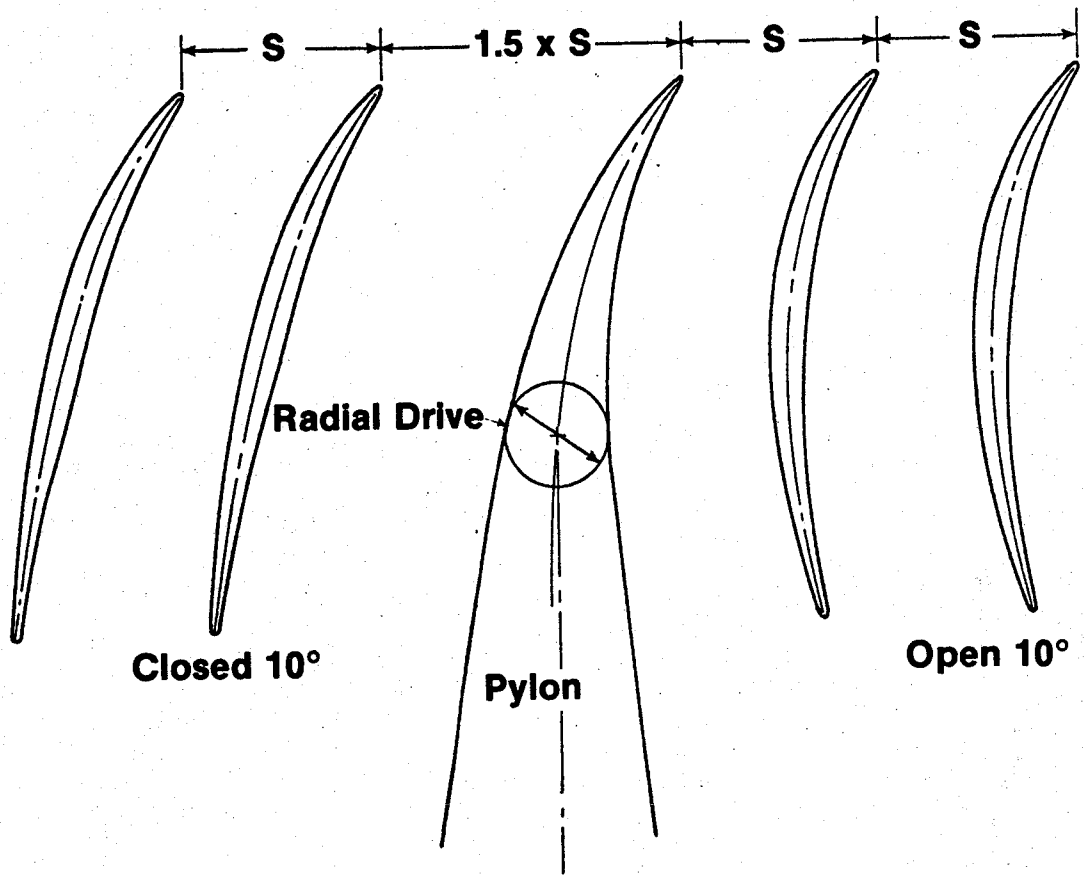
Figure 14.   UTW Fan Bypass OGV Design.
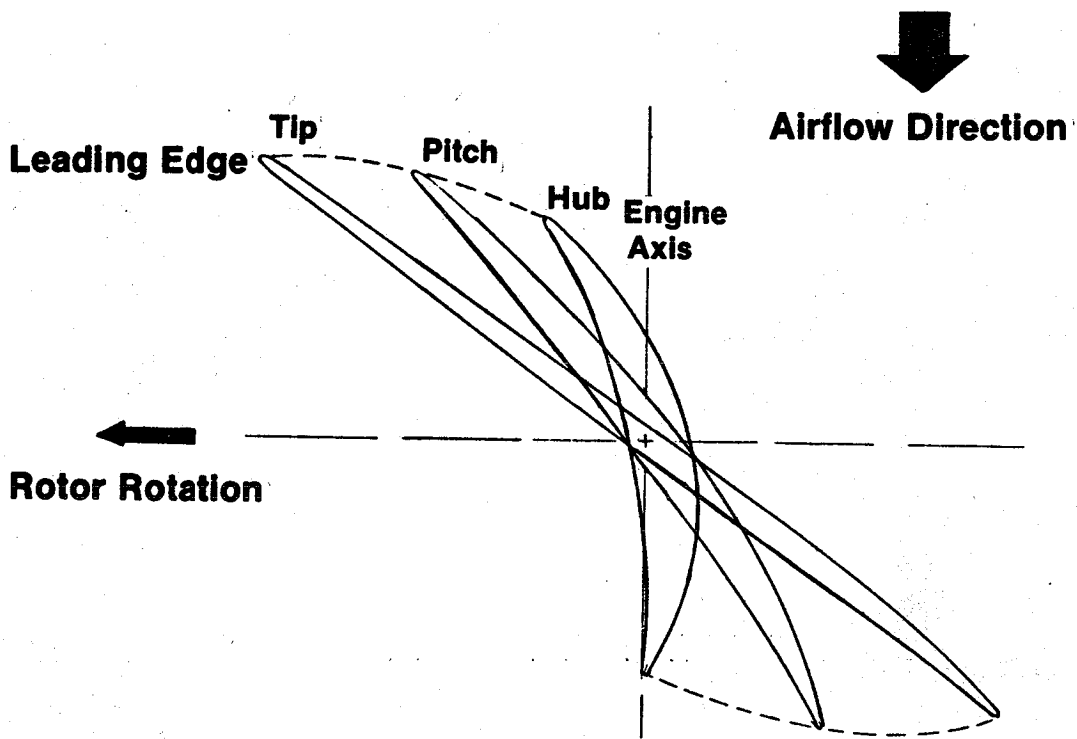
Figure 15. UTW Fan Rotor Blade; Forward-Mode
Operation.
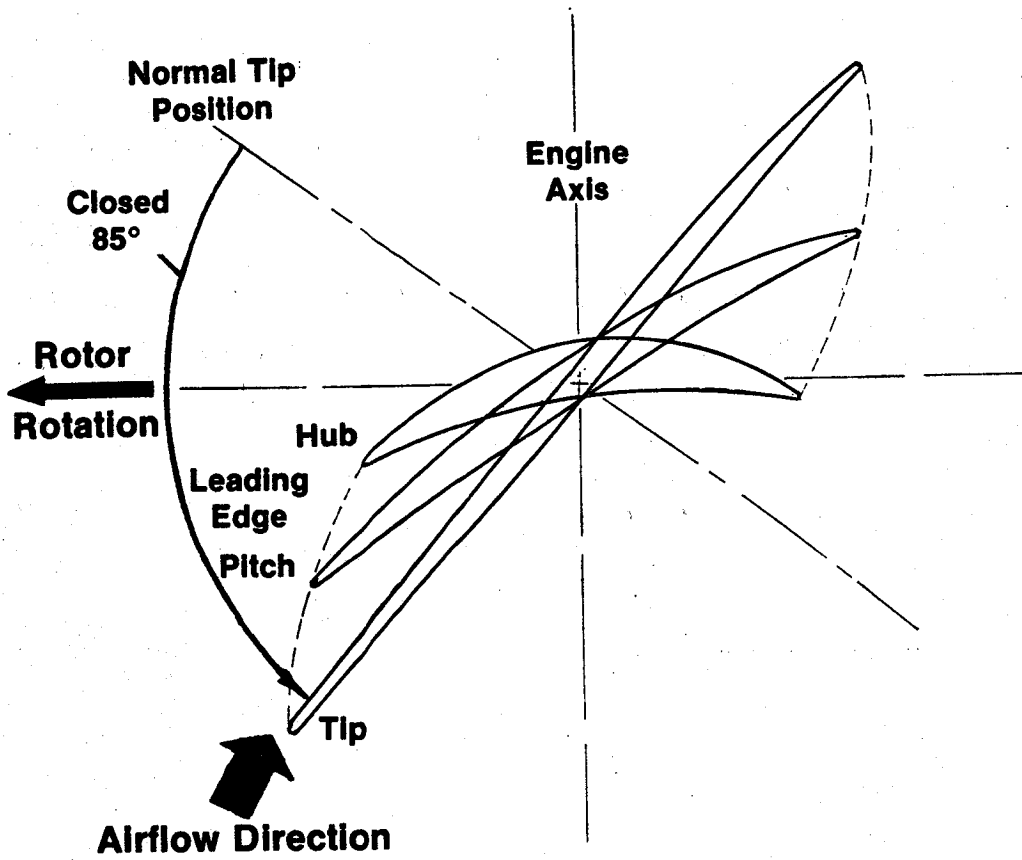
Figure 16. UTW Fan Rotor Blade; Reverse Through Flat Pitch Operation.
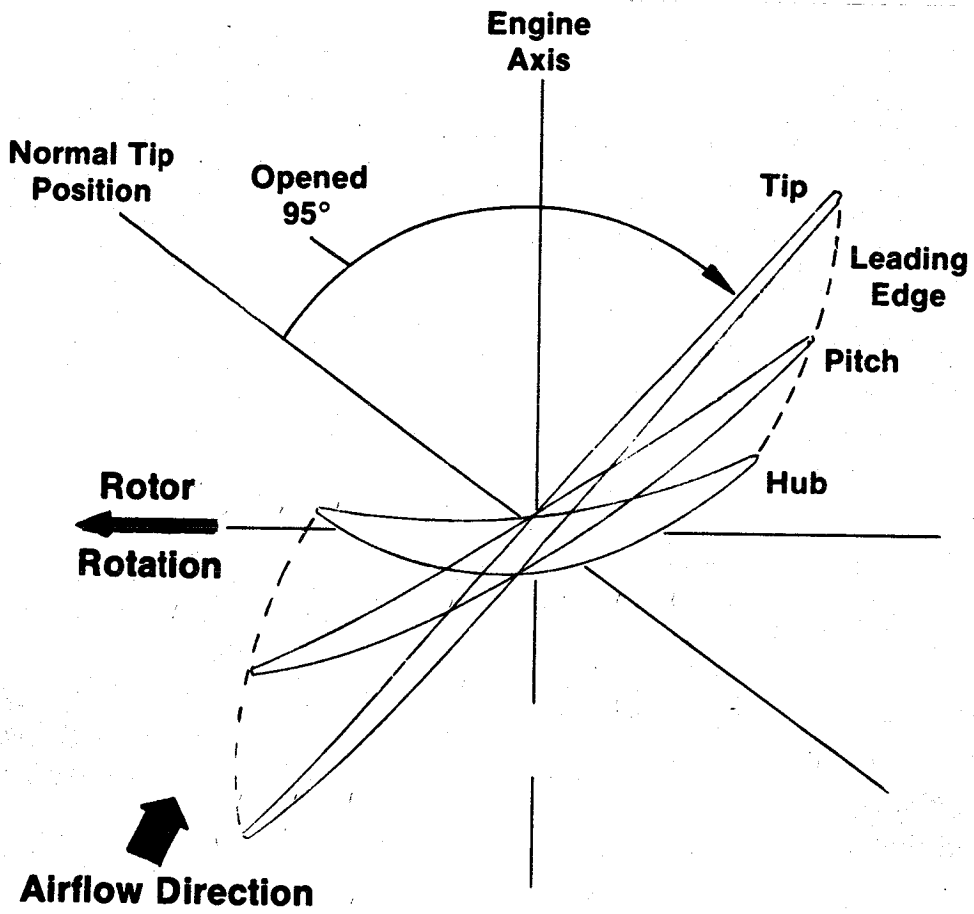
Figure 17. UTW Fan Rotor Blade; Reverse Through
Stall Operation.
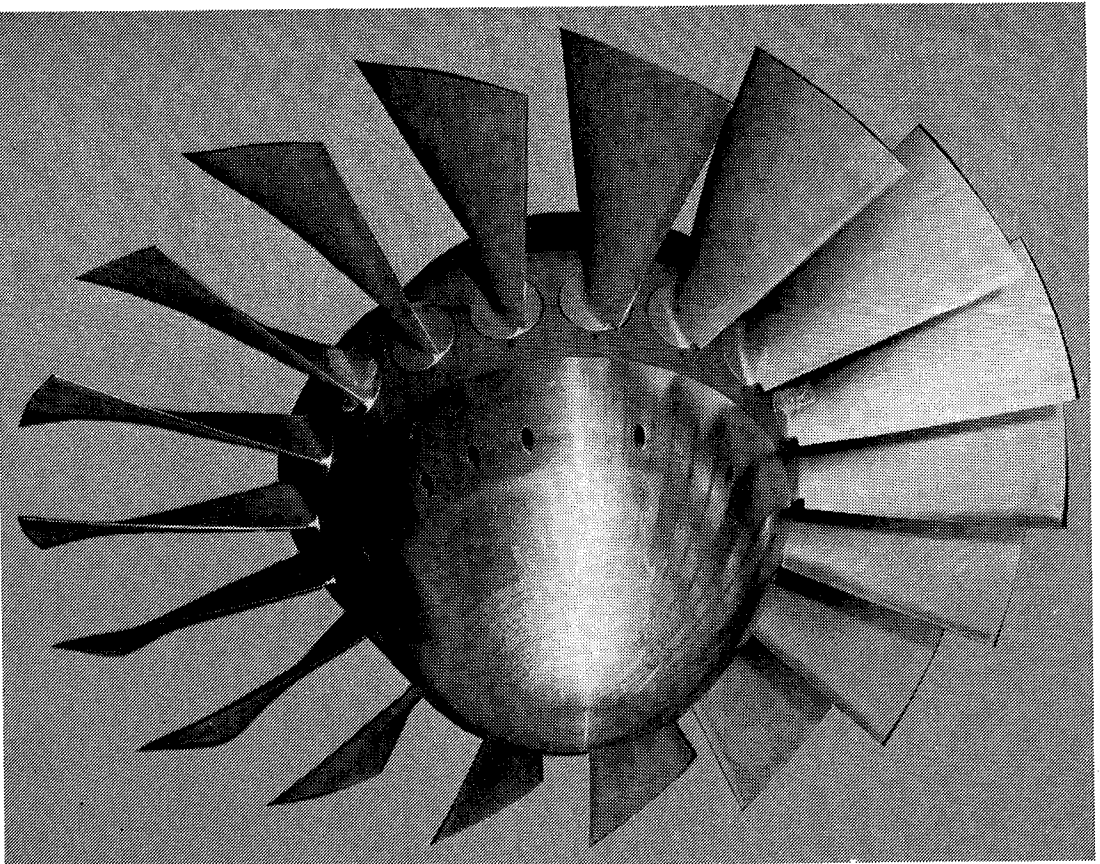
Figure 18. UTW Scale-Model Fan.

A performance map for the bypass portion of the fan flow in forward-mode operation at the nominal design rotor pitch angle is shown in Figure 19. The design pressure ratio, flow, and efficiency are indicated by the target symbols, and the objective stall line is shown dotted. Performance maps similar to the one shown were also obtained at 5° open and 5° closed rotor-pitch-angle settings. Test results indicated that stall margin goals and the design-point efficiency goal of 86.5% had been met. At 100% speed the design flow was achieved at low operating lines, but flow and pressure ratio were below objectives on an operating line through the design point. Analysis indicated that the rotor blade-tip sections lacked circulation capacity at higher loadings. A redesign to increase rotor camber would have increased the pumping of the fan on the design operating line, but (because of the low solidity) this might have reduced efficiency by opening the throat areas. For this reason, and because of a tight fabrication schedule, it was decided that the blades for the full-scale engine would not be redesigned.

The 95% speed lines obtained at the three pitch angles are shown in Figure 20. This is the fan speed at which takeoff thrust was to be obtained in the demonstrator engine; the objective takeoff flow, pressure ratio, and efficiency are indicated in the figure by solid symbols. Despite the lower-than-design pumping capacity, the flexibility of the variable-rotor-pitch feature enabled the fan to meet the very important flow and pressure-ratio goals of the engine system at takeoff simply by opening the rotor 3° from nominal instead of 2° as originally estimated.

Fan hub performance measured during scale-model tests at 100% design corrected speed, for the three rotor pitch angles, is shown in Figure 21. Design hub pressure ratio was nearly achieved at design flow with the nominal design pitch angle. The 78% hub efficiency goal was met at the design operating line and was exceeded by a substantial margin at higher operating lines.

Reverse-mode test results from the fan scale-model program are shown in Figure 22. Fan pressure ratio from the OGV exit to the engine inlet throat is plotted versus rotor corrected flow for five different reverse-pitch angle settings: closed through flat pitch to 73° and 79°; and opened through stall pitch to 95°, 100°, and 105°. The data points for a given pitch angle represent different speeds. Only a single operating line could be evaluated at each pitch angle since the engine inlet (which serves as the exhaust nozzle in reverse-mode operation) was a fixed-geometry device. The various combinations of flow and pressure ratio needed to achieve the reverse-thrust objective of 35% of takeoff thrust are indicated by the heavy, dark band. Although the reverse-thrust goal could not be met when reversing through flat pitch, because of speed limits or high rotor stresses, the reverse-thrust objective was met for all three of the reverse-through-stall-pitch angles tested.

3.2.2 OTW Fan Aerodynamics

A cross section of the fan for the OTW engine is shown in Figure 23. The OTW fan has a conventional, fixed-pitch rotor and has a higher tip speed, a
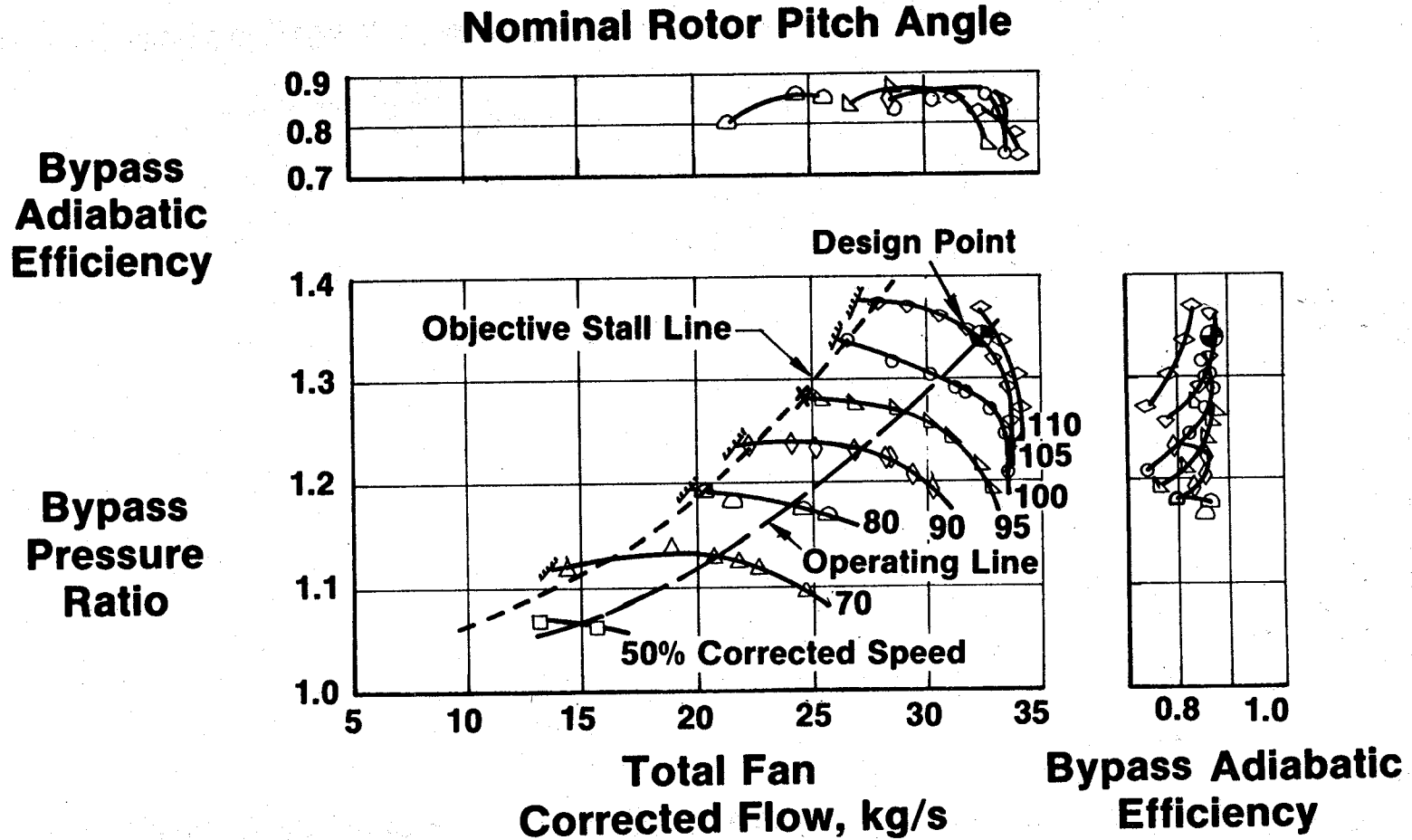
Figure 19. UTW Fan, Scale-Model, Bypass Performance.
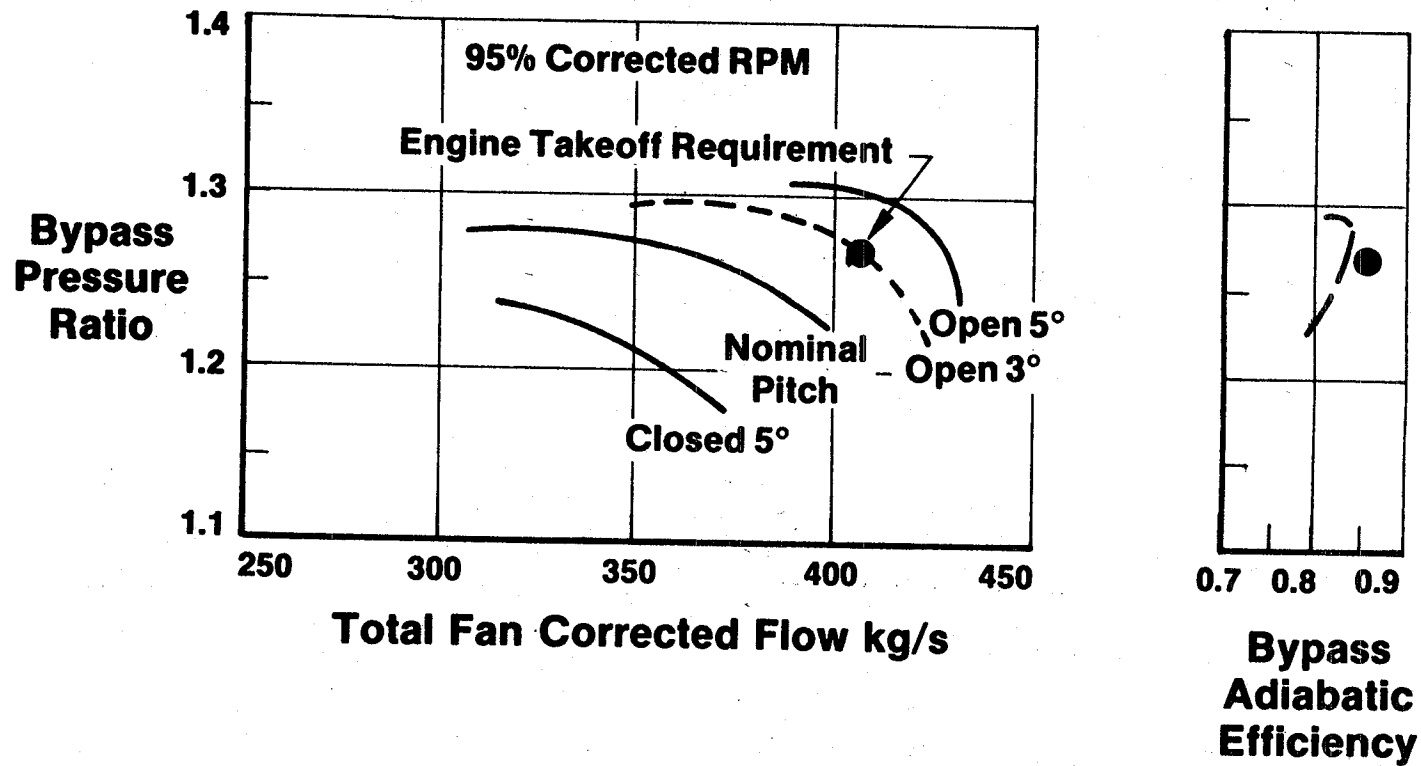
Figure 20. UTW Fan Takeoff Operation Scaled from Model Data.
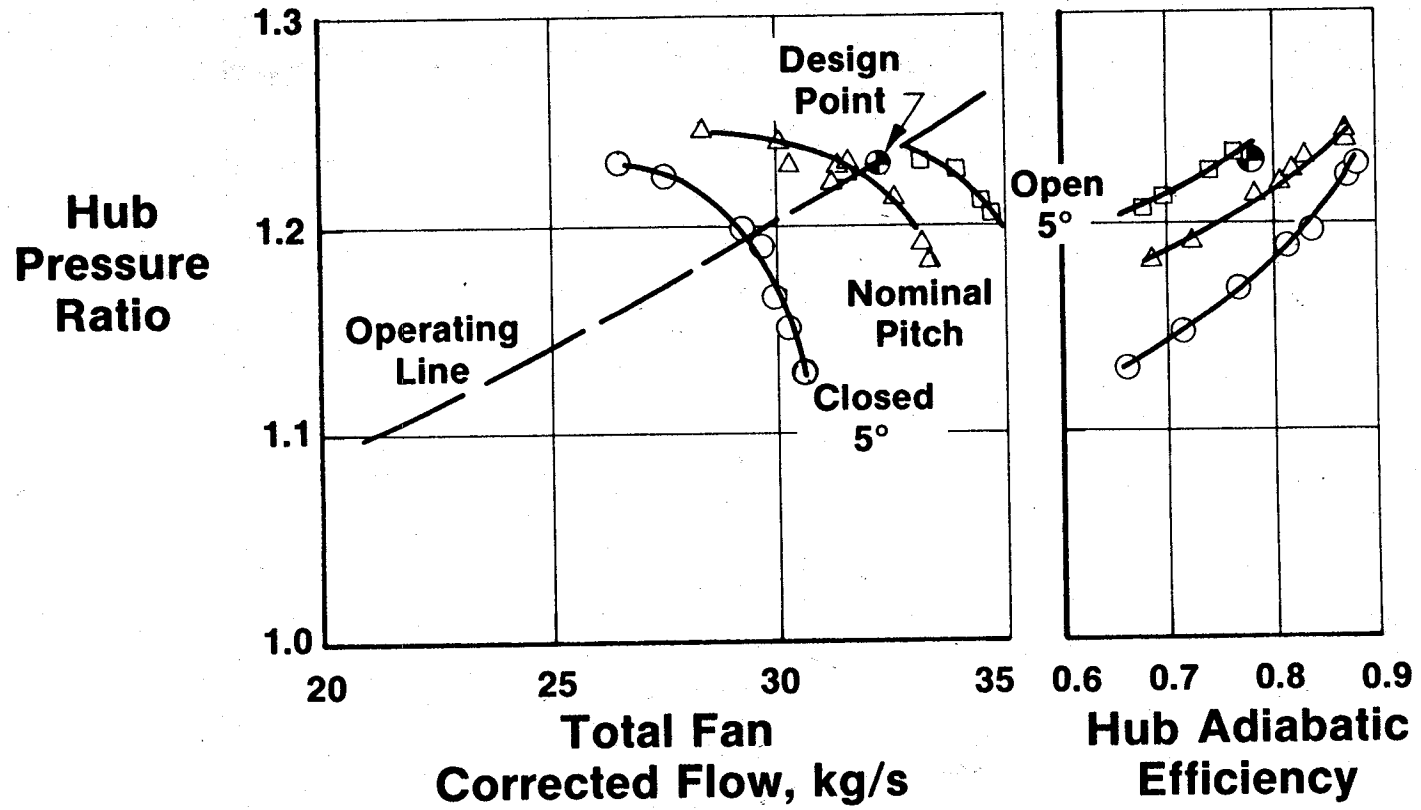
Figure 21.   UTW Fan, Scale-Model, Hub Performance at 100% Corrected Speed.
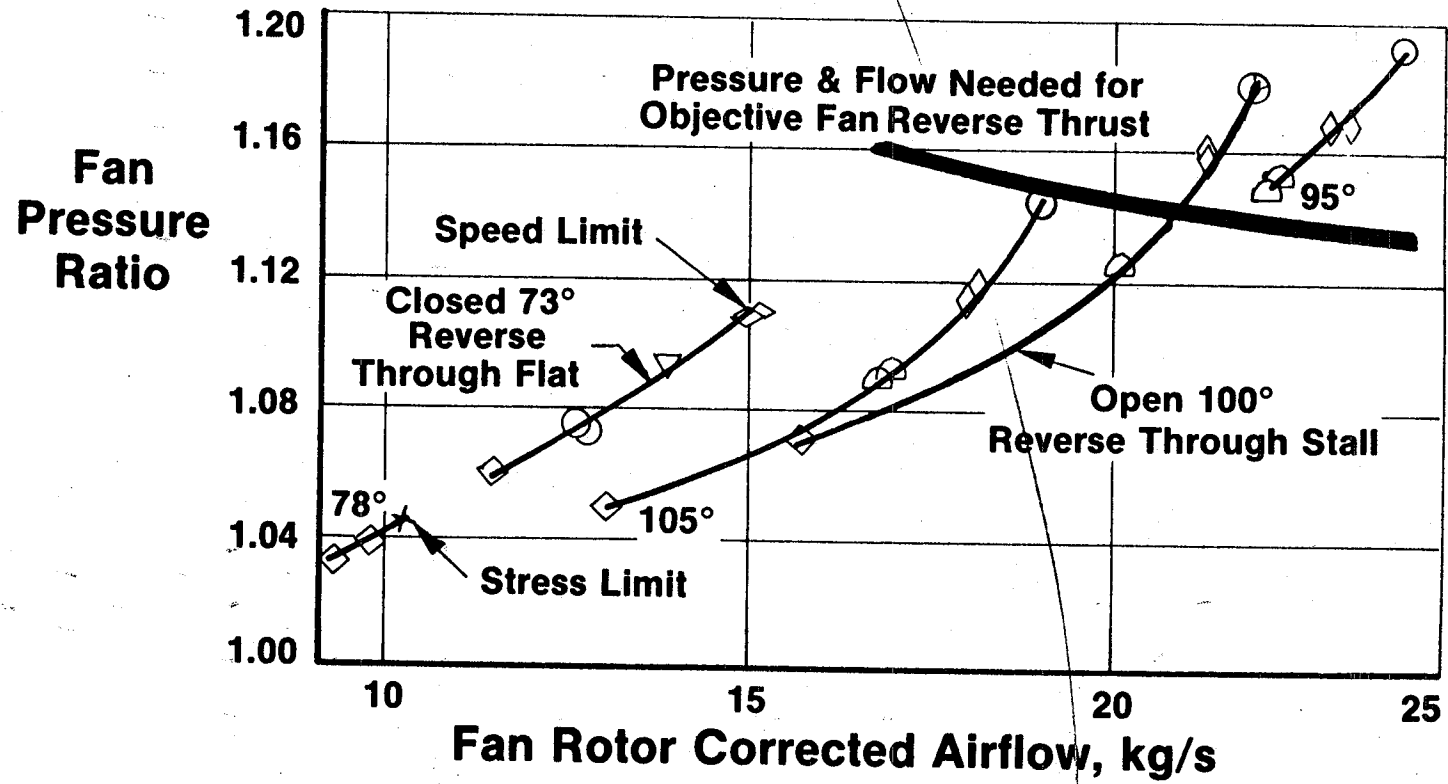
Figure 22. UTW Fan, Scale-Model, Reverse-Mode Performance.

Airflow

Bypass OGV/Frame

Core Duct Struts

Inner Stator
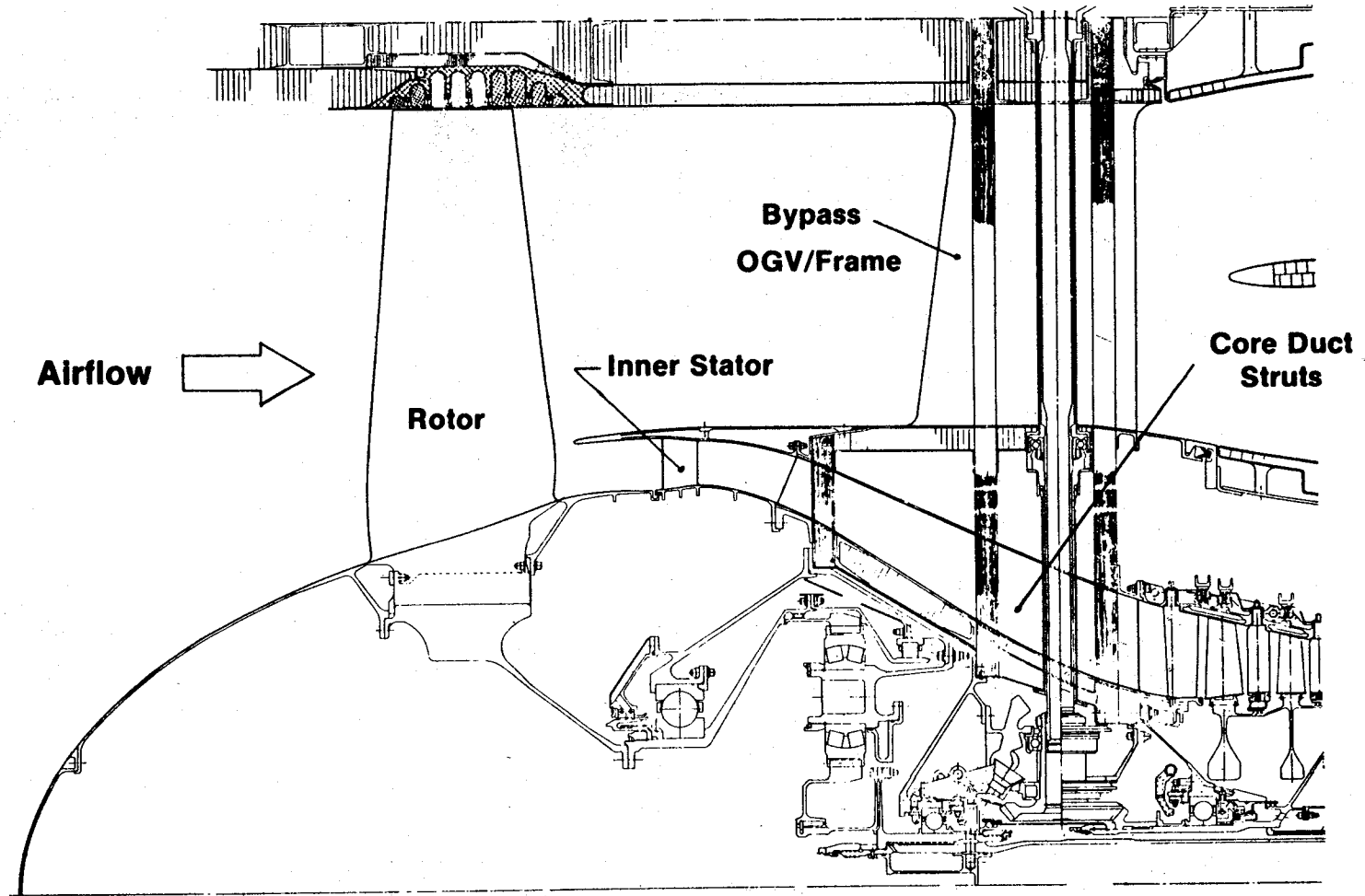
Rotor

Figure 23. OTW Fan Cross Section.

higher pressure ratio, and a higher rotor solidity compared to the UTW fan. It also has low-aspect-ratio, unshrouded, rotor blades that are designed to be fabricated from composite materials - although titanium blades were used in the QCSEE OTW demonstrator. A flow splitter and inner stator are closely coupled behind the rotor, and the composite bypass vane/frame is identical in aerodynamic design to that used in the UTW engine.

A portion of the predicted OTW fan-performance map is shown in Figure 24. The aerodesign-point bypass pressure ratio was 1.36. This point was selected to be midway between the lower, takeoff, operating line and the higher, cruise, operating line. A variable exhaust nozzle enabled the fan operating line to be adjusted to meet flight conditions. Maximum cruise and takeoff again occurred at the same flow because of inlet throat Mach number limits.

A summary of OTW fan aerodynamic design parameters is listed in Table VI. The fan-tip speed of 358 m/sec (1175 ft/sec), while higher than in the UTW engine, is still a relatively low value. Of those features listed, probably the aerodynamic design feature of greatest significance in the OTW fan is the effort to achieve a high hub pressure ratio. The design radial profile of total pressure ratio at the fan rotor exit is shown in Figure 25. The average hub pressure ratio is 1.43 - higher than the 1.36 average value in the bypass stream. The tip speed is 17% higher than the UTW fan, and a higher rotor hub solidity (made possible by use of a fixed-pitch rotor) is used to aid in achieving the high core supercharging.

A photograph of the rotor for the OTW fan is shown in Figure 26. The low aspect ratio (2.1) of the 28 unshrouded titanium blades is evident in this view.

3.3 COMPOSITE FAN BLADES

3.3.1 Design Requirements

The mechanical design and the materials selected for the UTW fan blades were dictated by the requirements associated with variable-pitch (VP) capability. The blades had to be capable of a very large angle of rotation over the whole engine-speed range. To allow blade rotation, the number of blades in the stage had to be kept small, with short chord lengths, so they could pass each other with no interference. To allow actuation of these blades at high rotor speeds, with reasonable actuation forces, the blades had to be very light. To provide acceptable elastic stability with the blade geometry dictated by the variable-pitch-capability, the materials required very high specific stiffness and strength-to-density ratios. Composite materials made of graphite, S-glass, Kevlar, and boron fibers in an epoxy matrix have these properties.

Figure 27 indicates the effects of the VP requirement on fan-blade geometry. On the left is a picture of the VP UTW fan, on the right is a picture of the OTW fan which did not have a VP requirement. Note the wide spaces
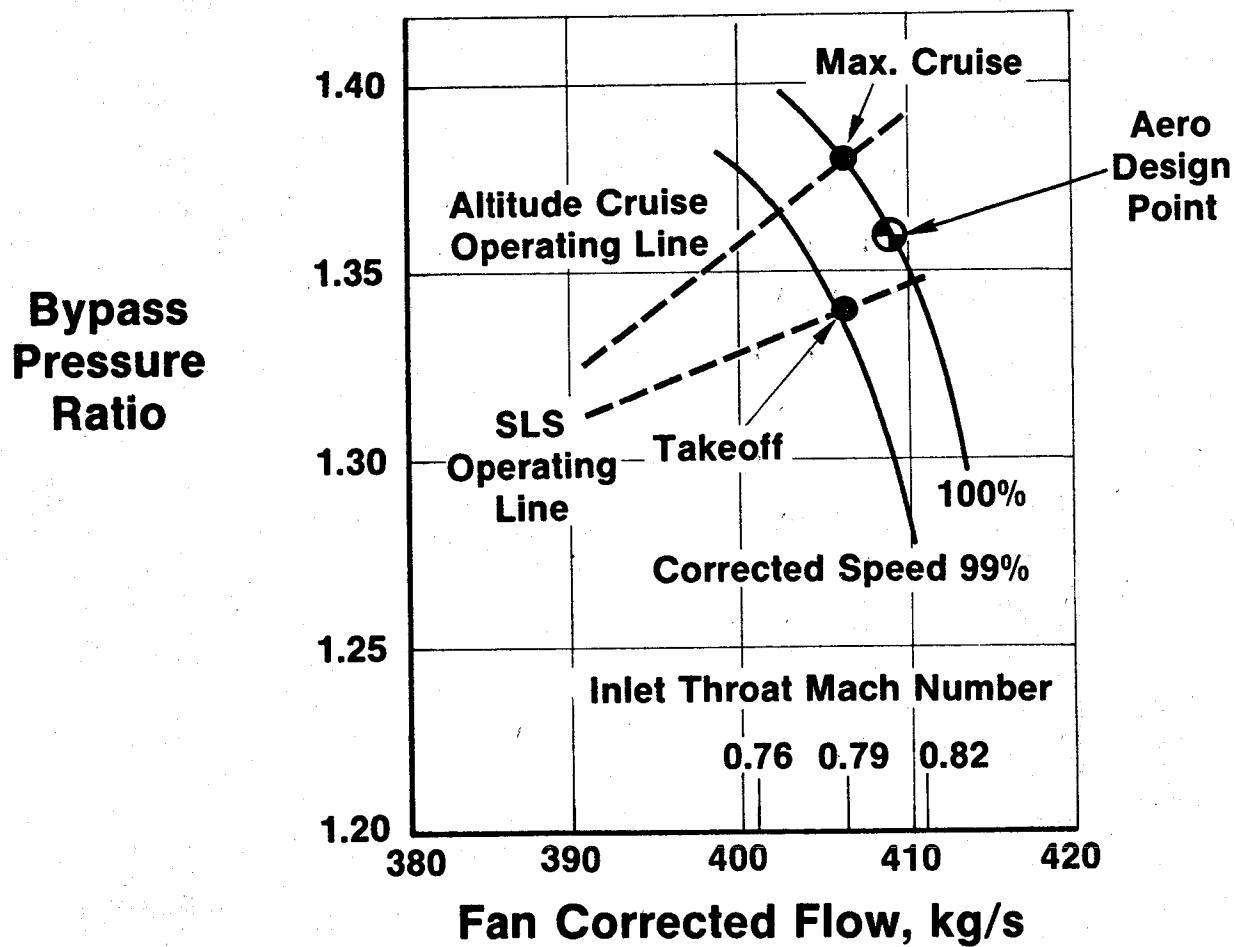
Figure 24. OTW Fan Design Map.

Table VI. OTW Fan Aerodynamic Design Features.

Tip Speed	358 m/s (1175 ft/sec)
Radius Ratio	0.42
Specific Flow	194 kg/sec-m^2 (39.8 lbm/sec-ft^2)
Bypass Pressure Ratio	1.36
Core Pressure Ratio	1.43
Bypass Ratio	9.9
Inlet Tip Relative Mach No.	1.22
Rotor Tip Solidity	1.30
Rotor Hub Solidity	2.23
Rotor Aspect Ratio	2.1
Number of Rotor Blades	28
Number of OGV's/Inner Stators	33/156
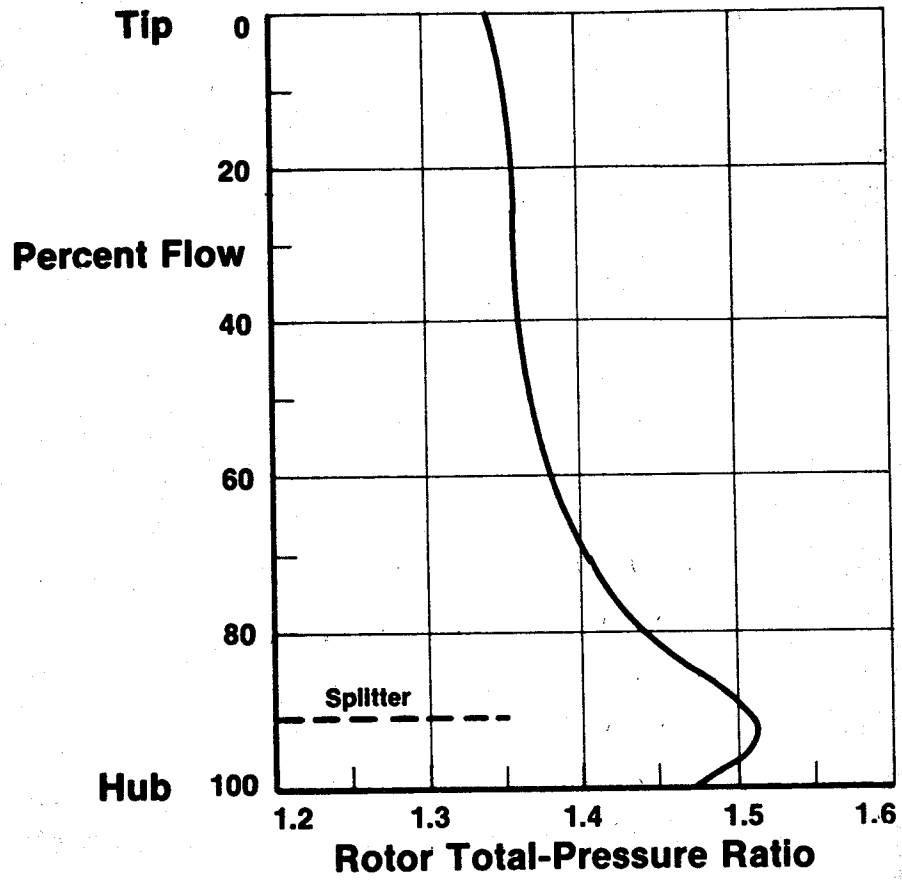
Figure 25. OTW Fan Rotor Design Total-Pressure
Ratio Radial Profile.
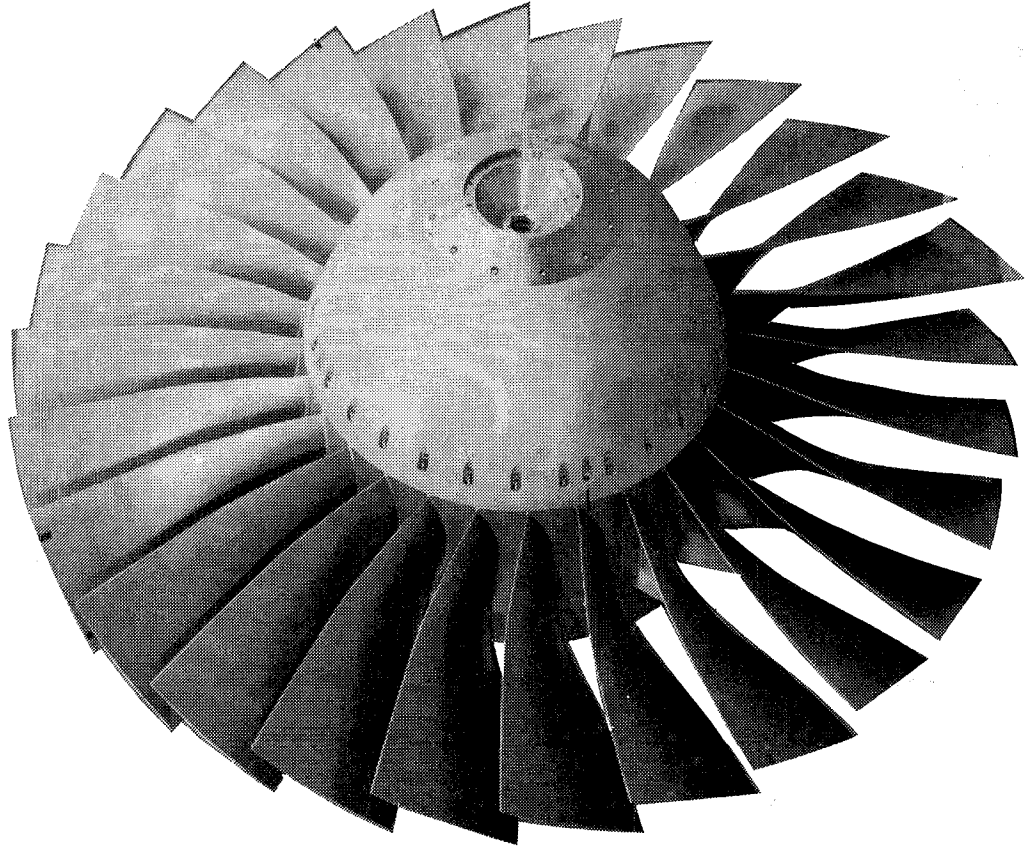
Figure 26. OTW Fan Rotor.

41

UTW
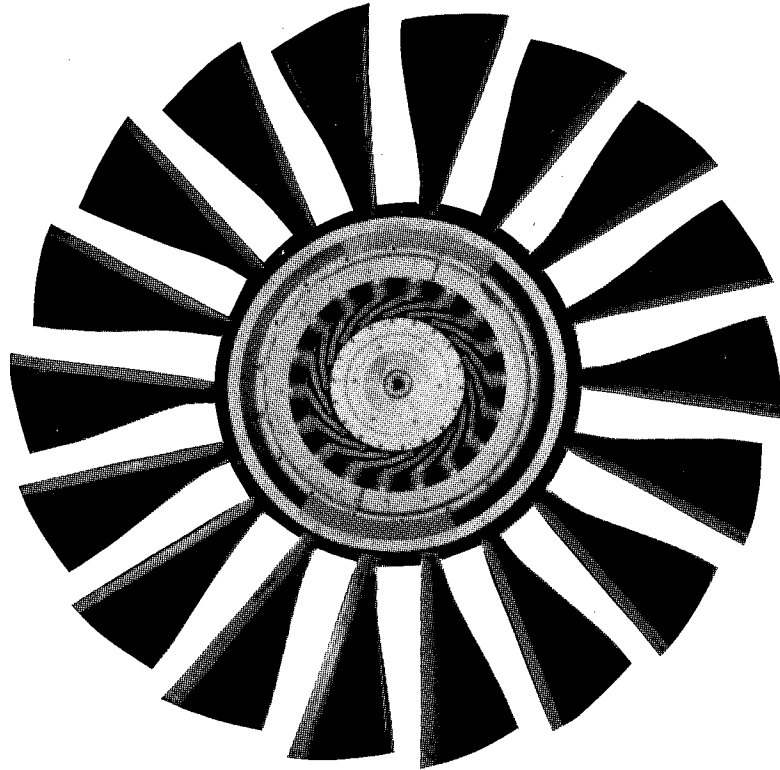
OTW
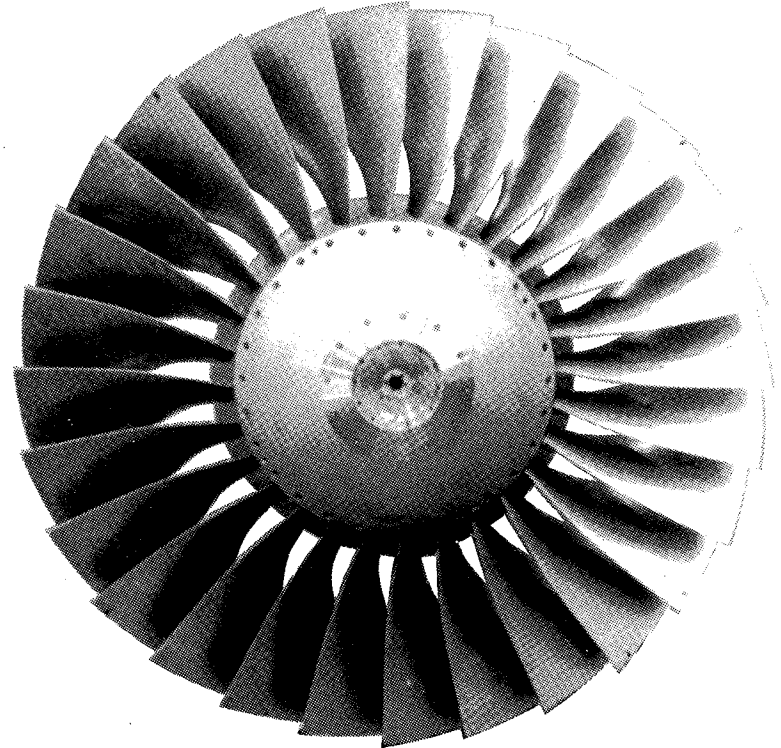
Figure 27. Fan Rotors.

between the UTW blades. This fan rotor has 18 blades with root-chord lengths of 14.7 cm (5.8 in.) compared to 28 blades with root chords of 20 cm (7.87 in.) used in the OTW rotor. Both blades were originally designed to use composite materials. The UTW blades weighed 43.3 kg (95.4 lb) while the composite OTW blades would have weighed 55.3 kg (122 lb). The OTW blades used in the experimental engine were fabricated from titanium.

The aerodynamic design requirements for the UTW fan blades are shown in Table VII. Note that the airfoil solidity is less than 1.0 at all radial sections.

The mechanical design requirements of the fan blade fall into two major categories: variable pitch and structural integrity. Those requirements associated with varible pitch are uniquely the result of the need to be able to rotate the blades. For the UTW application, the blades had to be capable of rotation from the flat pitch to the stall pitch position - which encompassed a blade rotation of over 170°. Obviously, to accomplish any rotation, shrouds could not be used. Finally, in order to be able to rotate the blades over the engine-rotor-speed range with reasonable actuation forces, the blade weight had to be limited to less than 2.5 kg (5.5 lb) each. The actual blade weight was 2.4 kg (5.3 lb).

The design requirements associated with structural integrity were defined based on GE blade-design practices and the engine-mission application. They encompass vibrational and steady-state stresses, fatigue, FOD resistance, and maintainability considerations. The design and materials selected for the blade were primarily dictated by the aeromechanical stability requirements, i.e., to avoid blade excitation at natural frequencies by forcing functions due to aerodynamic flow.

Short-term, steady-state, structural margin is defined as the capacity to operate the blade at 141% speed with no failure. (This represents a load factor of 2.) Thus, all blade stresses at this condition must be less than ultimate.

The blade must be capable of infinite high-cycle-fatigue life ($>10^6$ cycles) and have a low-cycle capability of 48,000 engine starts. For aircraft use, the blades must pass the FAA certification test which defines bird-strike tolerance. Finally, from an economic standpoint, the blade design must exhibit easy maintenance features such as on-the-wing replacement.

3.3.2 Design Description

Figure 28 shows the design features of the composite blade. The airfoil and dovetail were fabricated from a number of 0.25-cm (0.010-in.) thick plies of composite preimpregnated fibers cut to various shapes and carefully laid-up to satisfy the blade geometric requirements. These plies, of several different materials, were oriented in 0°, ±45°, and 90° directions to give the blade

Table VII. Aerodesign Requirements.

Aero Definition	UTW
Tip Speed	306 m/sec (1005 ft/sec)
Tip Diameter	180 cm (71 in.)
Radius Ratio	0.44
Number of Blades	18
Bypass Pressure Ratio	1.27 Takeoff
Aspect Ratio	2.11
Tip Chord	30.3 cm (11.91 in.)
Root Chord	14.8 cm (5.82 in.)
Solidity	
— Tip	0.95
— Root	0.98
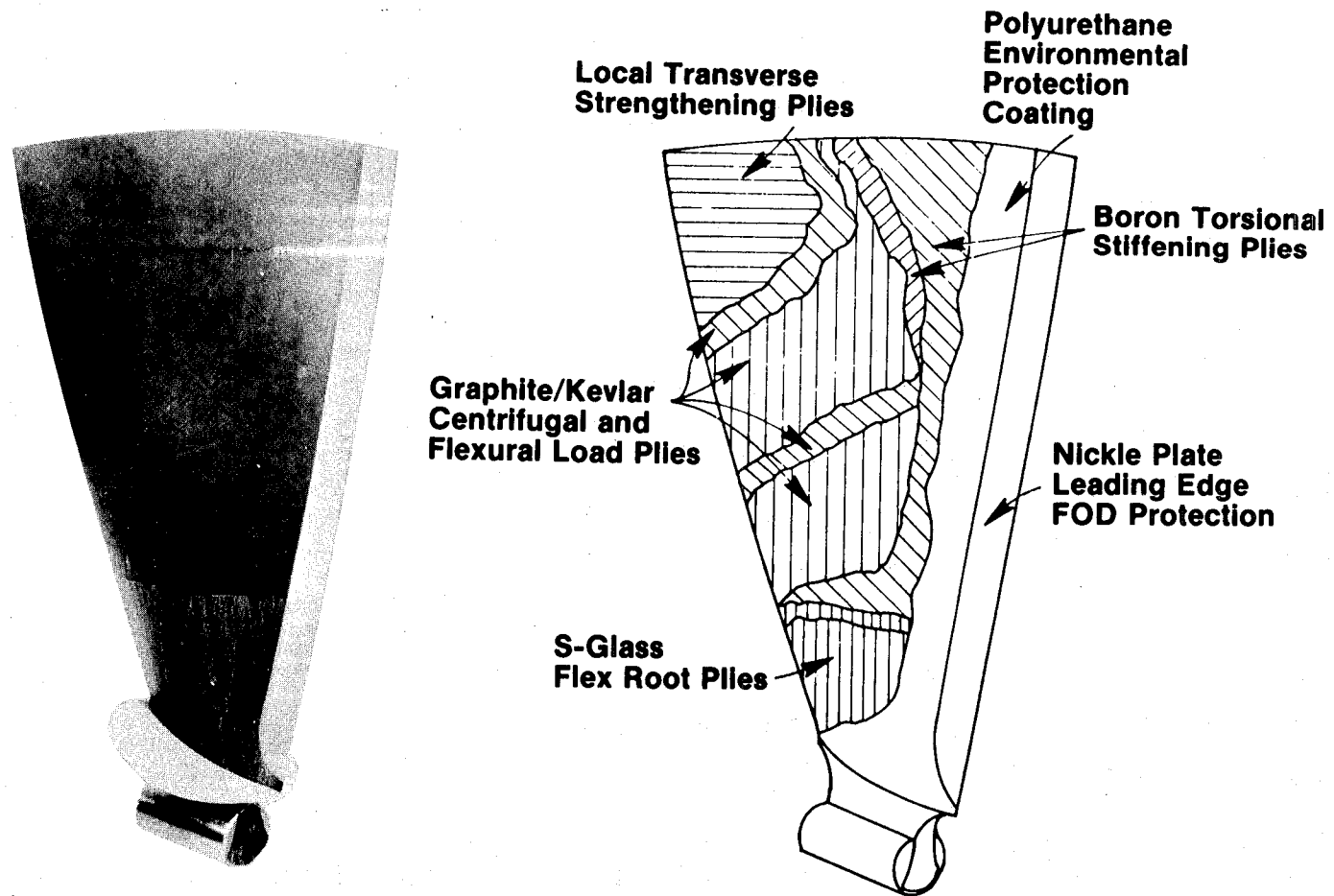
Figure 28. UTW Engine Composite Fan Blade Features.

The figure labels are:

Local Transverse Strengthening Plies

Polyurethane Environmental Protection Coating

Boron Torsional Stiffening Plies

Graphite/Kevlar Centrifugal and Flexural Load Plies

Nickle Plate Leading Edge FOD Protection

S-Glass Flex Root Plies

the directional strength and stiffness needed. The plies were laid-up in a die and pressed in a carefully controlled time/temperature/pressure cycle. The leading edge was nickel plated to improve the erosion and FOD character-istics of the blade. The nickel was plated onto a stainless steel wire mesh that was bonded to the airfoil in a secondary operation. The remaining area of the airfoil was coated with a thin layer of polyurethane to reduce erosion due to dust, sand, and water. The platform, which forms part of the inner-annulus flowpath, is round to allow blade rotation and still maintain a smooth inner flowpath for the air. The composite dovetail is bell-shaped and encased in a 7075-T6 aluminum outsert. The outsert is cylindrical and allows the blade to rotate during bird impacts. This feature is designed to help eliminate blade breakage at the root during foreign-object impact.

Figure 29 shows half of the composite material plies that make up the blade. Four different materials are used in the blade. Note that the shape of each ply is different. Also shown are the proportions of the various ma-terials used. The overall fiber volume fraction is 60%.

The platform is an integral part of the blade, as shown in Figure 30. It is put on the blade in a secondary operation. The round, flowpath portion is made up of a number of graphite-epoxy plies bonded to the airfoil. The flow-path piece is supported by a lower face sheet also made of graphite-epoxy. An aluminum-honeycomb core is sandwiched between the flowpath and lower face-sheets for stiffness. Finally, a leading-edge strap of graphite-epoxy is put all around the lower face sheet. The purpose of this strap is to hold the platform onto the blade in the event the shear bond fails; it is really a safety bandage.

The natural-frequency characteristics of the blade/disk are shown on the Campbell diagram (Figure 31) as a function of fan speed. The blade was sized to satisfy aeroelastic stability criteria. This required the level of first-torsional frequency shown. The second requirement was to have a good separa-tion between the blade natural frequencies and all excitation lines at the 100% speed condition. The third goal was to have the first-flexural natural frequency above the 2/rev excitation line. This could not be done within the other design requirements; thus, the first-flexural frequency was set to cross the 2/rev excitation line at about 67% speed - a transient condition. During engine testing, it was found that stresses exceeded scope limits at the first-flex, 2/rev, crossover condition. The OTW blade also had a crossover of the first flex with the 2/rev excitation line but, because the longer blade-hub chord and the higher fatigue strength of titanium, the stresses were well be-low scope limits.

The Goodman diagram (Figure 32) was constructed using blade and specimen test data. The allowable curve was defined as 85% of test data. The test data were based on no delamination of specimens and blades for 10^6 cycles. Thus, this diagram represents a very conservative estimate relative to Goodman diagrams, used for metals, which are based on material fracture. For engine testing, the scope limits were set at 5.86 kN/cm^2 (8.5 ksi) to account for

Airfoil Center

Airfoil Surface

Material	% By Volume
Type AS Graphite/PR288 Epoxy	36
S-Glass/PR288 Epoxy	5
Kevlar/PR288 Epoxy	37
Boron/PR288 Epoxy	22
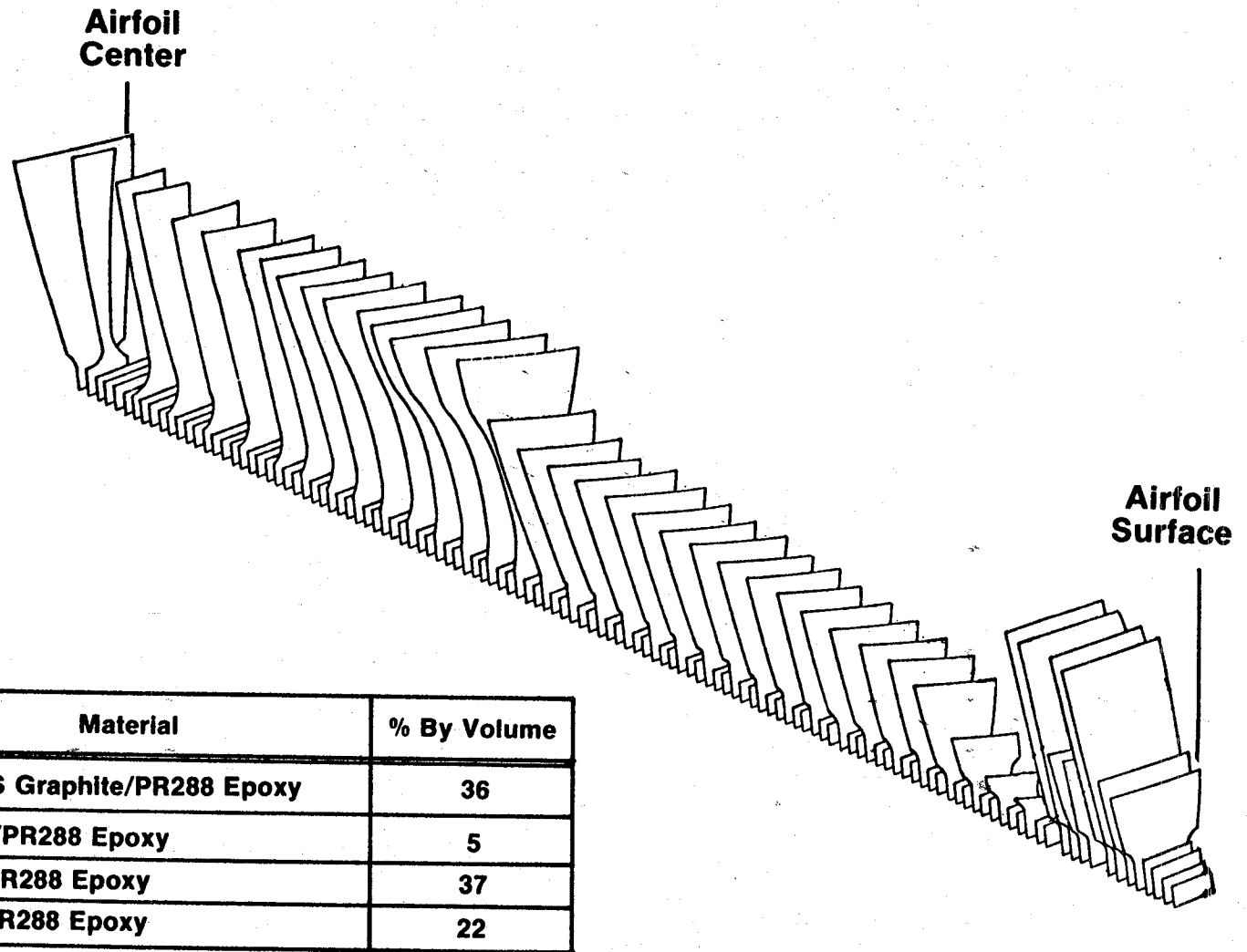
Figure 29.   Composite Fan Blade Ply Assembly.

47
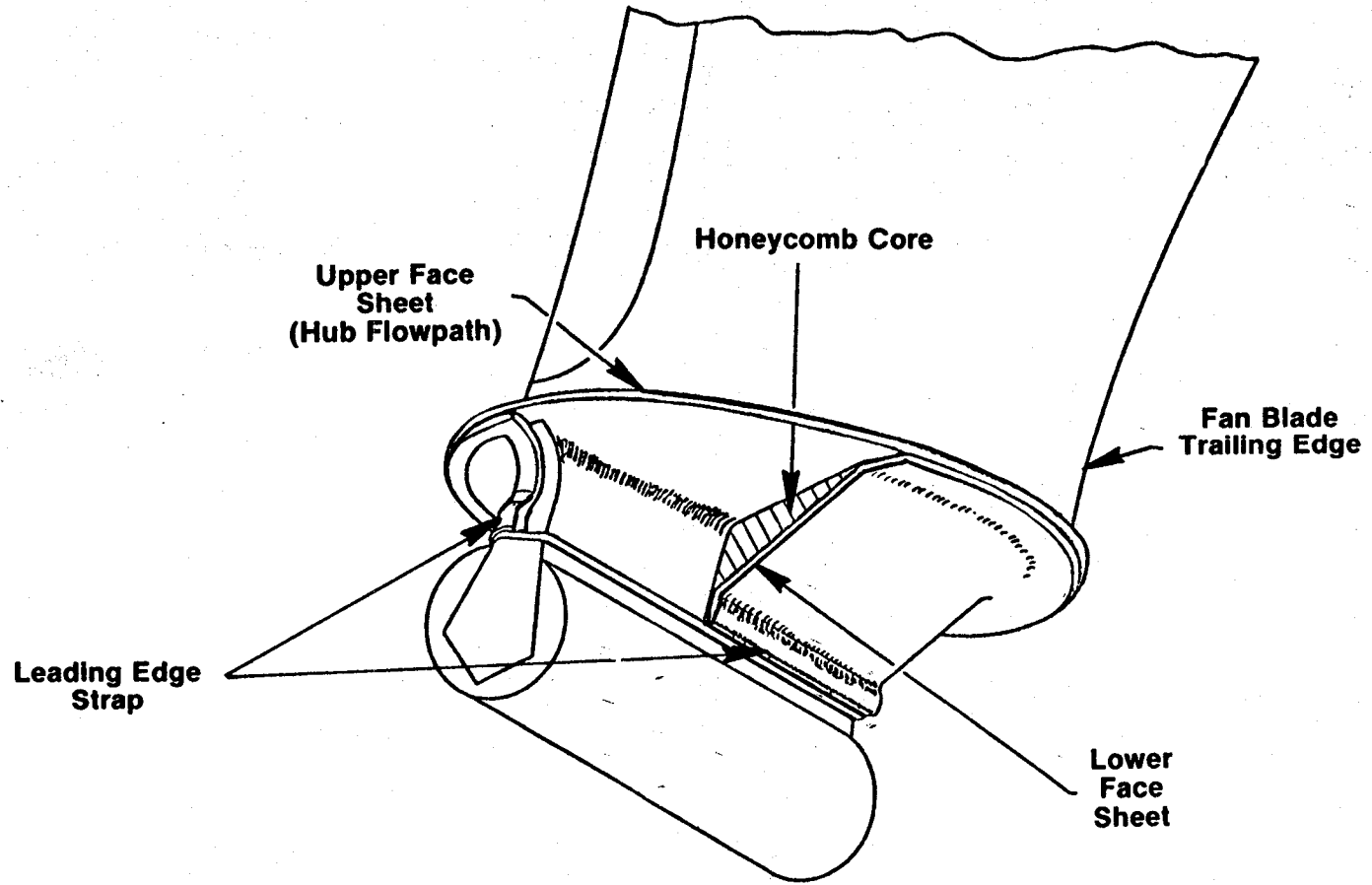
Figure 30. Composite Fan Blade Platform Construction.
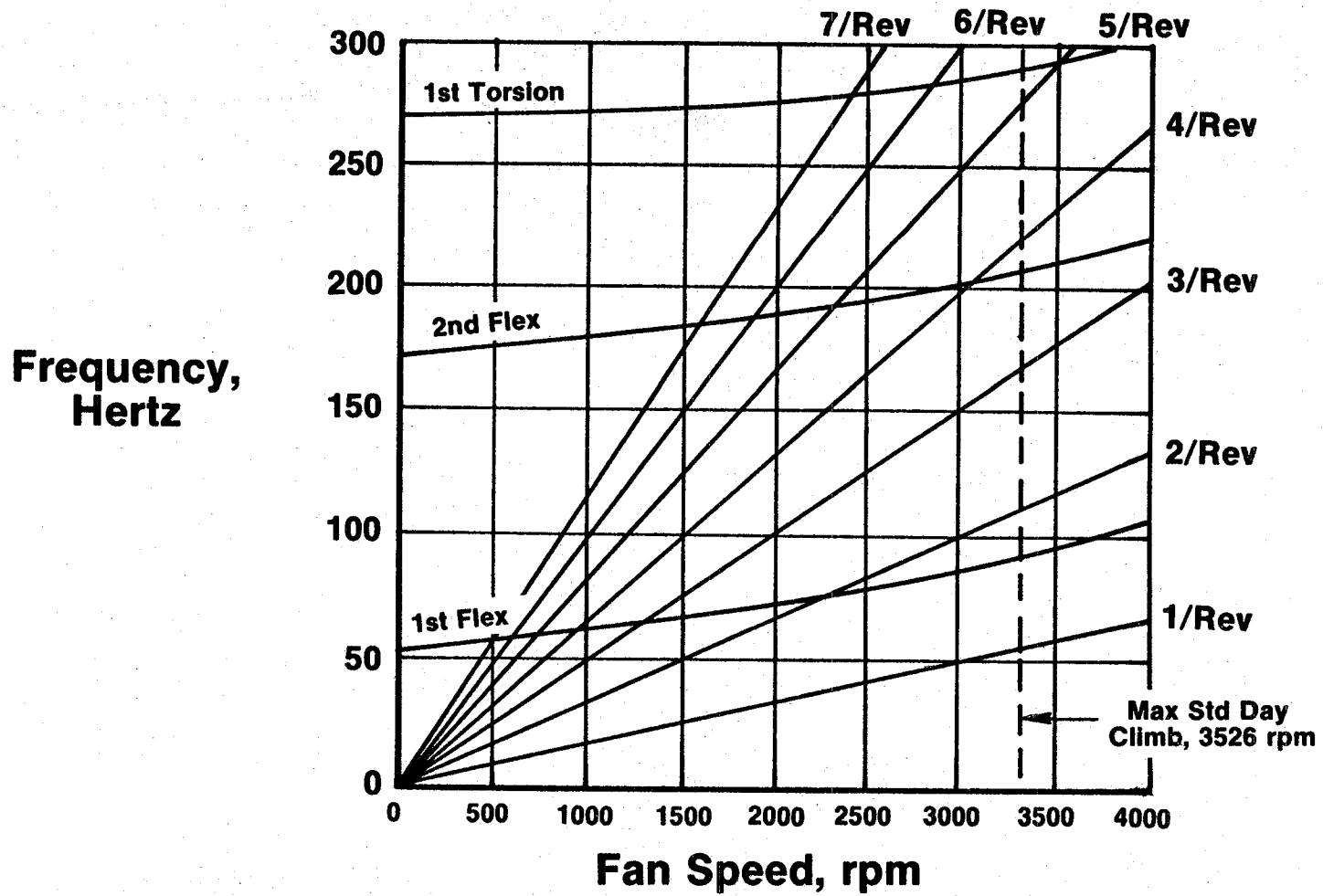
Figure 31. Composite Fan Blade Campbell Diagram.

Steady-State Mean Stress, ksi
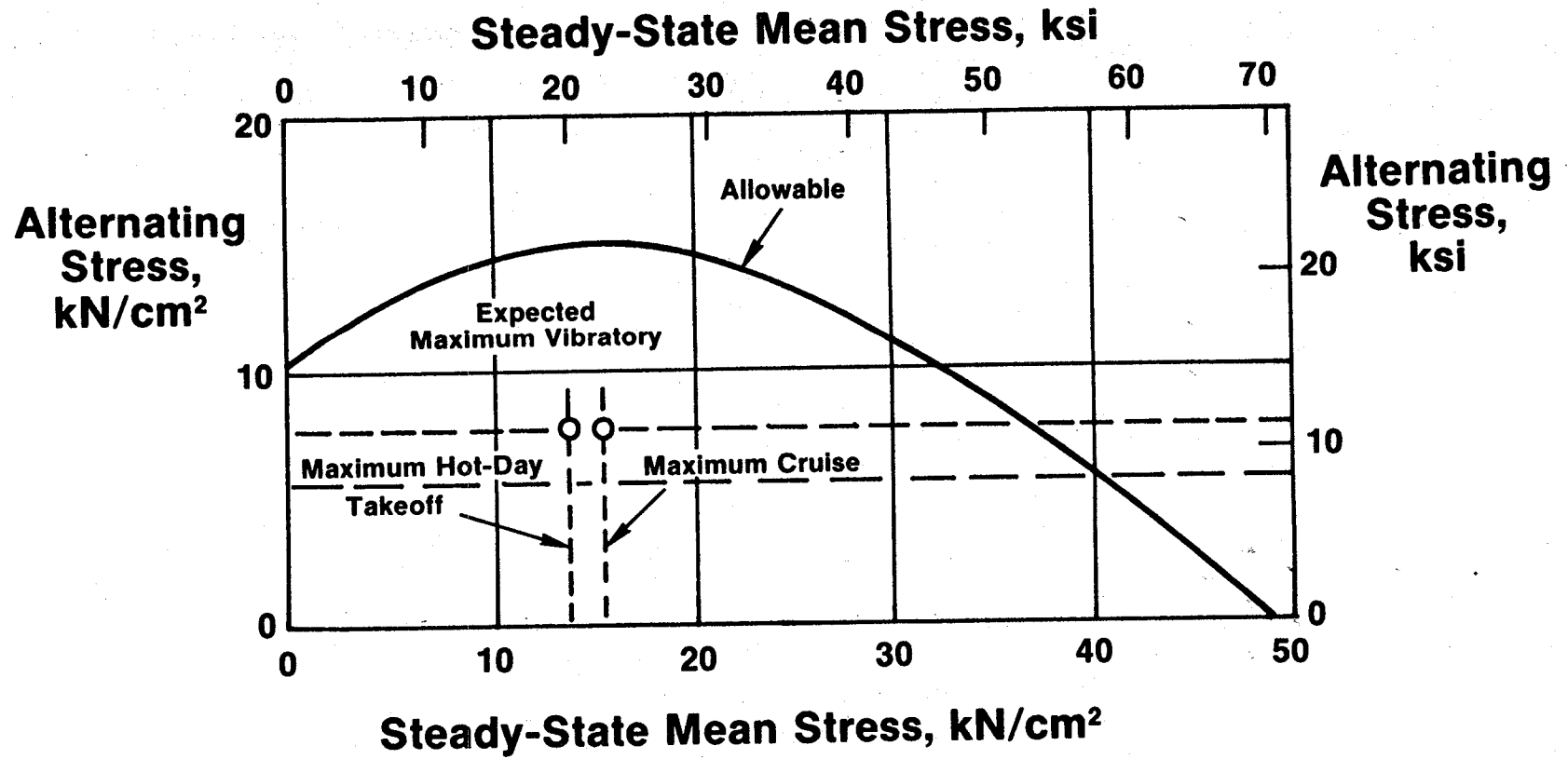
Figure 32. Composite Fan Blade Goodman Diagram.

blade-to-blade variations, electronic errors, etc. Thus scope limits were very conservative. During testing, scope limits were exceeded significantly a number of times; however, no delaminations have been found in the blades.

3.3.3 FOD Resistance

The initial blade-development effort was addressed to foreign object damage (FOD) requirements. The FAA requirements for bird impacts are shown in Table VIII. In addition, the more stringent GE goals are shown. GE's requirements are more demanding in the area of small birds. The rationale for the GE goals is based on experience with titanium blades and economics.

The FOD resistance of the preliminary blade design was evaluated in a whirligig impact facility (Figure 33). In these tests, the blades were rotated, and a simulated RTV rubber bird was injected into the path of the blade. The results of one of the two tests are shown in Figure 34. Blade serial number QP005 was impacted at simulated aircraft takeoff conditions with a 0.907-kg (2.0-lb) bird. The test conditions simulated an impact at the blade 80% span location for an aircraft forward veloctiy of 41.2 m/sec (80 knots). The bird-to-blade relative velocity was 275 m/sec (904 ft/sec), the incidence angle was 33°, and the weight of the bird slice was 0.227 kg (1/2 lb). The blade did not break at the root. Keyhole rotation was noted in the movies. Posttest inspection of the blade showed it had lost 7% of its weight, and approximately 90% of the airfoil was delaminated. Based on this result, it was concluded that the UTW composite fan blade design would not satisfy the FAA FOD requirements. Further, it was decided not to pursue the development of an FOD-resistant design under this program.

3.4 VARIABLE-PITCH-ACTUATION SYSTEMS

Because of the criticality of the actuation system to the operation of a variable-pitch fan, many concepts were evaluated. Two were selected for detail design and development. These were a cam/harmonic system, designed and produced by Hamilton Standard under subcontract, and a ball spline system designed and produced by General Electric. Both systems were engine-tested in the UTW propulsion system.

3.4.1 Cam/Harmonic Variable-Pitch System

Design Requirements - The design criteria for the actuation system were established consistent with the demands of commercial service. The mission cycles, major component life, and bearing life values used for the design, Table IX, reflect this philosophy. No compromises in design criteria or weight were made for the fact that the system was to be used in a short-test-life, experimental engine. The only deviation from this approach was in selection of readily available items such as hydraulic motors and servovalves.

Table VIII. UTW Composite Fan Blade Bird-Impact Design Requirements.

Bird Size kg (lbs)	Max No. Birds Ingested	FAA Requirement	GE Goals
.085 (.188)	16	Maintain 75% Engine Thrust	No Blade Damage
.68 (1.5)	8	Maintain 75% Engine Thrust	Maintain 75% Engine Thrust
1.8 (4)	1	Safe Shutdown	Safe Shutdown

Table IX. Design Requirements for Variable-Pitch-Actuation System.

- **48,000 Missions**
  36,000 Hours Major Components
  9,000 Hours Bearings and Expendables

- **Actuation Rate 135°/sec**

- **Feedback Accuracy ±¼°**

- **Net Blade Twisting Moment — Function of Blade Angle**
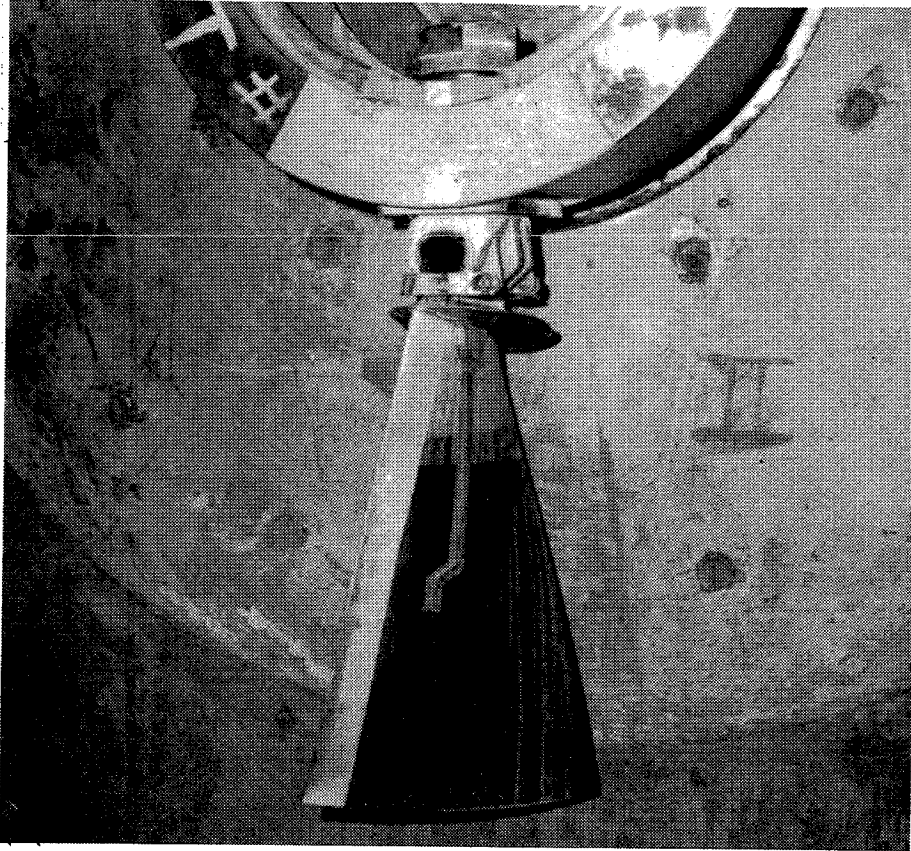
Figure 33. Composite Fan Blade Whirligig
Impact-Test Facility.
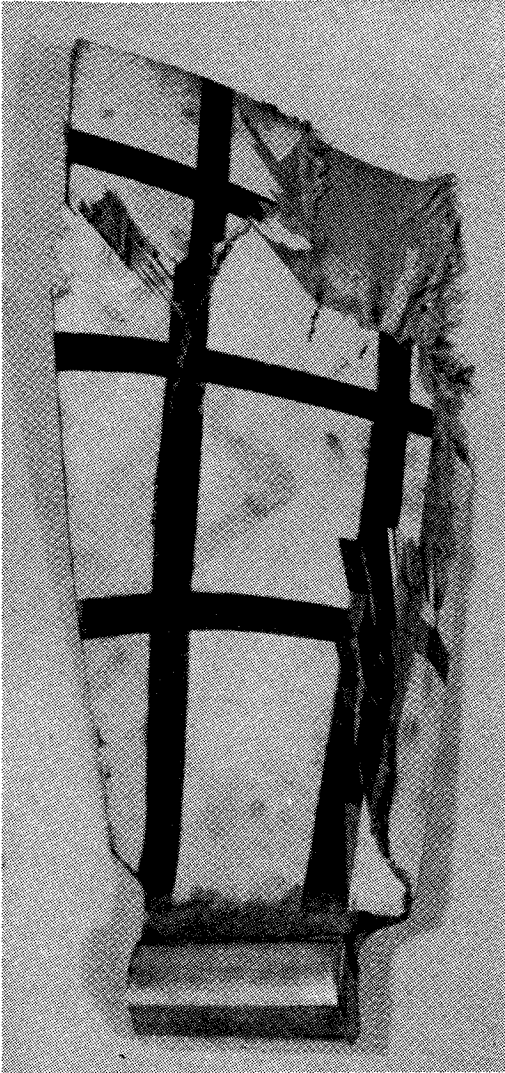
Test Conditions

- **Aircraft Takeoff**
- **1.5 Pound Bird**

Results

- **7% Weight Loss**
- **90% Delamination**
- **No Root Failure**

Figure 34. Bird-Impact-Test Results.

The high rate of pitch-change capability designed into the system (Table IX), reflects the need, dictated by STOL aircraft operation, to change very rapidly to reverse thrust; in addition, it facilitates rapid thrust response for go-around operation. The feedback accuracy stipulated in Table IX is important to obtain control-system accuracy. The actuation system is required to overcome the twisting (moment) loads inherently present in a variable-pitch system; these loads vary as a function of blade angle as shown in Figure 35. The centrifugal moment curve is sinusoidal, and it is a function of the mass distribution of the blade about the pitch-change axis and the centrifugal field. The aerodynamic-twisting moment is the torque generated by the center of pressure about the pitch-change axis. The sum of these two torques is the net value. The frictional moment of the blade-retention bearing due to centrifugal pull is assumed to be a constant, maximum value. The 0° setting is the static, takeoff setting.

The large range of blade-angle travel was initially established so that reversing of the fan could be accomplished through stall, that is the open-pitch direction, as well as in the closed-pitch direction. Scale-model fan testing conducted while the design was in process showed that much higher levels of reverse thrust could be achieved by the through-stall approach. As a result, the closed-pitch method was never implemented in the hardware phase.

Alternate Concepts Studied - Prior to initiation of the design effort, an in-depth study was conducted to select an optimum concept. Ten designs of various mechanical and hydraulic arrangements were studied, and a comparative assessment was made using weight plus six other criteria such as reliability and development risk. The matrix was reduced to six choices for more in-depth evaluation, and the matrix of criteria was increased to ten factors. The selected cam/harmonic system scored heavily in the areas of weight, reliability, simplicity, and accessibility of controls.

Description of Selected System - The key elements of the mechanism are depicted on the block diagram and schematic shown in Figures 36 and 37. The input from the digital control system is a blade-angle position command to the electrohydraulic servovalve; the servovalve meters flow from a remote hydraulic source to power a hydraulic motor, the output of which drives a high-speed, flexible shaft.

The output position of the hydraulic motor provides a feedback signal from a Linear-Variable Differential Transformer (LVDT) to the digital control. Although the remainder of the system is open loop, it does provide a high degree of positioning accuracy. A differential gear transfers the torque of the flex shaft from the stationary reference to the rotating fan. This torque is then increased, with a large corresponding speed decrease, by the harmonic drive. The output of the harmonic drive is transmitted to the blade through the cam, which rotates the trunnion arm. The combination of the trunnion arm and the contour of the cam track provides the desired output torque-versus-blade-angle characteristic. The no-back is a simple locking device that fixes blade angle in the absence of any input motion on the flex shaft. The key
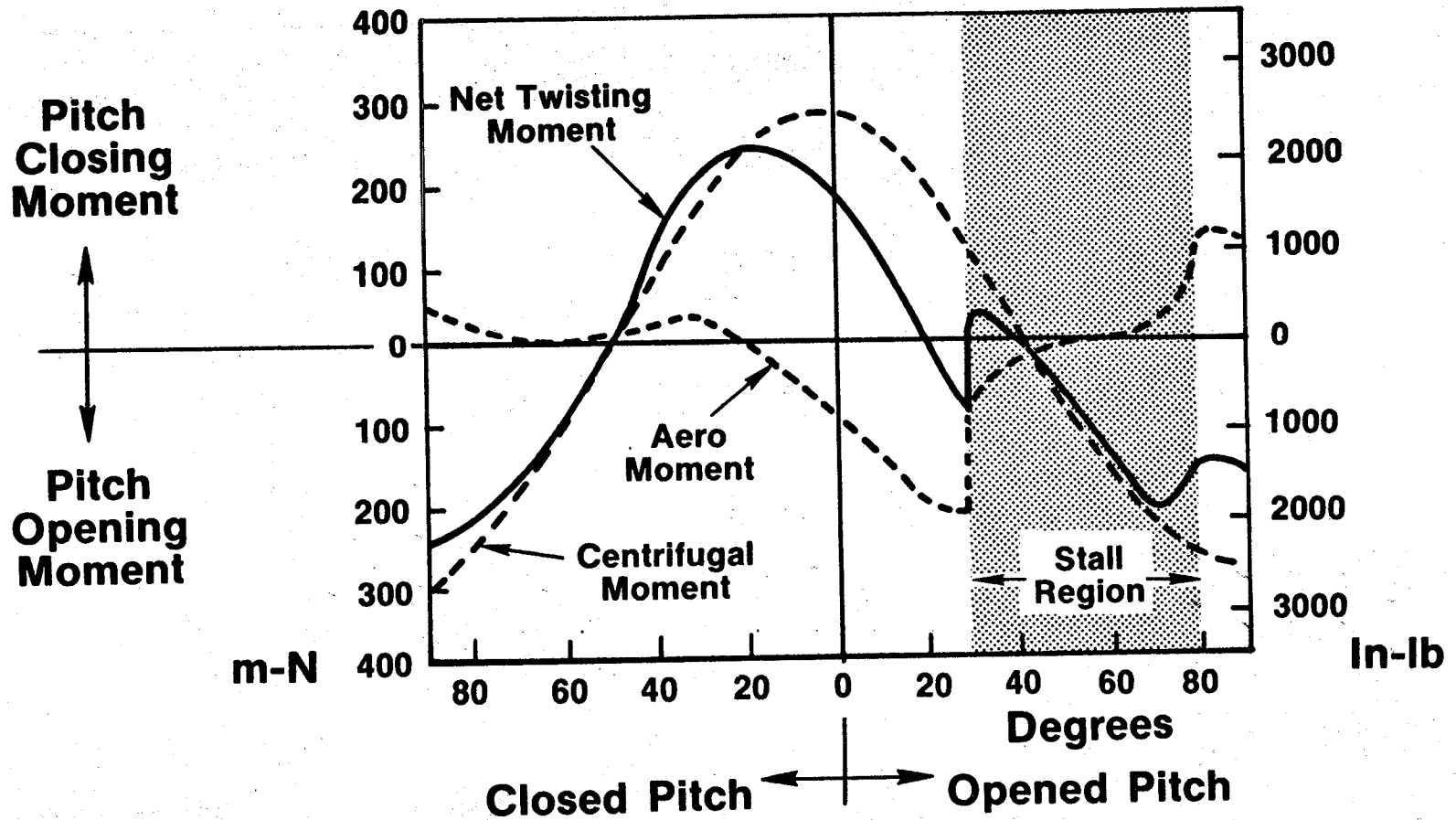
Figure 35. UTW Fan Blade Twisting (Moment) Loads.
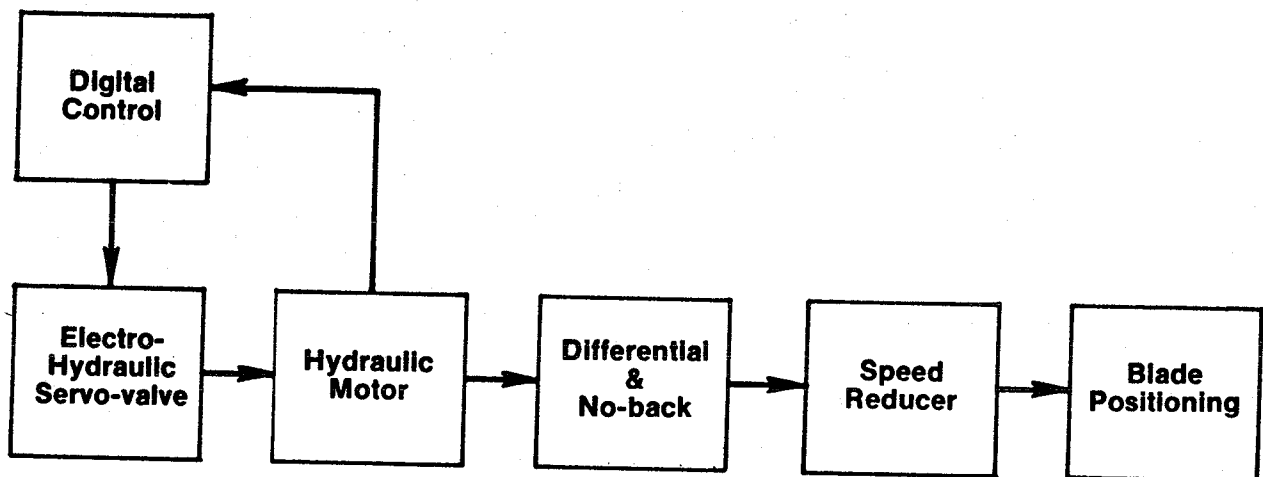
Figure 36. Block Diagram of Pitch-Change Mechanism.

Position
Feedback

Control
Input

Trunnion Arm
and Roller

Servo
Valve

Beta Regulator

No-Back

Harmonic Drive

Flexible
Shaft

Differential
Gearing

Spherical
Cam
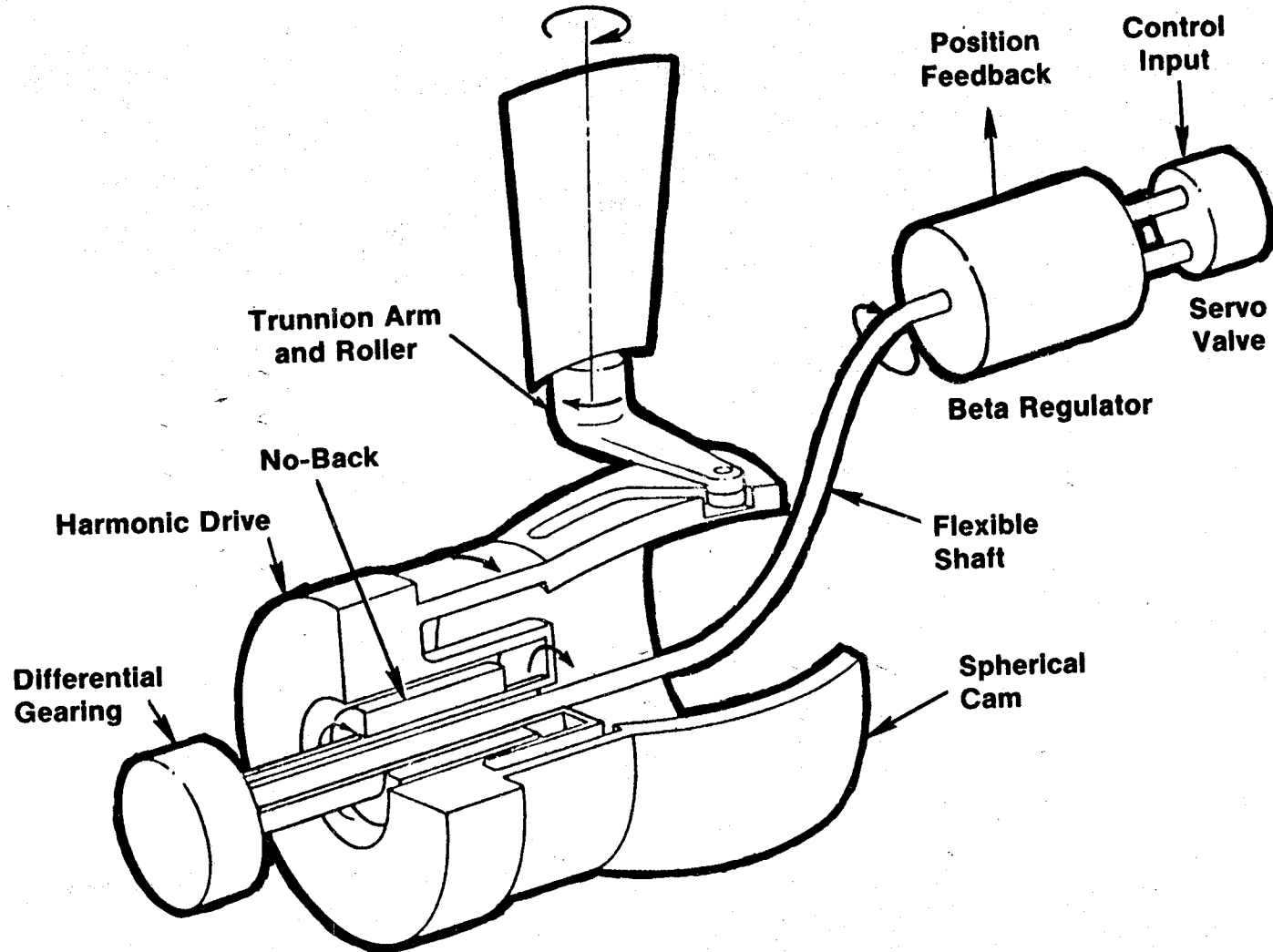
Figure 37. Schematic of Pitch-Change Mechanism.

design features of the system are more apparent in Figure 38. The beta regulator comprises a servovalve, hydraulic motor, and feedback signal. It is packaged as a unit and mounted remotely from the fan for ease of replacement since the control portion of actuation systems have historically been the major contributor to unscheduled removals. In addition, the remote mounting is a less hostile environment compared to a location inside the fan close to the gearbox.

The overall gear ratio between the hydraulic motor and the fan blade is 1000:1. Of this, 200:1 is provided by the harmonic drive. This high reduction is provided in a very small envelope and for a minimum weight. The no-back is a coil-spring device that, as noted earlier, locks the system when there is no input motion from the beta regulator. The system is self-energizing; a very low magnitude of back-drive torque will lock it. Similarly, it is released by extremely low levels of input drive torque.

The QCSEE fan has a large disk, and it operates at higher rpm than previous variable-pitch systems. This would result in a significant weight penalty of oil required to fill the disk; in addition, there is increased risk of leakage due to the high centrifugal-induced oil pressure. As a result of these considerations, dry lubrication was used for the cam track and roller. The blade retention used grease-packed bearings. As a consequence, the interior of the rotor is accessible for visual inspection.

Such features as the low-torque, high-speed drive between the beta regulator and the harmonic drive, elimination of oil in the disk, and the lightweight no-back made this concept the lightest of the 10 systems that were evaluated.

Lubrication for the flex shaft, no-back, differential gear, and harmonic drive is provided by a low oil flow from the beta regulator through the flexible-drive housing. This flow is centrifuged into these components and returns to the gearbox scavenge area. A benefit of this configuration is the elimination of high-pressure hydraulic transfer across the compressor inlet or through the gearbox, thereby improving safety and reliability.

Another maintenance feature is the ability to replace the flexible shaft from the beta regulator end without disturbing the fan assembly.

The harmonic drive is one of the key elements in achieving a lightweight design. The operating principle is illustrated by Figure 39. Rotation of the input-wave generator, which has three lobes, causes a distortion of the thin flex-spline member. The passage of two lobes past a given point on the output lobe causes the output circular spline to advance one tooth. Since there are three lobes, the output motion per revolution of the wave generator is three teeth, as indicated; combined with the number of teeth used, 600, this provides a 200:1 ratio. Because the teeth are quite small, a key design parameter is ratcheting capacity - that is, the ability to resist "skipping" or "slipping." The harmonic drive was tested as a component, under the combination of load-induced deflection and thermal effects, prior to initiation of

Cam Follower
Arm

Fan Blade
Trunnion

Harmonic
Drive

Differential
Gear Train

No-Back

Stop

Flexible Drive
Shaft & Lube Supply

Beta
Regulator
Module

Servo Valve (E.H.V.)
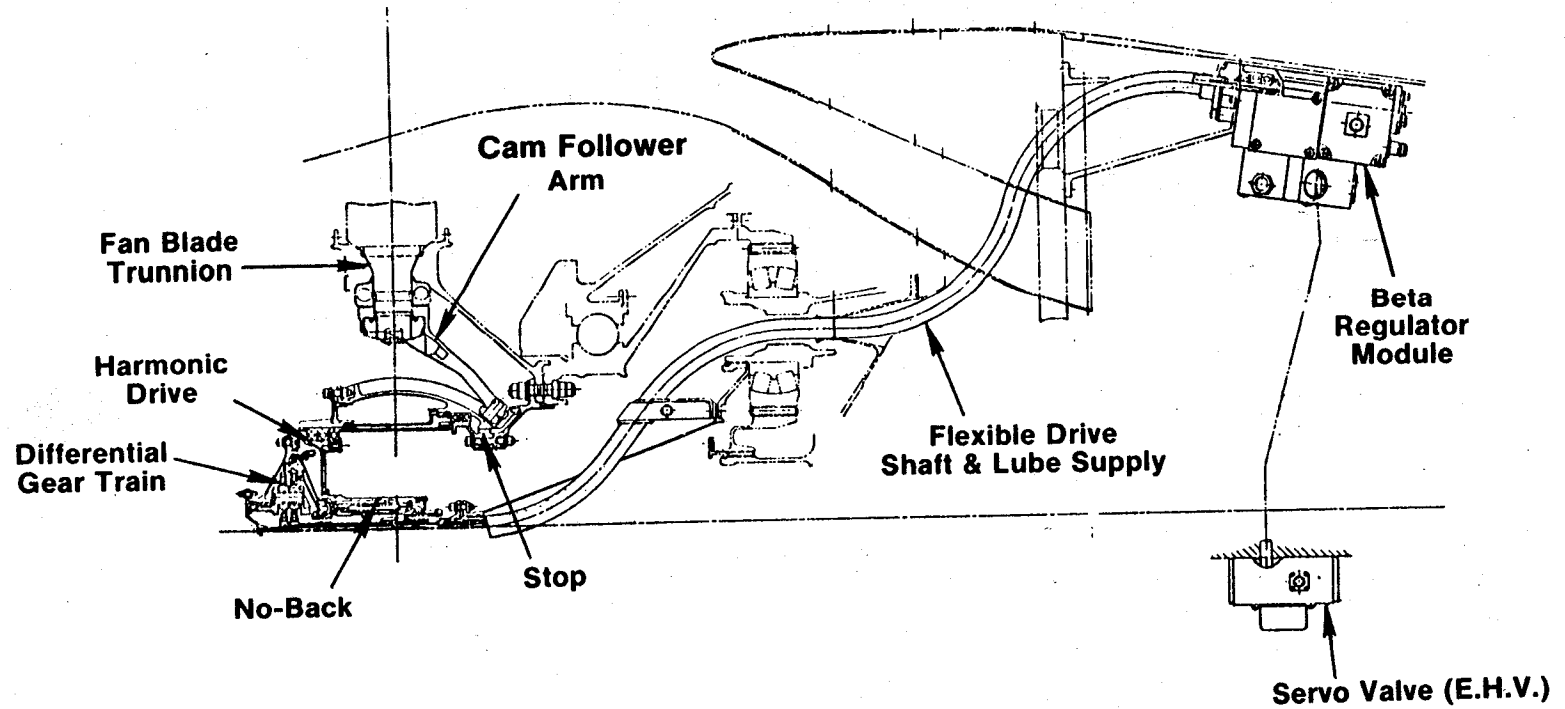
Figure 38. Cam/Harmonic Variable-Pitch Actuator System.

**Output Motion
Per Input Revolution
(200:1 Speed Ratio)**

**Flex Spline
(600 Teeth)**

**Input
Wave Generator
(3 Lobed)**

**Output
Circular Spline
(603 Teeth)**
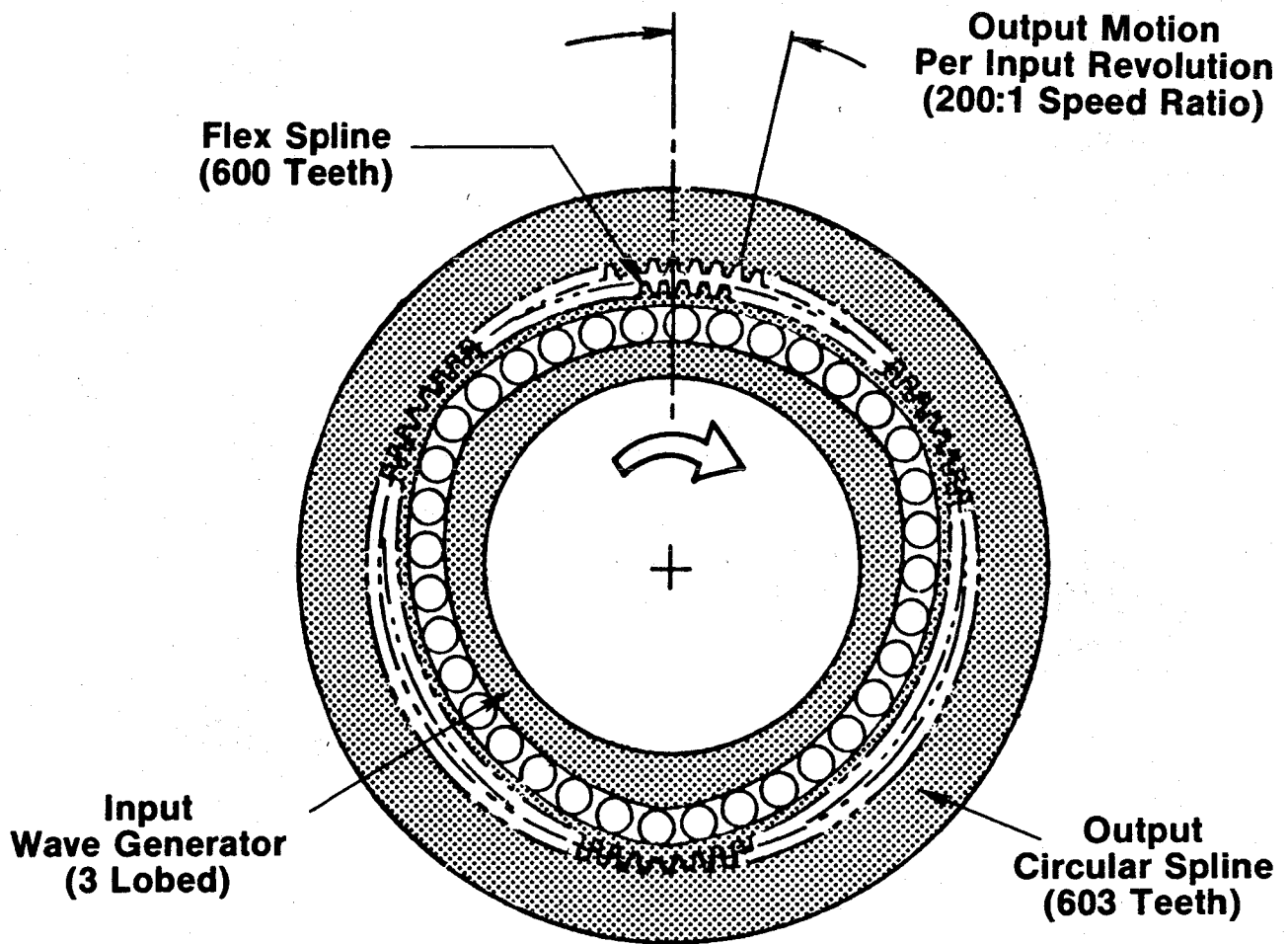
Figure 39. Harmonic Drive.

the whirl-rig test. This device has been used in such applications as the duct-tilting mechanisms on the Bell X-22 VTOL aircraft and on the wheel-drive system for the lunar rover.

The harmonic-drive components are shown in Figure 40; the wave generator and circular spline are designed for high radial stiffness to minimize radial deflection under load. The flex spline is, of course, designed to continually deform during its operating lifetime.

The cam, shown in Figure 41, provides contoured tracks for the 18 cam-follower arms and bearings. The cam contour, coupled with the variation in the effective moment arm, provides the variable torque ratio required to match the load-versus-blade-angle requirements shown earlier. This hollow structure is made of hardened steel; diameter is dictated by the envelope required to lo-locate the grooves on a spherical surface as well as by the structural require-ments of the groove walls.

Whirl-Rig Test - A 60-hour, whirl-rig test using an electric motor drive was performed on the system prior to engine test. A disk and 18 counterweights were used for this purpose. The counterweight provided twisting (moment) loads by virtue of mass distribution when operating in a centrifugal field. The whirl-rig test was conducted using the entire actuation system including the beta regulator assembly. The objectives of the program were designed to prove acceptable performance and durability characteristics prior to engine test by demonstrating actuation rates and position accuracy and by (limited) endurance operation.

Figure 42 is a photograph of the test rig. The rotor assembly is shown in the background; the 18 blade counterweights and cam arms are also visible. The housing in the foreground was used to mount the flexible drive shaft and the beta regulator. The drive shaft was configured exactly as it would be in the engine even though the fan in this test was being driven from the front; this method was used for ease of testing.

The test program consisted of functional, structural, and endurance test-ing. Test results produced an average pitch-change rate of 116°/sec with a maximum rate of 135°/sec. Although this was less than the 135°/sec average value specified, it was judged to be a satisfactory level of performance. Perhaps more important was the demonstration of blade travel from positive thrust to full reverse thrust through stall of approximately one second. The required blade-positioning accuracy of ±1/4° was attained, and (although not a requirement) a hysterisis of 1-1/2° was demonstrated - as was the ability to provide a minimum step change of 1/2° in blade angle.

The most important result of the test was demonstration of compliance with the load capability of the system as measured against the levels, speci-fied by GE, which were presented earlier. The no-back was demonstrated to hold the fan blade in a locked position under the maximum load or overspeed condi-tion. A total of 550 simulated mission cycles were accomplished; each cycle consisted of 16 blade-angle/rpm combinations including one reverse cycle.

Wave
Generator

Flex Spline

Circular
Spline
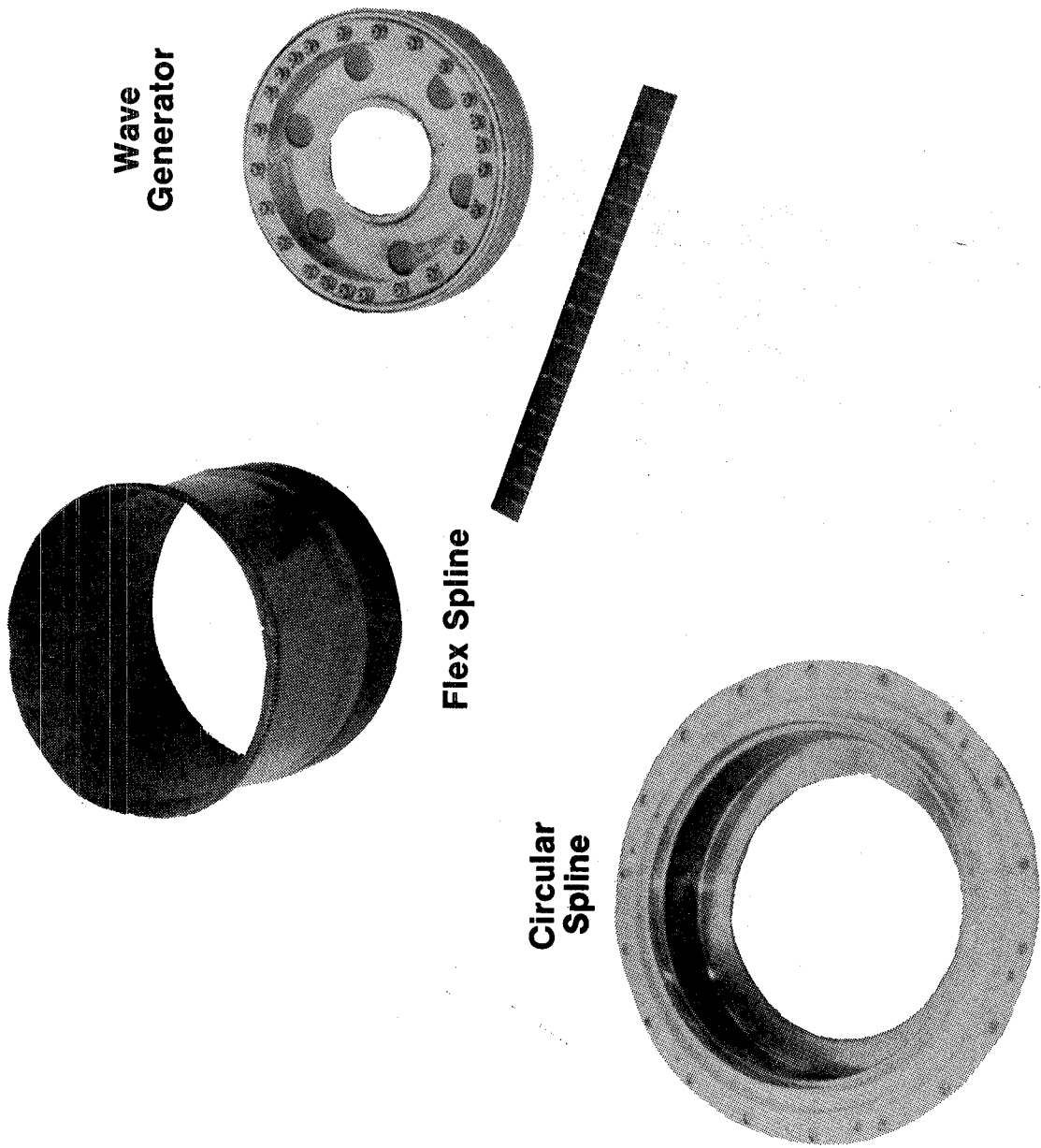
Figure 40. Harmonic-Drive Components.
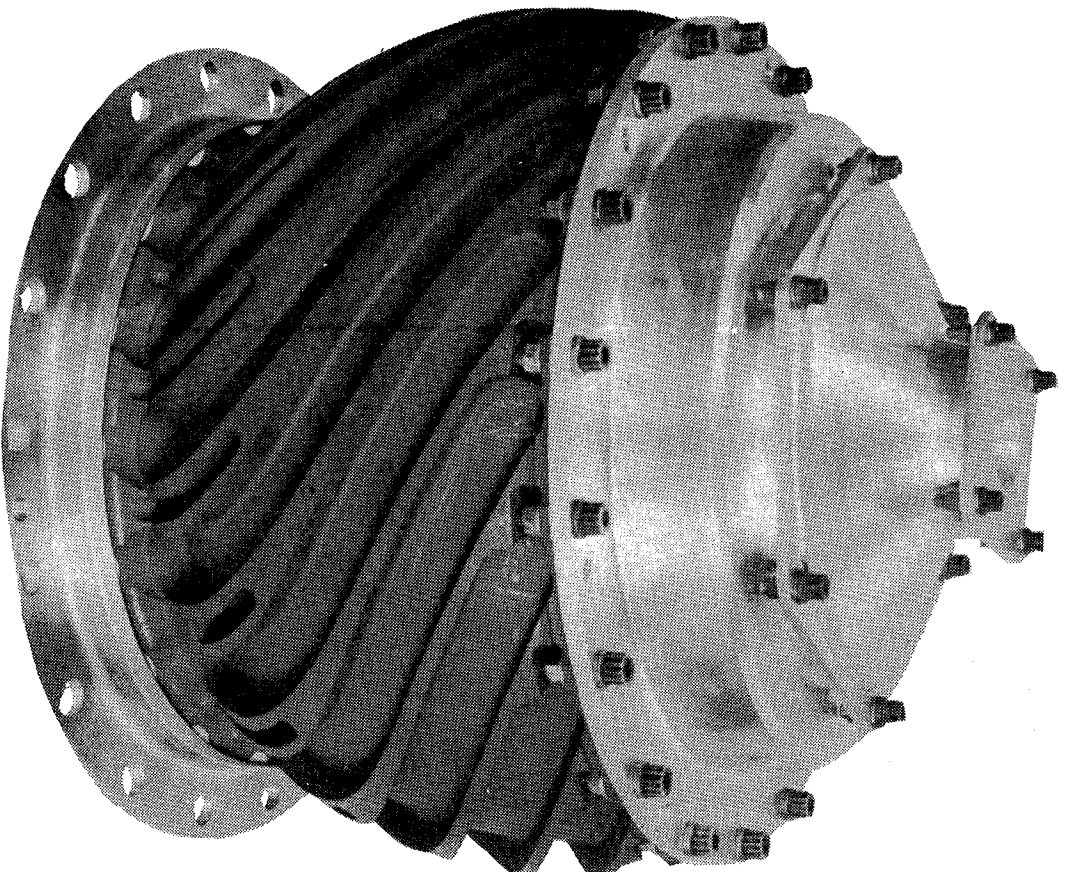
Figure 41. Harmonic-Drive Cam.
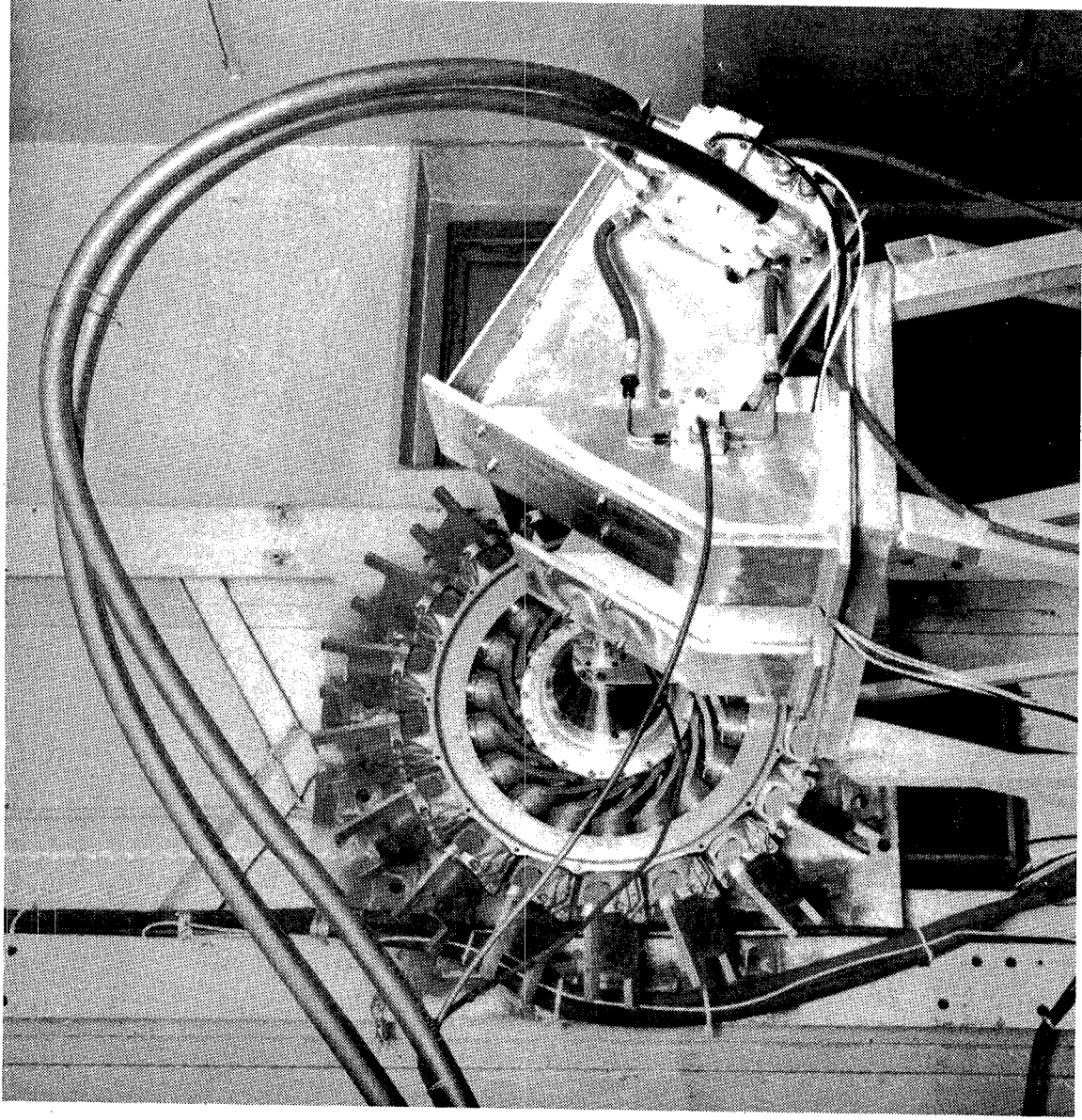
Figure 42. Actuator in Whirl Rig.

The results of the test were, in an overall sense, positive. Very little "fix" and retest was required. Moreover, the system was judged to have satisfied specification requirements; therefore, it was subsequently assembled into the under-the-wing QCSEE.

3.4.2 Ball Spline System

Design Requirements - The ball spline pitch-actuation system was designed to meet the same requirements specified for the cam/harmonic system (Table IX).

System Selection - Using technology demonstrated on previous variable- and reverse-pitch fan rigs, a second-generation ball spline actuator was studied. Several alternate concepts were also evaluated, including worm gearing, "mini" gearboxes, individual screwjacks, and a single planetary gear-box - all designed to the same conditions as the ball spline. The ball spline with two output ring gears was selected because it was the least complex and was extremely rugged. Its reduced parts count promised a lightweight, highly reliable design.

Description of System - The actuator system, as shown in Figure 43, is made up of a ball screw, ball spline, and two ring gears. The ring gears collect and synchronize the individual pinions that are attached to each of the 18 blade trunnions. As the input drive shaft is rotated, the two ring gears move in opposite directions. This imparts two equal reactions to each pinion, thus minimizing gear loads and providing a redundant load path.

The pitch-change mechanism is shown schematically in Figure 44 and as a block diagram in Figure 36. It is made up of blade positioning, speed reducer, differential, and no-back; it is driven by a piston-type hydraulic motor that is controlled by the servovalve. The servovalve is operated by the digital control while the control, in turn, receives position intelligence from the feedback. Motor output drives through the differential gearing and no-back. The no-back accommodates input movement in either direction of rotation but prevents fan blade torque from back-driving the system. A stage of reduction gearing is required to match the output of the motor with the blade-position-ing mechanism. Figure 45 shows the details of the system including: hydrau-lic motor, feedback, gearing, no-back, thrust bearings, ball screw, ball spline, torsion stops, ring gears, and pinions.

In order to actuate the fan blades, large axial forces must be generated in the load path formed by the ball screw, thrust bearings, and inner member of the ball spline. The key to minimizing actuator weight is keeping this closed-loop load path short and on a small radius.

Key design features include the motor and feedback location near the actu-ator for crisp blade movement and accurate positioning. Redundant ring gears reduce steady-state loads and improve reliability. The ball spline and ball screw are rugged, proven designs. The differential gearing and no-back are packaged together in order to simplify actuator assembly.
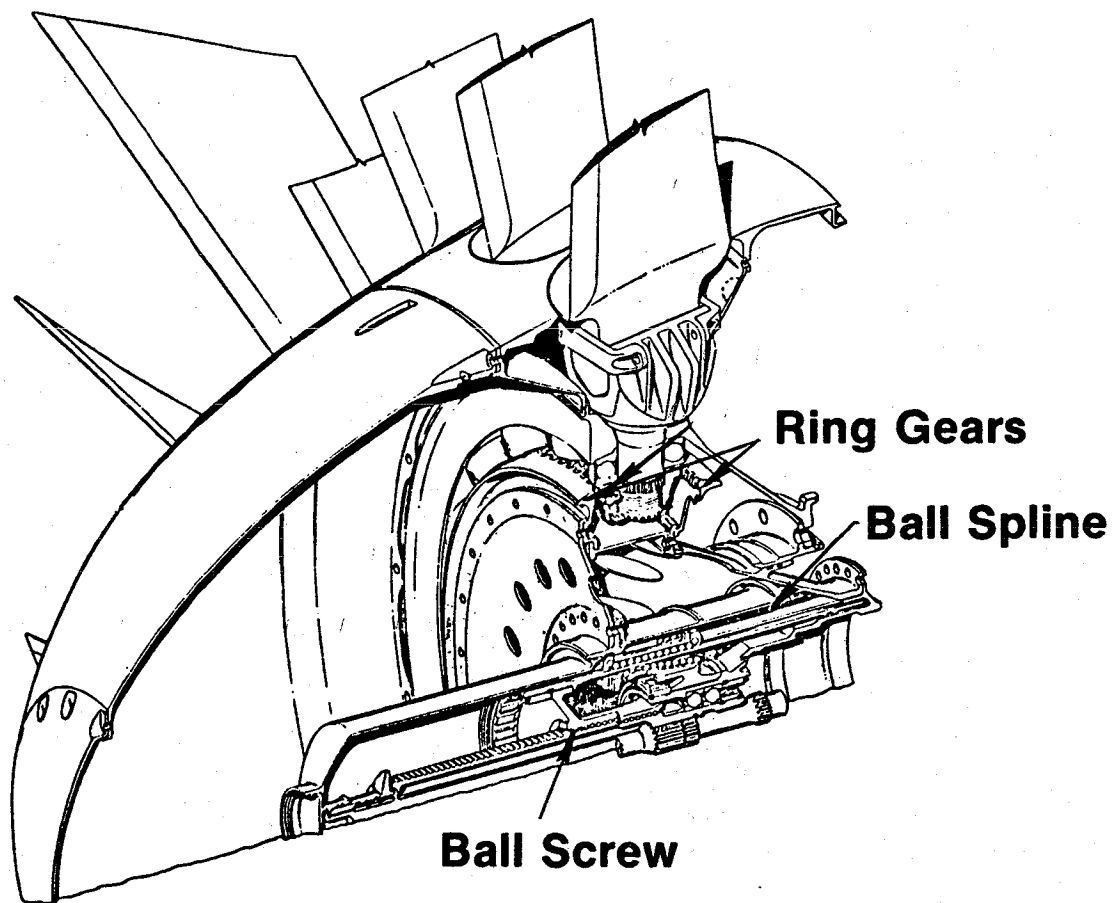
Figure 43. GE Ball Spline Actuator System.

Digital Control

Servo Valve

Position Feedback

Blade Positioning Mechanism

Speed Reducer Differential No-back
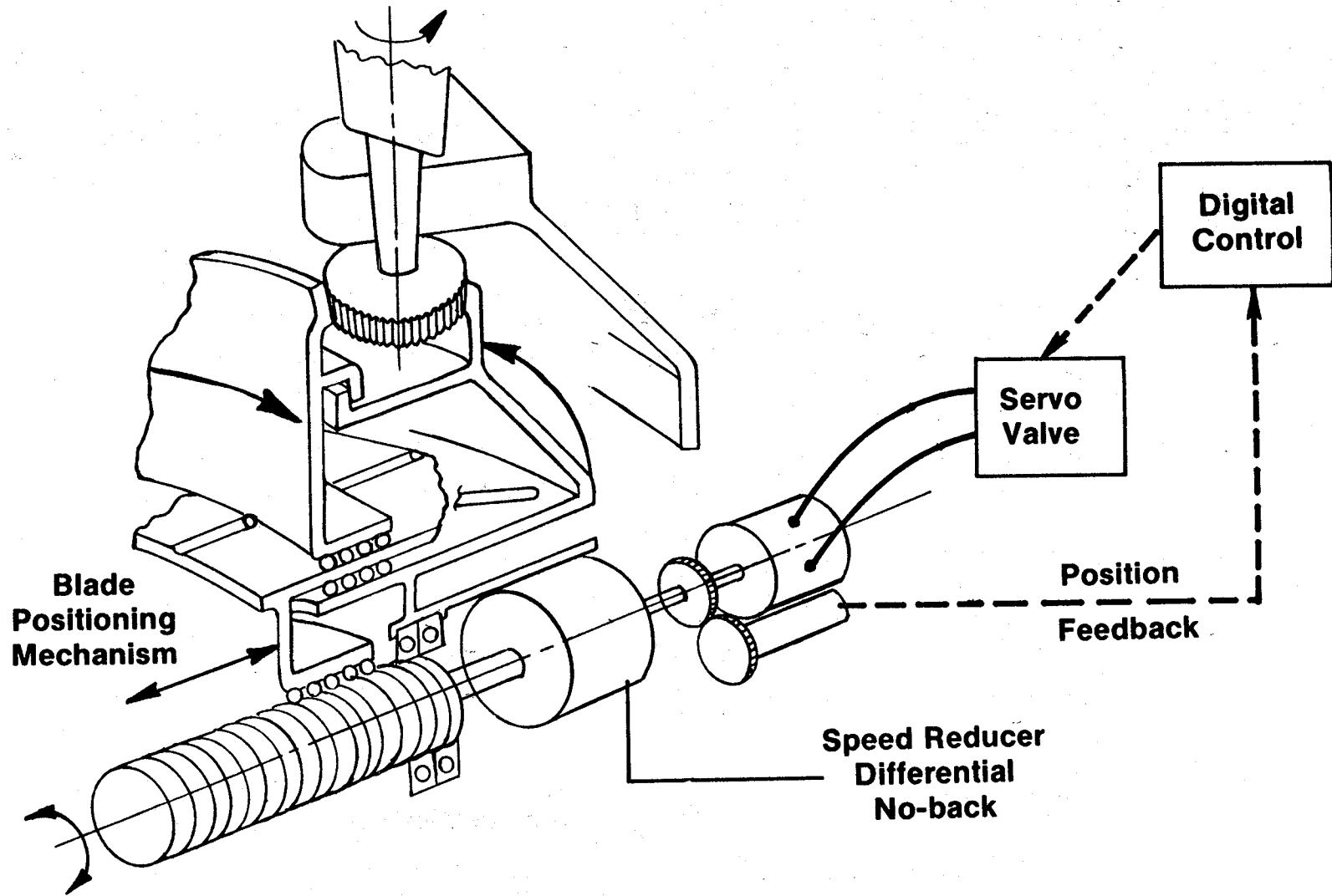
Figure 44. Pitch-Change Mechanism.
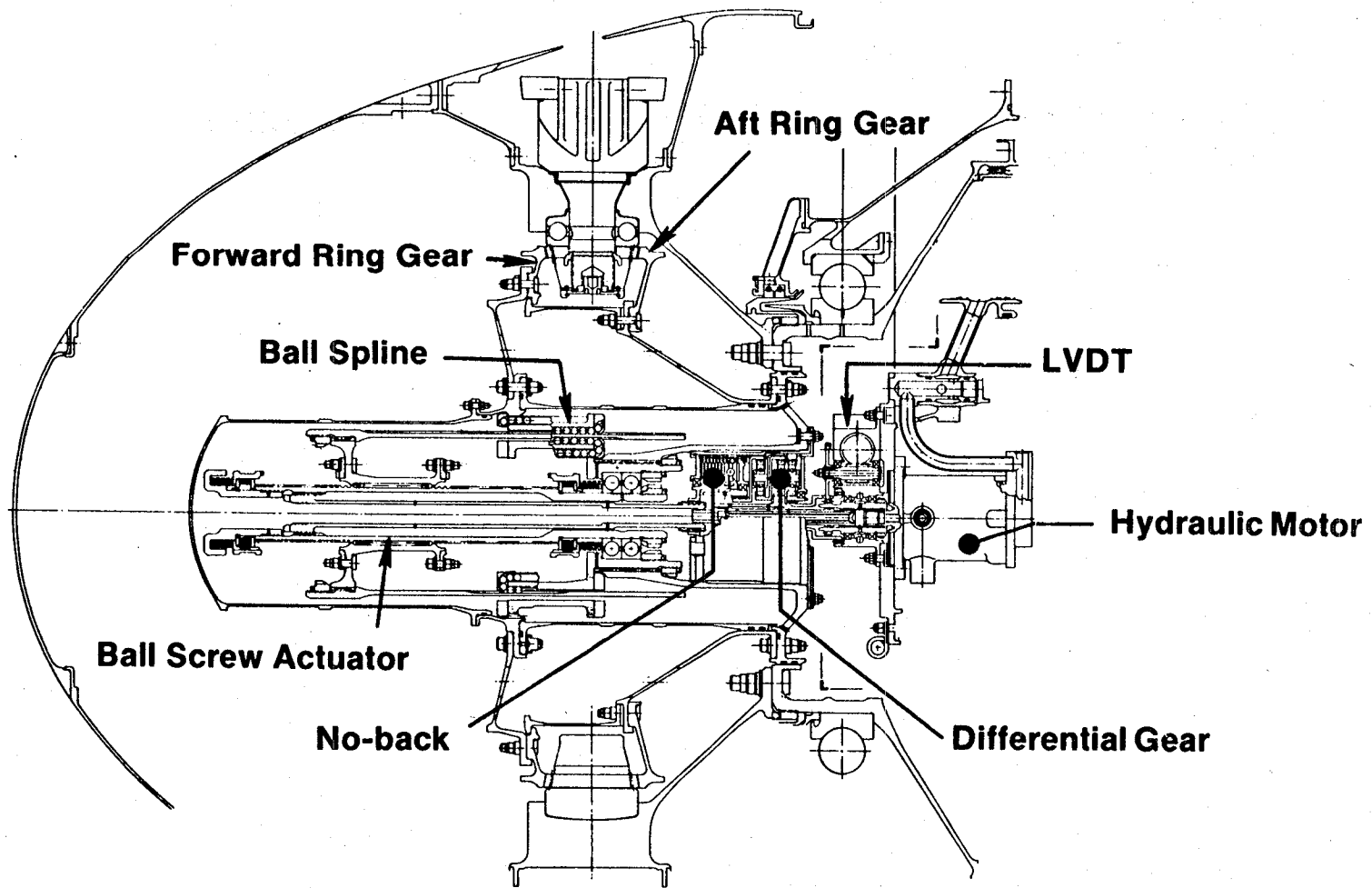
Figure 45. Ball Spline Actuation System.

The ball spline and ball screw shown in Figure 46 are the heart of the actuator assembly. Recirculating tracks of balls are lubricated by engine oil and transmit the required forces smoothly and efficiently. Ball tracks are hardened steel to assure long life. The drive package provides the input force and position intelligence for the actuation system. Two motion-feedback transducers are mechanically coupled to the motor output shaft by gears and a spring-loaded thread arrangement.

Rig Testing - An actuator whirl-rig test was run at General Electric using the breadboard digital control. Test objectives were:

- Proof test prior to engine running

- Demonstrate actuation rates and propulsion accuracy

- Demonstrate endurance during limited testing

- Investigate compatibility with digital control

Figure 47 shows the GE system mounted in the whirl rig. This view is aft looking forward with respect to the engine. The drive package and the simulated fan blades are clearly visible.

Testing of the GE system was completed in less than two weeks. Demonstrated average actuation rate was 125°/sec. The system was compatible with the breadboard digital control, and blade positioning accuracy was demonstrated within 1/4° in the forward-thrust mode. A system hysteresis of 3° was uncovered when actuated back and forth at zero speed, but it did not compromise testing, and no effort was made to reduce the value. Clearances that exceed design predictions in the actuator assembly appear to be responsible for this observed hysteresis.

No-back holding above maximum fan speed was demonstrated, and 50 mission cycles were run.

3.5 MAIN REDUCTION GEAR

The NASA/GE QCSEE concept is based on a lightweight, high-speed, power turbine driving a slower speed, quiet fan. This objective required a compatible, compact, lightweight, high-power-capability, main reduction gear. Two reduction gears designed, manufactured, and rig-tested by Curtiss-Wright under subcontract to General Electric have given trouble-free performance throughout the engine-demonstration program.

3.5.1 Design Requirements

The UTW QCSEE main reduction gear is shown in Figure 48. One point of interest is the maximum diameter of the gear, only 63.5 cm (25 in.). This is

70

Ball Spline

33 cm
(13 in.)

Ball Screw

36.3 cm
(14.3 in.)

48.3 cm
(19 in.)
Dia.

25.4cm
(10 in.)
Dia.

Assembly

Drive Package
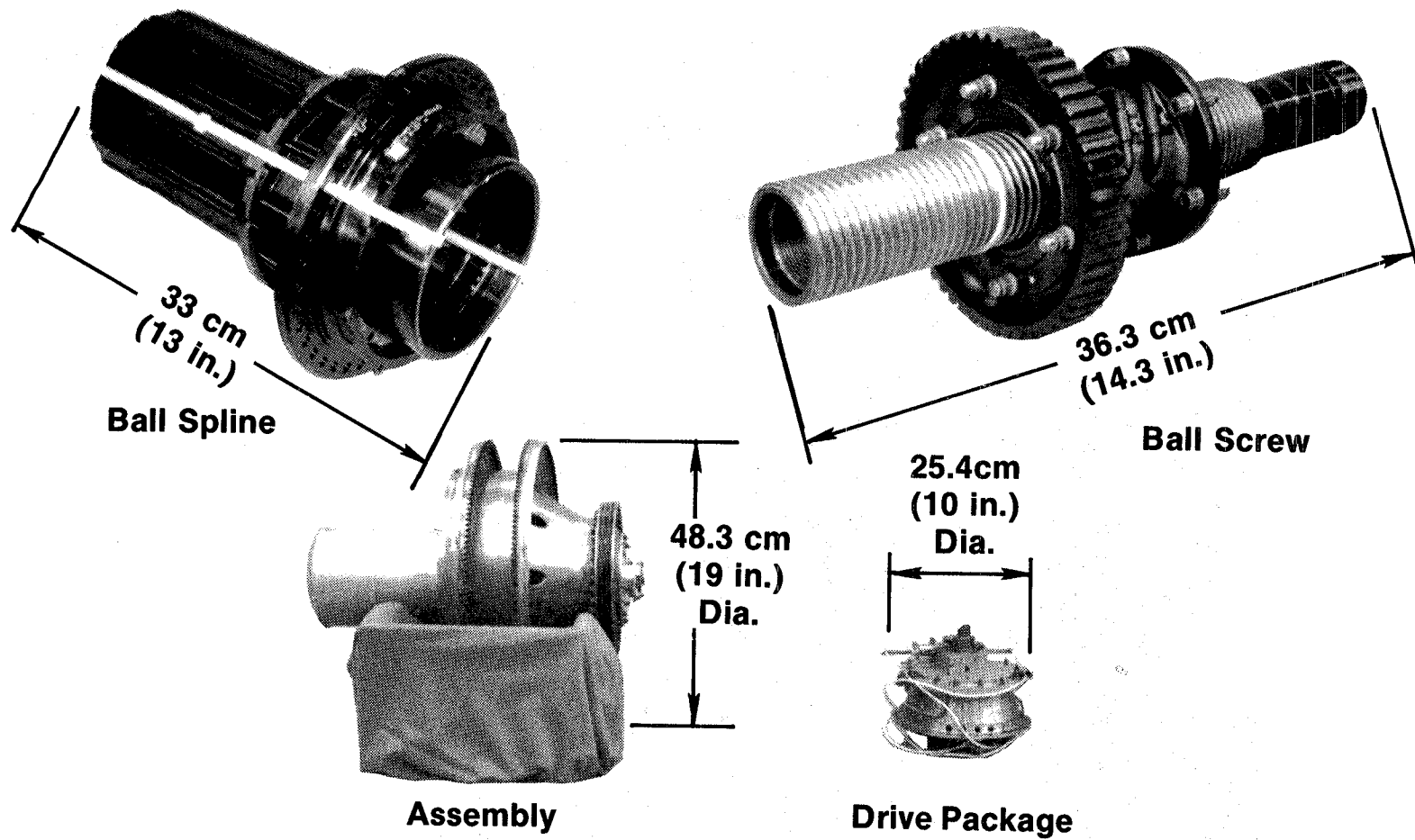
Figure 46. Pitch-Actuator Components.

72
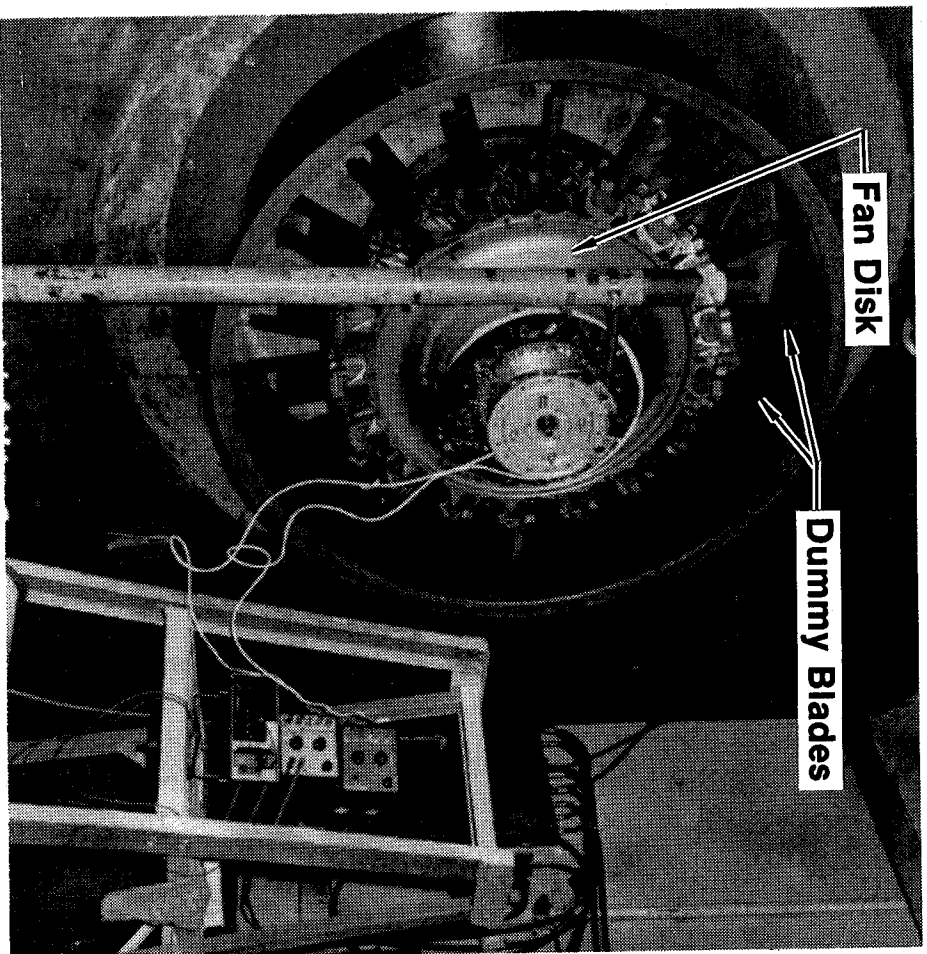
Figure 47. Whirl-Rig Test Setup.

63.5 cm
(25 in.) Dia

Star Gear

Star Carrier

Ring Gear
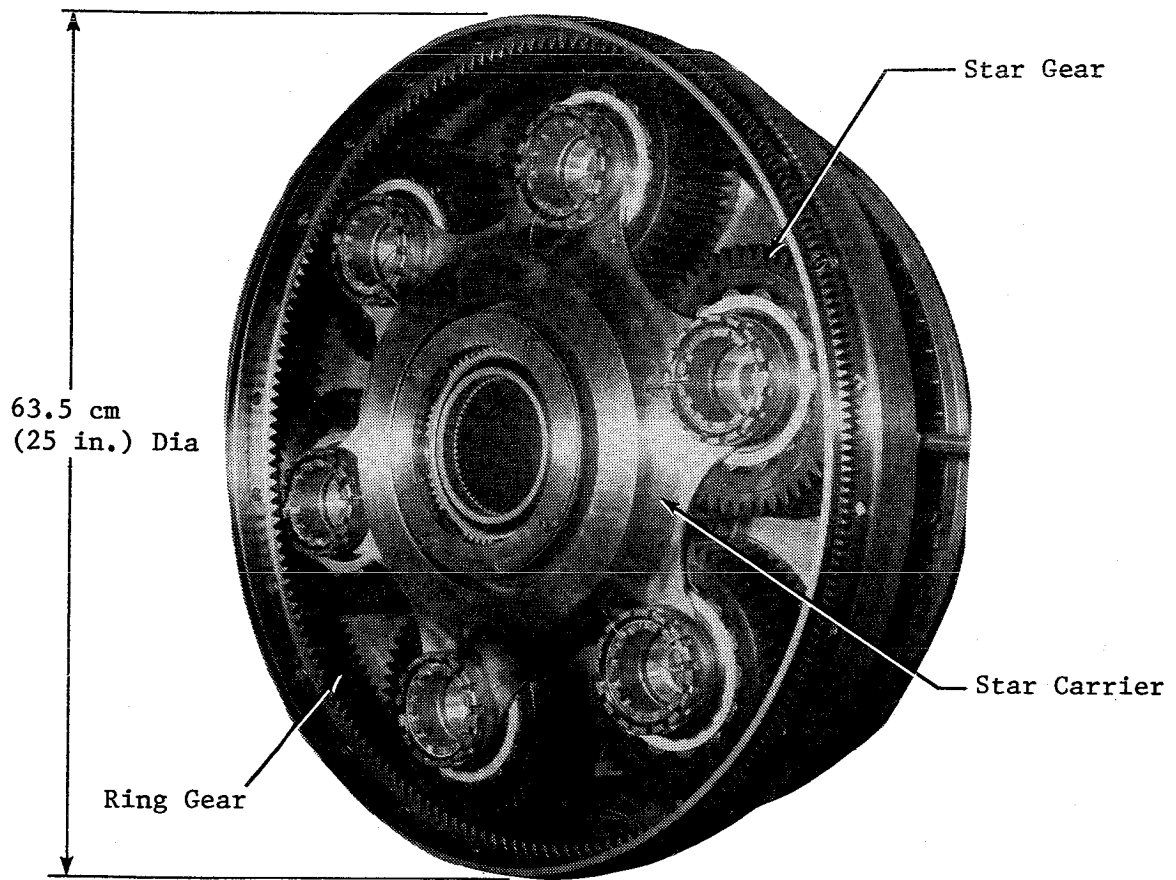
Figure 48. QCSEE UTW Main Reduction Gear.

the maximum permissible to be compatible with the required engine-housing airflow paths.

The under-the-wing (UTW) and over-the-wing (OTW) engine concepts were based on using the same core engine but differing fan-performance characteristics. This dictated different reduction ratios and power ratings. The main reduction gear feasibility studies were directed toward approximately 2.5:1 ratio and 9321 kW (12,500 hp) at 3197 rpm fan speed for the UTW engine and approximately 2.1:1 ratio and 11,282 kW (15,130 hp) at 3782 rpm fan speed for the OTW engine. The specified operating life objectives included 36,000 hours with a minimum of 6000 hours time between overhauls (TBO).

Since light weight and minimum complexity were prime requirements for the engines, a single lubrication system for the turbine, accessory drive, and main reduction gear, using either MIL-L-7808 or MIL-L-23699 lubricant, was specified. This also meant that special attention to gear design factors (such as tooth-spacing accuracy, involute-profile modification, surface finish, gear misalignment, and contact stress) was required to ensure against scoring for these high performance gears.

Since the UTW and OTW reduction gears were both to be used on the same basic engine, identical interfaces between the reduction gears and the engine were specified. These interface points included:

- Power turbine coupling to input gear

- Gear support attachment to engine housing

- Power output gear to fan shaft

- Lubrication supply connection

Other important considerations were the capability of the reduction gear unit to be installed and removed as an assembled module and a low noise level for the reduction gear.

3.5.2 Design Approach

A number of years ago, Curtiss-Wright developed a 671-kW (9000-hp) turboprop military engine that included a two-stage, epicyclic, reduction gear. That reduction gear, Figure 49, had an overall reduction ratio of 7.0:1 which included a 2.67:1 reduction in the primary stage. During an early conceptual phase of the QCSEE program, use of the original YT-49 primary-stage gear was considered. As engine design studies progressed, the need for higher power capability and a different ratio were indicated, but the YT-49 reduction gear technology was still applicable. Features of the YT-49 gear utilized in the QCSEE main reduction gears include the fixed carrier star configuration, flexibility in the sun and ring gears and supports, straight spur gears, and double-row spherical roller bearings with the outer race integral with the star gear.
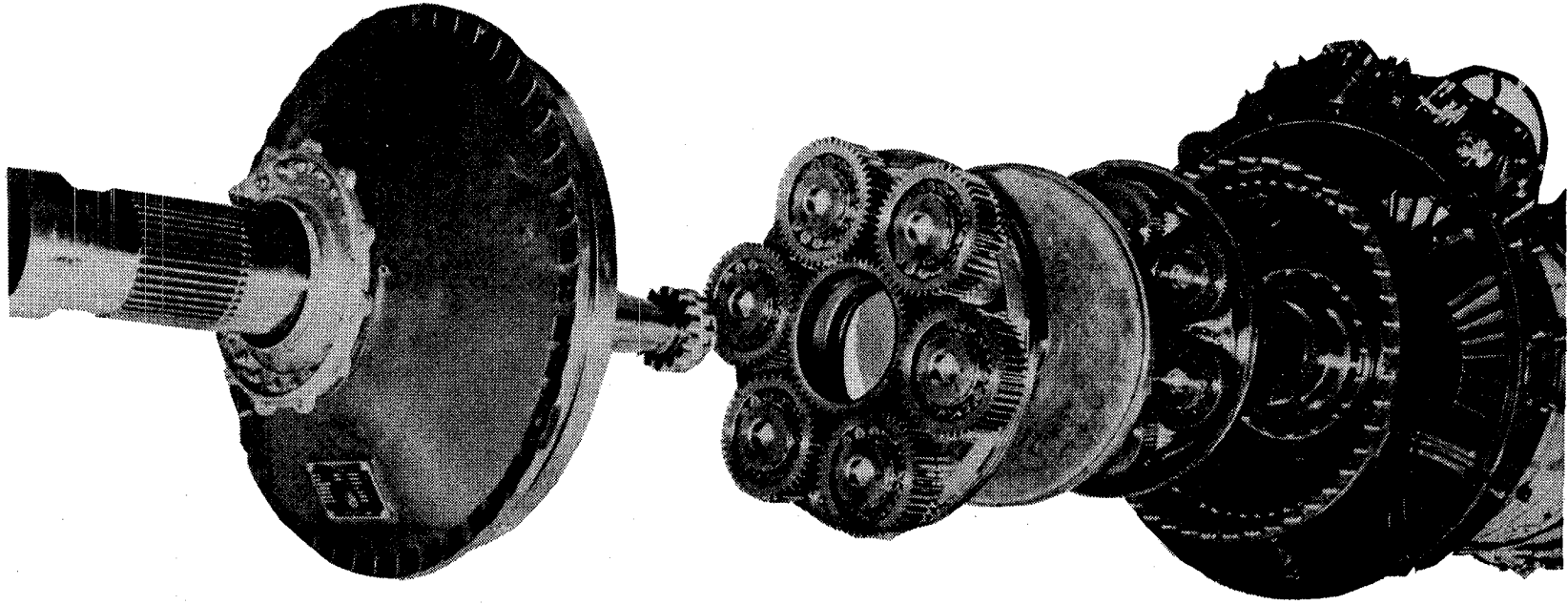
Figure 49. YT49-W-1 Reduction Gear.

A cross section of a QCSEE fixed-carrier, epicyclic, star-system reduction is shown in Figure 50.

The major components of this epicyclic star gear system are:

- Fixed star gear support

- Diaphragm-type sun gear coupling

- Sun gear

- Star gears

- Ring gear

- Lubrication system components

These gearsets were to be installed within the engine housing with the star carrier supported by the engine frame, the input gear supported by the power turbine shaft, and the output gear supported by the fan shaft.

The power input to the reduction gear is through the sun gear. With the fixed star gear carrier or support, the star gears serve as idler gears providing multiple power paths between the input sun gear and the output ring gear. In this configuration, the star gear bearings are subjected to only the tangential gear tooth loads and not to added centrifugal loads as they would be in the case of a conventional planetary with the carrier rotating.

Lubrication of the gearing is provided from the engine system through a single connecting tube to an oil manifold attached to the star gear trunnion support. An annular passage distributes oil to the individual trunnions where radial passages in the trunnions and bearing inner races provide lubrication to the star gear bearings. Spray tubes on the forward side of the manifold provide lubrication and cooling to the sun and star gear teeth. The spray tubes, which are not shown in this figure, have a number of jets spaced to distribute oil across the faces of the gear teeth.

Flexibly mounted gears are important for achieving load equalization between power paths and across the faces of the gear teeth. A double-diaphragm-type coupling is used between the turbine shaft and the sun gear. The sun gear also incorporates flexibility in the web. The objective here is to allow the sun gear to be positioned by the mesh contacts with the star gears and be subjected to minimum influence of any relative radial motion between the turbine shaft and the star gear support. With the accurate machining of the star gear bearing trunnion locations and the gears, a very high degree of load equalization with the individual star gears is achieved. A flexible section between the ring gear and the spline attachment to the fan shaft allows this gear also to be positioned by the mesh contacts with the star gears and be subjected to minimum influence of any relative radial motion between the fan shaft and the star support. A cylindrical roller bearing between the aft end

76
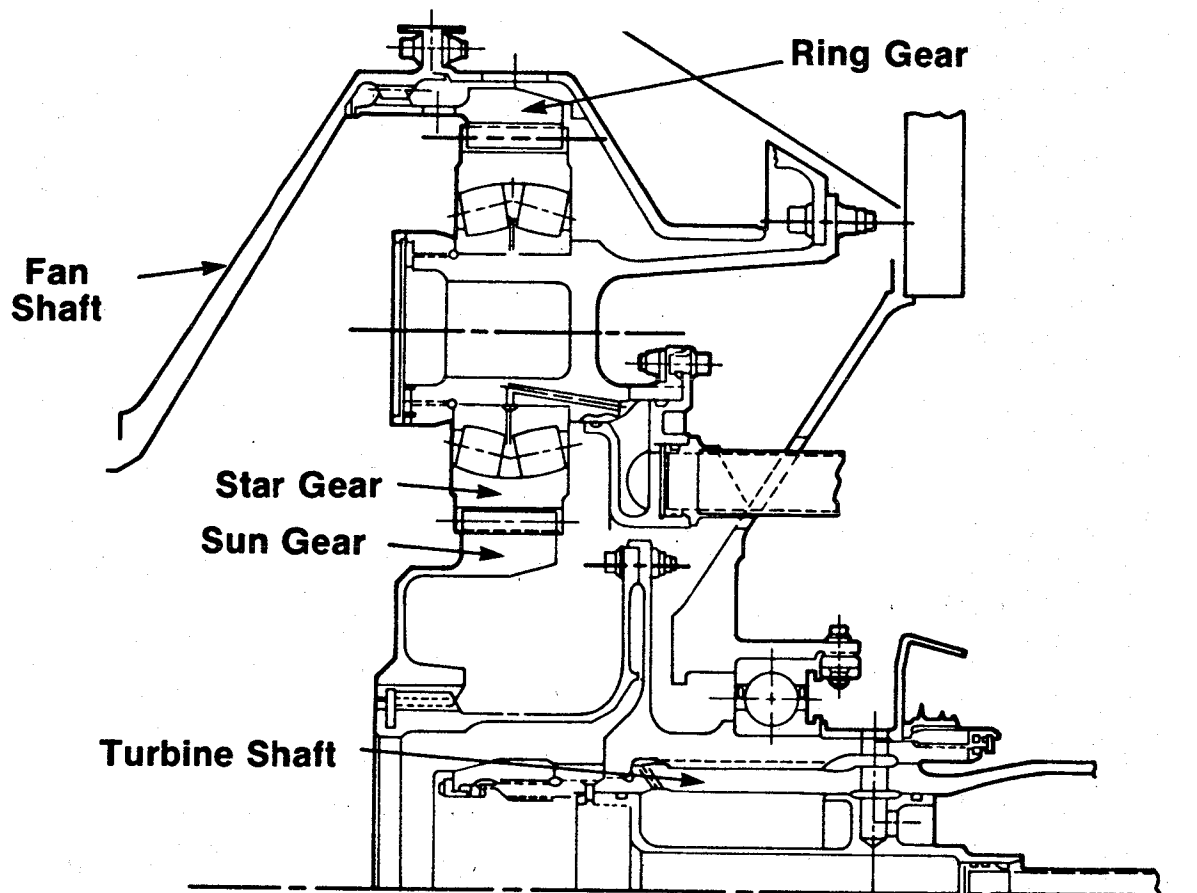
Figure 50. Reduction Gear.

of the fan shaft and the member to which the star gear support is attached also helps to maintain the relative position of the fan shaft to the star gears.

Mounting of the star gear on a double-row, spherical roller bearing allows the gear to operate in a plane defined by the loaded tooth contacts with the sun and ring gears, thus providing good load distribution across the face width. In the design of the gear rims and star gear trunnion supports, section modulii are selected to provide relatively close matching of gear and tooth deflections for the mating gear teeth at each mesh. Consequently, deviation of the plane of rotation for the star gear bearing outer race from the plane of the inner race is very small.

Design factors contibuting to smooth operation and low gear noise are the use of a minimum gear-contact ratio (2) and numbers of gear teeth selected for hunting and nonfactorizing. A minimum contact ratio of 2 means that there are never less than two teeth in each gear in contact at each mesh.

In designing for hunting and nonfactorizing, the number of teeth in each gear is selected such that no two teeth in the gearset enter engagement simultaneously, and the same two teeth in mating gears repeat engagement only after engagement with all other teeth in the mating gear.

3.5.3 Design Summary

Engine and fan trade-off performance studies resulted in changes in power requirements and speed for the final UTW and OTW main reduction gear designs as shown in Table X. The UTW power increased approximately 4%, and the fan speed decreased slightly to 3157 rpm. The OTW power increased approximately 12%, and the fan speed increased to 3860 rpm. These requirements were accommodated within the originally specified envelope. The number of star gears shown, six for the UTW gear and eight for the OTW gear, are the maximum that can fit in the available space allowed by the reduction ratios.

The UTW pitch-line velocity of 97.5 m/sec (19,200 ft/min) is only slightly higher than in the YT-49 gear; that for the OTW unit is approximately 30% greater. Neither of these are considered excessive.

The star gear bearing 0.74×10^6 DN value [bearing bore (mm) x outer race rpm] for the UTW gear compares favorably with the 0.72×10^6 DN value for the YT-49 reduction gear. The 0.90×10^6 DN value for the OTW star gear bearing is higher than any known previous experience for a double-row, spherical roller bearing.

Design oil-flow rates shown are divided between the star gear bearings and the gears. Approximately 35% of the flow goes to the bearings and 65% goes to the gear through the spray-tube jets. The flow split for each spray tube is approximately 50% to the sun gear and 50% to the star gear on the out-of-mesh side.

Table X. Main Reduction Gear Design Summary.

	UTW	OTW
• Gear Ratio	2.465	2.062
• Power Transmitted, kW (HP)	9708 (13,019)	12,610 (16,910)
• Maximum Fan Speed, RPM	3157	3860
• Number of Star Gears	6	8
• Pitch Line Velocity, m/s (ft/min)	97.5 (19,200)	119.3 (23,450)
• Pressure Angle, Degrees	21	21
• Diametral Pitch	7.5321	7.1884
• Bearing dN	$.74 \times 10^6$	$.9 \times 10^6$
• Oil Flow, m³/s (GPM)	.0833 (22)	.0945 (25)
• Heat Rejection, kJ/s (BTU/min)	116 (6600)	190 (10,800)
• Maximum bearing Temp., K (°F)	417 (290°)	417 (290°)

Materials selected for the QCSEE main reduction gears were carburized AMS 6265 for the sun gear, star gears, and the coupling; nitrided AMS 6470 for the ring gear; and AMS 6415 for the star gear carrier. Heat-treat data for the gears are:

Sun and star gear teeth:

Finished case depth - 0.635-0.889 mm (0.025-0.035 in.)

Case hardness   - R_c 60-63

Core hardness   - R_c 32-40

Star gear spherical raceway:

Finished case depth - 1.524-1.778 mm (0.060-0.070 in.)

Case hardness   - R_c 60-63

Ring gear -

Nitride depth   - 0.51 m (0.020 in.)

Case hardness   - 15N91 minimum

Maximum limits selected for the gear design stresses were approximately 24.1 kN/cm^2 (35 ksi) bending and 93.1 kN/cm^2 (135 ksi) contact. These are well below AGMA allowables and Curtiss-Wright operating experience.

The spherical roller bearings have CEVM M-50 steel inner races and rollers and AMS 4616 silicon bronze, silver-plated cages.

3.5.4 Hardware Fabrication

Two UTW gearsets and three OTW sets were manufactured. Two sets of each were required for the back-to-back rig test, and one each of these test gearsets were subsequently installed in the engines.

3.5.5 Rig Testing

Primary objectives of the rig test program were to demonstrate satisfactory operation and to determine operating characteristics of each of the reduction gear designs prior to installation in the engine. Testing was conducted with two essentially identical reduction gears installed in a back-to-back test rig and torque-loaded to simulate engine operating conditions.

Figure 51 shows a schematic cross section of the upper half of the test rig in which some engine reduction gear cavity and oil scavenging characteristics are simulated. The reduction gears are mounted by the star gear support in each end of the rig. The sun gears are connected through engine-type
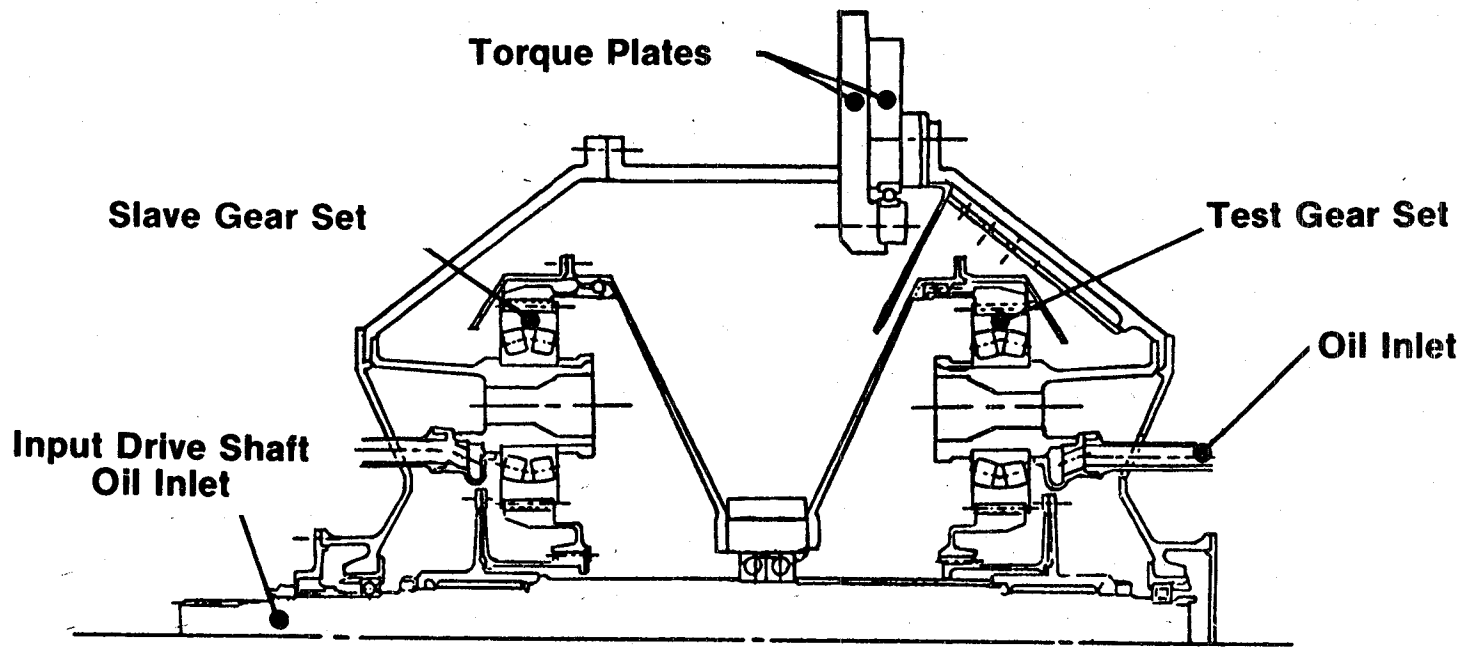
Figure 51.   Main Reduction Gear Test Rig Schematic.

diaphragm couplings and the input drive shaft. The ring gears are supported and connected by simulated fan shafts. An engine-type antichurning and scavenging oil screen was installed in the test gear end of the rig. Oil is supplied to the gears through engine-type oil-inlet tubes. Rotation of one gear assembly relative to the other introduces the torques into the gear system.

Figure 52 shows the drive end of the test rig and also the torque-loading hydraulic cylinders that, by the application of hydrauic pressure, rotate one end of the rig relative to the other and apply the load to the gears.

Significant results of the rig test are shown on Table XI. The reason for the OTW unit not being operated to 100% speed at 100% torque was not the fault of the gear but rather an overestimate of the capability of an aged motoring dynamometer when planning the test program.

The reduction gear efficiencies were a little lower than had been expected, but it is believed improvement could have been accomplished through some lubrication and scavenging development in the vicinity of the sun and star gears.

The engine-hardware oil-baffle screen was installed in the test gear end of the rig at the start of the test program to verify or predict the scavenging characteristics of the engine. The rig operation appeared to indicate marginal scavenging accompanied by oil churning. Several scavenging and baffle-screen modifications were evaluated. The OTW gear, with the higher pitch-line velocity, appeared to be the more critical.

Upon conclusion of the rig test programs, the test gears were thoroughly inspected and prepared for installation in the engines.

3.6 COMPOSITE FAN FRAME

One of the major areas of new technology investigated under the QCSEE program was the application of advanced composite materials to major engine hardware. Two types of static structure were demonstrated during the program. The first of these was the fan frame, a structure requiring both high strength and stiffness. This is the main support point for the engine and will be discussed in some detail covering the frame requirements, structural description, design, analysis, fabrication, and testing. The second type of static structure that utilized advanced composite material was the nacelle; the nacelle is discussed in the next section.

The graphite/epoxy fan frame, shown in Figure 53, is the largest highly loaded advanced-composite structure yet built for a turbofan engine. It is the first time the major structural support for such an engine was constructed utilizing advanced composite materials for virtually all components. It has been estimated, based on two smaller composite-frame programs conducted in 1972 through 1974, that this type of application could save from 25% to 35% in weight over an equivalent metal frame. These previous programs generated sufficient technical confidence to undertake the design and fabrication of advanced composite frames without a backup metal frame.

82
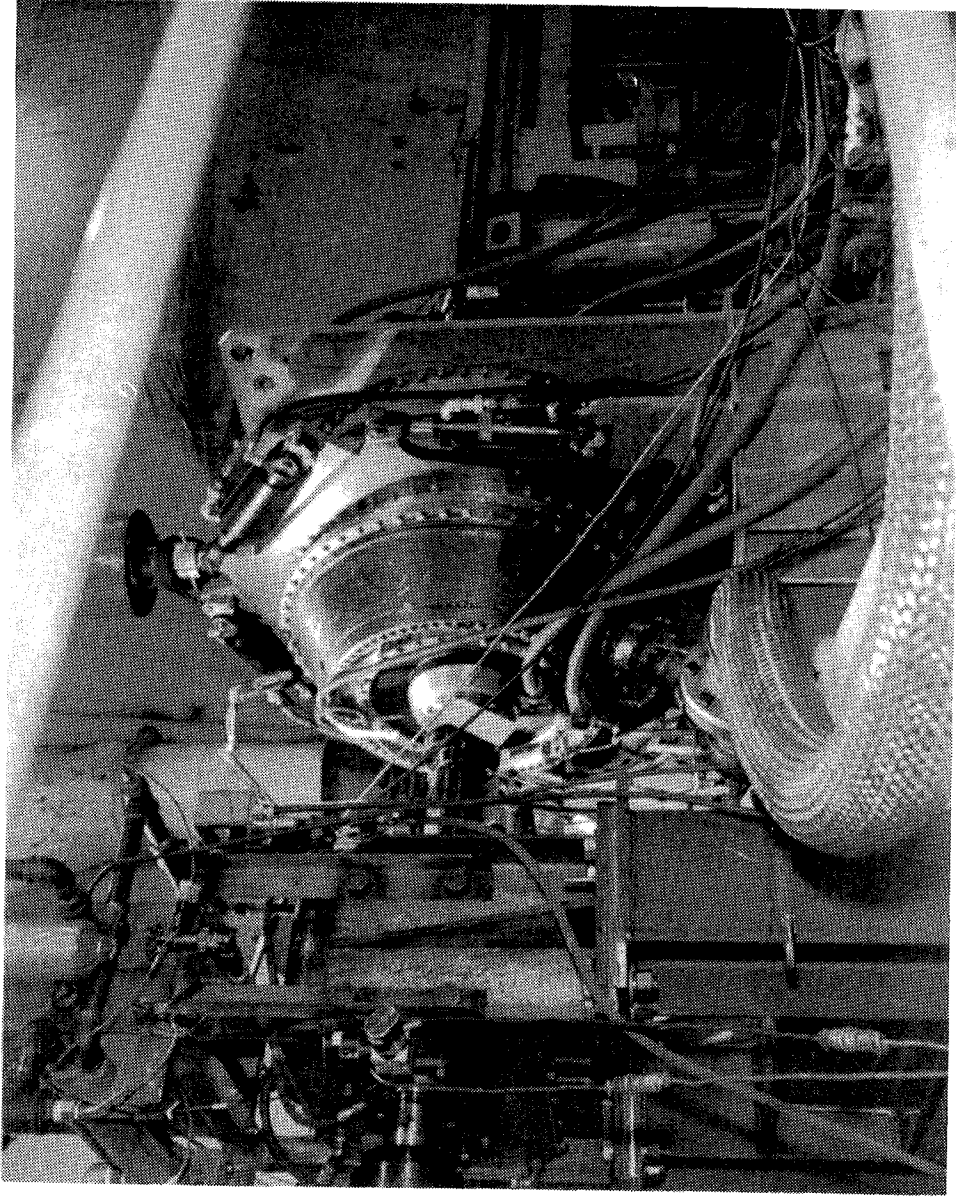
Figure 52. Main Reduction Gear Test Rig, Slave Unit (Drive) End.

Table XI. Rig-Test Results.

	UTW	OTW
• **Demonstrated**		
Speed/Torque, %	100/125	80/109*
	105/50	95/50*
		*Limited by Drive Power
• **Completed**	48.8 hr	36 hr

• **At Max Speed and Torque, 344K (160°F) Oil Inlet**

		UTW	OTW
Oil ΔT	=	294K (70°F)	321K (119°F)
Oil Flow	=	80 kg/min (177 lb/min)	91 kg/min (200 lb/min)
η Mech	=	98.9%	98.7%

• **Developed Lube/Scavenging System Through Several Configurations**
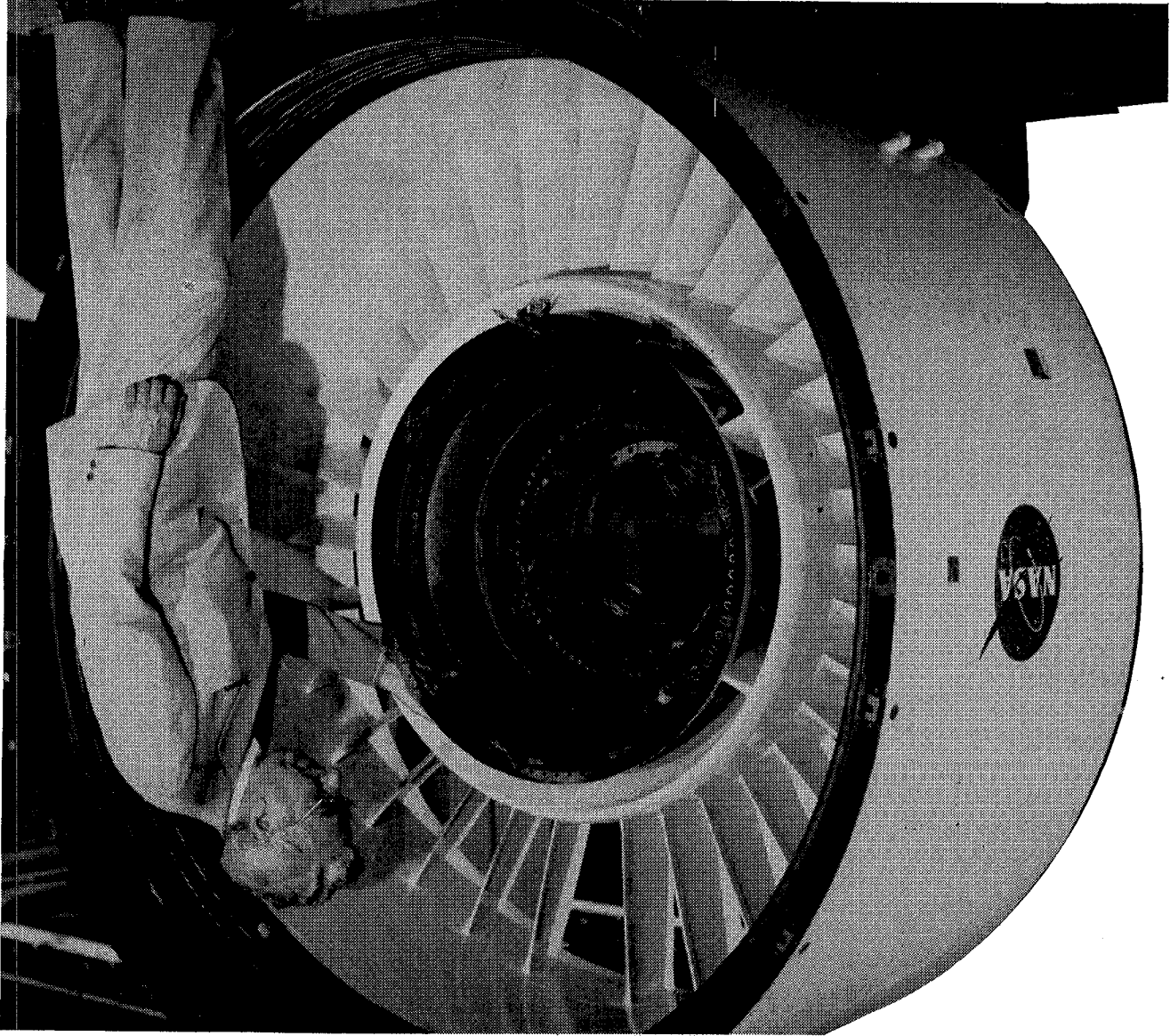
Figure 53. QCSEE Fan Frame.

This program thus provided the somewhat unique opportunity to design a major composite structure from an original-equipment point of view rather than a replacement component in an existing-engine design. This permitted a much more integrated structure than is possible when constrained by the necessity of mating with existing hardware.

The differences between the OTW and UTW frames were so minor as to have no effect on the basic frame structure. For simplicity, all further discussion will pertain to the frame used in the UTW propulsion system.

3.6.1 Design Requirements

The QCSEE frame design was governed by the necessity for performing the following major structural and aerodynamic functions:

- Provide the main engine forward-attachment points for thrust, vertical, and side loads.

- Support the fan thrust bearing, variable-pitch system, reduction gear, and compressor thrust bearing.

- Support the inlet, aft outer, and aft inner core cowls.

- Support the core compressor at the forward casing flange.

- Support the fan hub OGV's.

- Provide the mounting position for the accessory gearbox and digital control.

3.6.2 Structural Description

As can be seen in Figure 54, the QCSEE integrated fan frame is a graphite/epoxy structure that incorporates the fan casing, fan bypass stator vanes, and core frame into one all-bonded structure. It provides the primary support for the engine. Fan blade-tip treatment and containment are provided by the grooved and Kevlar-filled structure integrated in the forward portion of the outer casing. Positioning of the fan and core engine-bearing supports relative to the integral nacelle/outer casing is provided by 33 bypass vanes that also provide flow-turning of the fan discharge. Due to the blockage caused by a pylon at the 12 o'clock position, the camber of these vanes is tailored individually depending on circumferential position.

The hub of the frame is connected to the frame splitter through six equally spaced struts. The inner shell of the outer casing, the bypass duct and core duct surfaces of the frame splitter, and the pressure faces of the bypass vanes are perforated to provide acoustic suppression within the frame structure.
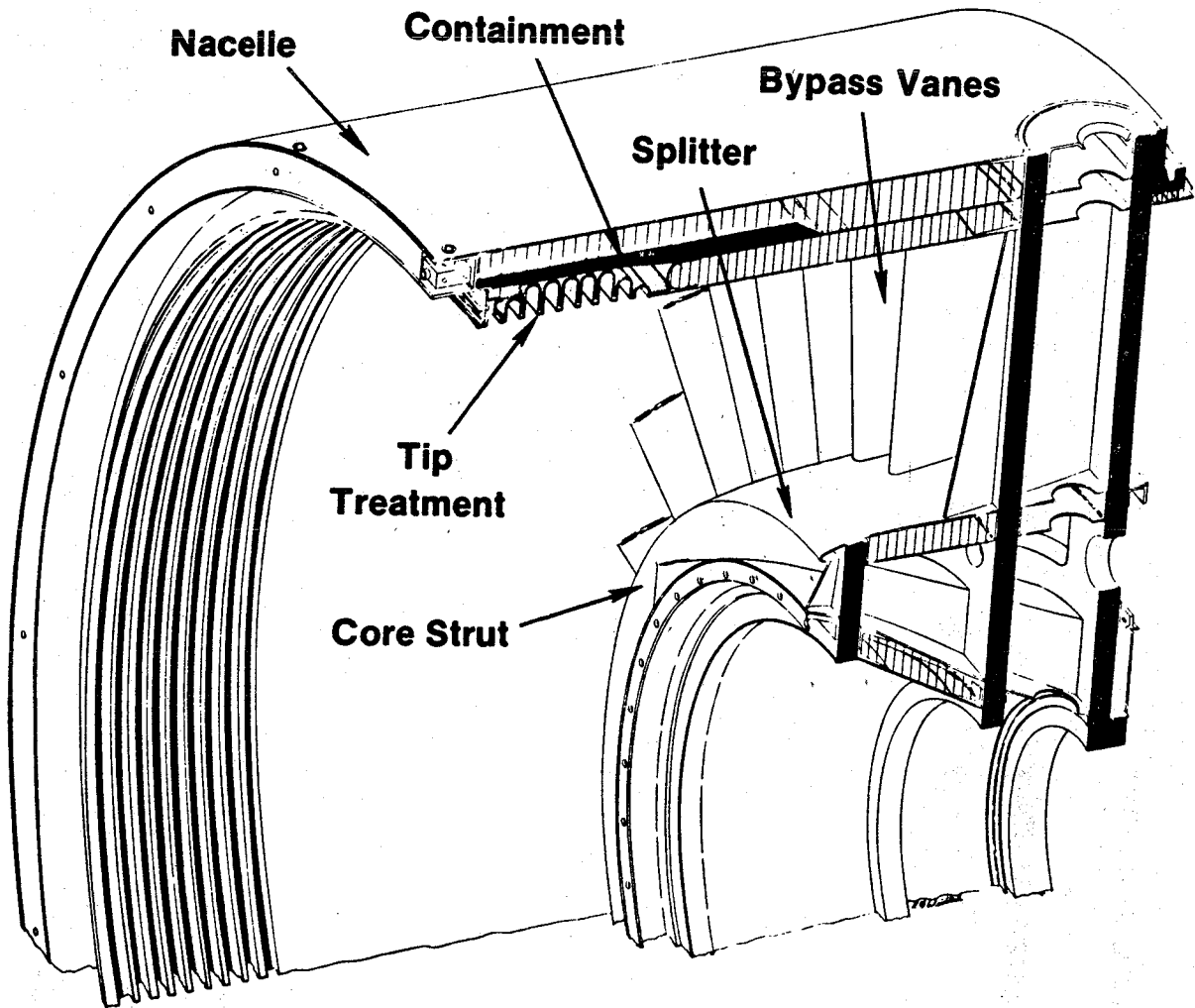
Figure 54. QCSEE Integrated Fan Frame.

The frame was designed based on the load conditions shown in Table XII. The magnitudes of some of the more critical of these loads are shown in Figure 55. The basic structural concept used in the frame design is also shown in this figure. The primary radial members of the frame consist of three wheel-like structures. The forward wheel is a flat-spoked wheel comprised of a splitter ring, hub ring, and six spokes. The middle and aft wheels are flat-spoked wheels consisting of an outer casing ring, splitter rings, and 33 spokes connecting the outer casing ring to the splitter ring. Shear panels of the proper aerodynamic shape are bonded to these wheels to form the fan bypass stator vanes and the struts in the core flowpath.

The aft splitter ring contains the engine-mount attachment points. These consist of a metal uniball at the 12 o'clock position, to react vertical and side load, and two metal thrust brackets located 45° down on either side of the uniball.

The internal load distribution for the frame was determined using a finite-element computer program which represented the frame structure as a combination of curved beams, straight beams, and plates, all capable of having orthotropic material properties. A graphic comparison of the analytical model to the actual hardware is shown in Figure 56. In the core region of the frame, the struts were modeled as three straight beams (representing the spokes of the wheels) connected to curved beams in the hub and splitter region (rims of the wheels), all tied together by plates representing the flowpath and splitter walls. The fan flowpath area was represented by radial beams representing the bypass vanes (wheel spokes and flowpath panels were lumped together and appropriate section properties used for these pseudobeams) tied to plates representing the outer casing forward to the inlet. Appropriate structure was also included to represent the mount structure and the compressor case back to the turbine frame.

Several iterations were made on thickness and orientations of the various elements of the model to arrive at an efficient structure which would meet the design requirements. By these iterations it was possible to take advantage of the ability to tailor composite materials to the specific load requirements of the individual components. As can be seen in Table XIII, a considerable amount of tailoring was possible.

Once the material configurations were selected, the computer model was used to determine the final internal stresses in the frame components. Several of the most critical of these are shown in Table XIV along with the allowable stress for the specific layup pattern for the component. The "design calculated stress" for the "critical flight" conditions shown is a conservative three times the actual calculated stress for that condition. As can be seen in Table XIV, the stress allowable, as verified by material-properties tests, always exceeded the design calculated - indicating a safe design. The effect of different thermal coefficients where the titanium bearing cones attached to the composite structure was also accounted for, as shown in Table XV.

Table XII. Frame Loading Conditions.

● Operating

— Flight and Landing
— Gust Load Plus Crosswind and Max Thrust
— Side Load — 4g Plus 1/3 of Gust Load

● Emergency

— Seizure — Decelerating From Max. Speed to Zero in One Second
— Crash — 9g Fwd, 2.25g Side, 4.5g Down,
  Max Thrust — 12g Fwd at Zero Thrust
— Blade Out — Loss of Five Adjacent Composite Fan Blades at Max. RPM

Cowl Loads

0.9525 m
(37.5 in.)

2.0 m dia
(78.8 in.)

Inlet Loads

Cowl Loads

Mount Loads

Thrust 93,410 N
(21,000 lb)

Gear Torque 2,204,000 cmN
(14,600 in-lb)

Core Loads

867,400 N
(195,000 lb)

5 Blades Out

Core Loads
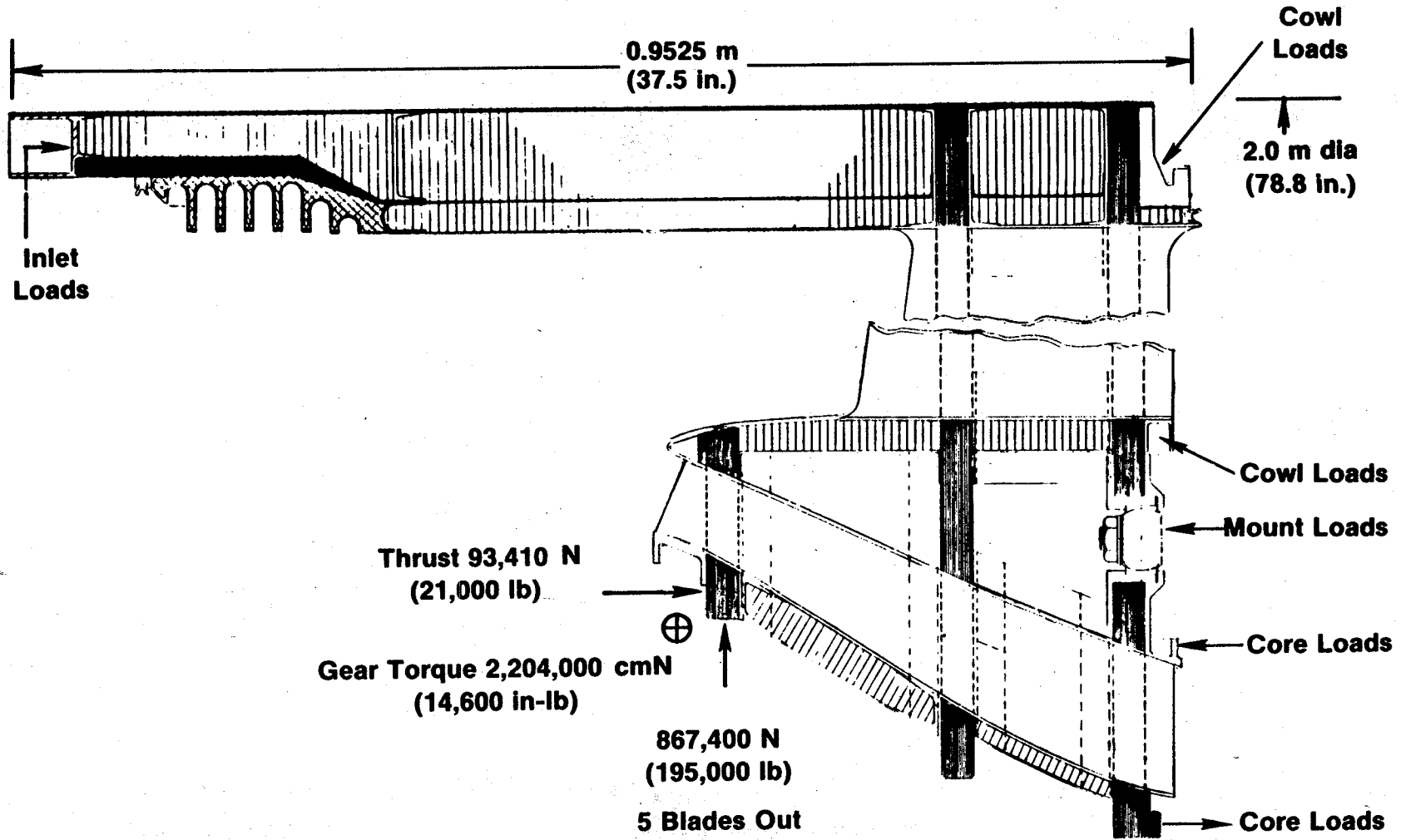
Figure 55.   QCSEE Composite Frame.
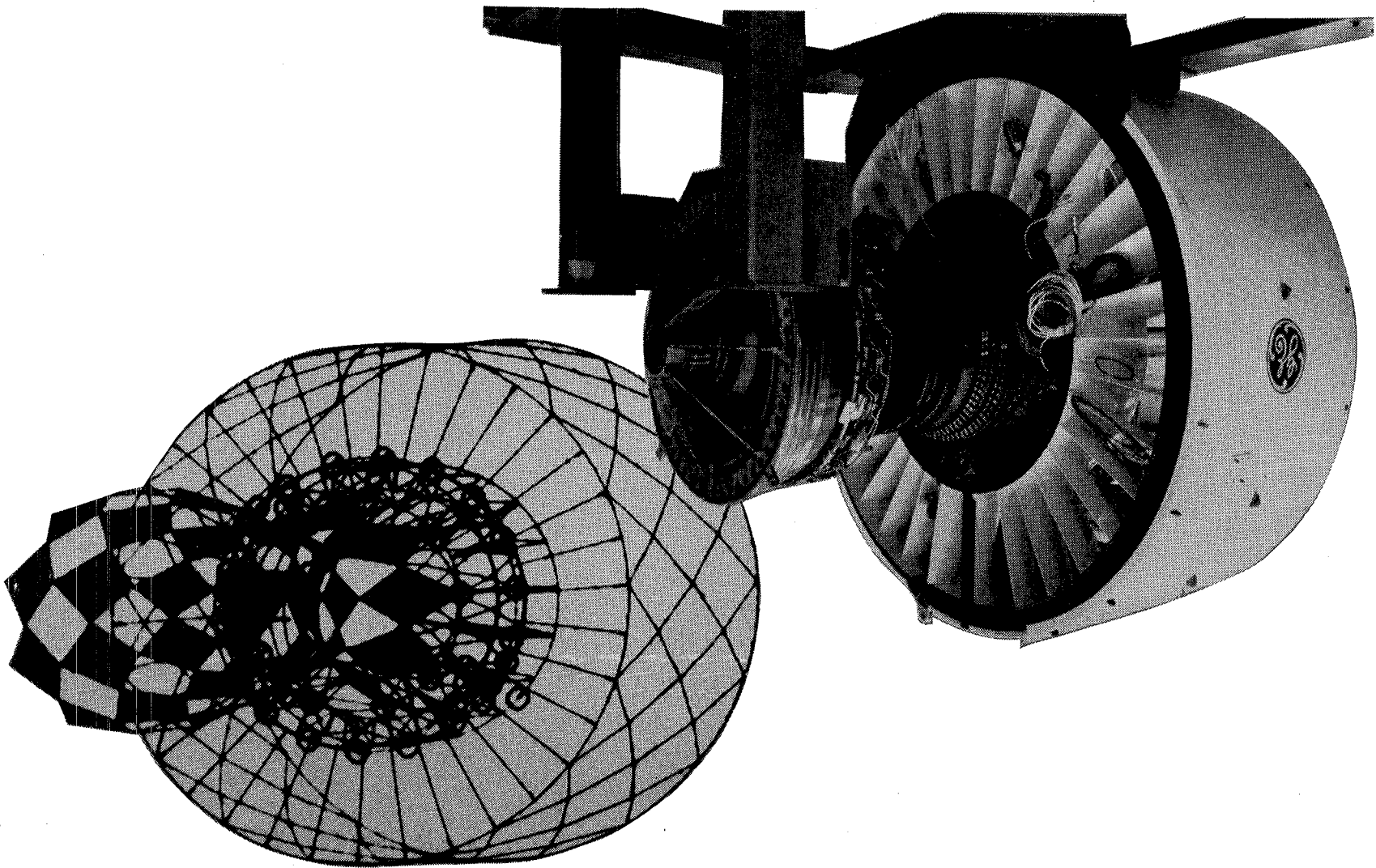
Figure 56.   Analytical Model Comparison.

Table XIII. Geometry of Composite Frame Components.

Material Type-AS Graphite/3501 Epoxy

Item	Layup Conf.			0° Datum
	0°	± 45°	90°	
Forward "Wheel"	50%	20%	30%	Radial
Middle "Wheel" and Aft	30%	20%	50%	Radial
Nacelle Panel	28.5%	57%	14.5%	Axial
Bypass Vane Panel	40%	40%	20%	Radial
Bypass Vane Spoke	80%	20%	0%	Radial
Bypass Vane Outer Ring	30%	20%	50%	Radial
Core Vane Panel	25%	50%	25%	Axial
	40%	40%	20%	Axial

Table XIV. Frame Component Stress.

Load Condition	Location	Design Calculated Stress N/cm² (psi)	Stress Allowable N/cm² (psi)
5 Airfoils Out	Forward "Wheel" Hub Ring	37,230 (54,000)	42,750 (62,000)
5 Airfoils Out	Forward "Wheel" Spoke	53,570 (77,700)	65,500 (95,000)
Critical Flight	Bypass Vane Panel	40,920 (59,349)	57,230 (83,000)
5 Airfoils Out	Core Panel	8600 (12,471)	17,240 (25,000)
Critical Flight	Nacelle Panel	12,700 (18,417)	27,580 (40,000)

Table XV. Effect of Different Thermal Coefficients.

Ring	α(RING — G/E) cm/cm/°K x 10⁻⁶ (in/in/°F x 10⁻⁶)	α(BRG — T 6-4) cm/cm/°K x 10⁻⁶ (in/in/°F x 10-6)	Thermal Stress N/cm² (psi)	Total Ring Stress Ncm² (psi)	Allowable Stress N/cm² (psi)
FWD HUB	4.5 (2.5)	8.46 (4.7)	2070 (3000)	39,300 (57,000)	42,700 (62,000)
MID HUB	2.34 (1.3)	8.46 (4.7)	4830 (7000)	25,500 (37,000)	60,000 (87,000)
AFT HUB	2.34 (1.3)	8.46 (4.7)	4830 (7000)	18,600 (27,000)	60,000 (87,000)

Since one of the most critical areas of composite stuctures is the joining of the individually molded pieces, either by bonding or mechanical fastening, the critical joint areas of the frame were investigated by a series of individual subcomponent tests representing these areas. A total of 36 specimens representing 21 different areas of the frame were fabricated and tested to failure. In all cases, the failing load of the subcomponent was in excess of the maximum design requirements of the area represented. A summary of some of the more critical of these tests is shown in Table XVI, and a typical failed subcomponent is shown in Figure 57.

3.6.3 Fabrication

Designing the frame was only the first part of the problem. It then remained to devise means for fabricating this large composite structure that, by its very nature, required new frame-fabrication concepts.

The fabrication of the QCSEE composite frame was a cyclic manufacturing process of bonding numerous premolded-graphite/epoxy parts and then machining the required interfaces in preparation for the next bonding cycle.

Since only two frames were to be fabricated, the fabrication process was designed to require a minimum amount of tooling - substituting hand benching and machining in its place. Although this is counter to the approach that would be employed in a production situation, it was felt that this would result in a lower overall cost in this case.

The frame was fabricated as two major subassemblies: the basic frame structure and the fan casing.

The basic frame subassembly required the prefabrication of the three wheels that provide the frame backbone. The forward wheel was cured-out as one piece; however, the much larger middle and aft wheels were made by adhesively bonding a great many precured pieces in a steam-heated press. The assembly of the pieces of such a wheel is shown in Figure 58, and the completed wheel, just out of the press and prior to machining, can be seen in Figure 59.

After these wheels were complete, the frame assembly was initiated by bonding the middle wheel to the aft wheel using preassembled honeycomb-box structures to space the wheels axially at both the outer rings and the splitter rings. The forward wheel was then added in the same fashion. This assembled wheel structure is shown in Figure 60.

To complete this subassembly, the precured sump cone was bonded in place as well as the precured core-strut skins and bypass-vane skins. With the addition of appropriate reinforcing structure, this completed the frame subassembly.

Table XVI. Subcomponent Test Results.

Type	Location	Required	Test
Core Strut/Ring	FWD	177,900 N (40,000 lb)	245,530 N (55,200 lb)
Core Strut/Ring	MID	214,000 N (48,100 lb)	298,000 N (67,000 lb)
Core Strut/Ring	AFT	20,000 N (4,500 lb)	105,000 N (23,700 lb)
Core Strut/Ring (Bending)	FWD	128,800 cmN (11,400 in.-lb)	165,000 cmN (14,600 in.-lb)
Core Ring (I.D. in Comp.)	FWD	18,080 cmN 1,600 in.-lb	427,140 cmN 37,800 in.-lb)

Tensile Failure
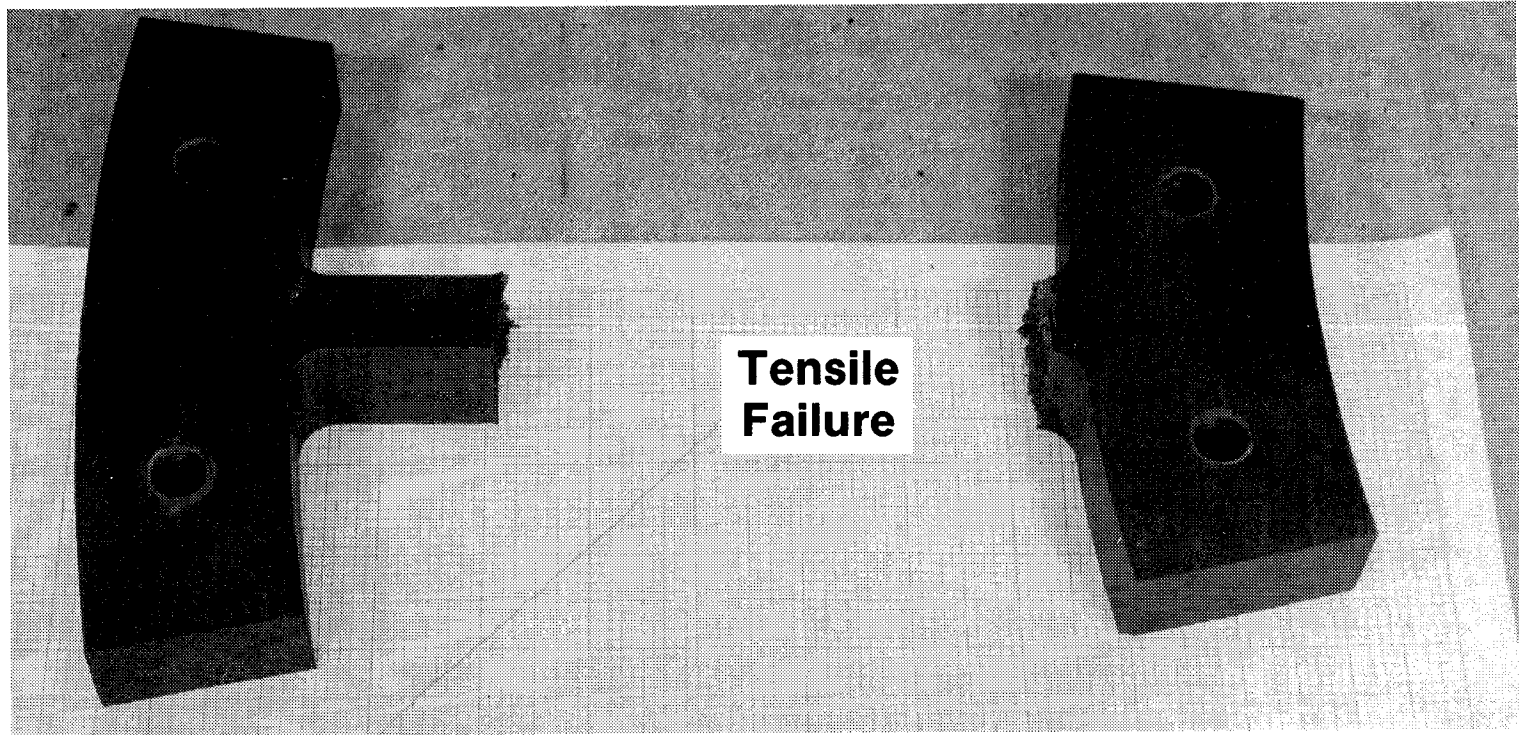
Figure 57. Spoke Subcomponent Test.
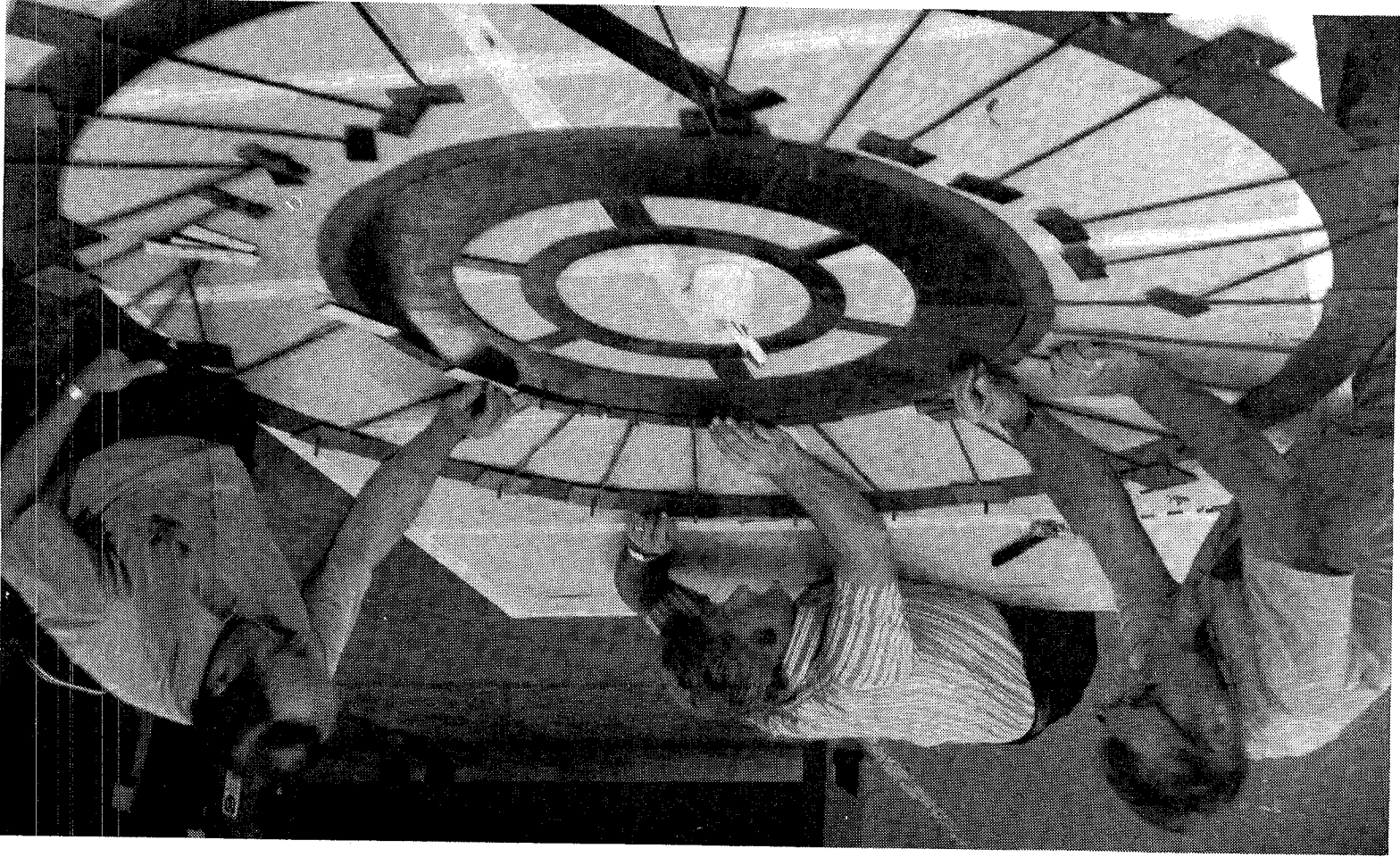
Figure 58.   Assembly of Aft Wheel.

Figure 59. QCSEE Aft Wheel.

98
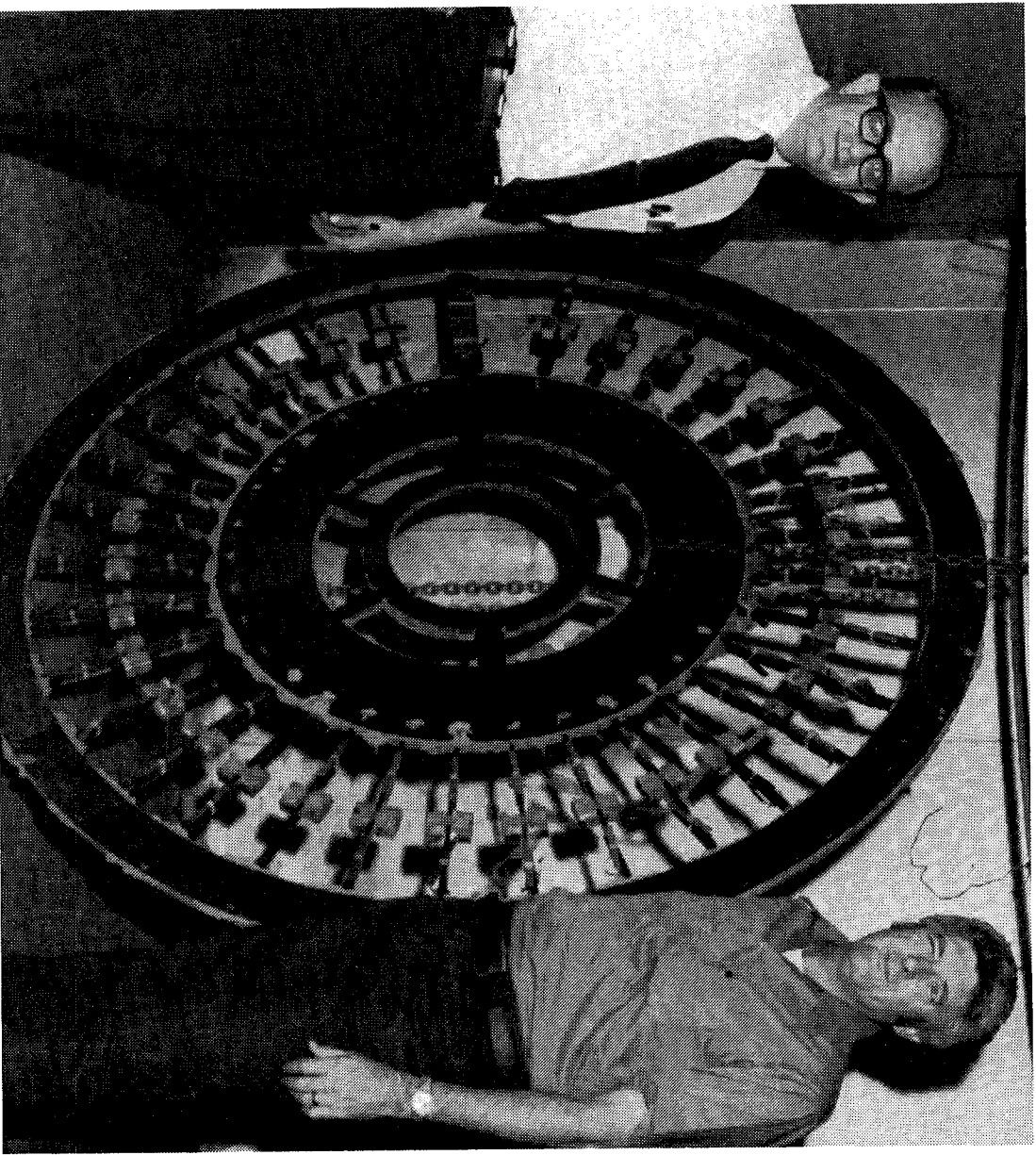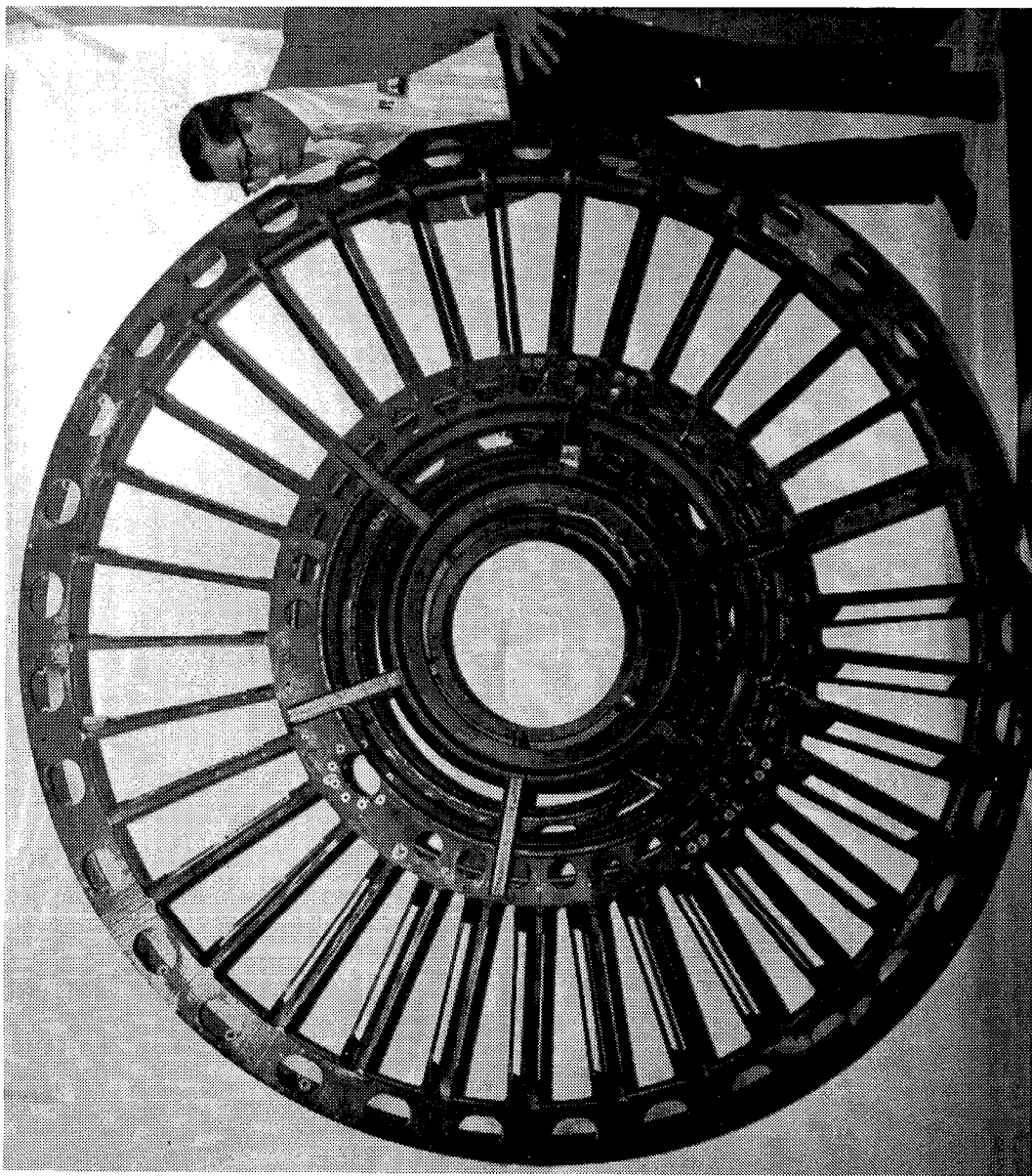
Figure 60. Assembled Wheel Structure.

The outer casing subassembly was sequentially assembled on a male tool, cylindrical in shape, while the skins that went into the assembly were pre-cured in 120° segments in a female tool.

The first step was to precure the fan flowpath skins. This was the surface requiring acoustic holes. These holes were laser drilled as shown in Figure 61. This skin was put on the male tool and the tip-treatment components bonded in place as shown in Figure 62. A layer of aluminum honeycomb of the proper depth for the acoustic requirements was then bonded in place and a septum skin added to provide the back face of the acoustic panel. The containment system was installed at this time. Another layer of honeycomb was then added to obtain the proper casing depth. This completed the basic structure of the fan casing subassembly, seen in Figure 63, since the outer skin would not be attached until the casing was assembled to the basic frame.

At this point, the two major subassemblies were mated (Figure 64), the fan casing outer diameter ground to the proper dimensions, and the fan casing outer skin bonded in place. this completed the frame structure. All penetrations into the core were sealed, instrumentation and services installed, and the frame painted. The completed frame is shown in Figures 65 and 66.

3.6.4 Testing

The fan frame ws subjected to a series of static-load tests to verify the overall structural adequacy. All loads were applied to the frame through a simulated forward-fan-bearing cone and a simulated inlet. To simulate the proper boundary conditions on the frame, it was bolted to a simulated core engine. This assembly was then supported from the facility through the actual engine-mount locations (Figure 67). In addition to determining the actual frame stiffnesses, the frame was tested to the loads imposed by the maximum operating thrust, thrust plus a 51.4-m/sec (100-knot) crosswind, and thrust plus the unbalance due to one blade out. The frame survived these tests with no damage, and recorded stress levels were in good agreement with predictions.

3.7 COMPOSITE NACELLE

The flight-type nacelle for the UTW engine was a major area of composite application to static structures in the QCSEE program. Virtually everything shown in Figure 68, except for the test facility and some tubing, is constructed from advanced composite materials. In addition to the fan frame discussed in the previous section, the inlet, outer cowl, and the fan nozzle can be seen. In addition, the inner cowl was also constructed of advanced composite material. These can be seen in the cut-away drawing shown in Figure 69.

3.7.1 Inlet

The inlet is of fairly conventional composite construction utilizing Kevlar/epoxy skins on aluminum-honeycomb core. The inner barrel comprises
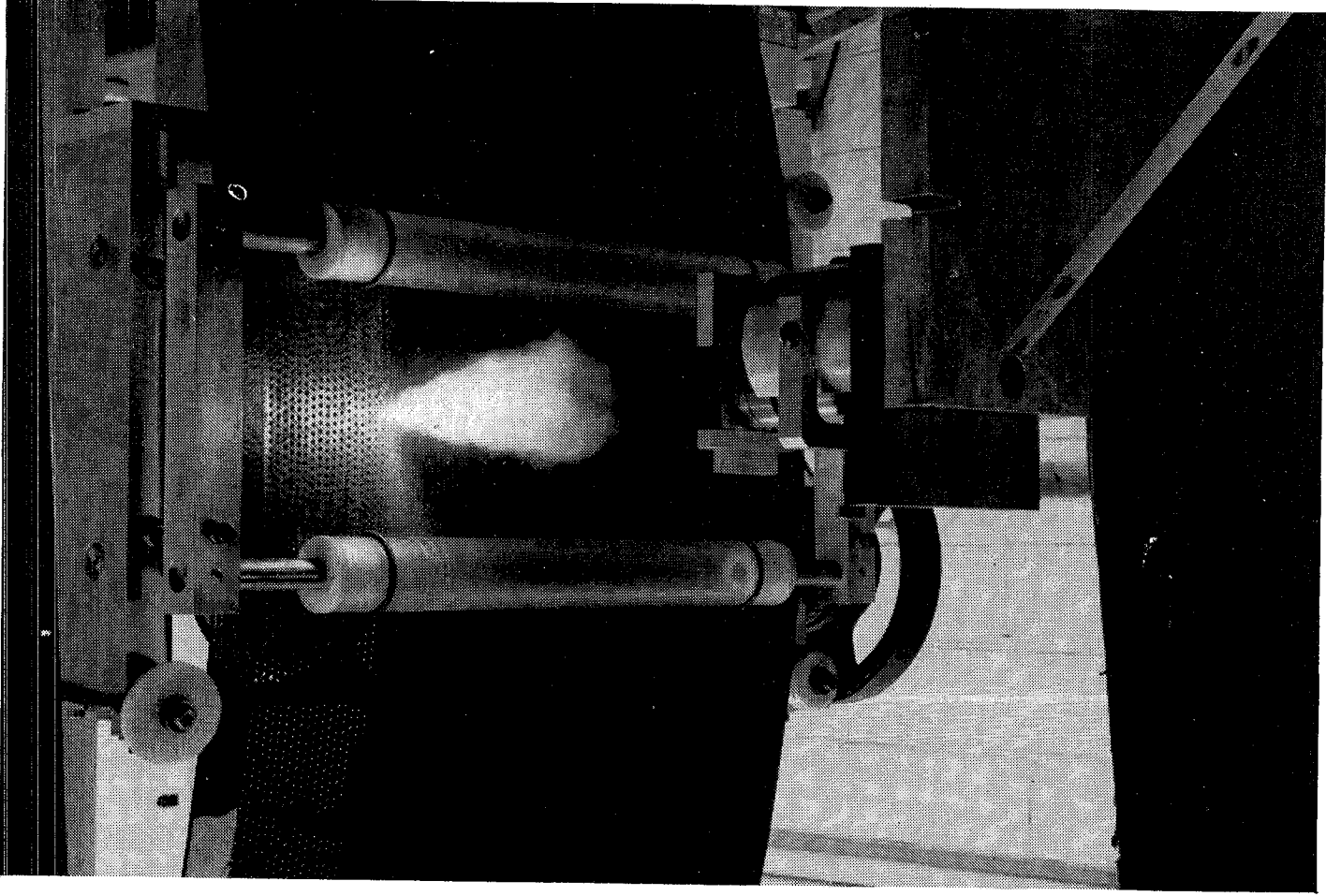
Figure 61.   Laser Drilling of Acoustic Holes.
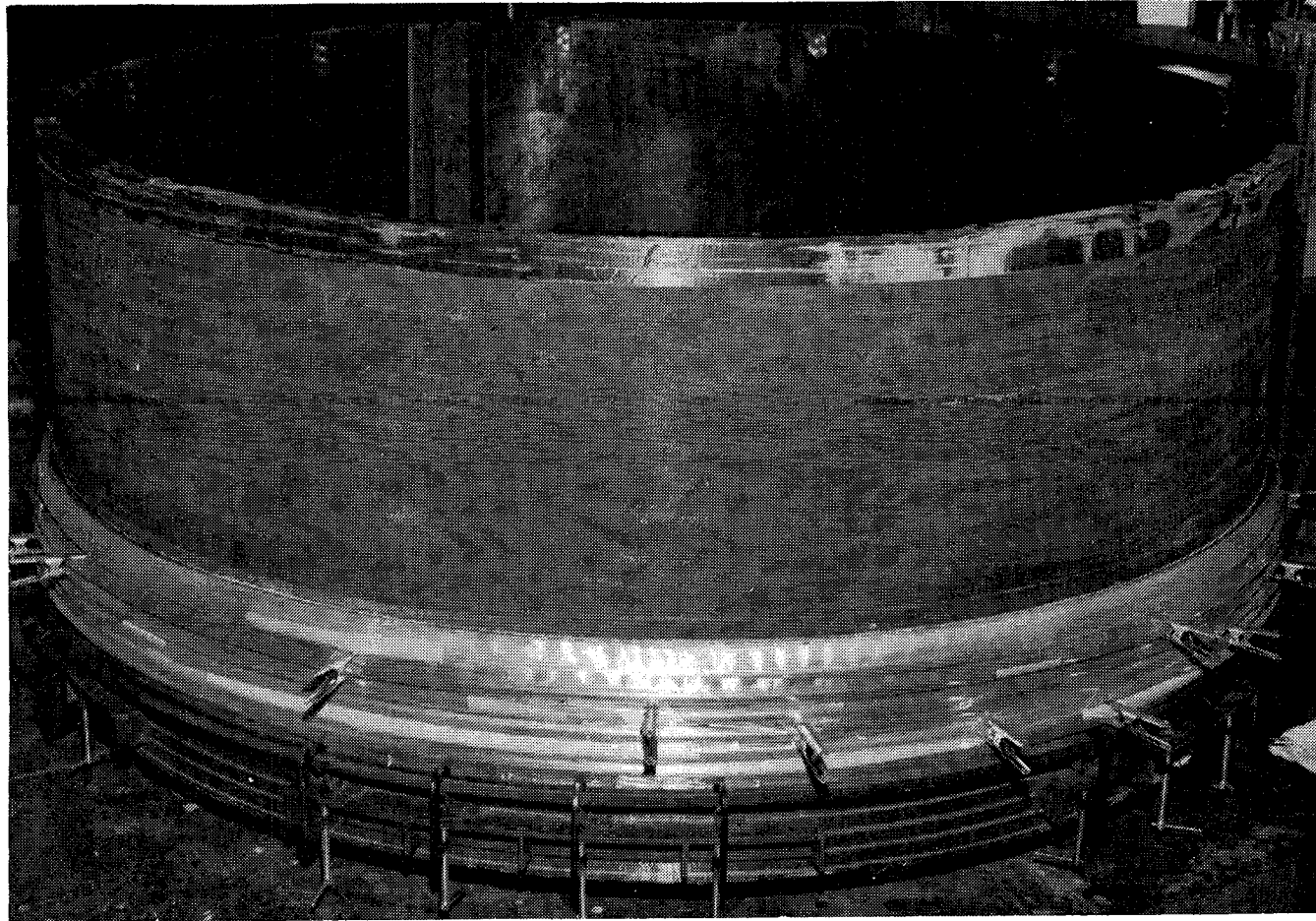
Figure 62. Fan Casing Fabrication.
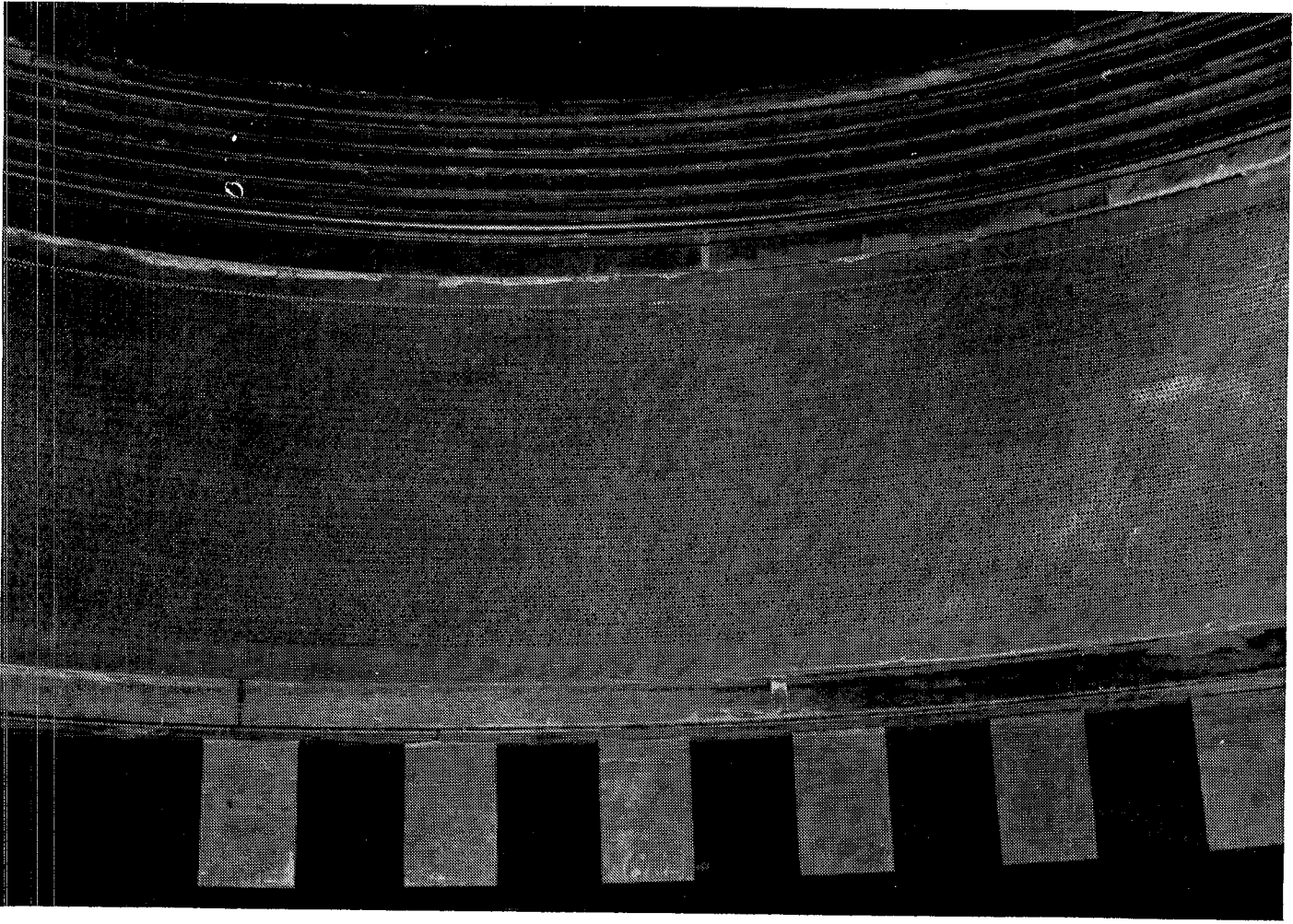
Figure 63.   Fan Casing Subassembly.
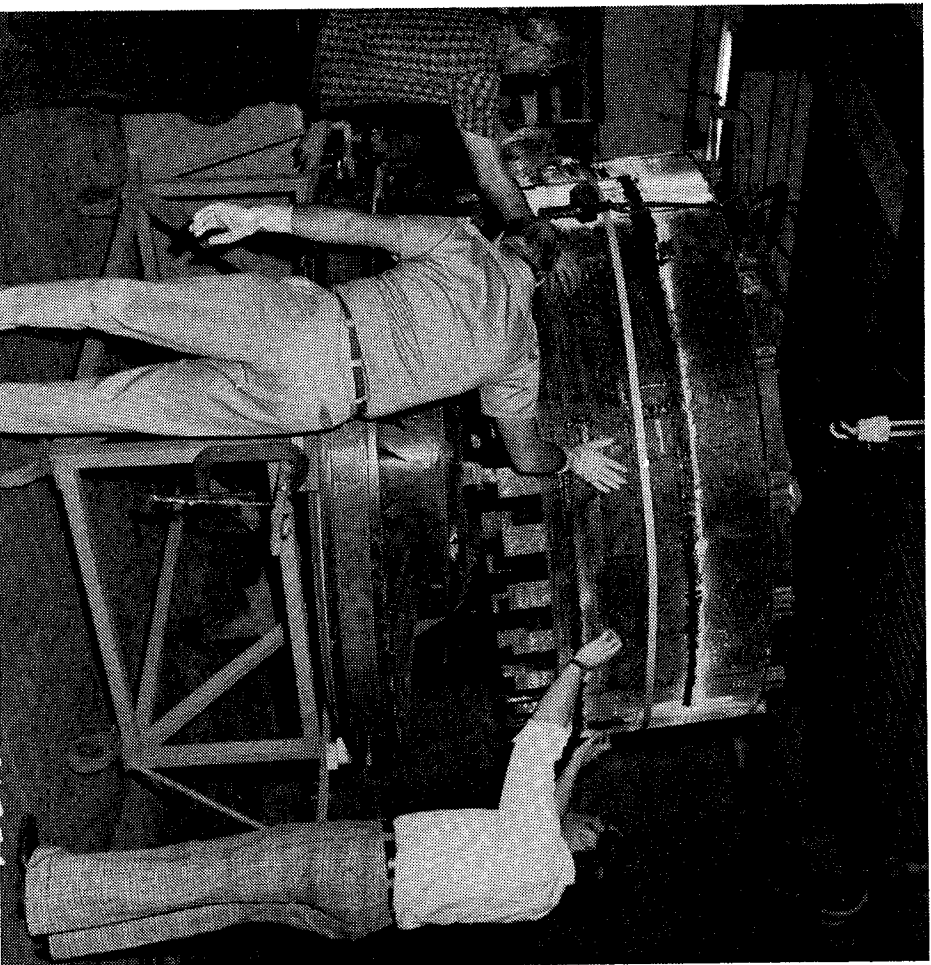
Figure 64. Assembling Fan Case to Frame.
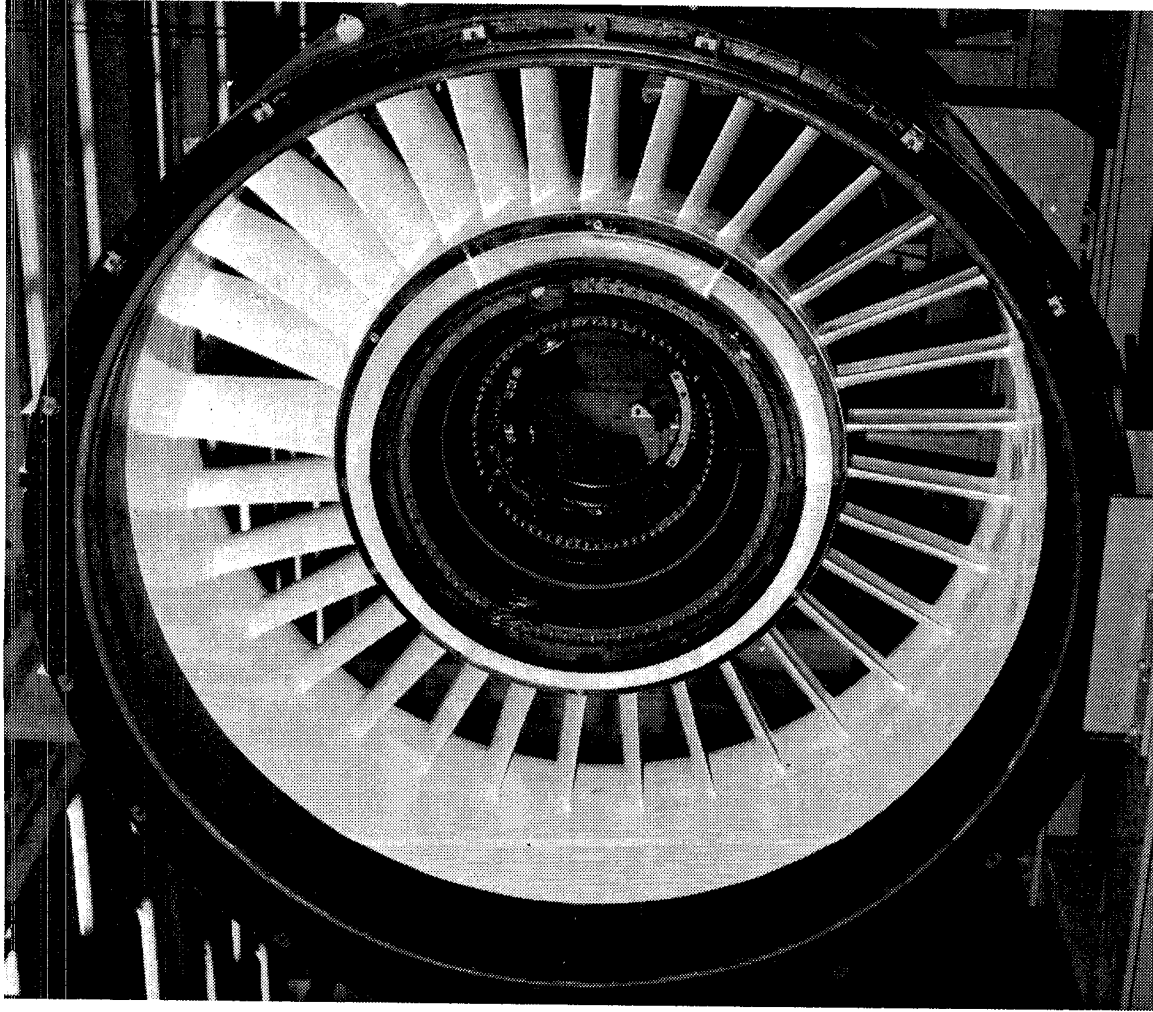
Figure 65. QCSEE Fan Frame.
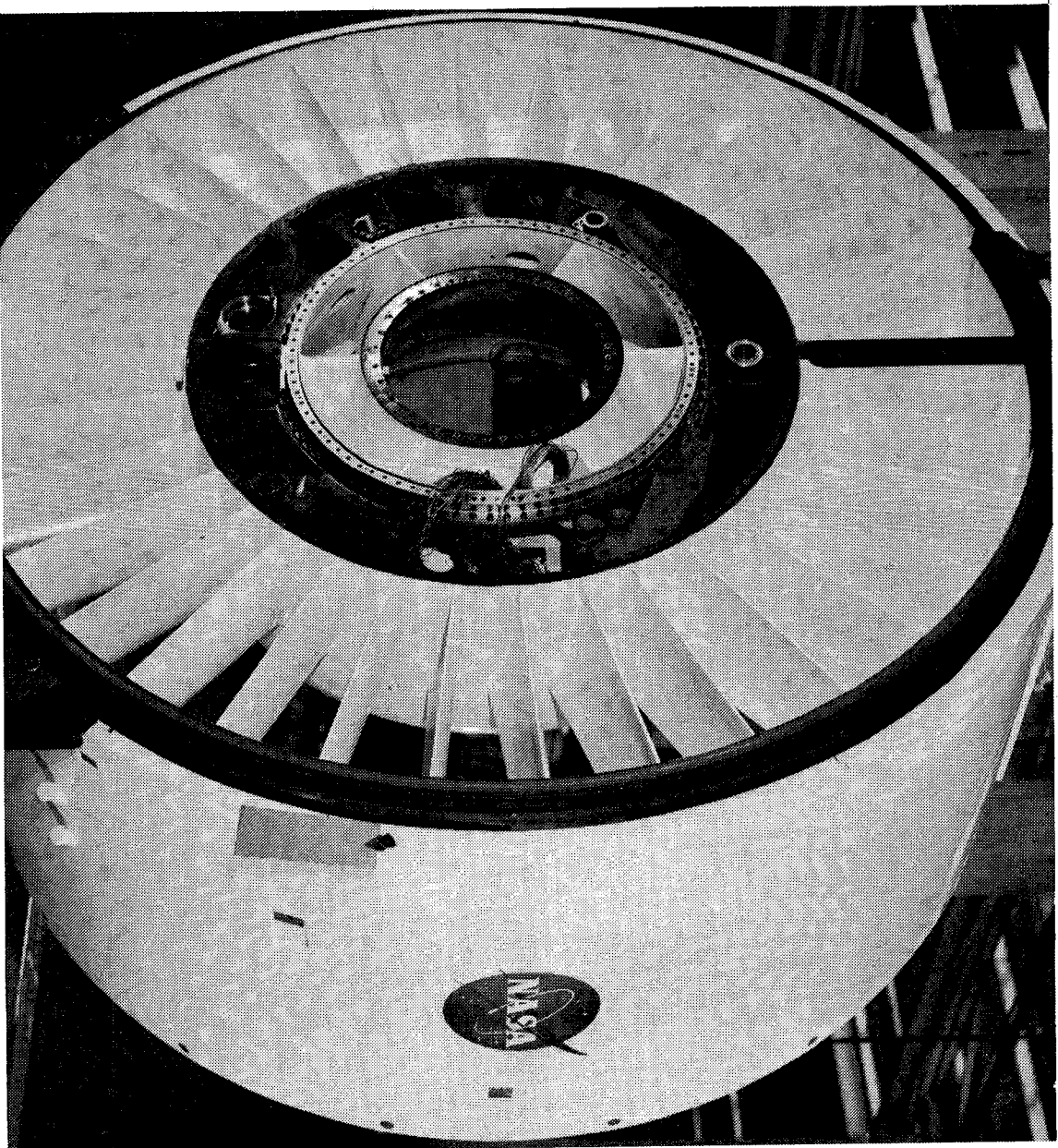
Figure 66. QCSEE Fan Frame.
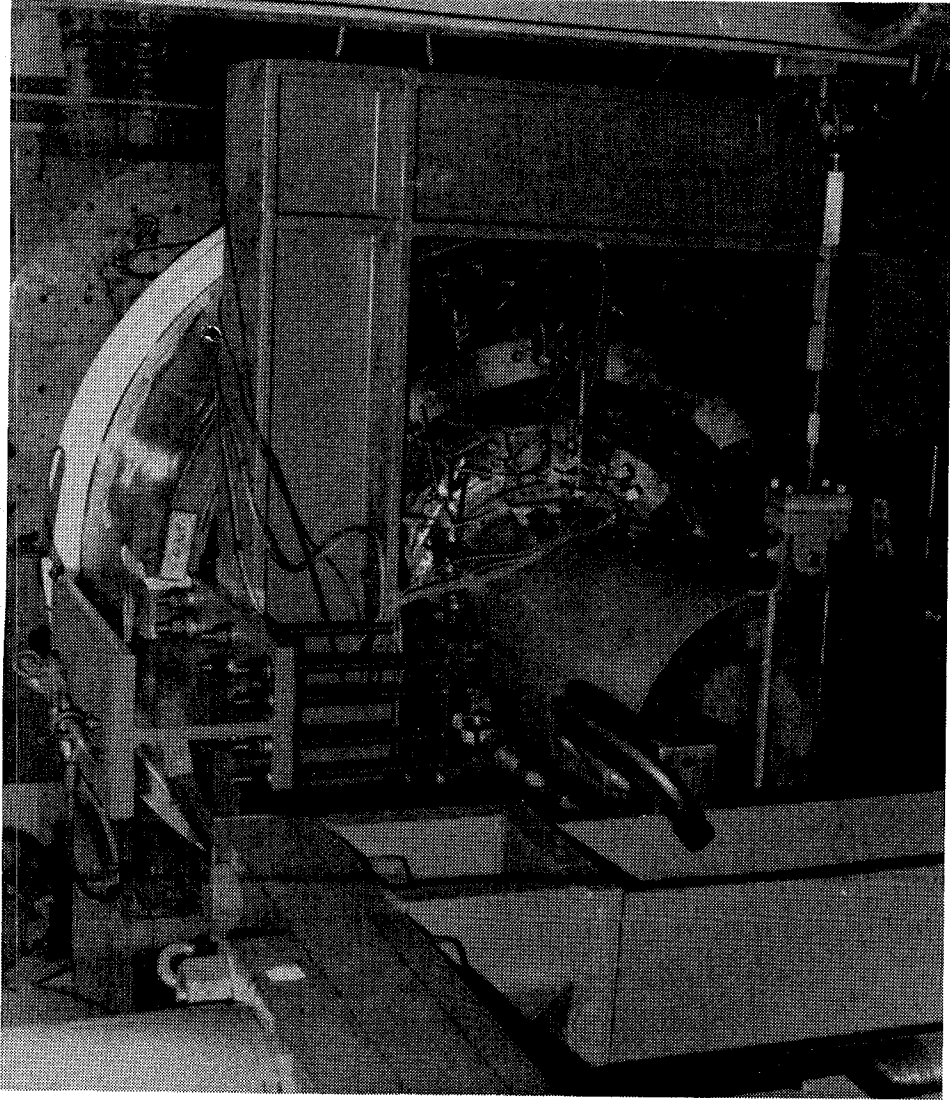
Figure 67. Static Test Setup.
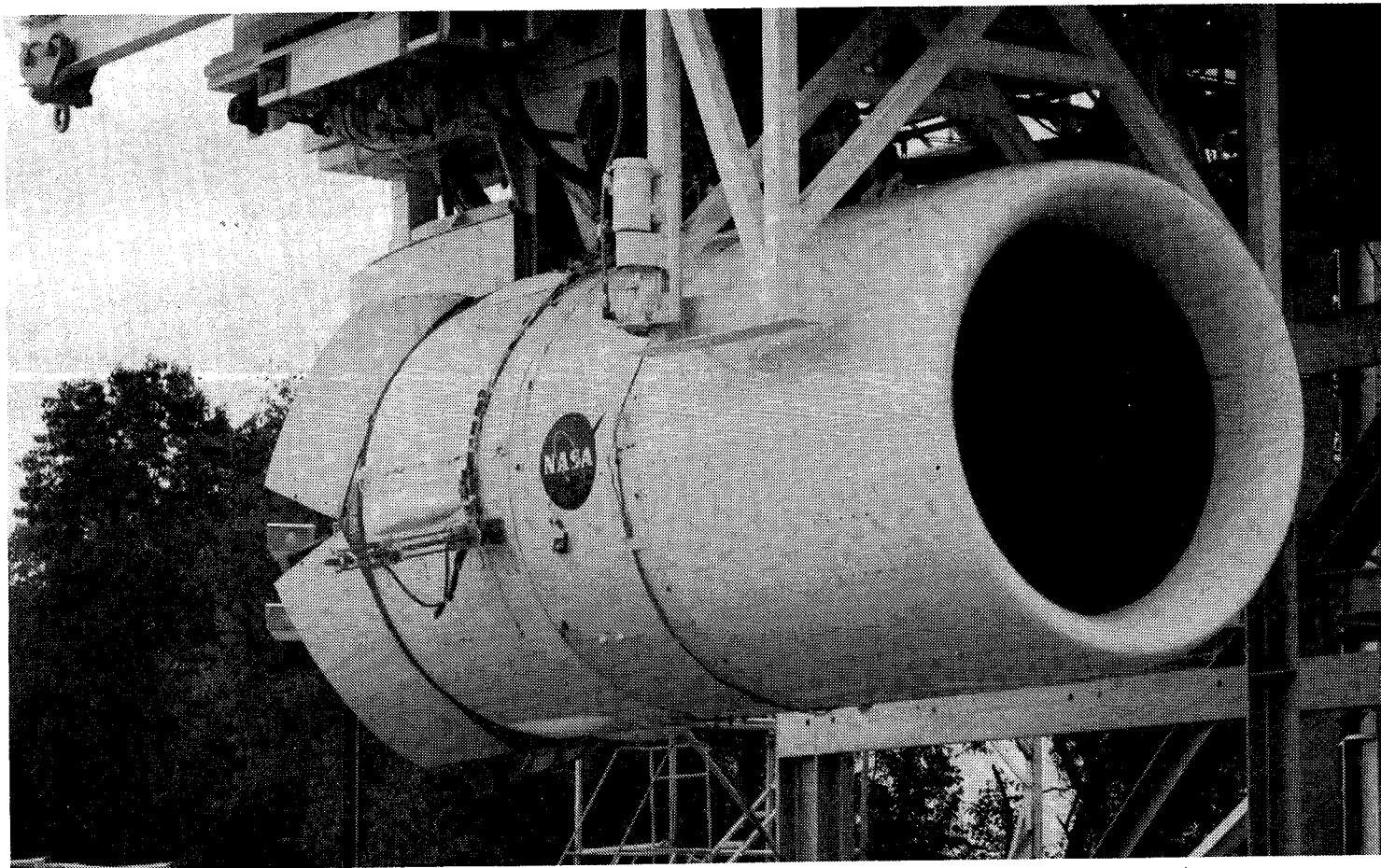
Figure 68. UTW Composite Nacelle.
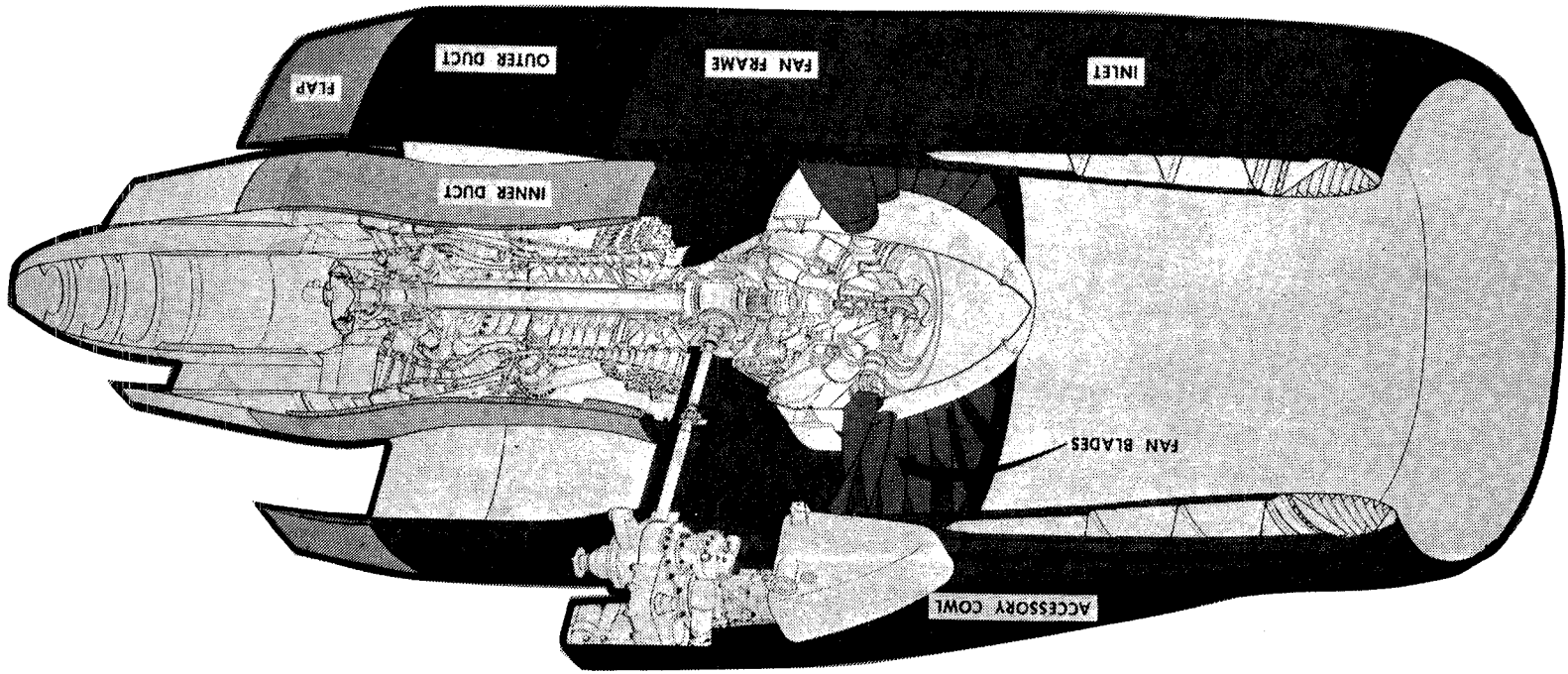
the integral acoustic treatment with a 10% open-area face sheet on the inner flowpath. The depth of the honeycomb core on the inner barrel varies as dictated by acoustic requirements. The porosity is molded into the face sheet as it is cured; this is now the practice in making CF6 fiberglass sound panels. The outer barrel is the primary load path. Both barrels are additionally supported by composite ring stiffeners. The leading edge was made from glass/epoxy for the QCSEE demonstrator but would be titanium for a flight engine due to anti-icing requirements. The critical inlet loads result from a 3-g stall in combination with a dynamic landing. Typical stresses, deflections, and margins of safety are shown in Table XVII.

The inlet is attached to the fan casing by 16 rotating latches. These points are the only critical local loads applied to the inlet; therefore, a subcomponent test, see Figure 70, was conducted of this area. The latch-housing failure was within 1% of the rated latch capability. Analysis indicates that six consecutive latches would have to be open before failure would occur at maximum load.

3.7.2 Outer Cowl and Fan Nozzle

Both of these components were fabricated in the same manner as the inlet, using the same materials. They are of full-depth honeycomb-sandwich construction with Kevlar/epoxy outer skin, aluminum-honeycomb flex core, and graphite/epoxy inner skin and structural rings. The only purpose for using graphite for the inner skins was the 15% to 20% porosity required for acoustics. At that time, it was felt that this porosity could best be obtained by laser drilling, and the initial attempts at laser drilling Kevlar/epoxy had not been as successful as laser drilling graphite/epoxy.

The pressure loading of these components is shown in Figure 71. Typical stresses resulting from this loading are shown in Table XVIII along with the allowable stresses obtained from coupon testing. Several critical joint areas were also checked by subcomponent tests.

The fabrication of these components was reasonably straightforward; both were built-up on male tooling. The outer cowl is shown in Figure 72 as the outer surface of the honeycomb is being machined prior to bonding on the outer skin - the last major operation. The nozzle-actuator housing pans can be seen as well as the tunnels for routing the hydraulics and sync cables to the actuators. The completed outer cowl is shown in Figure 73. The piano hinge which attaches the cowl to the pylon can be seen. The external fairings for the actuators can also be noted.

The only difference in construction of the fan nozzle was in inclusion of spring-loaded seals in the ends of the nozzle flaps which sealed the flaps against leakage in the forward-flight nozzle position. These seals separated when the nozzle was in the reverse-thrust position as shown in Figure 74.

Table XVII. Inlet Stresses and Deflections at Maximum Load Conditions.

3g Stall Plus Dynamic Landing

Type	Stress Calculated N/cm² (psi)	Stress Allowable N/cm² (psi)	Safety Factor	Deflection cm (in.)
Compression	1400 (2034)	12,377 (17,950)	7.8	0.058 (0.023)
Tension	1583 (2296)	27,097 (39,300)	16.1	
Shear	378 (584)	6033 (8750)	14.1	0.414 (0.163)
Burst	1806 (2620)	27,097 (39,300)	14.0	
Crush	3910 (5672)	12,377 (17,950)	2.2	

Table XVIII. Typical Outer-Cowl Stresses.

Component	Mode	Calculated Stress/Load	Allowable Stress/Load
Outer Skin	Buckling	18,450 N/cm² (26,760 psi)	45,330 N/cm² (65,740 psi)
Forward Ring	Compression	165 N/cm² (240 psi)	910 N/cm² (1320 psi)
Aft Ring	Bending	23,277 N/cm² (33,760 psi)	77,221 N/cm² (112,000 psi)
Piano Hinge Fast.	Bearing	10,782 N (2,424 lb)	52,698 N (11,847 lb)
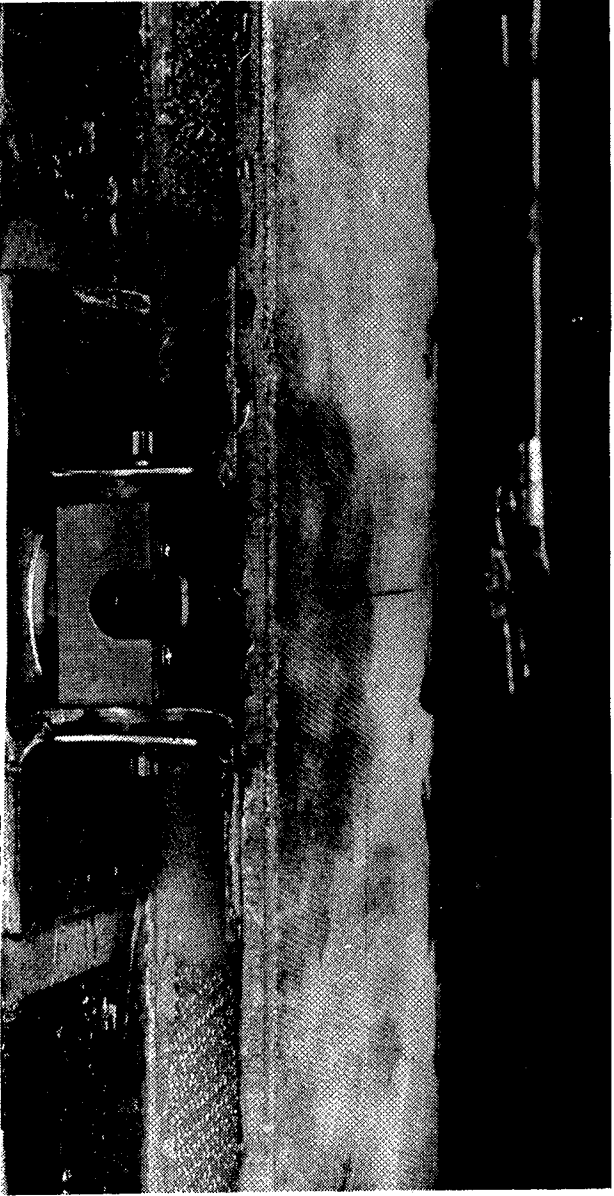
Figure 70. Inlet-to-Frame Attachement Test.
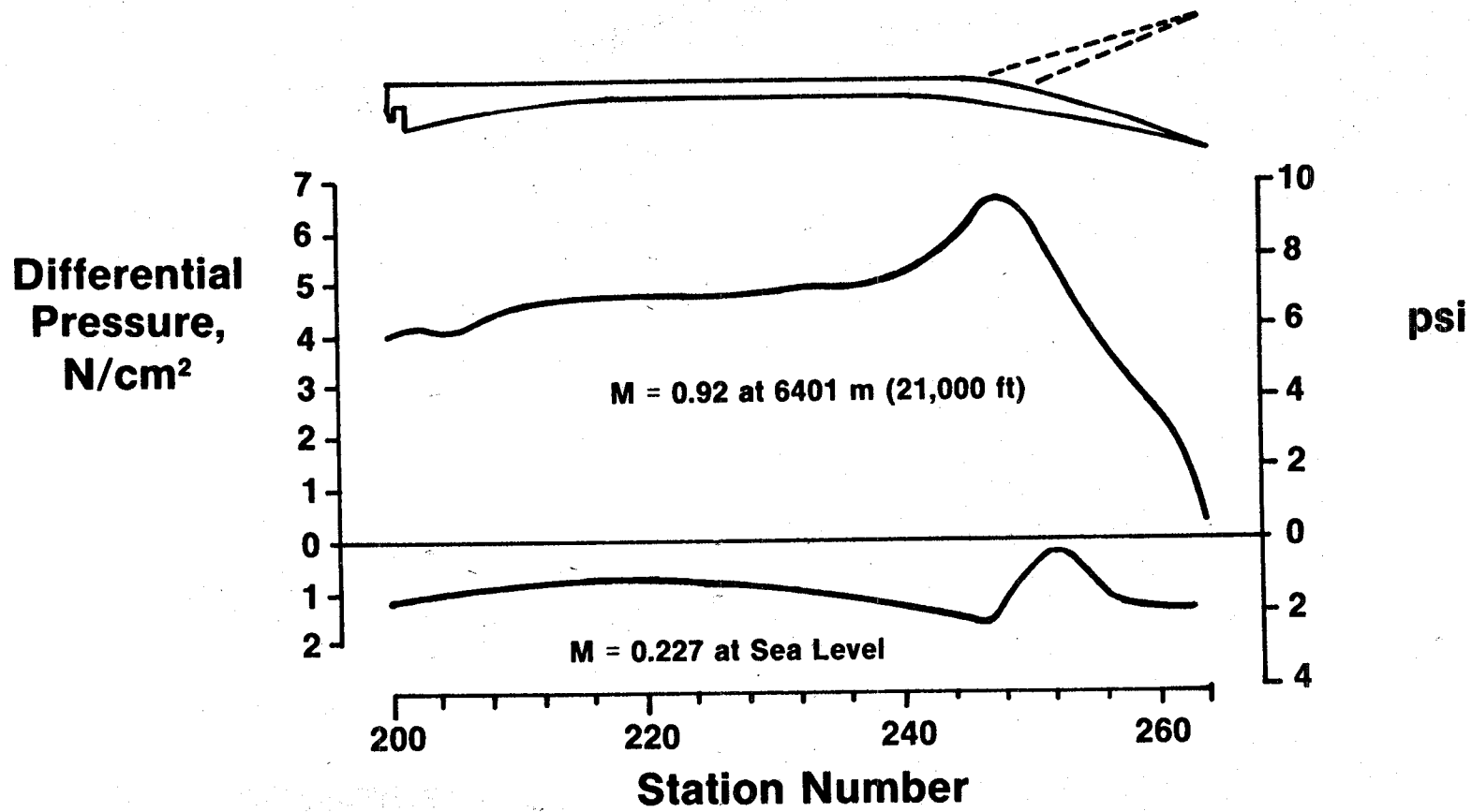
Figure 71. Differential Pressures.
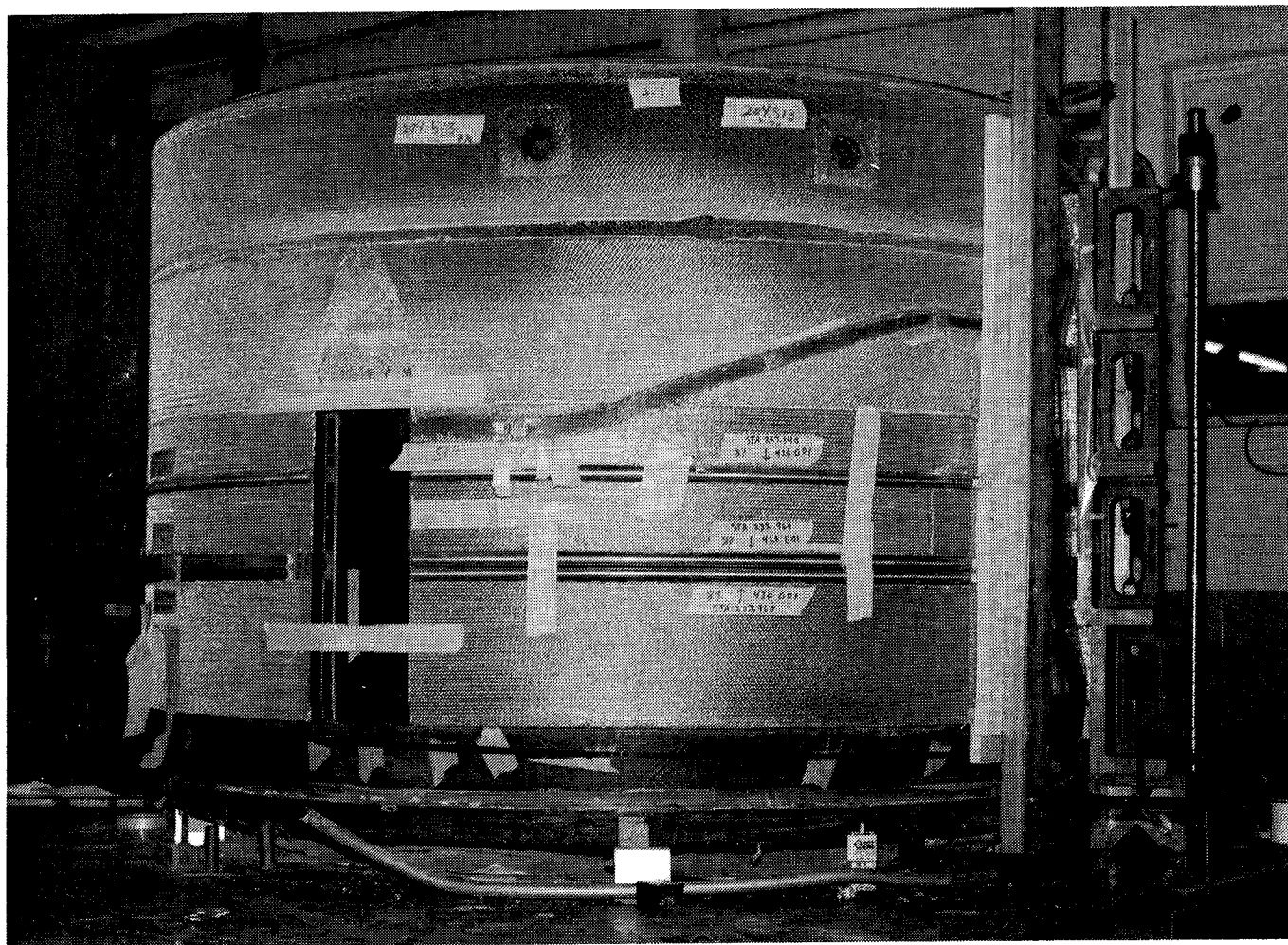
Figure 72. Outer Cowl Fabrication.
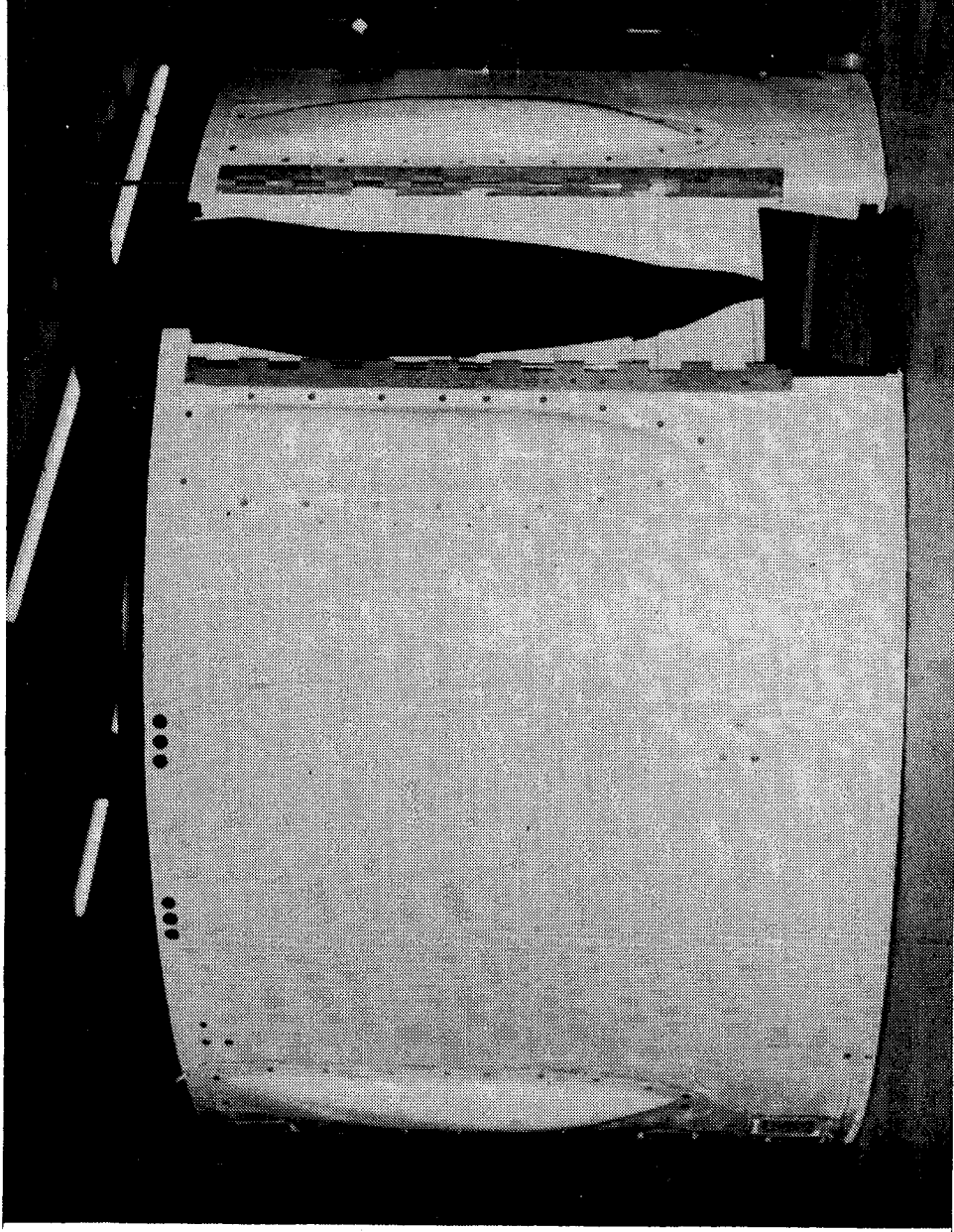
Figure 73. Completed Outer Cowl.

115
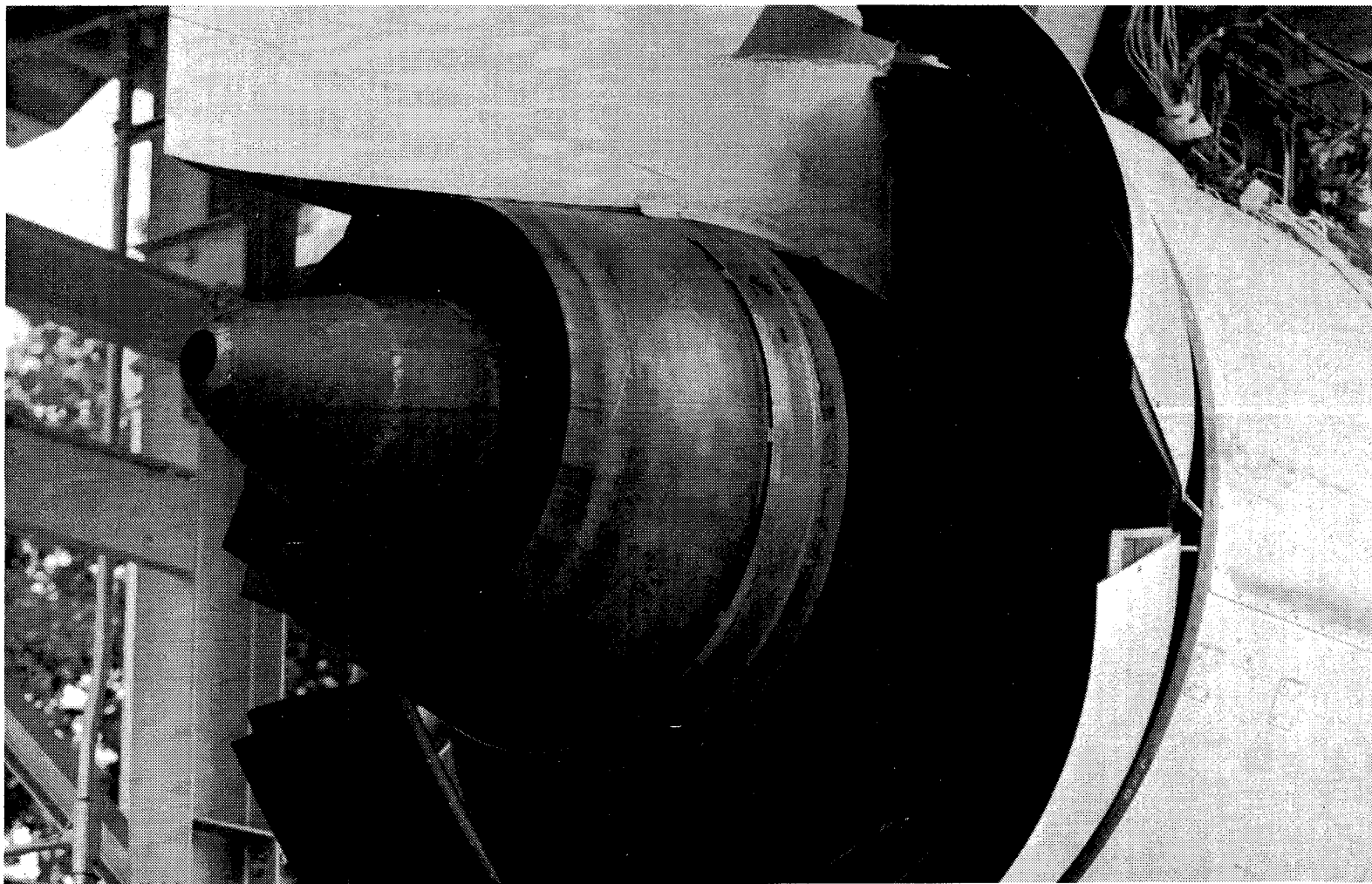
Figure 74. Fan Nozzle.

The most critical area in the outer-cowl/fan-nozzle system was the hinge ring in the back end of the outer cowl which supports the fan nozzle. This area was proof-tested satisfactorally in the test shown in Figure 75.

3.7.3 Inner Cowl

The most ambitious application of composites to the QCSEE nacelle-type hardware was in the area of the cowl; temperatures precluded the use of the familiar reinforced-epoxy materials. Even with a typical heat shield installed, the operating-temperature requirements were beyond epoxy capabilities, as shown in Figure 76.

Based on this information, it was decided to employ the NASA-developed PMR 15 polyimide type resin system. This system not only met the temperature requirements but is relatively easy to process and produces low-void-content laminates. Woven graphite T300 cloth was chosen as the reinforcement because it provided the needed stiffness and was easier to fabricate with than tape. This is particularly true when using the PMR system because of its lack of tack compared to epoxies. This material could also be laser drilled to get the 15% to 25% porosity required for acoustic treatment in this component. The HRH 327 fiberglass/polyimide core was used because of temperature considerations.

Using these materials, a core-cowl design was developed that resulted in a structure with typical ultimate calculated applied stresses as shown in Table XIX. Coupon-test results were used to determine the allowable stresses in the table. The completed core cowl is shown in Figure 77. The steel aft ring that forms the slip joint with the outer side of the core nozzle can be seen along with the hinges that attach the core cowl to the pylon. Each half of the core cowl was fabricated in two pieces due to the size of the laboratory autoclave; this would not be necessary in production. The split line can be seen in the photograph. An interior view of the core is shown in Figure 78. The flight-weight core cowl would incorporate a standoff heat shield (steel) in the aft portion of the cowl. This heat shield was not built for the demonstrator engine, so a heat blanket was installed in its place and shop air introduced in sufficient quantities to keep the core-cowl temperature at the levels they would have been if the heat shield had been installed.

3.8 DIGITAL CONTROL SYSTEM

A digital control was specified for the QCSEE propulsion system in anticipation that this technology would be required for an advanced, short-haul, aircraft system. This anticipated need, in conjunction with the general trend toward the use of digital computation in aircraft controls, led to the requirement that the control be engine mounted for exposure to the vibratory and thermal environment. As a result of this development effort, a digital control technology base has been established for the application of digital controls on many kinds of future aircraft-propulsion systems.
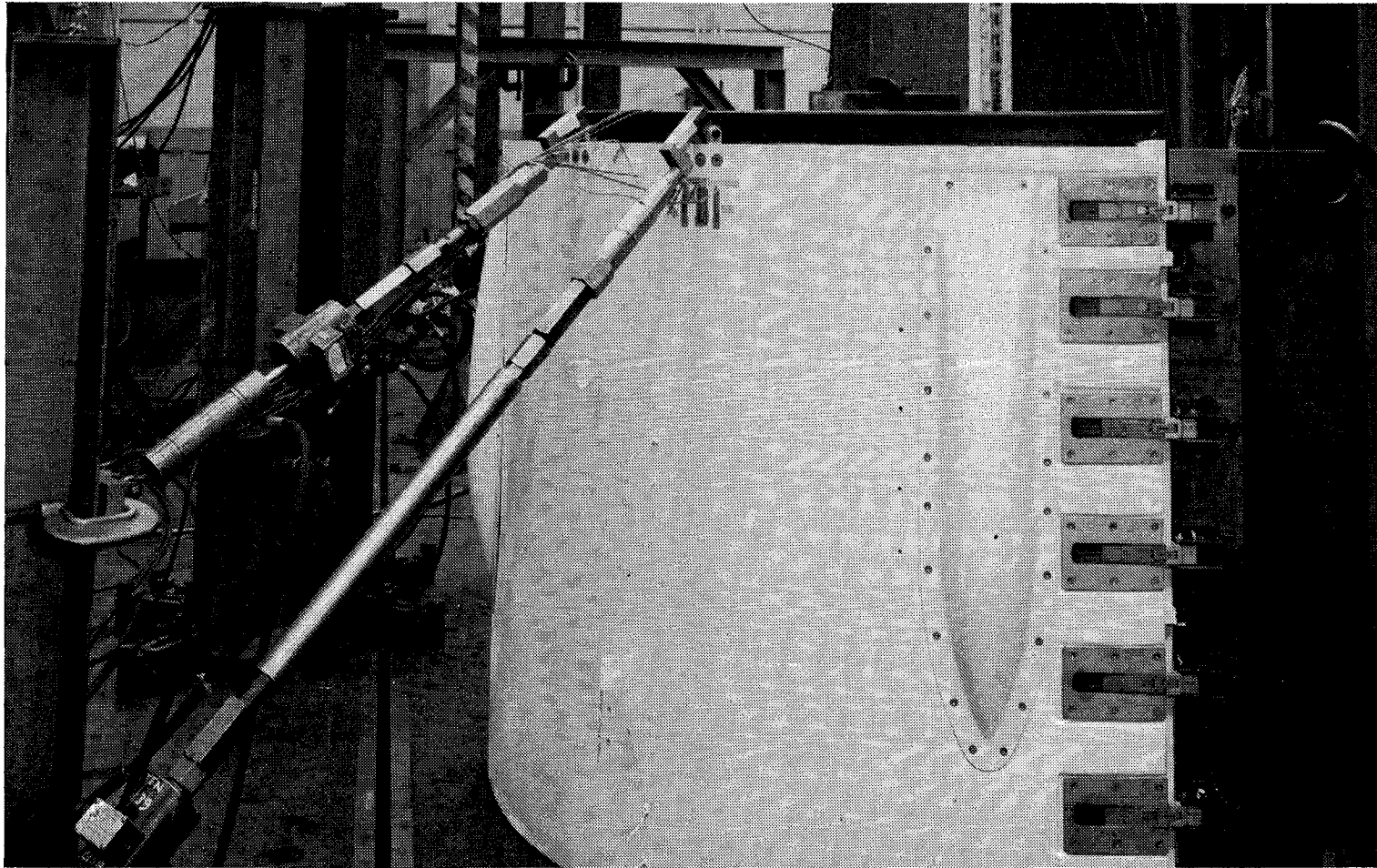
Figure 75. Outer Cowl Static Load Test.
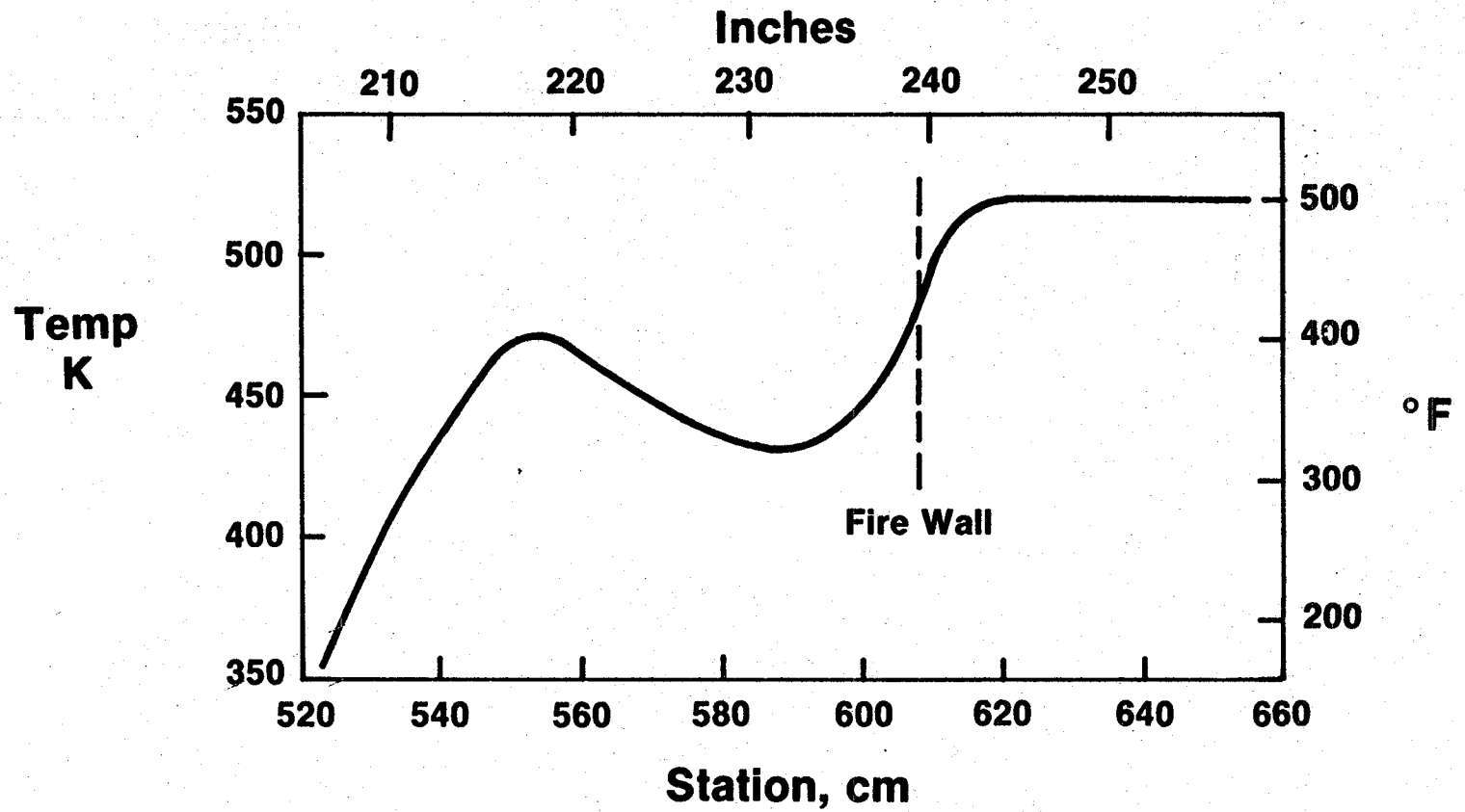
Figure 76. Inner Core Cowl Estimated Temperatures (Heat Shield Installed).

Table XIX. Typical Core-Cowl Stresses.

Load Condition	Component	Ultimate Calc. Stress N/cm² (psi)	Allowable Stress N/cm² (psi)
Forward Thrust	Outer Face Sheet Tension	8480 (12,300)	19,240 (27,900)
Reverse Thrust	Outer Face Sheet Compression	2290 (3324)	12,480 (18,100)
Forward Thrust	Inner Face Sheet Compression	11,420 (16,560)	29,990 (43,500)
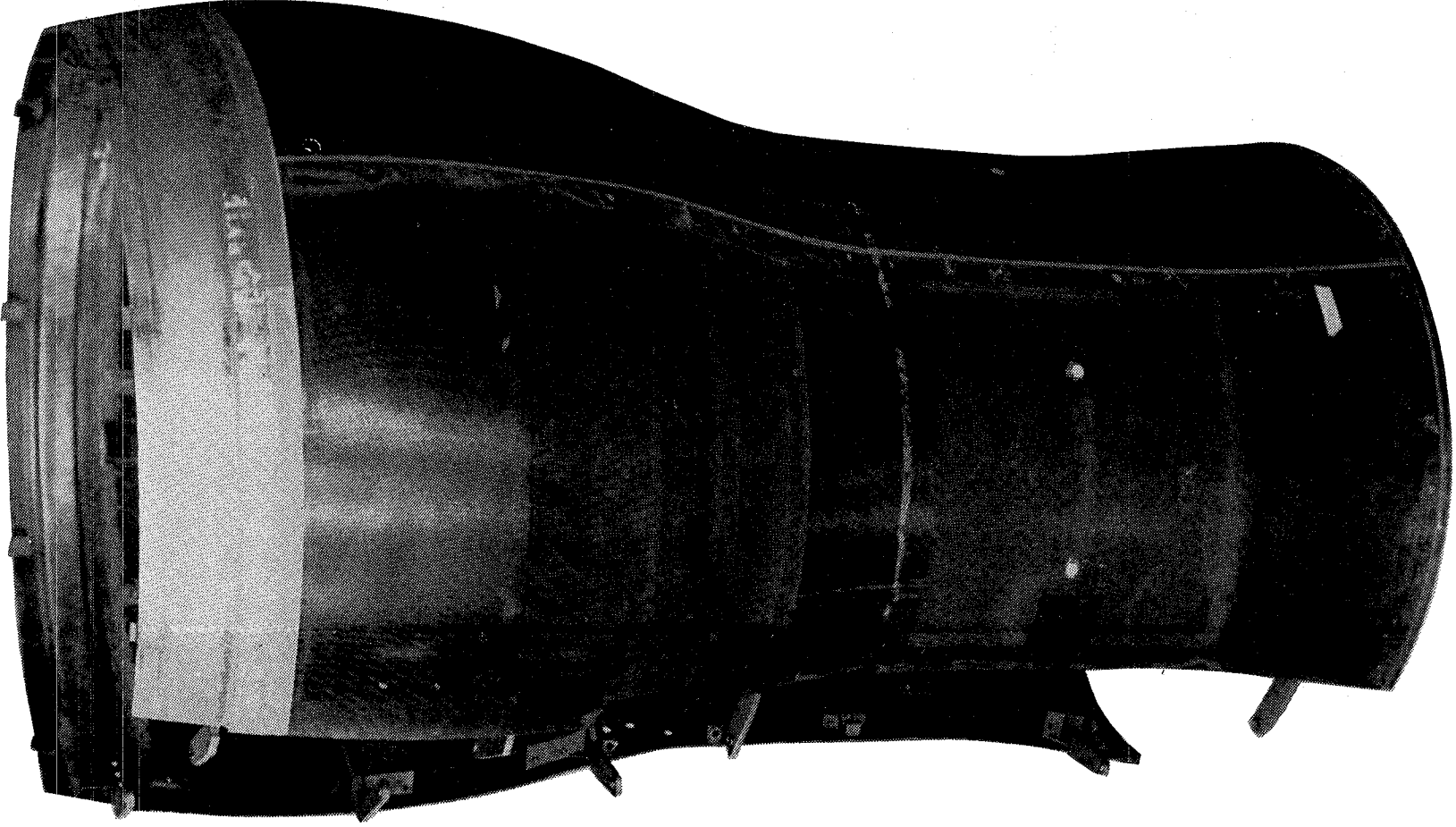
Figure 77. Completed Core Cowl.
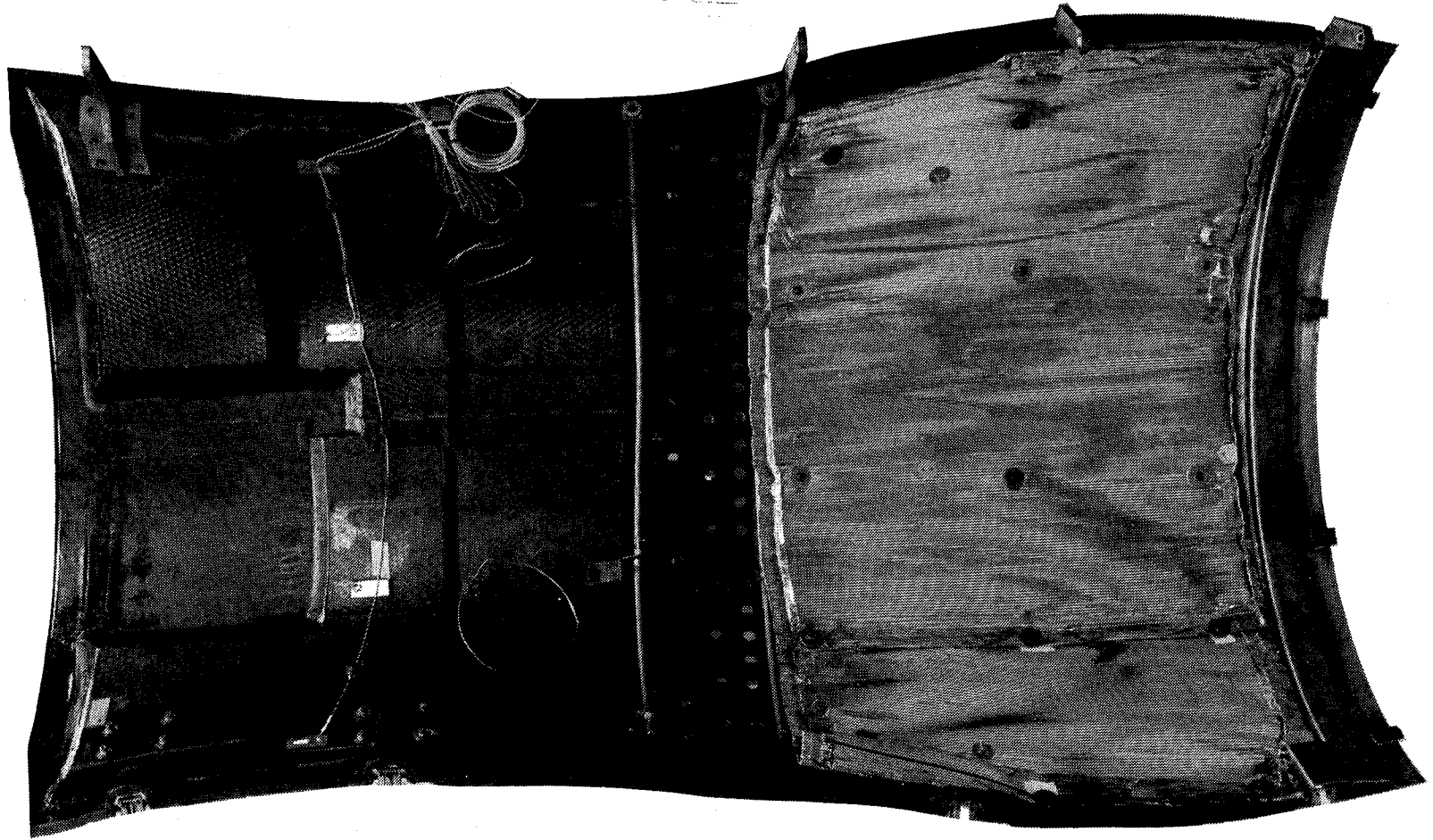
Figure 78. Core Cowl Interior View.

3.8.1 UTW Design Requirements

The control system design was based on a set of control-system requirements developed from the needs of a short-haul aircraft system. The primary control-system requirements are:

- Set Percent Rated Thrust

- Maintain Engine Safety Limits

- Reduce Pilot Work Load

- Control Inlet Mach Number

- Provide Rapid Thrust Response

- Facilitate Engine-Condition Monitoring

- Interface with Aircraft Digital Computer

One of the primary functions of the propulsion control is to manipulate the engine variables to achieve the design thrust levels. The use of a digital control allowed the development of control-system logic that related engine thrust to measurable engine parameters. These parameters were integrated and scheduled so that cockpit power-lever position (percent power setting) was directly related to percent of rated thrust. The thrust parameter selected for the UTW engine was propulsion system pressure ratio: compressor-discharge static pressure divided by free-stream total pressure (P_{S3}/P_{T0}). The basic pressure ratio schedule was biased by engine inlet and aircraft operating conditions to achieve a relationship between rated thrust and cockpit power-lever position over the flight envelope.

To achieve safe operation over the flight envelope, the control system was designed to automatically maintain engine operation within normal physical limits. The control system incorporated logic to prevent engine overspeed or overtemperature. The specific mechanization of the limits will be discussed later.

Since operation of a short-haul aircraft into intercity airports could place heavy demands upon the pilot, it was required that the system design should attempt to reduce pilot work load. To accommodate this objective the system was designed to automatically integrate the propulsion-system variables and engine safety limits.

One of the primary objectives of the QCSEE program was the development of noise-reduction technology. Previous experiments have shown that operation with a high inlet-throat Mach number provides a substantial reduction in fan noise. To achieve this noise-reduction benefit, it is necessary to provide automatic control of inlet-throat Mach number at high power settings, and demonstration of this capability was a UTW engine control requirement.

Studies by NASA prior to initiating the QCSEE program revealed that short-haul aircraft require rapid thrust response to achieve a safe go-around in the event of an engine failure during landing approach. As a result of these studies, the propulsion system was required to provide a thrust change from 62% to 95% in one second. This thrust-response rate is approximately twice as fast as current engines.

Digital computers have the inherent capability to process and transmit massive amounts of data rapidly. It was decided to utilize this capability, and the QCSEE digital control was designed to collect and transmit 48 engine-condition parameters such as speeds, pressures, temperatures, and operating modes. The data were stored and displayed in the engine control room. With appropriate integration of the engine and aircraft digital controls, a comprehensive condition-monitoring system could be provided to provide maintenance-action information.

To be utilized effectively, a propulsion-system digital control should have the capability to interface with an aircraft digital control system. Propulsion-system commands from the aircraft and propulsion-system operational data would be transmitted through this interface. Recognition of this need led to the requirement for a digital interface and transmission system between the experimental propulsion system and the engine control room.

3.8.2 UTW System Description

Figure 79 is a simplified schematic of the UTW propulsion control system. The UTW engine incorporated four manipulated variables: fan nozzle area, fan pitch angle, engine fuel flow, and core stator angle. The system to control these variables can be divided into three functional groups: the system sensors, represented by the engine sensors and digital commands from the control room; the computer, representd by the digital control; and the system power, represented by the system actuators. The digital control is the heart of the system; hence, it incorporates all of the control laws and logic to regulate the variables from engine idle to takeoff thrust. The other major components in the system are: fuel pump, hydromechanical control, and hydraulic pump.

In this control system, the fan nozzle and fan-pitch actuators were manipulated solely by the digital control. Fuel flow was varied as programmed by the digital control; however, the hydromechanical control had the authority to override the digital control, and it also schedules the core stator-angle position. This mechanical override capability was incorporated for several reasons: development program cost, digital control memory size, and experimental engine safety. A secondary electromechanical power-demand link to actuate the fuel stopcock and set a core-speed limit was also implemented for experimental engine safety.

The command and data link was a serial, time-multiplexed, data-transmission system consisting of digital serializers, optical isolators, line
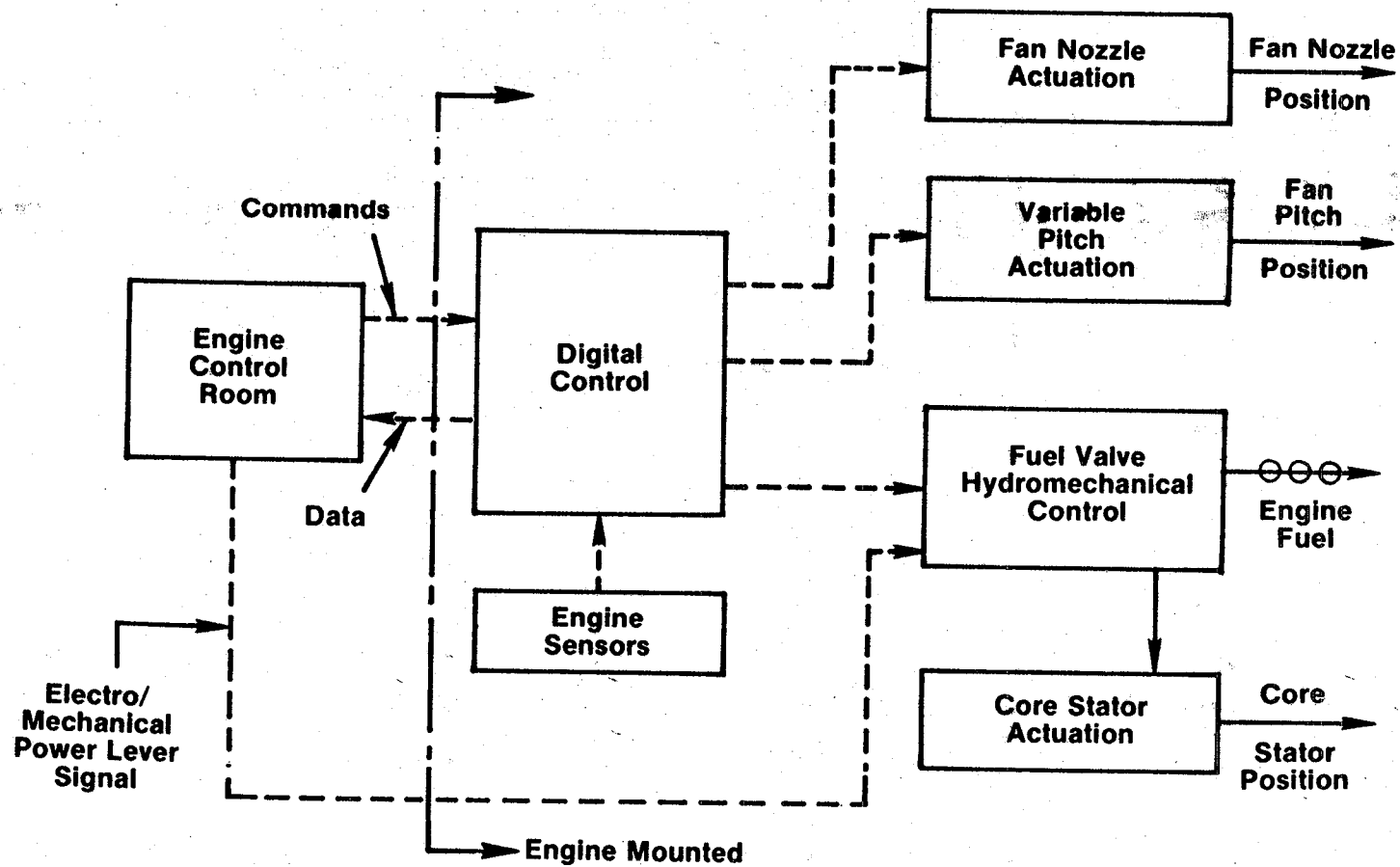
Figure 79. UTW Control System Schematic.

drivers, and line receivers. Data were transmitted and received at a one-megahertz rate. The command and data-transmission process was regulated by the engine-mounted digital control.

An engine-driven, accessory-gearbox-mounted, F101 engine fuel pump was utilized for fuel system pressurization and fuel delivery. The pump incorporates a fixed-displacement vane element and a centrifugal boost element to charge the intake of the vane element. Rated pump speed is 6690 rpm; at this speed it has a capacity of 2.7 dm^3/sec (42.8 gpm) with a pressure rise of 6.93 MN/m^2 (1000 psi). The pump was designed and manufactured by Sperry-Vickers.

A modified F101 engine fuel control was used for fuel metering. This control uses a constant metering head and incorporates a servo-operated bypass valve to accommodate excess pump flow. The control incorporates hydromechanical devices for speed governing and for fuel and core stator scheduling and provides a fuel-system interface with the digital control. The control was designed and constructed by Woodward Governor Company.

The UTW engine incorporated an engine-driven, piston-type, pressure-compensated, hydraulic pump as a power supply for variable nozzle and variable fan-pitch actuation. The pump supplies a constant-pressure, variable flow to the system servovalves - which are regulated by the digital control. The pump capability at 100% speed is 3.08 dm^3/sec (48.8 gpm) with a pressure rise of 23.6 MN/m^2 (3350 psi). This relatively large flow capacity was required to provide rapid variable-pitch actuation at low engine speeds. The pump was designed and manufactured by Abex Corporation.

Figure 80 shows a photograph of the engine-mounted digital control. The package shown in the figure incorporates pressure transducers for sensing the pressures used in engine control, a separately powered analog control for limiting fan overspeed, and the digital control. The unit is powered by a variable-frequency, variable-voltage, engine-driven alternator. Power dissipation is in the order of 100 watts and is handled by air cooling. The cooling-air source is free-stream total pressure, and the pressure sink is the fan inlet.

The digital control integrates the following functions: sensor excitation and signal conditioning, data acquisition, digital-to-analog conversion, output-signal conditioning, power-supply regulation, and special-purpose digital computation. The digital computer is composed of five major sections: program memory, read/write memory, clock, central processor, and input/output unit. The computer has the capability to add, substract, multiply, divide, and branch upon command. The machine data word is 12 bits in length. The computer instruction set consists of 31 different instructions.

The program memory incorporates instructions that define the control laws and logic. The UTW QCSEE control memory incorportes 3071 instructions to define the complete control strategy. Each instruction in the program memory

126
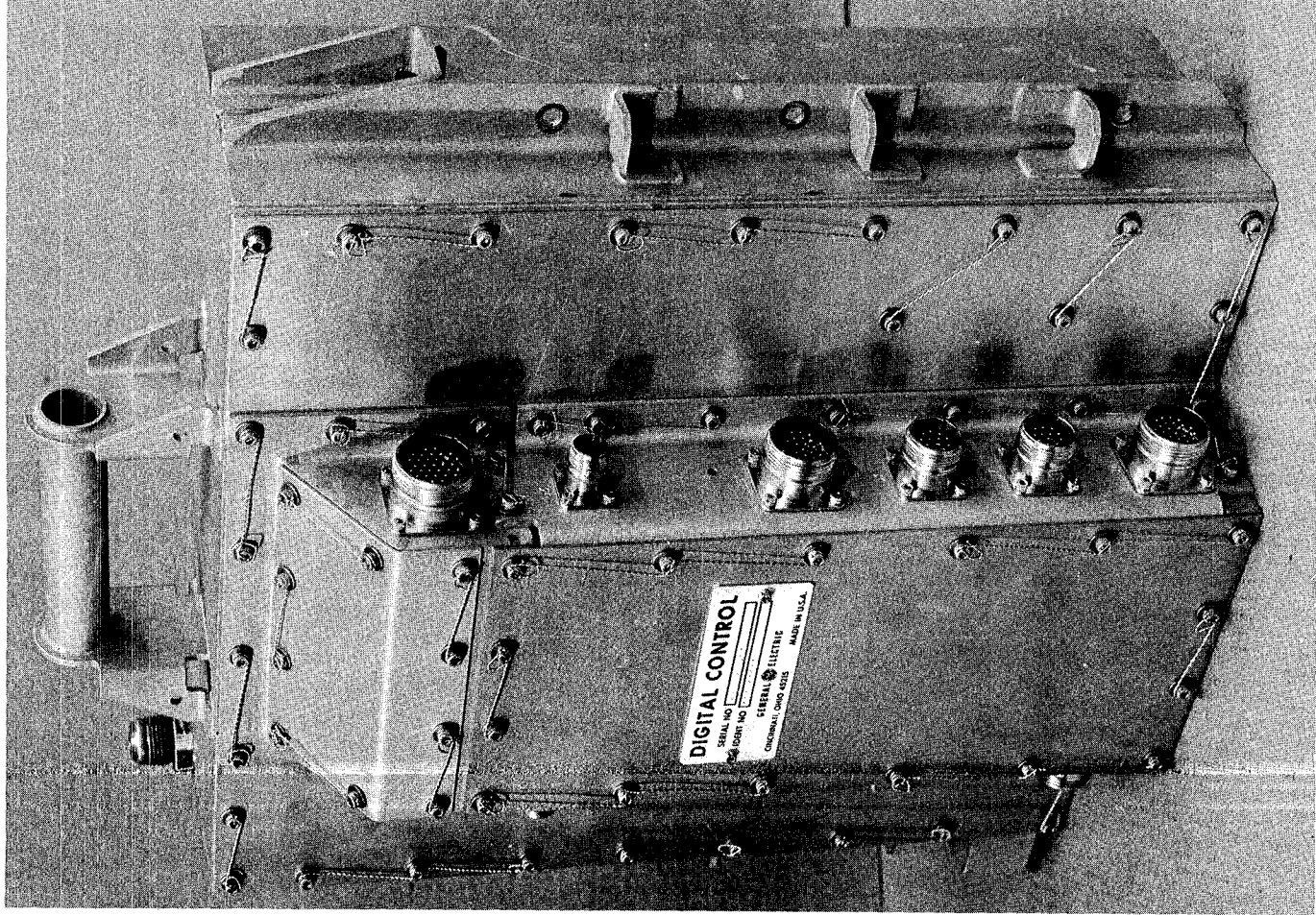
Figure 80. UTW QCSEE Digital Control.

is sequentially transmitted to the central processor for execution. The timing for instruction execution is controlled by the central processor. Execution time for the UTW QCSEE program is 7.46 milliseconds. Hence, the program repeats 134 times per second.

The electrical components in the digital control consist of a combination of discrete and medium-scale integrated components. A type of logic called the low power Schottky TTL was selected for digital components. These devices were selected because they offer the best speed-power product. The digital control was designed and fabricated by the General Electric Company.

Figure 81 is a schematic of the UTW engine showing the control system sensors. All of the measured parameters, except core stator angle, and core inlet temperature, were collected by the digital control and used in the propulsion control logic. In addition, they were subsequently transmitted to the control room for display.

Fan inlet total temperatures and free-stream total pressures were measured to evaluate flight conditions and used for power-control scheduling.

Inlet static pressure was combined with free-stream total pressure and used as a representation of inlet Mach number. The static pressure was measured at the 40% axial station in the inlet duct. This was done to eliminate pressure variations due to crosswinds. An empirical equation was used to convert the measured pressure ratio to average inlet-throat Mach number.

Free-stream total pressure was also used along with measured compressor-discharge pressure to establish propulsion system pressure ratio - which is related to system thrust.

Fan pitch angle, fan nozzle area, and core stator angle were measured to allow for a loop closure in the control logic.

Fuel flow, compressor discharge temperature, and pressure were measured for use in the computation of turbine inlet temperature.

Core inlet temperature, core speed, and low pressure turbine speed were measured for use in physical speed limits, corrected speed limits, acceleration schedules, and core stator schedule compuations.

All of the sensors used in the system were current, state-of-the-art-type devices.

3.8.3 UTW Operating Characteristics

One fundamental task performed in designing an automatic control system was to define the system control mode. This control-mode-definition process relates the engine cycle variables (speeds, pressures, temperatures, etc.) to the available manipulated variables (fuel flow, fan pitch, nozzle area) to

128

Fan Inlet Total
Temperature

Free
Stream
Total
Pressure

Compressor
Discharge Total
Temp. +
Static Pressure

Fan Nozzle Area

Fan Pitch
Angle

Core Inlet
Total Temp.

Core
Speed

Low Pressure
Turbine
Speed

Inlet Static
Pressure

Core Stator
Angle

Fuel
Flow
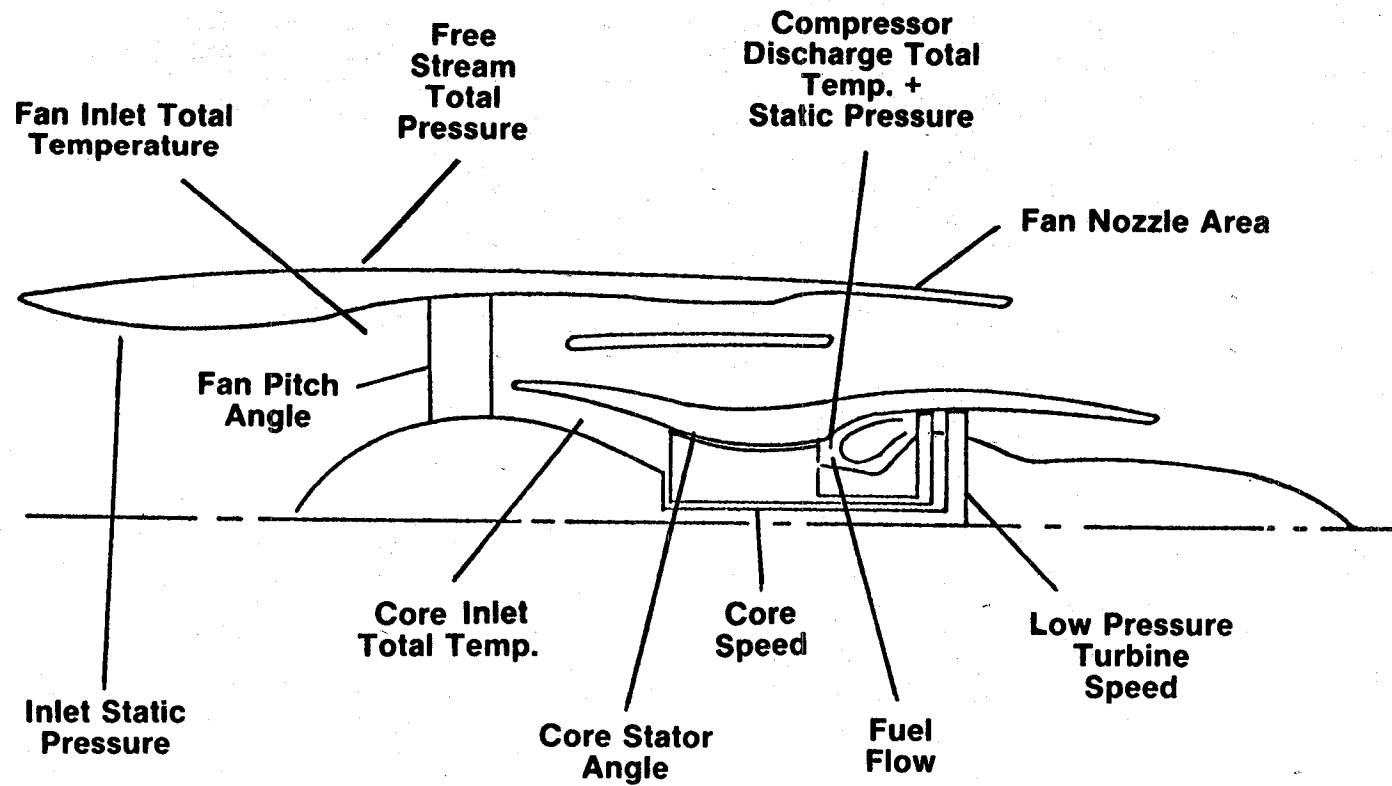
Figure 81.   UTW Control System Sensors.

achieve control of the vehicle and to obtain the desired operating character-
istics. The objective of the analysis is to choose practical combinations of
cycle parameters and manipulated variables which result in small variations
in the engine-cycle-dependent variables (i.e., thrust, sfc, stall margin) at
important operating conditions. The analysis process involves the comparison
of potential control modes on the basis of accuracy, schedulability, stability,
response, and other performance considerations.

The UTW QCSEE incorporated three prime manipulated variables: fuel flow,
fan pitch, and fan nozzle area. During the mode-selection process these vari-
ables were paired with many combinations of engine cycle variables. The anal-
ysis resulted in selection of engine pressure ratio (P_{S3}/P_{T0}), fan speed,
and inlet Mach number as controlled variables. These variables were paired
with fuel flow, fan pitch, and fan nozzle area.

As a result of this pairing of variables, selection of a percent power
setting through movement of the power lever causes the following: engine
fuel flow is varied to hold a scheduled engine pressure ratio, fan pitch is
varied to hold a scheduled fan speed, and fan nozzle area is varied to hold
a scheduled inlet Mach number. The above actions are implemented through
the digital control. This variation of the manipulated variables is con-
strained by both physical limits and cycle considerations. For example,
maximum fan nozzle area was limited to 1.87 m^2 (2900 in.^{2}) because at
this point the fan nozzle exit area became larger than the fan duct area,
and nozzle variations no longer affected inlet Mach number. Fan pitch was
limited to 10° closed from nominal due to actuator mechanical limits.

Figure 82 shows the relationship between fan nozzle area, inlet Mach
number, and percent power demand at sea level conditions. Over the com-
plete power setting range, the digital control tries to position the fan
nozzle to maintain an inlet Mach number of 0.79. However, in the lower
percent power setting region (<70%) the nozzle is scheduled to the maximum
area, and inlet Mach number varies as a function of power setting. As the
power demand is increased beyond approximtely 70% the fan nozzle area
begins to close to maintain a constant inlet Mach number.

Figure 83 shows the relationship between fan blade pitch angle, cor-
rected speed, and percent power setting at sea level standard conditions.
In the lower power-setting region fan speed varies with percent power setting
because the fan pitch is closed to its minimum position. As the percent
power setting is increased beyond approximately 55%, the fan pitch begins
to open toward the takeoff position to hold fan speed constant at approxi-
mately 95% - the scheduled fan speed for takeoff power. The fan speed is
held constant at the higher power settings for transient-response reasons
which will be discussed later.

3.8.4 UTW Automatic Safety Limits

As noted earlier, one of the primary control-system functions is to pre-
vent the engine from exceeding speed or temperature limits. To meet this

130

**Fan Nozzle
Area**

**Inlet
Mach
Number**
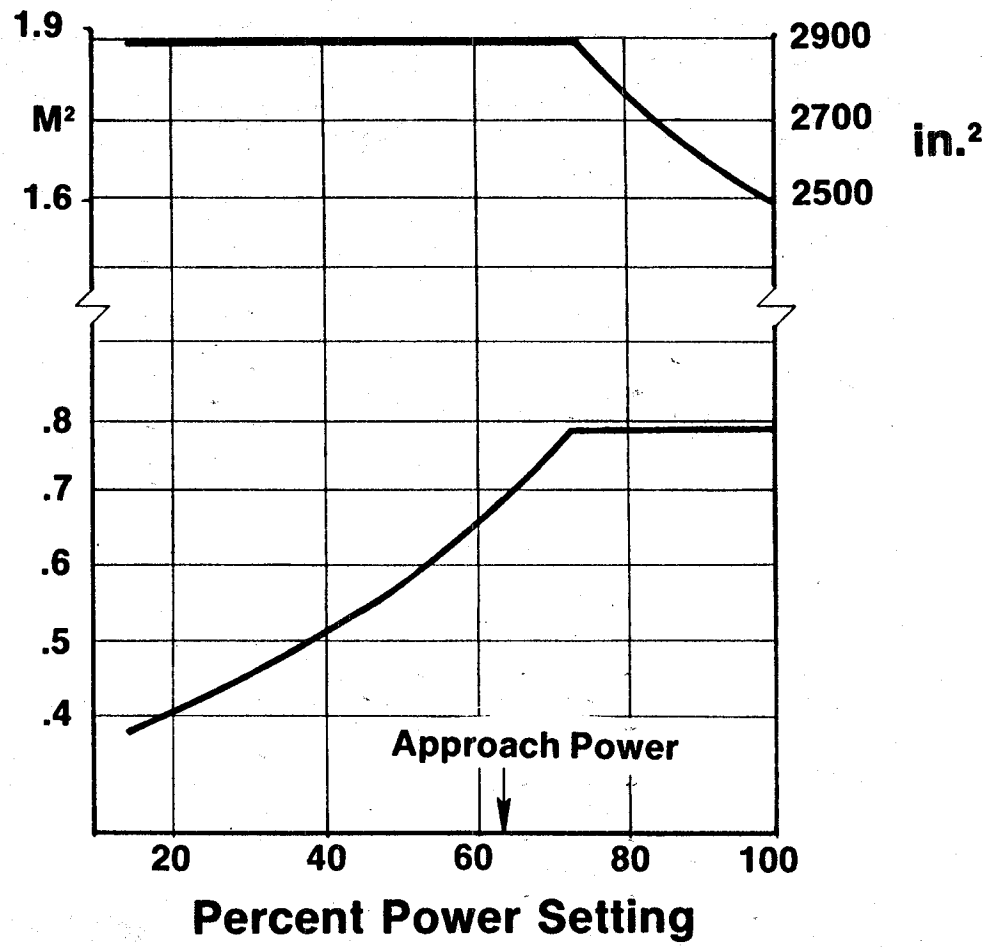
Figure 82. UTW Fan Nozzle Control Characteristics.
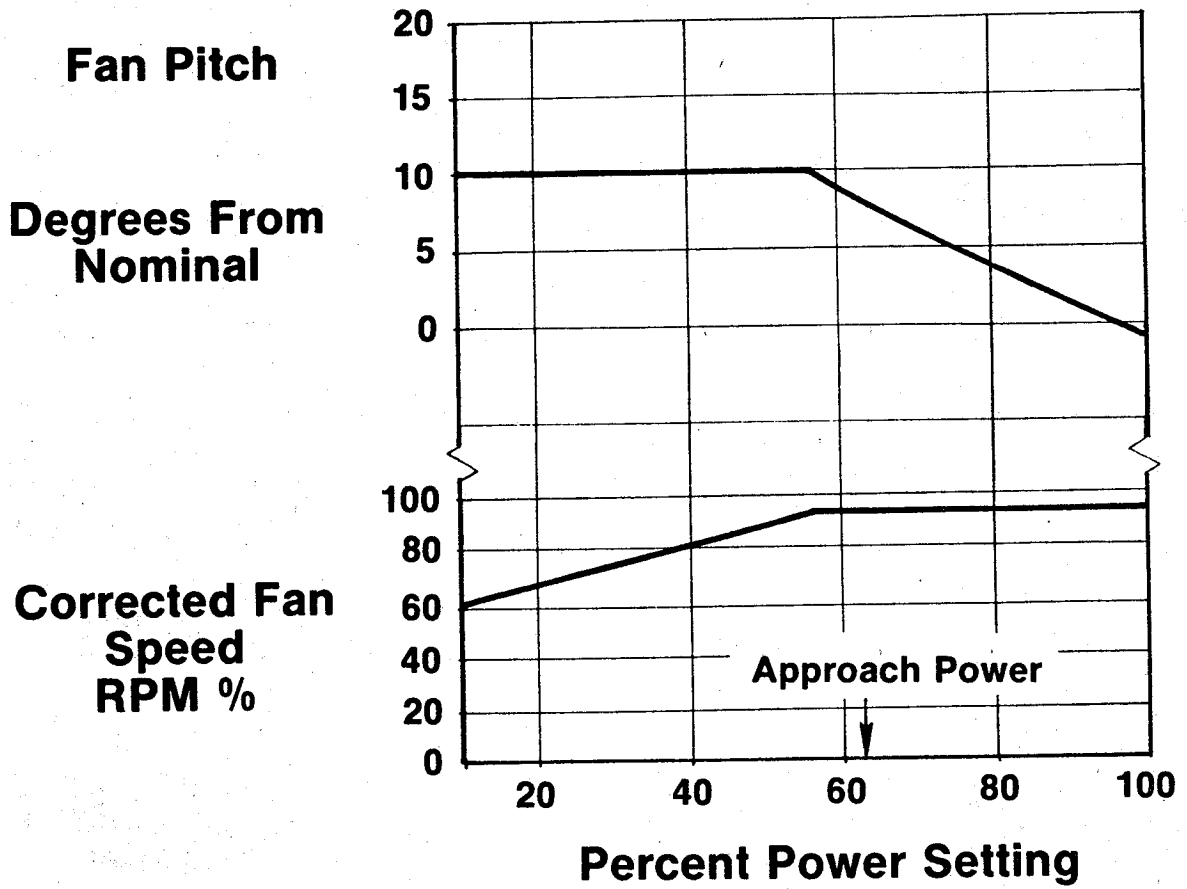
Figure 83. UTW Fan Pitch Control Characteristics.

requirement, limiting functions were incorporated in the hydromechanical and digital controls. The hydromechanical control incorporated a full-range, fly-ball governor on core speed; this would override the digital control input and reduce fuel flow if core speed attempted to exceed the scheduled value. The digital control memory incorporated fan speed and core speed limits which would cut-back fuel flow if the speed limit was reached. The digital control unit also incorporated a separate analog control to cut-off fuel flow on the experimental engine if overspeed occurred in the low pressure turbine due to loss of load. Loss of load could occur with a reduction gear failure or an extreme closure of the fan pitch at high power.

Turbine temperature was limited by a digital control function. The control memory incorporated an equation that calculated turbine inlet temperature as a function of fuel flow, compressor discharge pressure, and temperature. The control compared the calculated turbine inlet temperature with a limit and acted to cut-back fuel flow to prevent operation beyond this limit. The digital control received fan-case vibration signals from test facility instruments. The control program memory incorporated logic to automatically retard the experimental engine to idle power if vibration signals exceeded a safe level.

3.8.5 UTW Transient Response

As noted earlier, the QCSEE's were required to have rapid thrust-response capability. The specific requirement was to achieve a thrust change from 62% to 95% thrust in one second. Figure 84 shows the results of a study using a transient model of the UTW engine. The QCSEE requirement is noted on the figure. The dashed line shows the response of a conventional turbofan in which fan speed and core speed are both varied with fuel flow. The required response could not be achieved, with a conventional system, due to compressor stall and turbine inlet temperature considerations.

The solid line on Figure 84 shows the predicted thrust response with fan speed held constant through variation in the fan pitch angle. Holding fan speed constant results in the achievement of the required response since acceleration of the fan rotor is not required, and changes in fan pitch angle result in rapid changes in fan airflow.

3.8.6 OTW Design Requirements

The control-system requirements for the OTW engine were essentially the same as the UTW engine. However, the inlet Mach number control requirement was eliminated because the exhaust nozzle was manually varied, and two new requirements were added. These new requirements were:

● Failure indication and corrective action

● Full authority digital control

Figure 84. UTW Predicted Transient Response.

The first of these requirements is associated with a concept which allows continued operation after failure of an engine control-system sensor. The second requirement was added to allow further development of engine digital-control-system technology. The manner in which these requirements were implemented and demonstrated is discussed in the following sections.

3.8.7 OTW Control System Description

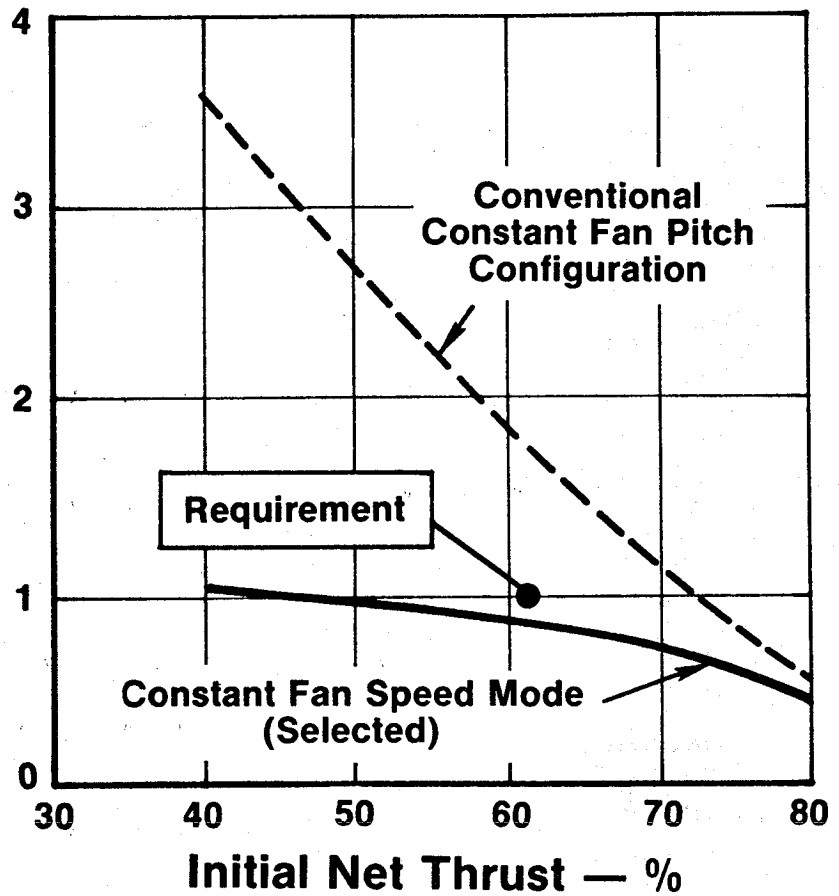Figure 85 is a simplified schematic of the OTW propulsion control system. The experimental engine incorporated two manipulated variables: engine fuel flow and core compressor stator angle. The system to control these variables can be divided into three functional groups. These are the system sensors, the digital control, and the system actuators. The digital control is the heart of the system; it incorporates all of the control laws and logic to regulate the variables from engine start to maximum thrust. The digital control is identical to the UTW control except the control program memory has been revised to incorporate the OTW engine characteristics. The other major components in the system are the fuel pump, hydromechanical control, and core stator actuators. These components are the same as on the UTW engine except for functional changes in the hydromechanical control. On the OTW engine, the hydromechanical functions associated with acceleration fuel and core stator scheduling were eliminated. These important functions were incorporated into the full-authority digital control program memory.

Figure 86 is a schematic of the OTW engine and shows the control system sensors. The schematic is similar to the UTW system except for the following: the fan pitch and fan nozzle sensors have been eliminated, the core stator angle is sensed with an electrical transducer, and the core inlet temperature is calculated from fan inlet temperature, fan speed, and a fan-efficiency function. This calculated value of core inlet temperature is used in a subsequent calculation by the digital control to establish corrected core speed.

3.8.8 OTW Operating Characteristics

A control system analysis similar to the UTW engine effort was performed to select the controlled- and manipulated-variable pairs. Since the OTW experimental engine incorporated only one primary manipulated variable (fuel flow), the analysis process was less complicated. The analysis resulted in the pairing of corrected fan speed with engine fuel flow. Corrected fan speed was chosen because of its close correlation with turbofan thrust. Furthermore, the analysis resulted in the decision to schedule the core compressor stators with corrected core speed because this relationship provides good control of compressor stall margin. As a result of the above selection, movement of the percent-power-demand selector causes the digital control to vary fuel flow to hold a scheduled corrected fan speed and to schedule the core stator angle as a function of corrected core speed.

The digital control also incorporates the engine acceleration fuel schedule. This acceleration fuel limit is composed of two primary schedules.

Electro/Mechanical Fuel Cutoff Signal

Commands

Engine Control Room

Full Authority Digital Control

Hydromechanical Fuel Valve (Control)

Engine Fuel

Data

Core Stator Actuation

Core Stator Position

Engine Sensors

Engine Mounted

Figure 85. OTW Control System Schematic.

Fan Inlet Total
Temperature

Free Stream
Total Pressure

Compressor
Discharge Total
Temp. +
Static Pressure

Inlet Static
Pressure

Core Speed

Core Stator Angle

Fuel Flow

Low Pressure
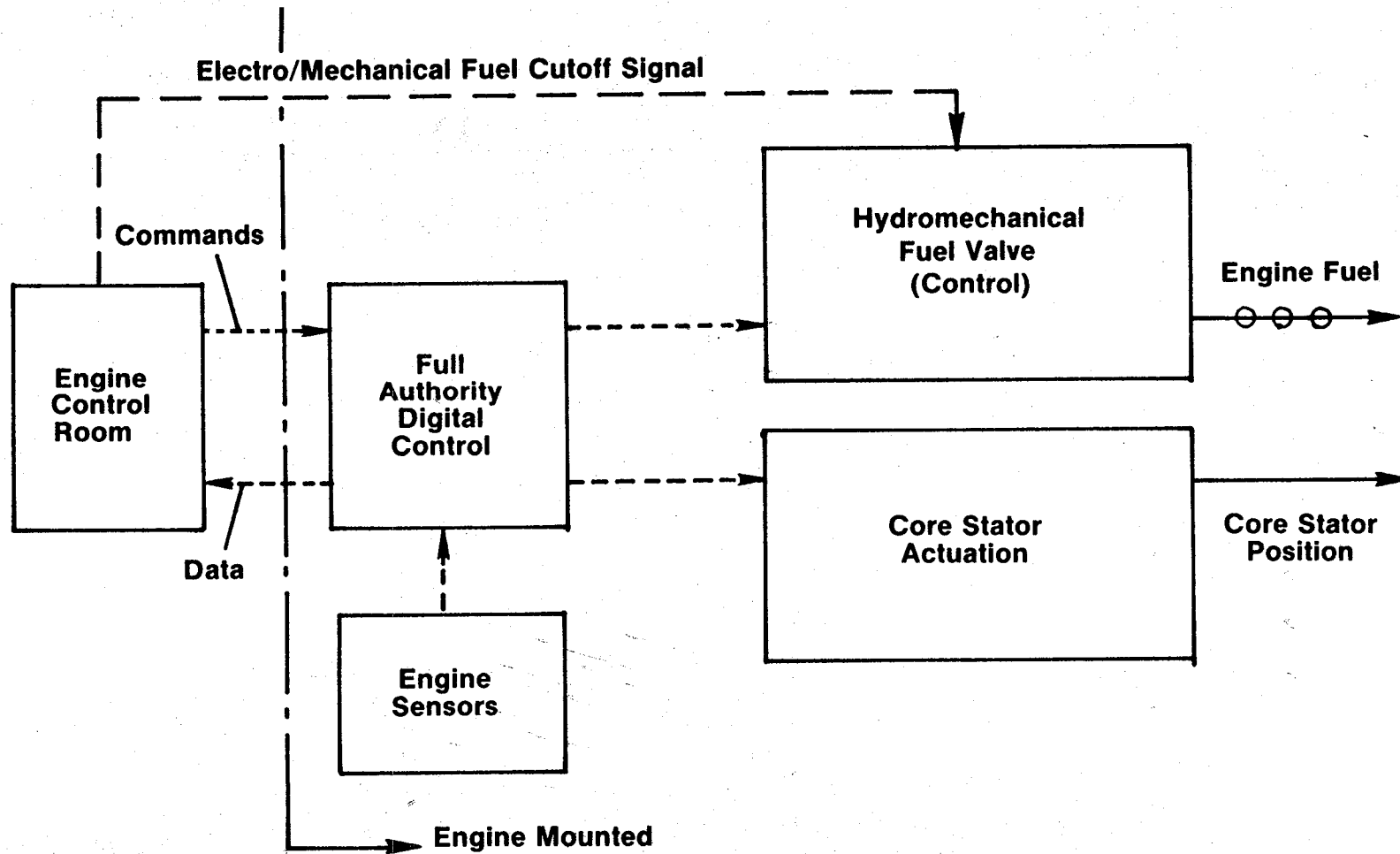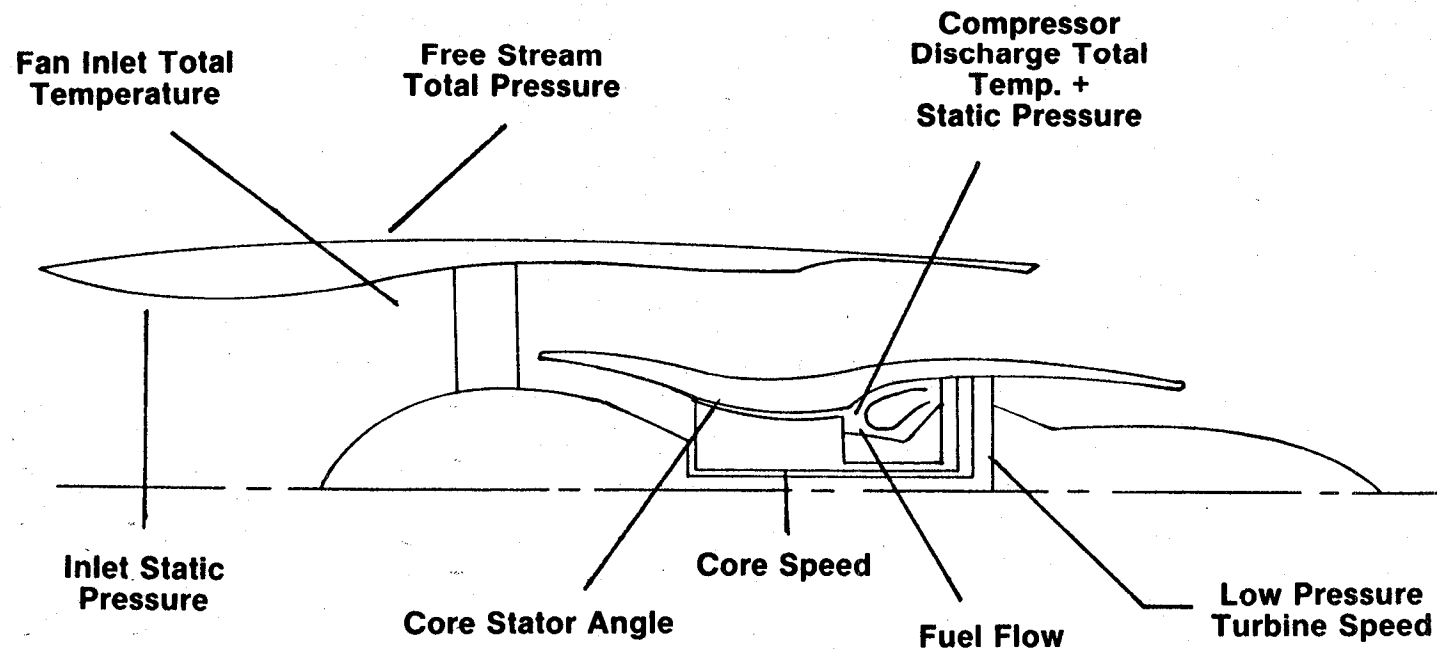Turbine Speed

Figure 86. OTW Control System Sensors.

The first schedule protects against compressor stall, and the second protects against turbine overtemperature. Both functions are scheduled as functions of corrected core speed. The digital control memory incorporates logic to select the lower of the acceleration fuel limits which are computed from the two functions. Figure 87 depicts the OTW engine acceleration fuel schedule. The corrected core speed function is calculated from measured core speed, fan speed, and fan inlet temperature. The corrected acceleration fuel limit is a function of fuel flow, compressor discharge pressure, fan speed, and fan inlet temperature. The digital control logic compares the scheduled acceleration fuel limit with the real-time calculated level of the acceleration fuel function and multiplies the difference by compressor discharge pressure to establish the actual engine-fuel-flow limit. This calculation process is repeated approximately 80 times per second.

The OTW control also incorporates limits for engine protection.

3.8.9 OTW Transient Thrust Response

As noted earlier the QCSEE was required to have rapid thrust-response capability. The UTW and OTW requirements were the same. Figure 88 shows the results of a thrust-response study using a transient model of the OTW engine. The thrust-response requirement is noted on the figure. The dashed line on the figure shows the predicted response of a conventional turbofan in which fan speed and core speed are both varied with changes in engine fuel flow. With a conventional system, the required response could not be achieved due to the acceleration fuel schedule - which is designed to prevent compressor stall and turbine overtemperature.

Since the required response could not be achieved using conventional methods, a study was conducted to determine if the thrust-response time could be improved by more effective use of the core stators. It was determined that, by setting the stators closed from the nominal schedule, the thrust-response rate could be increased. When the core stators are closed, the core speed increases to maintain sufficient power to hold the fan speed and maintain the thrust setting. Therefore, with closed core stators the core engine was not required to accelerate to achieve thrust response. The core stator closure was implemented by biasing the base stator schedule with the power-demand signal and by an operating-mode signal. With a step increase in the power-demand signal, the core stators would open rapidly to provide the power for fan acceleration to takeoff speed. The solid line on Figure 88 shows the predicted thrust response of the OTW engine with the core stator reset function.

3.8.10 Failure Indication and Corrective Action

One propulsion-control-technology objective in the QCSEE program was to reduce the impact of control-system sensor failures. This concept was implemented by using the inherent capability of a digital computer to rapidly compare and act on a large amount of data.

138

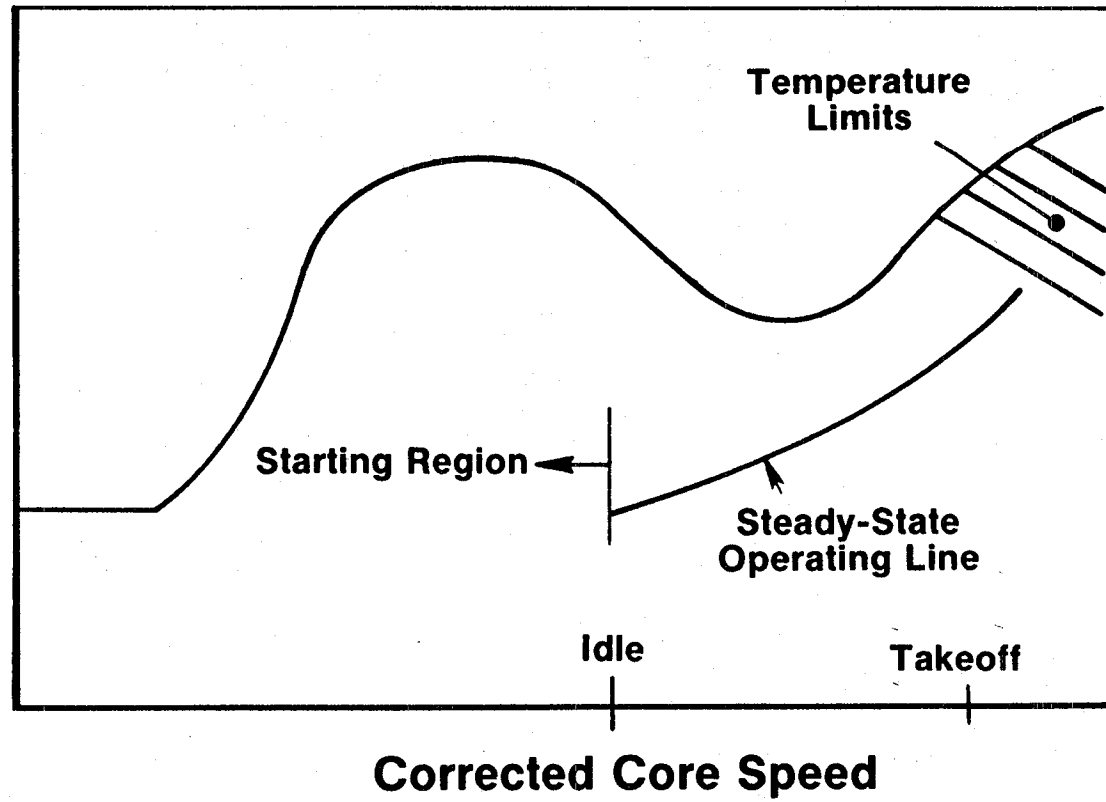**Corrected Acceleration Fuel Limit**

Temperature Limits

Starting Region ←

Steady-State Operating Line

Idle

Takeoff

Corrected Core Speed
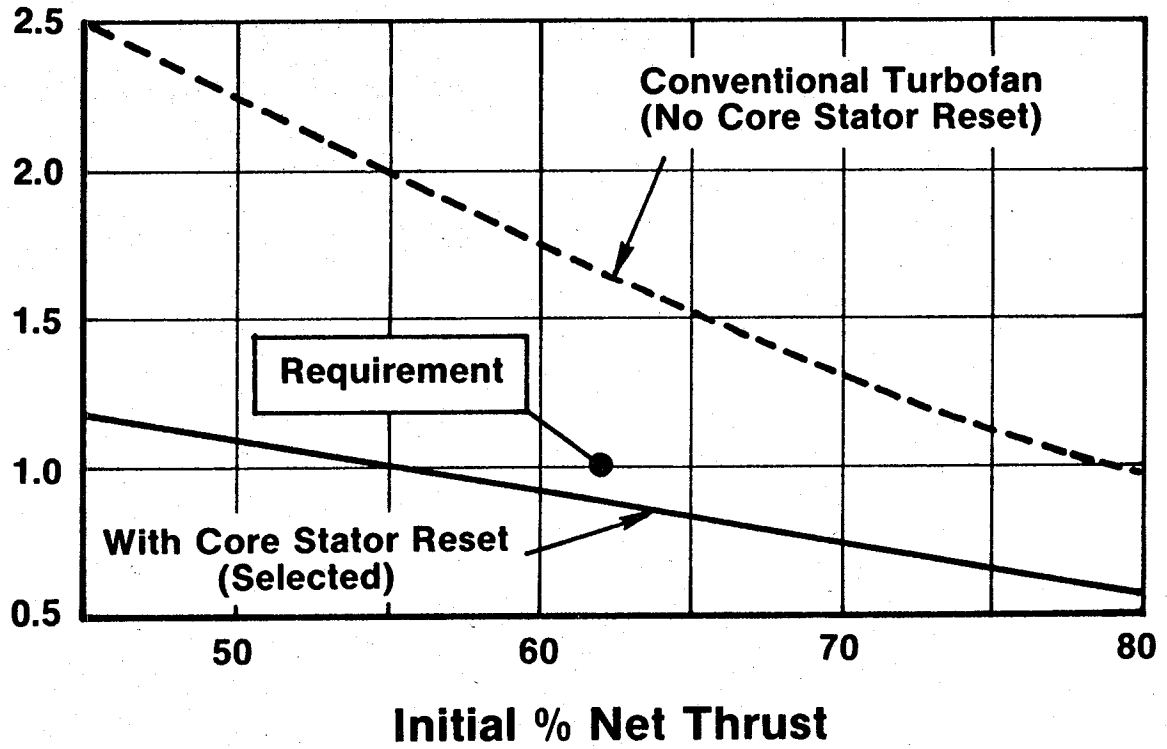
Figure 87. OTW Acceleration Fuel Schedule.

Figure 88. OTW Predicted Transient Response.

The digital control memory incorporated a nonlinear model of the OTW engine cycle. This model was combined with a logic-update scheme to form an extended Kalman-Bucy filter which provided a calculated estimate of the engine sensor outputs. These calculated sensor values were compared with the measured sensor values. If the difference was small, the engine model was updated to calculate new estimated sensor outputs. If an engine sensor fails excessive error is detected, the engine sensor is automatically disconnected, and the engine continues to operate using the calculated value of the sensed output. The calculated value of a given sensor is based on the fact that sensed variables are interrelated through the engine model. Figure 89 is a schematic of the sensor failure indication and corrective action (FICA) concept. Figure 90 shows the results of dynamic-simulator study on the OTW engine with the FICA concept incorporated. The data on the far left show normal system operation with all sensors operating during a power chop and a power burst. The center set of data shows engine operation with a compressor-discharge sensor failure. The data on the right show operation with a fan-speed sensor failure. Even with the failed sensors, the dynamic simulation indicates that the engine should perform satisfactorily.

3.9 LOW-EMISSIONS COMBUSTOR

In July 1973, the U.S. Environmental Protection Agency (EPA) issued standards to regulate and minimize the quantities of carbon monoxide (CO), hydrocarbons (HC), oxides of nitrogen (NO_x), and smoke emissions that may be discharged by aircraft operating within or near airports. These standards were defined for several different categories and types of fixed-wing, commercial-aircraft engines and are presented in terms of a calculated parameter called the EPA Parameter (EPAP). This parameter is based on an EPA-defined, landing/takeoff cycle consisting of specific operating times at engine power settings for ground idle, takeoff, climbout, and approach. The CO and HC emissions are mostly generated at the low-power ground idle conditions while the NO_x emissions are generated at the higher power settings including takeoff, climbout, and approach.

3.9.1 Design Requirements

The requirements for the QCSEE combustor were predicated on meeting the very stringent EPA standards for certified Class T2 subsonic engines. These standards, shown below, are presently scheduled to become effective in 1979:

- CO   4.3
- HC   0.8   lbm/1000 lbf/hr
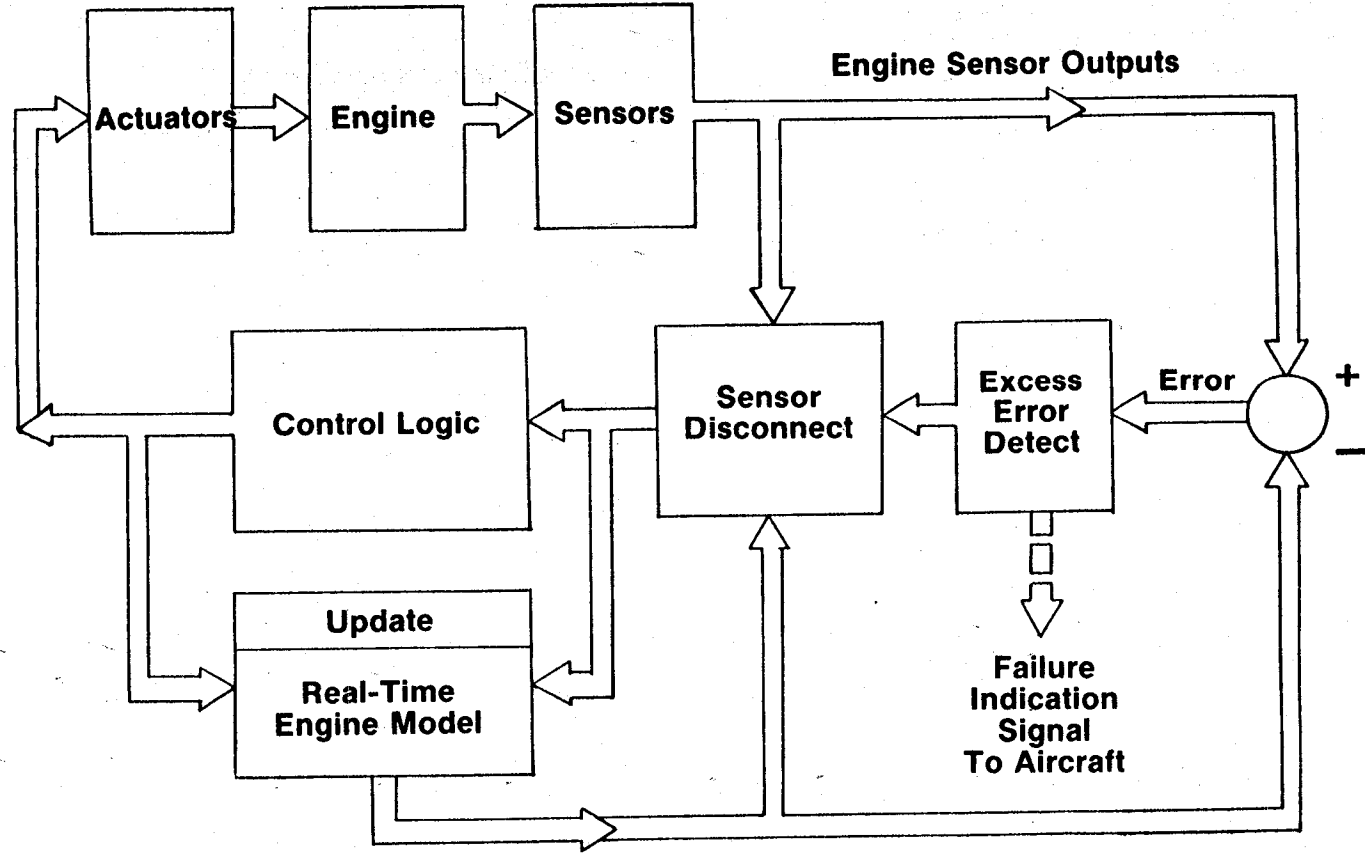- NO_x 3.0
- Smoke   22   SAE-SN

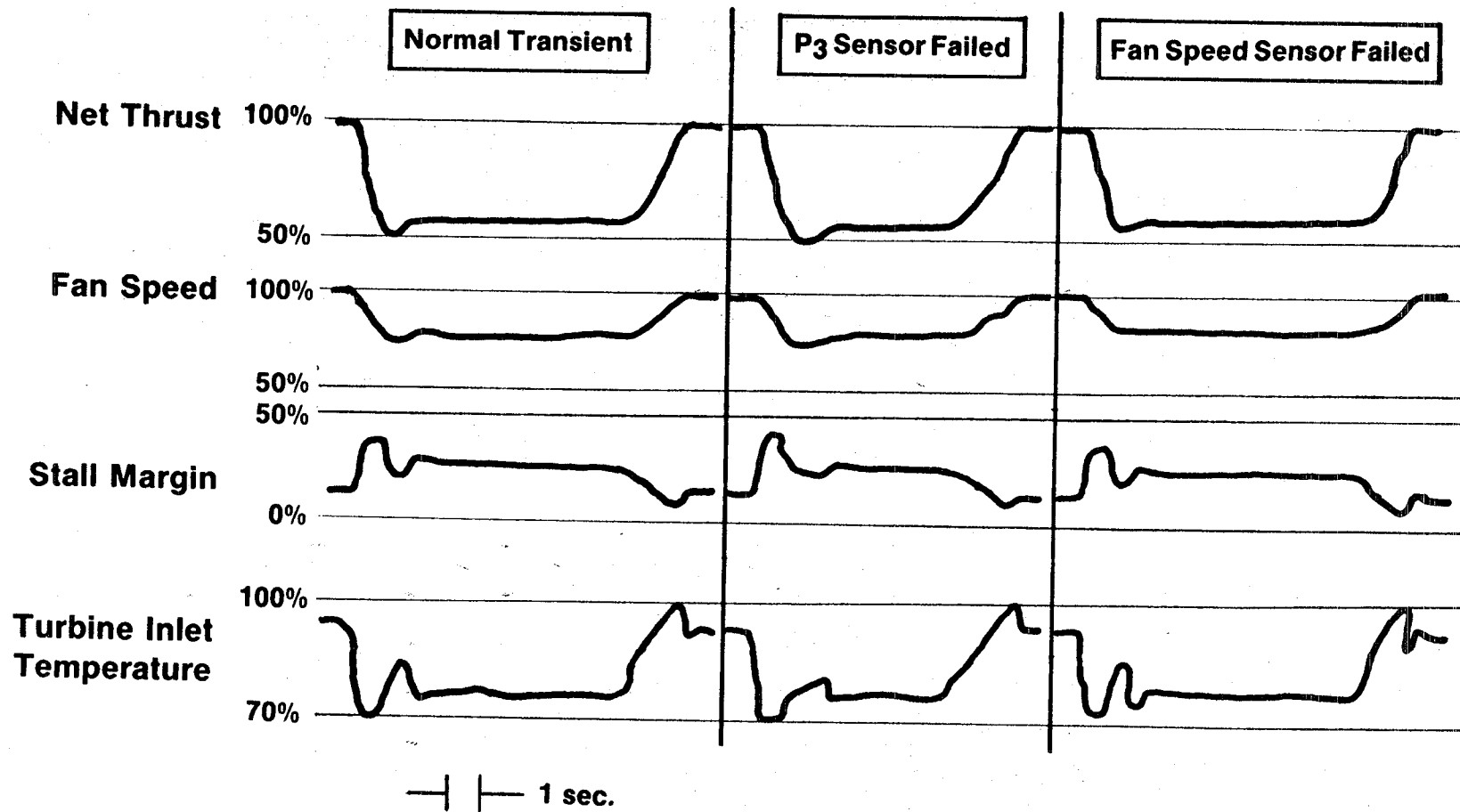Figure 89. OTW Failure Indication and Corrective Action.

Figure 90. FICA Dynamic Simulation Results; Power Chop to 60% and Power Burst to 100%.

Proposed amendments to these standards are currently being reviewed by the EPA. Revised standards could possibly result in relaxation of the requirements and the effectivity dates for Class T2 engines.

In addition to the combustor-emissions requirements, the combustor must be sized to fit within the dimensional envelope of the existing core engine and meet performance requirements such as combustion efficiency, exhaust-temperature distribution, and altitude ignition typically required for any advanced, high-bypass engine.

As shown in Table XX, meeting the CO and HC emissions requirements in the QCSEE applications is particularly challenging because of severe combustor-inlet operating conditions at ground idle compared to those of a current state-of-the-art engine such as the CF6-50. The CO and HC emissions of the QCSEE are strongly and adversely affected by these lower combustor-inlet temperatures and pressures. In addition, the requirements must be met with a combustor sized to fit within the confines of the very short, compact envelope of the F101 combustor casing. Figure 91 shows the most recent version of a single-annular combustor configuration sized to fit the QCSEE and designed specifically for low emissions.

The QCSEE UTW and OTW configurations both use the F101 core, resulting in low-pressure-ratio cycle designs. With the low combustor-inlet temperatures and pressures associated with this low cycle pressure ratio, the NO_x emissions would not be expected to be a problem. Since the technology being developed was intended for higher-pressure-ratio engines, the development was carried out in a test rig using the higher-pressure-ratio cycle conditions listed in Table XXI. The use of this "emissions program" cycle did result in improved combustor inlet conditions at the QCSEE ground idle power setting of 4.5% of sea level takeoff thrust. In addition, the higher combustor inlet temperatures and pressures associated with this higher-pressure-ratio cycle result in higher NO_x emission levels than would be expected with the original QCSEE cycles, making the EPA NO_x emissions standard more challenging.

Table XXII shows the CO, HC, and NO_x emission levels of the single-annular combustor in terms of the EPA parameter compared to the program goals. As is shown in the table, the combustor did not meet the program goals for CO or NO_x emissions with the high-pressure-ratio cycle. Therefore, to meet the emissions goals in the short, compact, combustor envelope, a more advanced combustor concept was required.

3.9.2 Approach

The primary approach was to design and develop a double-annular dome combustor, as shown in Figure 92, based on technology developed previously in the NASA/GE Experimental Clean Combustor Program (ECCP). Figure 93 shows the much smaller size of QCSEE double-annular combustor compared to the CF6-50 size double-annular combustor developed in the ECCP. The QCSEE double-annular dome combustor uses many of the features of the CF6-50 double-annular combustor,

144

Table XX.   QCSEE Combustor Design Challenges.

- **Meet 1979 CO/HC Emissions Standards with Low Ground Idle Combustor Inlet Operating Conditions**

	QCSEE	CF6-50
Combustor Inlet Temperature	415K (287 F)	429K (313 F)
Combustor Inlet Pressure	2.4 Atm. (36 psia)	2.9 Atm. (43 psia)
Engine Thrust at Idle (% Takeoff)	4.0	3.4

- **Meet Very Stringent NOX Emissions Goals**
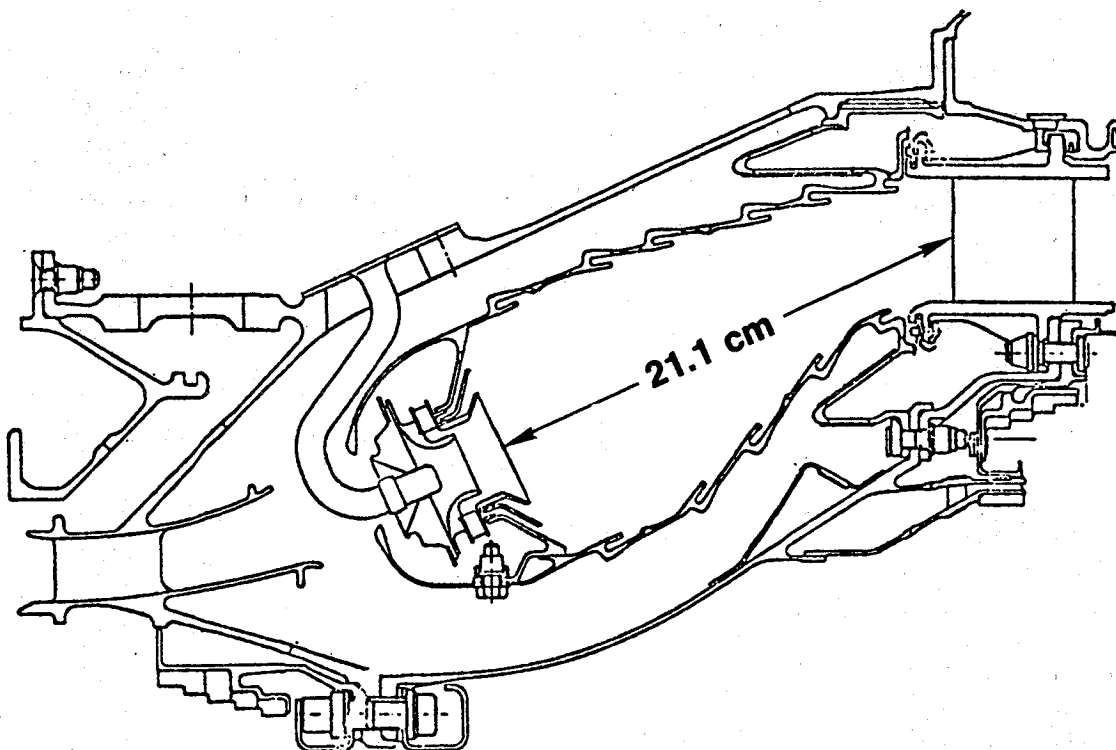
Figure 91.   QCSEE Single-Annular, Low-Emissions Combustor.

Table XXI. Emissions Program Cycle Selection.

	UTW Engine	OTW Engine	Emissions Program
Pressure Ratio	14	17	25
Pressure, N/cm² (psi)	143 (208)	172 (250)	245 (356)
Temperature, K(°R)	684 (1231)	726 (1307)	789 (1416)

Table XXII. QCSEE Single-Annular Combustor.

- With 4% Ground Idle Thrust
- With Sectorized Burning at Idle
- High P/P QCSEE Cycle
- Jet A Fuel

		Emissions Status	Goals
CO	Pounds Per 1000 Pounds Thrust Per Hour Per Cycle	7.2	4.3
HC		.6	.8
NOX		3.8	3.0

Conclusion:
Advanced Combustor Concept Required to Meet Emissions Goals
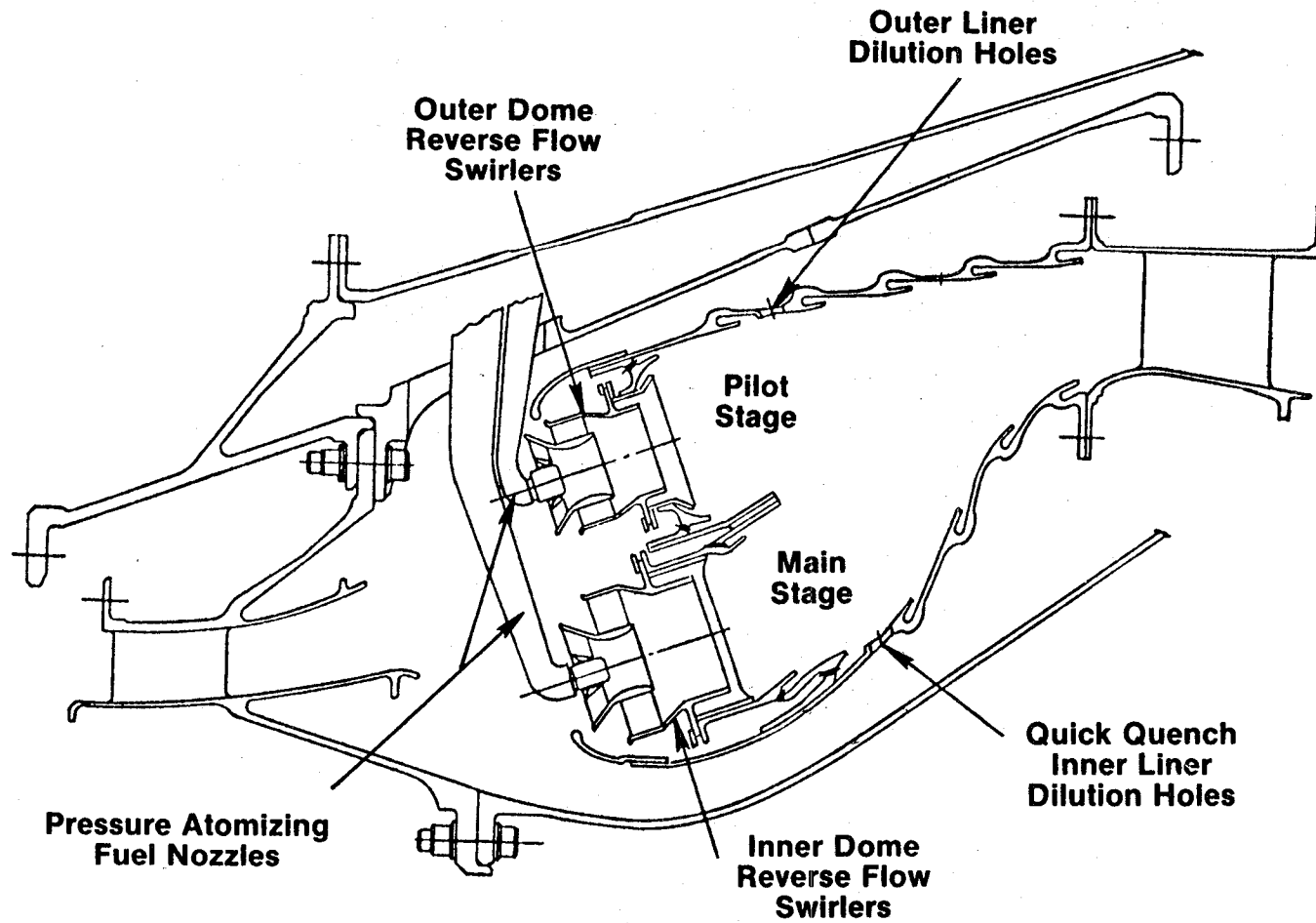
Figure 92. QCSEE Double-Annular Dome Combustor.

CF6-50

32.8 cm

QCSEE

17.7 cm
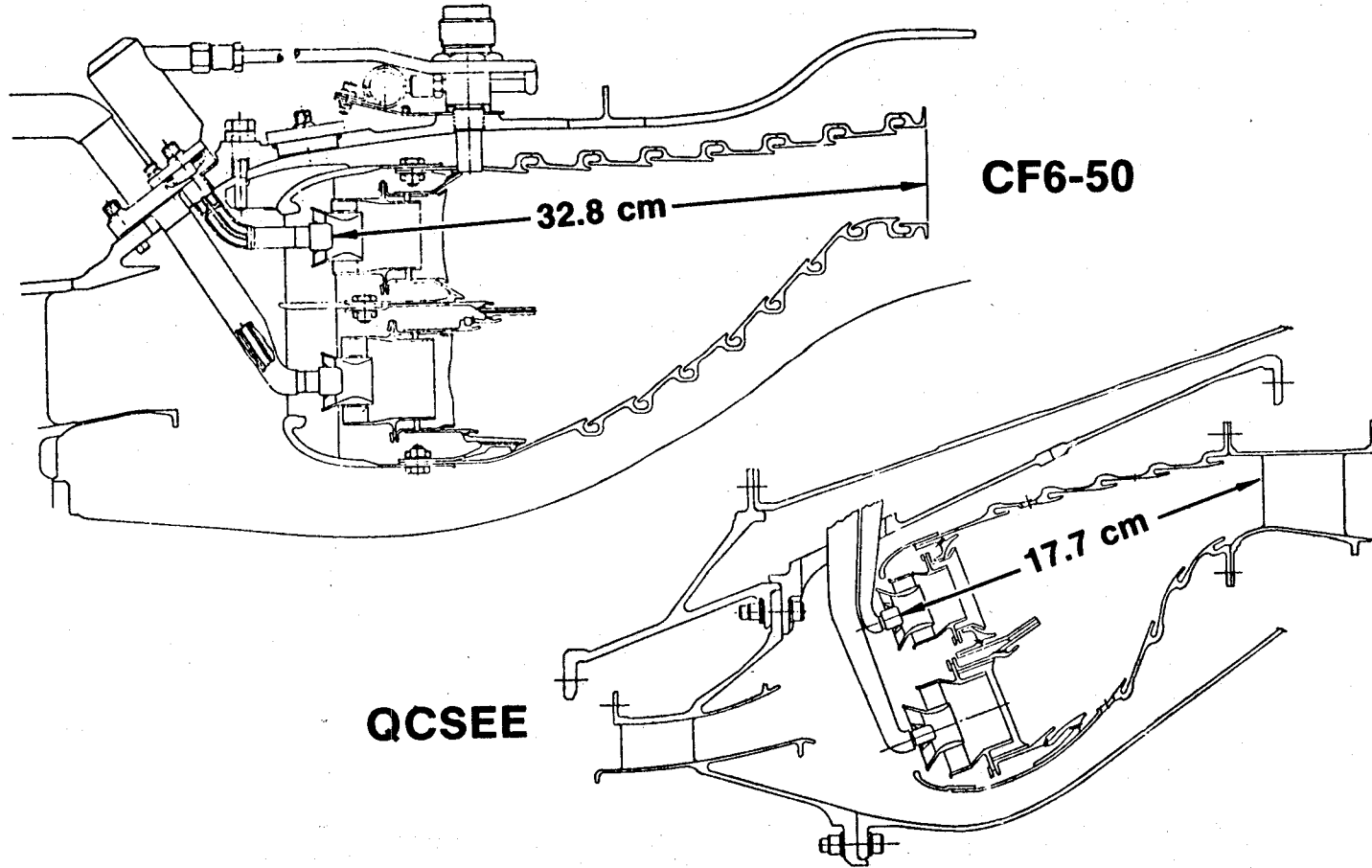
Figure 93. NASA QCSEE Double-Annular Combustor.

such as independently staged domes, counterrotating air-blast swirl cups, and pressure-atomizing fuel nozzles. However, a substantial scale-down was needed, particularly in length and dome heights, compared to the ECCP design. The staged combustor concept permits operation of only the pilot-stage dome, which is designed specifically to obtain low CO and HC emissions levels, at the low-power operating conditions. At the high-power operating condition both domes are operated with fuel staging selected to obtain low NO_x emission levels.

3.9.3 Development Program

The development program was conducted using a sector combustor, shown in Figure 94. A disassembled view of this five-swirl-cup, 90° sector combustor is shown in Figure 95. The tests were conducted in a rig designed to accept the sector combustor and duplicate exactly the flowpath of the F101 engine. Figure 96 shows a photograph of the test rig with the sector combustor installed. Although the major effort was focused on developing low CO and HC emissions at idle, the NO_x emissions levels of the QCSEE double-annular combustor were also evaluated at simulated high-power conditions; however, it was necessary to derate the pressure at higher power conditions and to adjust the measured NO_x emissions for the pressure difference.

3.9.4 Test Results

The number and types of combustor development tests conducted in the sector combustor program and the total number of test conditions at which data were acquired for each test category are shown below.

	Number of Test Configurations	Data Points
Emissions Development	32	310
Ignition Development	2	26
Combustor Performance	1	8
Fuel Spray Development	6	18

Figure 97 shows the four major categories of combustor configurations tested and the key design features of each. As shown in Figure 98, the baseline configuration exceeded the emissions goals by a large margin. Significant improvements were obtained with modified geometry by increasing the pilot-zone length in conjunction with cooling- and dilution-airflow modifications. Even further improvements in CO emissions were obtained by reducing the cup spacing in the pilot dome. Reduced cup spacing was obtained by relocating the pilot stage to the inner annulus. This configuration produced lower CO and HC emission levels than any of the previous configurations. The lower CO and HC emissions are believed to result from a reduction or elimination of the quenching regions between swirl cups. However, the very low CO and HC emission levels occurred at a fuel/air ratio below the QCSEE ground
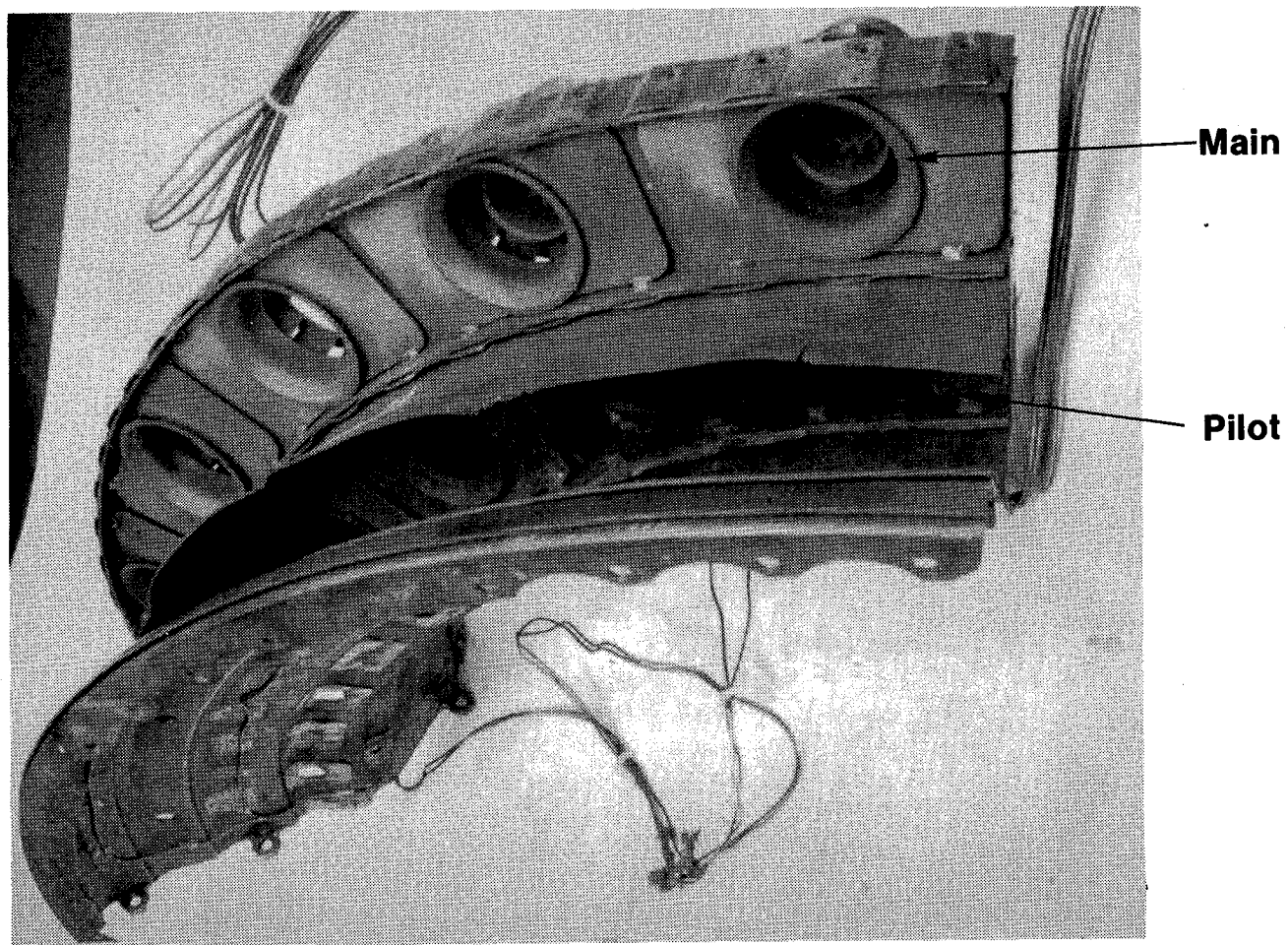
Figure 94. Double-Annular Test Sector.
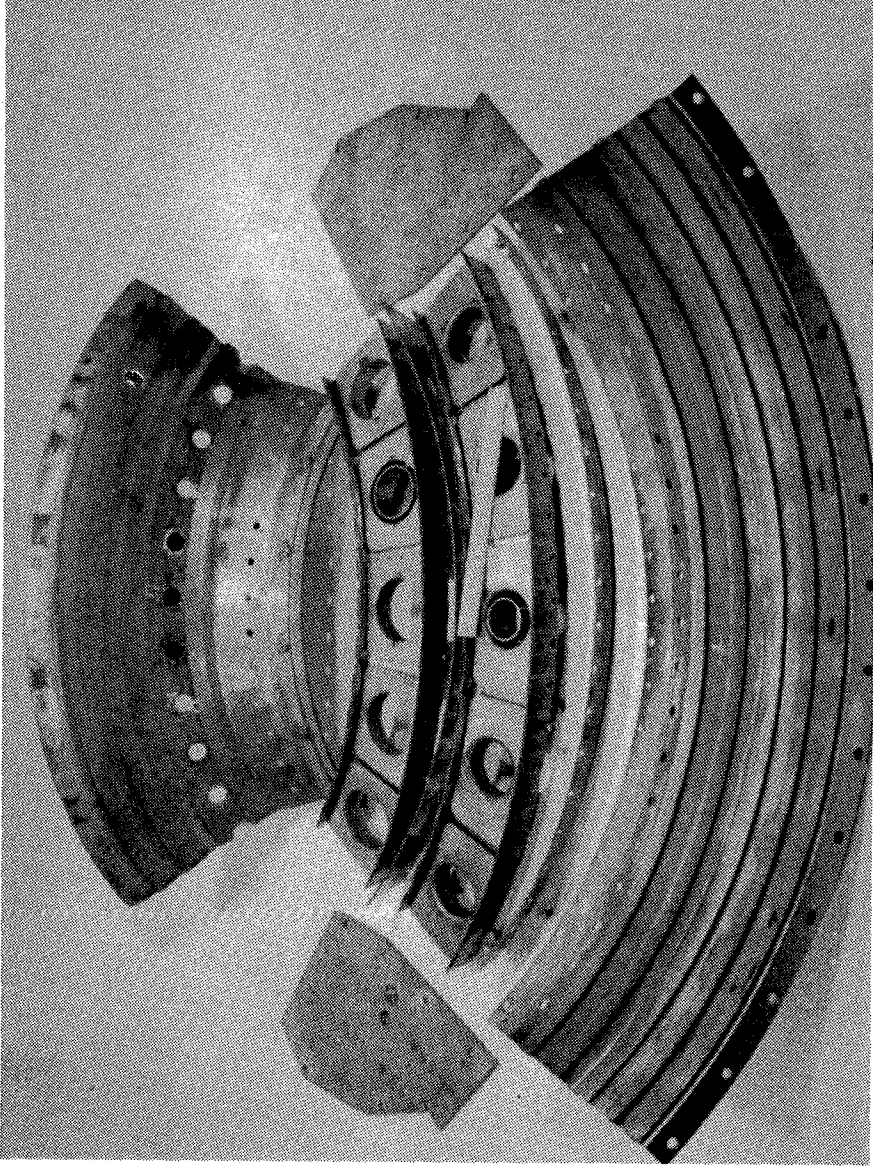
Figure 95. Double-Annular Sector Prior to Assembly.
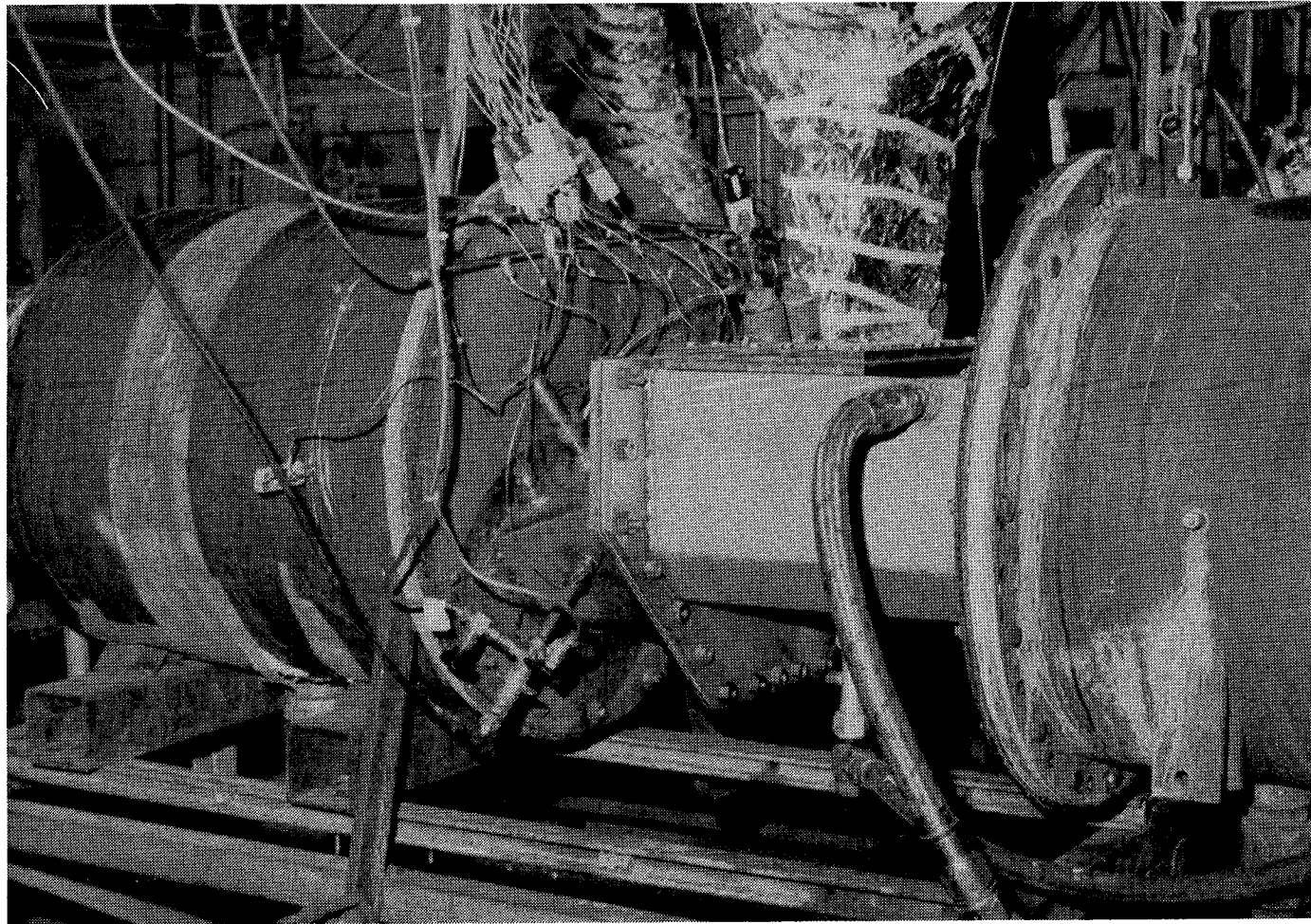
Figure 96. Double-Annular Combustor Test Rig.

Combustor Configurations

- **Baseline**

- **Modified Geometry**
  (Increased Combustion
  Zone Length)

PILOT

MAIN
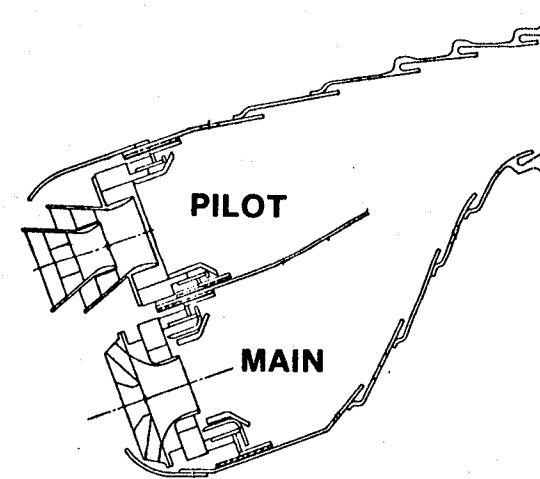
- **Inner Annular Pilot Dome**

- **Selected Final Design**
  (Radial Axial Air Blast Swirlers)

MAIN
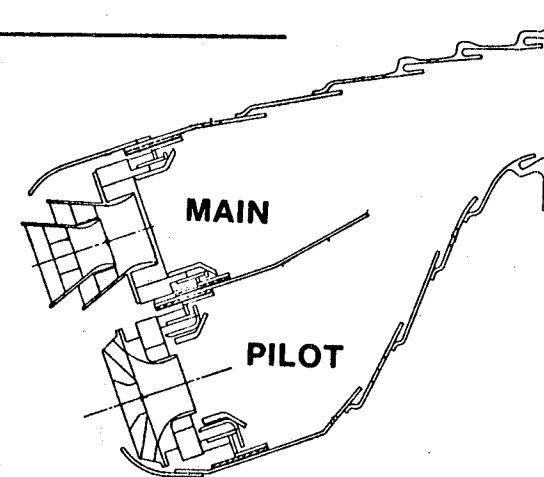
PILOT

Figure 97. Key Development-Test Results.
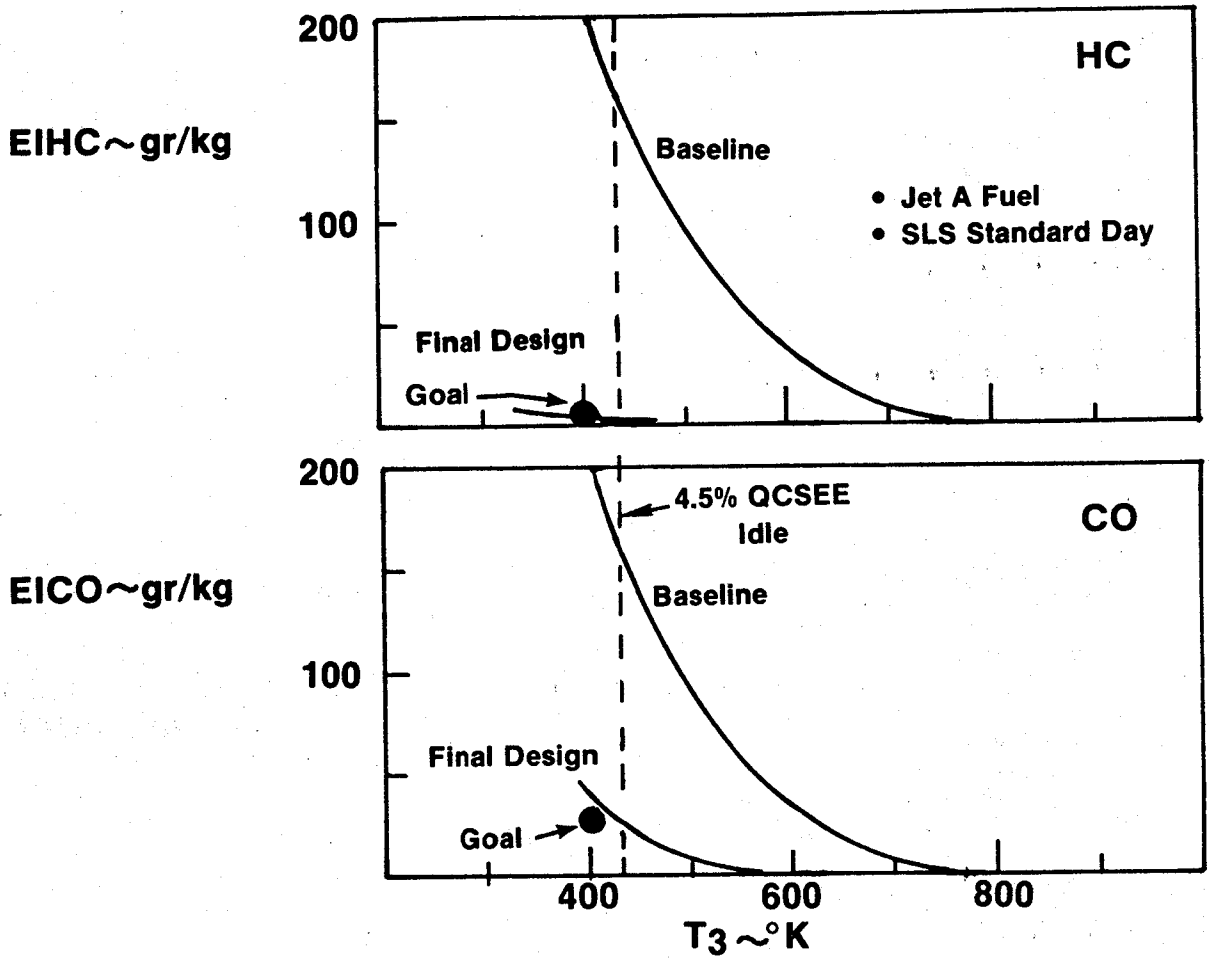
Figure 98. Key Emissions-Test Results.

idle design fuel/air ratio. Therefore, to further reduce the CO emission levels at the QCSEE ground idle fuel/air ratio, an improved pilot-stage swirl-cup design with higher airflow capacity and improved atomization was developed as the final design.

Figure 99 shows the improved pilot swirl-cup design and a similar design developed for the main stage. These design-improvement features were incorporated with the previously developed design features to obtain the final configuration. Figure 100 shows the preferred sector combustor configuration and the key dimensions.

Table XXIII shows the emissions levels for the final double-annular combustor configuration compared to those expected with the best single-annular combustor. Compliance with the program emissions goals, with a ground idle thrust of 4.5% takeoff thrust, is projected with this selected configuration.

The final configuration was also tested to investigate other important combustor-performance characteristics. Figure 101 shows the altitude ignition results obtained with the final double-annular combustor configuration. These tests were conducted with the sector combustor subjected to combustor-inlet conditions based on the altitude windmilling characteristics expected with QCSEE. The Jet A fuel temperatures were maintained at 244 K to simulate in-flight conditions. As shown, excellent altitude-relight results were obtained with successful ignition obtained in all regions tested within the flight envelope.

Although sector combustors are not generally conducive to accurate measurement of exhaust gas temperature-pattern factors, due to their limited circumferential size, data were acquired to examine trends. Because of the limited combustor airflow available for profile control and the very short length of this combustor design, it is expected that additional tailoring of the combustor profile would be required before introduction into a production engine.

In conclusion, it was demonstrated in a prototype sector combustor test that a double-annular dome combustor suitable for the QCSEE application can be developed which will satisfy the emissions goals of the program at a ground idle thrust of 4.5%. Furthermore, the selected final configuration demonstrated excellent altitude-relight performance for a combustor at this early stage of development. Other performance characteristics of this double-annular design will require further development before engine testing.

3.10 ACOUSTIC DESIGN

A schematic showing the QCSEE noise objectives is presented in Figure 102. These objectives are for a four-engine aircraft operating in the powered-lift mode from a 610-m (2000-ft) runway. The noise levels are those that would be heard by an observer on a 152-m (500-ft) sideline parallel to the runway centerline. At takeoff, the noise goal was 95 EPNdB with the engines at 100% thrust and on a 12.5° flight path. Under approach conditions, with the engines
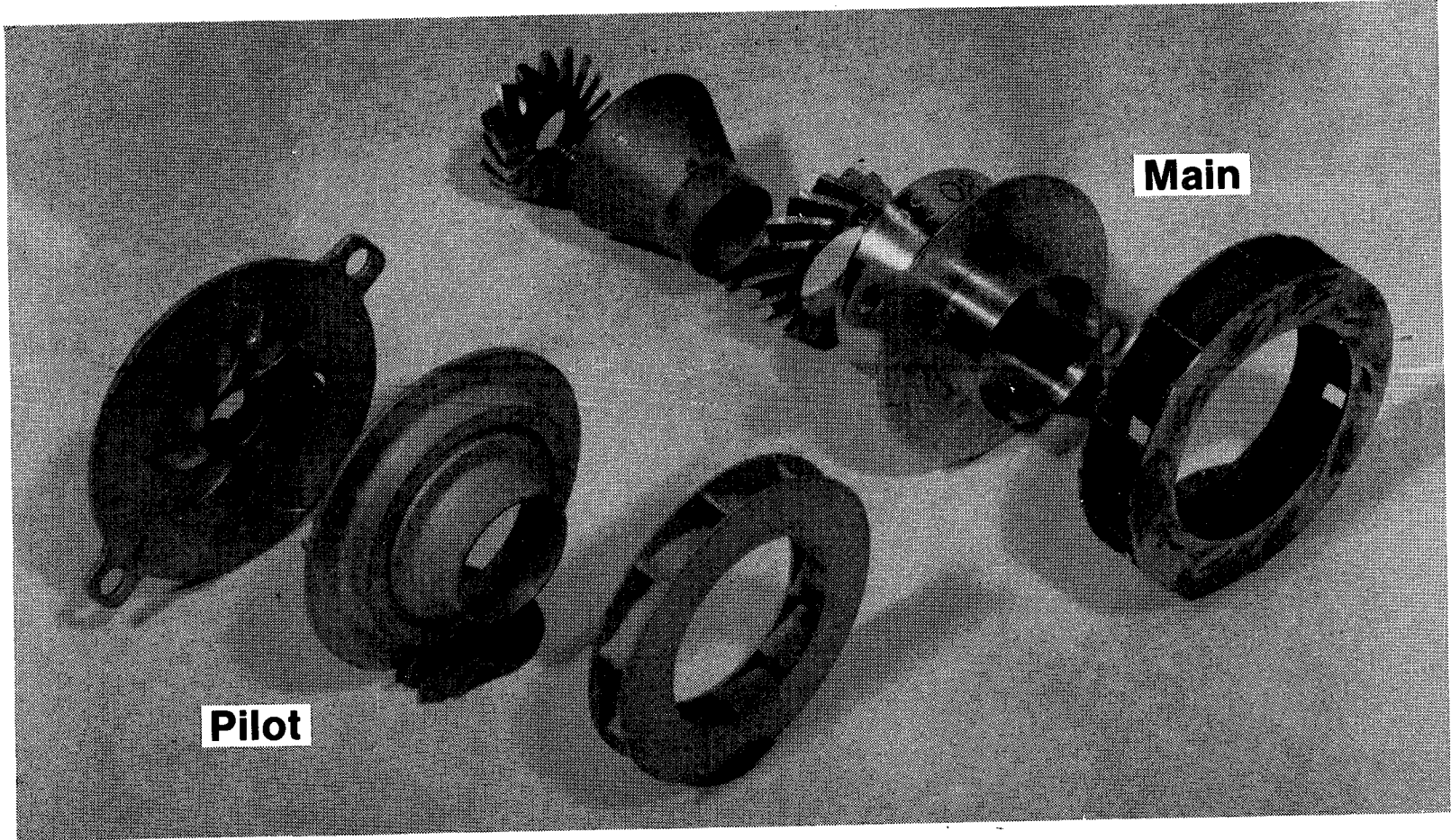
Figure 99. Swirl Cups.
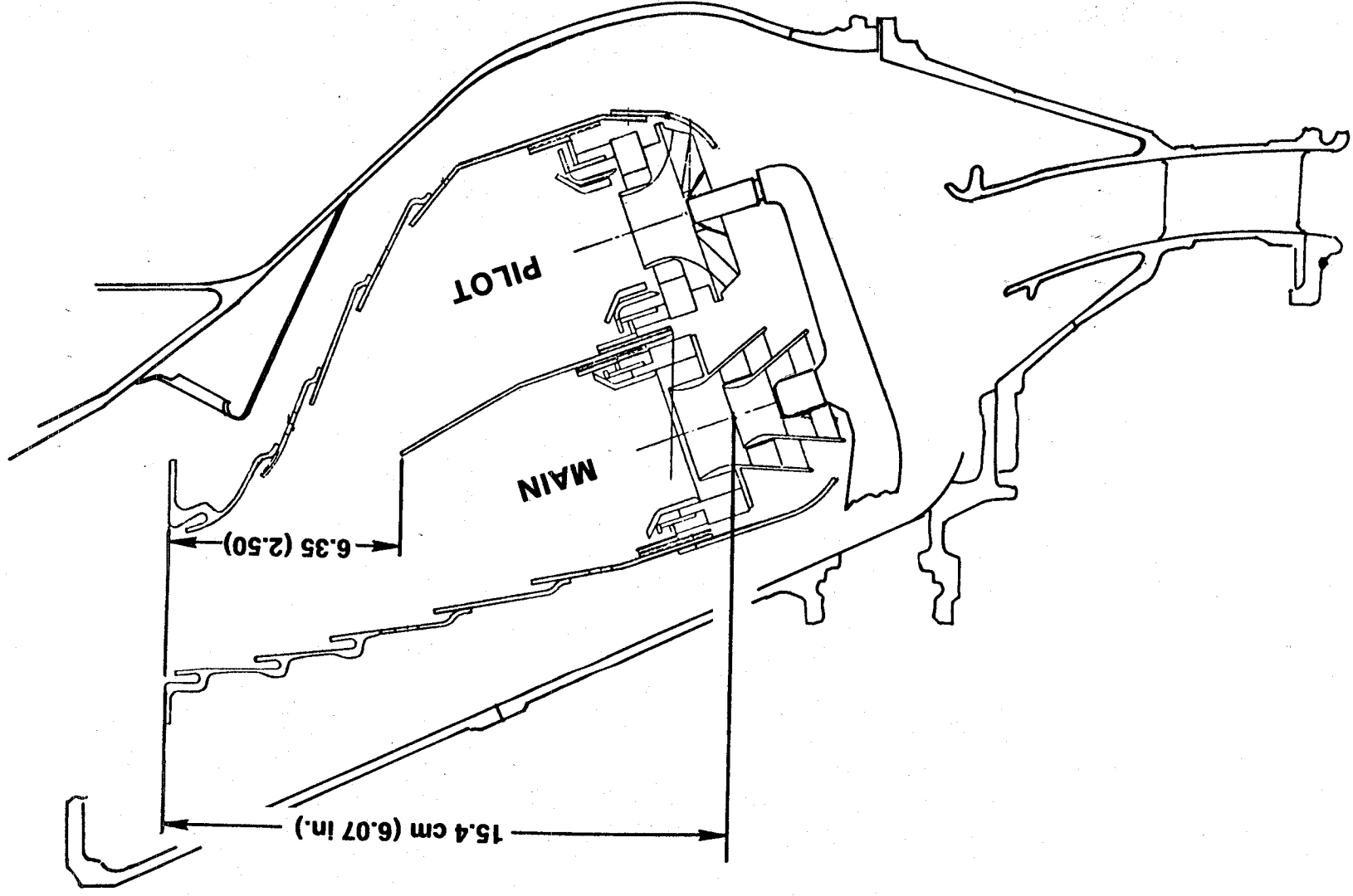
Figure 100. Final Configuration.

Table XXIII. Emission Results for QCSEE Double-Annular Combustor.

High P/P QCSEE Cycle

Idle Thrust	Double Annular		Best Single Annular with Sector Burn at Idle		Goals	
	4.0%	4.5%	4.0%	4.5%		
CO	5.6	4.3	7.2	6.7	4.3	
HC	.32	.13	.57	.43	.8	lb/1000 lb Thrust Per Hour-Cycle
NOX	3.0*	3.0*	3.8	3.8	3.0	

* **Estimated Based on Sector Combustor Results at Simulated High Power Conditions**

158
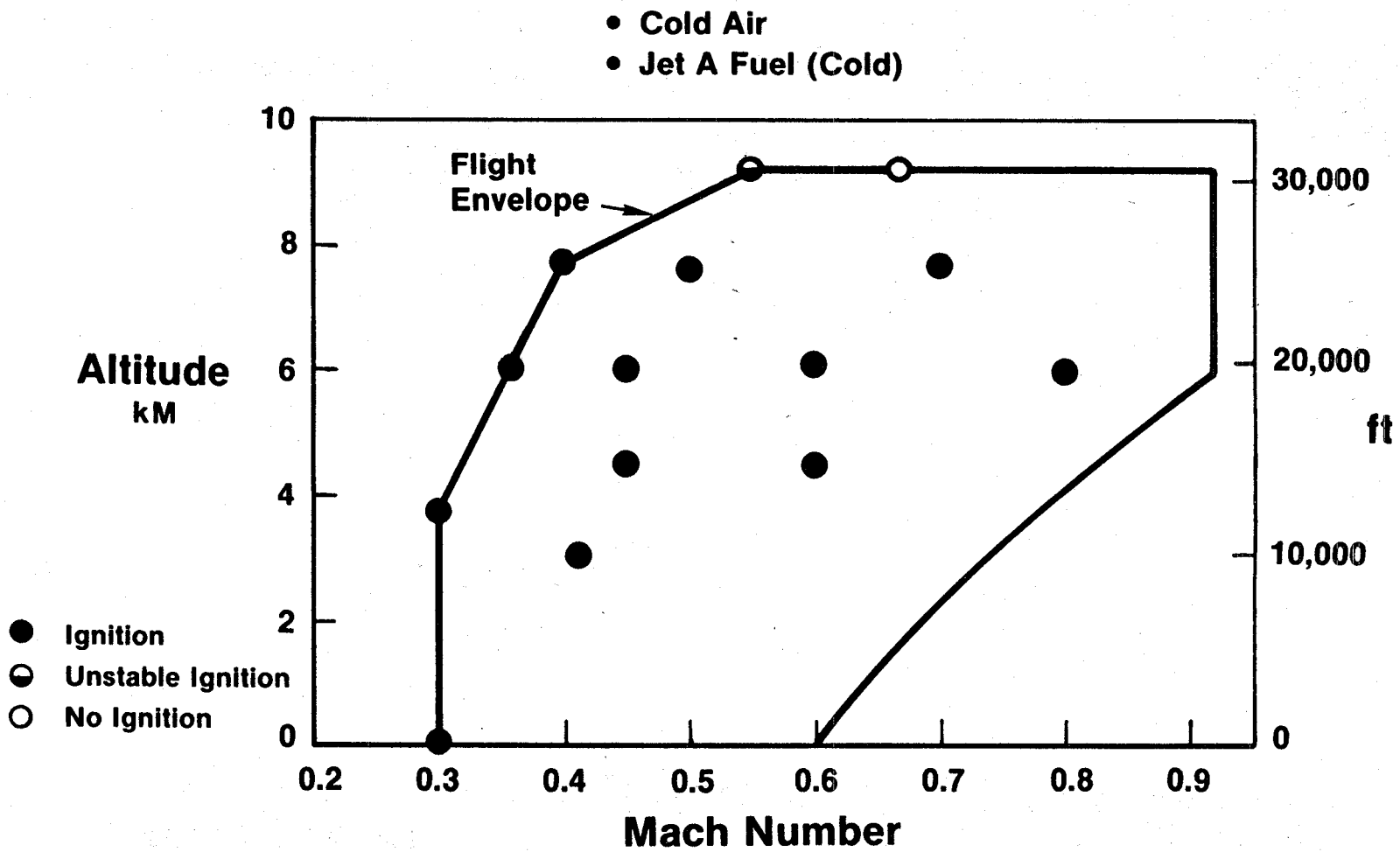
Figure 101. Altitude Ignition Results.

- **4 Engines**
- **400 KN (90,000 lbs) Installed Thrust (Fn)**
- **610m (2000 ft) Runway**

100% Fn
61m (200 ft) Alt.

Reverse 35% Fn

95 EPNdB Takeoff

65% Fn 61m (200 ft) Alt.

100 PNdB Reverse

152.4m (500 ft) Sideline

95 EPNdB Approach

Figure 102. QCSEE Acoustic Objectives.

developing 65% of takeoff thrust and the aircraft on a 6° glide path, the goal was also 95 EPNdB. After touchdown on the 610-m (2000-ft) runway, with the engines developing reverse thrust at 35% of takeoff thrust, the noise goal was 100 PNdB on the 152-m (500-ft) sideline. These noise objectives were very challenging; this can be seen more clearly by examination of Figure 103. The figure shows the relative decrease in EPNL over the years for the older narrow-body aircraft, current widebody, next-generation widebody, and finally an Energy Efficient Engine (E^3) powered aircraft. QCSEE powered aircraft that meet the 95 EPNdB goal are about 10 EPNdB below the next-generation aircraft.

These stringent noise goals meant that any noise source on the engine which had the potential for contributing to the far field had to be evaluated. The sources which were considered are listed below:

- Fan-inlet-radiated noise

- Fan-exhaust-radiated noise
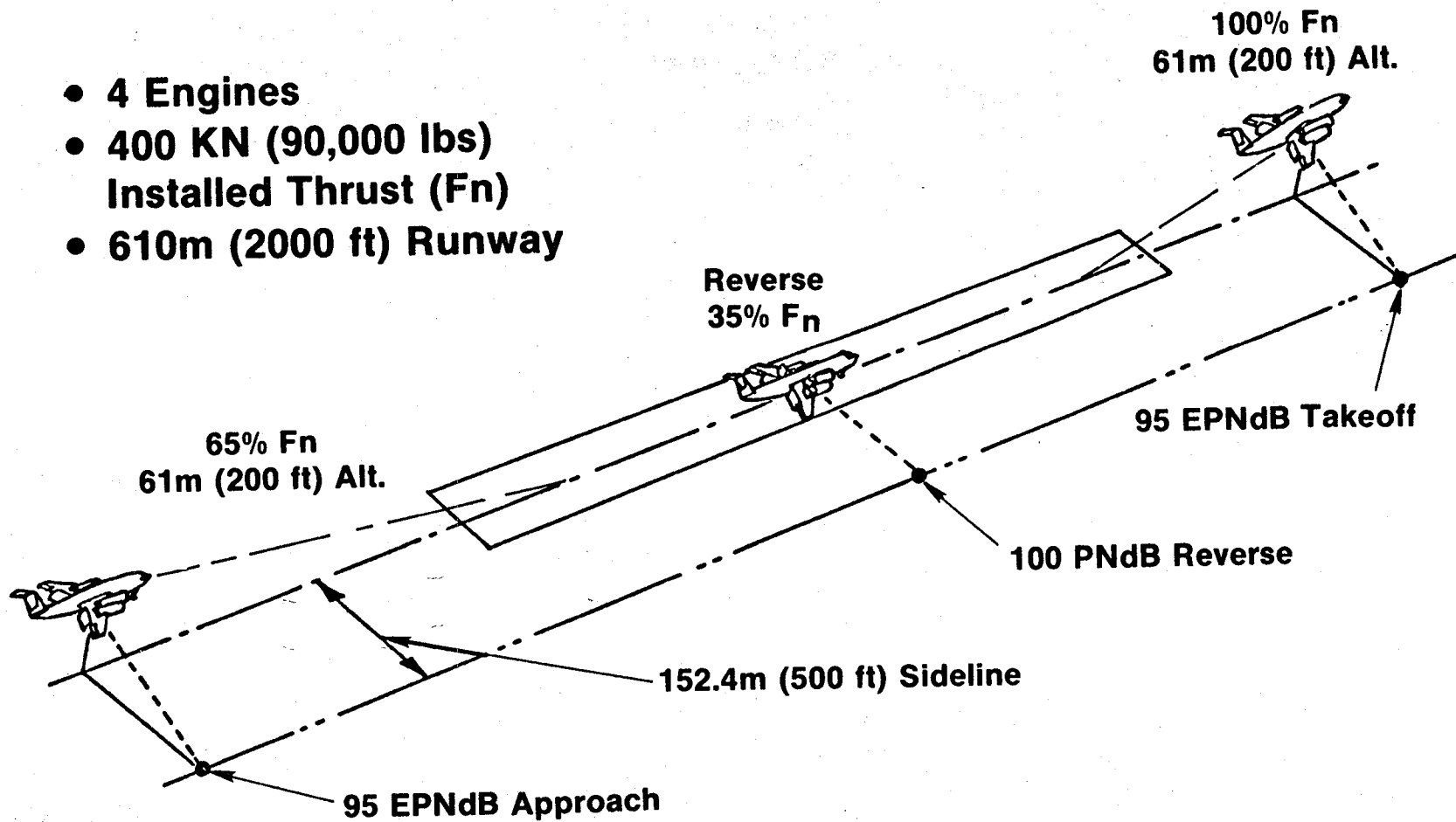
- Turbine noise

- Combustor noise

- Jet/flap noise

- Compressor noise

- Gear noise

- Treatment regenerated flow noise

- Strut noise

- Splitter trailing-edge noise

The design procedure for each noise constituent was to estimate the level by scaling existing test data from similar fan and core engines or by using the latest analytical techniques available. These estimated levels were then extrapolated to a simulated-flight condition of 61-m (200-ft) altitude, 152-m (500-ft) sideline. Precontract studies had indicated that maximum noise levels would occur with the aircraft at 61-m (200-ft) altitude during either takeoff or approach. As an example the predicted, unsuppressed, fan-exhaust-radiated noise spectrum for the UTW engine at takeoff is shown in Figure 104. This spectrum was then noy-weighted to determine the frequencies at which suppression or source-noise reduction techniques should be applied for maximum acoustic benefit. It can be seen that the second-harmonic tone required more reduction than the blade-passing frequency and that, after noy-weighting, treatment should be tuned to 2500 to 3150 Hz to provide the best broadband suppression.

A similar procedure was followed for each potential noise source for each of the three operating conditions. After several iterations, the levels of suppression which were required to meet the noise goals were established. Test and component programs were then conducted to verify that the required levels of suppression could be achieved and that the basic source noise (unsuppressed) levels were correct. System noise levels were updated and revised continuously as new data became available.
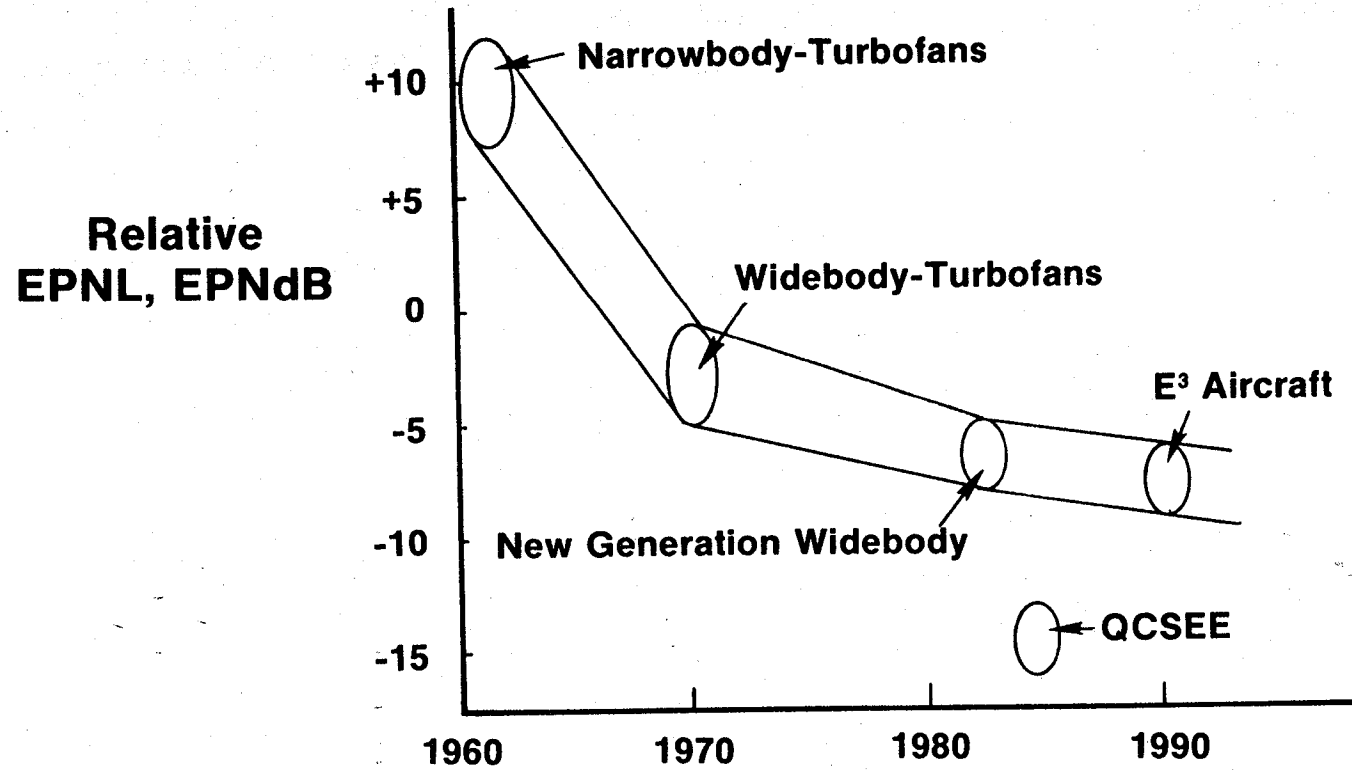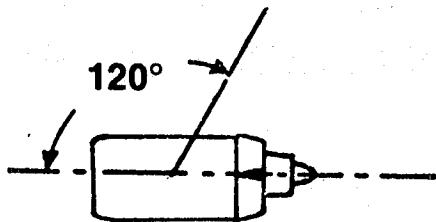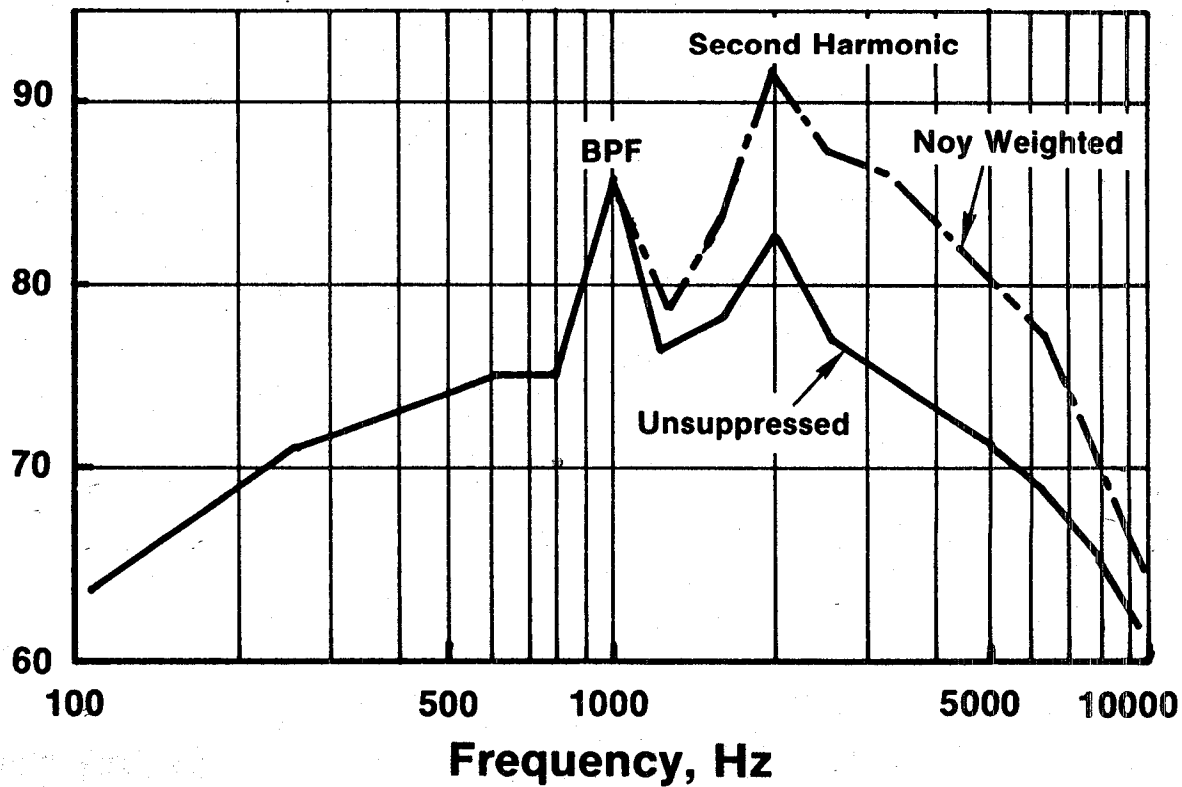
Figure 103. Aircraft Noise Trends.

Figure 104. Unsuppressed Fan Exhaust Spectra.

3.10.1 Engine Acoustic Features

Before discussing the component tests which led to the treatment designs, the basic acoustic features on each engine will be reviewed. These acoustic features can be divided into two main categories: those dealing with reduction of the source itself and those dealing with the reduction of noise after it has been generated.

UTW features are shown in Figure 105. A low-pressure-ratio fan was selected primarily to keep jet/flap interaction noise as low as possible by reducing the fan-bypass exit velocity. This low pressure ratio also aided in keeping exhaust-radiated fan noise low. The fan had a subsonic tip speed of 290 m/sec (950 ft/sec) at takeoff which eliminated high noise levels from multiple pure tones associated with supersonic tip-speed fans. A wide rotor/stator spacing of 1.5 rotor tip chords was selected to lower rotor/stator interaction noise. Additional reduction could have been achieved with wider spacing; however, an acoustic splitter could achieve the reduction with less weight penalty than that associated with a fan frame weight increase due to wider spacing. The vane/blade ratio of 1.83 was selected based upon analysis to minimize propagation of the UTW fan second-harmonic tone - which makes a major contribution to the noy-weighted spectrum.

A high throat Mach number (0.79) inlet was used to suppress inlet-radiated fan noise at takeoff; wall treatment having a length equal to 0.74 fan diameters was added to provide suppression at approach and in reverse thrust.

Fan exhaust suppression utilized inner- and outer-wall suppression with variable-depth, variable-porosity treatment sections to provide wide suppression bandwidth. Preliminary design studies indicated that wall treatment alone would not achieve sufficient suppression in the length allowable; therefore, a 1.02-m (40-in.) acoustic splitter was added to provide the required exhaust suppression. Mach number in the fan exhaust duct was limited to 0.47 to minimize strut noise, treatment regenerated noise, and splitter trailing-edge noise. Treatment was added to the core inlet to suppress high-frequency compressor tones. Fan frame treatment consisted of wall treatment to suppress fan blade-passing-frequency tones and treatment on the pressure surface of the outlet guide vanes (OGV's) to attenuate high-frequency, broadband, fan noise.

The single-degree-of-freedom (SDOF) treatment that was specified on the UTW was an integral part of the support and load-carrying structure of the composite nacelle.

The engine utilized a "stacked" treatment core suppressor which was designed to attenuate both low-frequency combustor noise and high-frequency turbine noise.

In order to maintain commonality, the OTW engine shown in Figure 106 utilized essentially the same composite fan frame design as the UTW. With the 33 vanes and 28 fan blades, the OTW vane/blade ratio is a low 1.18. This low vane/blade ratio was a departure from the usual design practice of

164

- **p/p = 1.27**
- **Tip Speed = 290m/sec (950 ft/sec)**
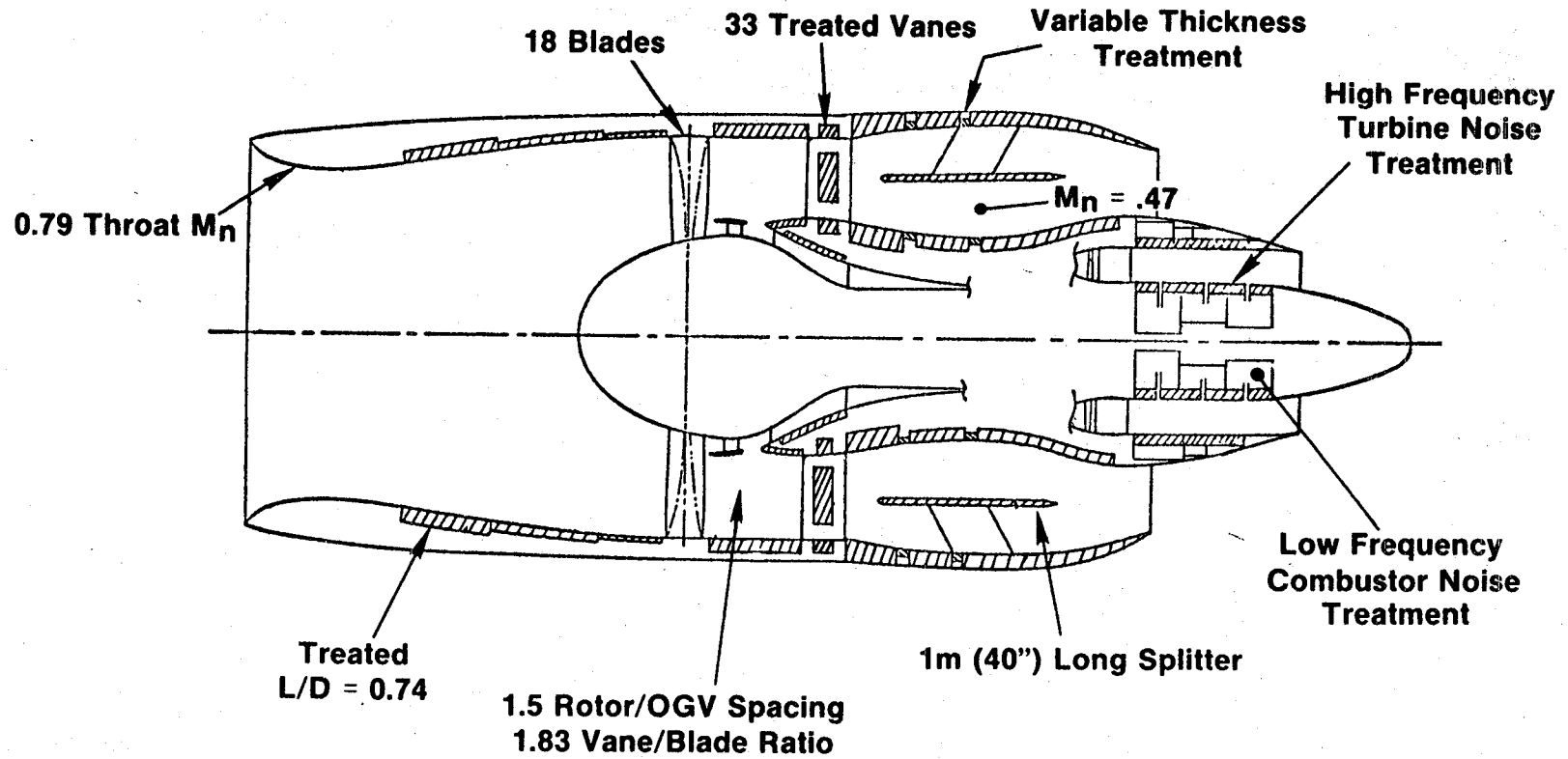
Figure 105. UTW Engine Acoustic Features.

- **p/p = 1.34**

- **Tip Speed = 350m/sec (1150 ft/sec)**

Bulk Absorber Treated L/D = 0.74

33 Treated Vanes

Variable Thickness Treatment

High Frequency Turbine Noise Treatment

.79 Throat Mach No.

$M_n = .47$

28 Rotor Blades

1.93 Rotor/OGV Spacing
1.18 Vane/Blade Ratio

1m (40") Long Splitter

Low Frequency Combustor Noise Treatment

Figure 106. OTW Engine Acoustic Features.

having a vane/blade ratio value near 2 to cut-off rotor/stator interaction
noise. It was felt that the wide spacing of 1.93 rotor tip chords for the
OGV/fan rotor would reduce rotor/stator interaction noise to the point where
it would not be a major contributor; thus, there was no need for "overkill"
by selecting a high vane/blade ratio.

Other acoustic features of the OTW are very similar to the UTW including
the treated vanes, "stacked" core treatment, variable-depth and variable-
porosity fan exhaust wall treatment, 1.02-m (40-in.) acoustic splitter, and
high throat Mach number inlet. At approach and reverse thrust, the OTW inlet
provides suppression with bulk absorber wall treatment.

3.10.2 Fan Inlet Design

Preliminary system studies conducted on both engines indicated that
achieving a balanced design would require the following levels of inlet PNL
suppression:

	UTW (PNdB)	OTW (PNdB)
Takeoff	12.8	13.5
Approach	6.3	10.4
Reverse Thrust	4.5	11.5

These high levels of required suppression could be achieved with a conventional
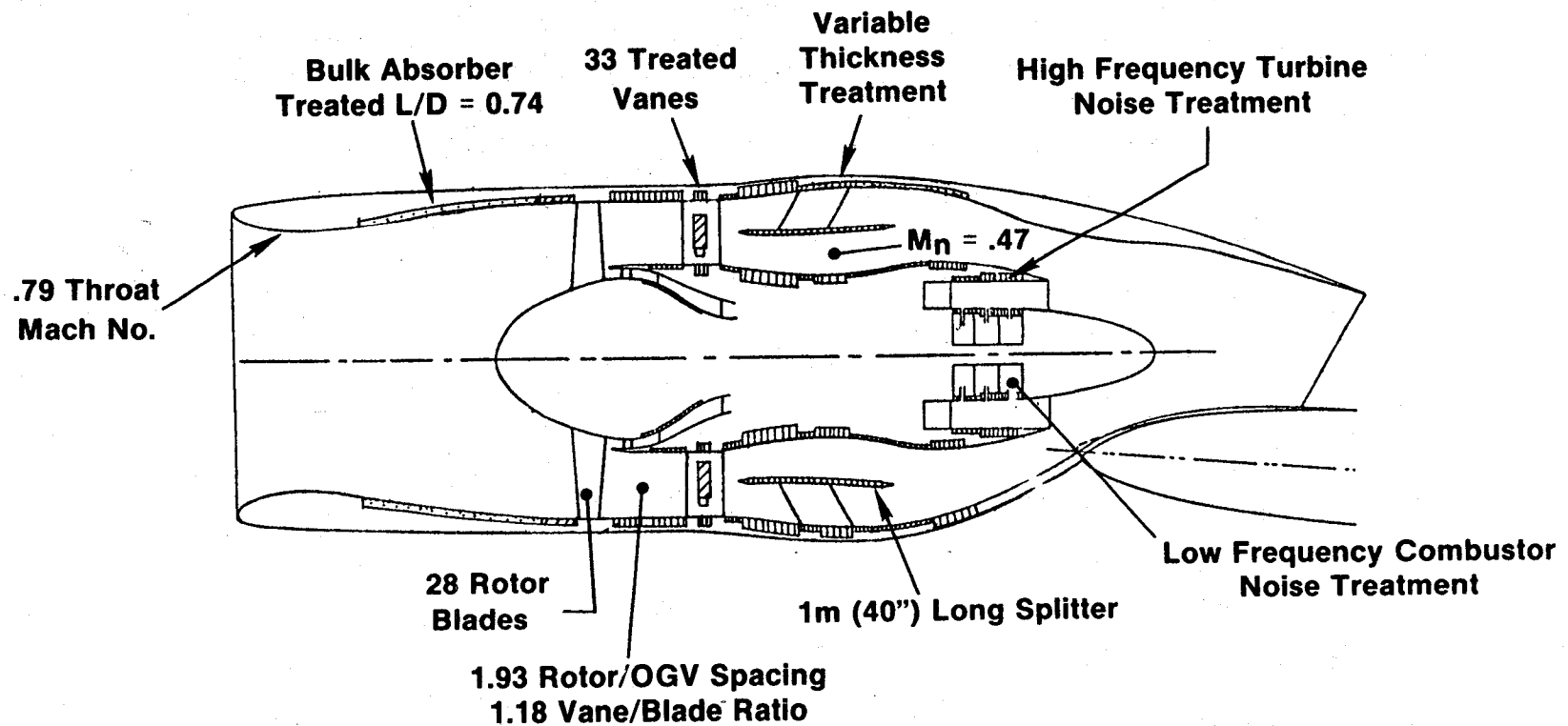inlet; however, with wall treatment only the treated-length-to-diameter ratio
would be much greater than 1.0 and/or inlet splitters would be required. Pre-
vious experience has shown that large levels of inlet suppression can be
achieved from high throat Mach number inlets. As shown in Figure 107, which
compares inlet-noise-reduction concepts, takeoff suppression can be achieved
with a treated high throat Mach number inlet. At approach and reverse thrust,
suppression is achieved with the wall treatment only since the inlet Mach num-
ber is much lower.

In order to demonstrate that the high levels of inlet suppression can be
achieved, a scale-model test program was conducted in the General Electric
anechoic chamber shown in Figure 108. The anechoic chamber can handle models
for inlet-radiated-noise studies or for exhaust-radiated noise as will be dis-
cussed later. The models are powered by a 1.86-MW (2500-hp) drive system.
Physical dimensions of the chamber are approximately 10.7 m (35 ft) long by
7.6 m (25 ft) wide by 3 m (10 ft) high with microphones located at model-
centerline height on a 5.2-m (17-ft) arc.

An exact scale model of the UTW fan was used for these studies. It was
5.8 cm (20 in.) in diameter and could be manually adjusted for various blade
angles including those required to demonstrate reverse thrust. Test objec-
tives are summarized below:

- **Takeoff**

$M_T = .79$

Mach Number Suppression

Δ **PNdB**

Increasing Mach Number

- **Approach**
- **Reverse Thrust**

L_T

D

Treatment Suppression

Δ **PNdB**

Reverse Thrust — UTW

Increasing L$_T$/D
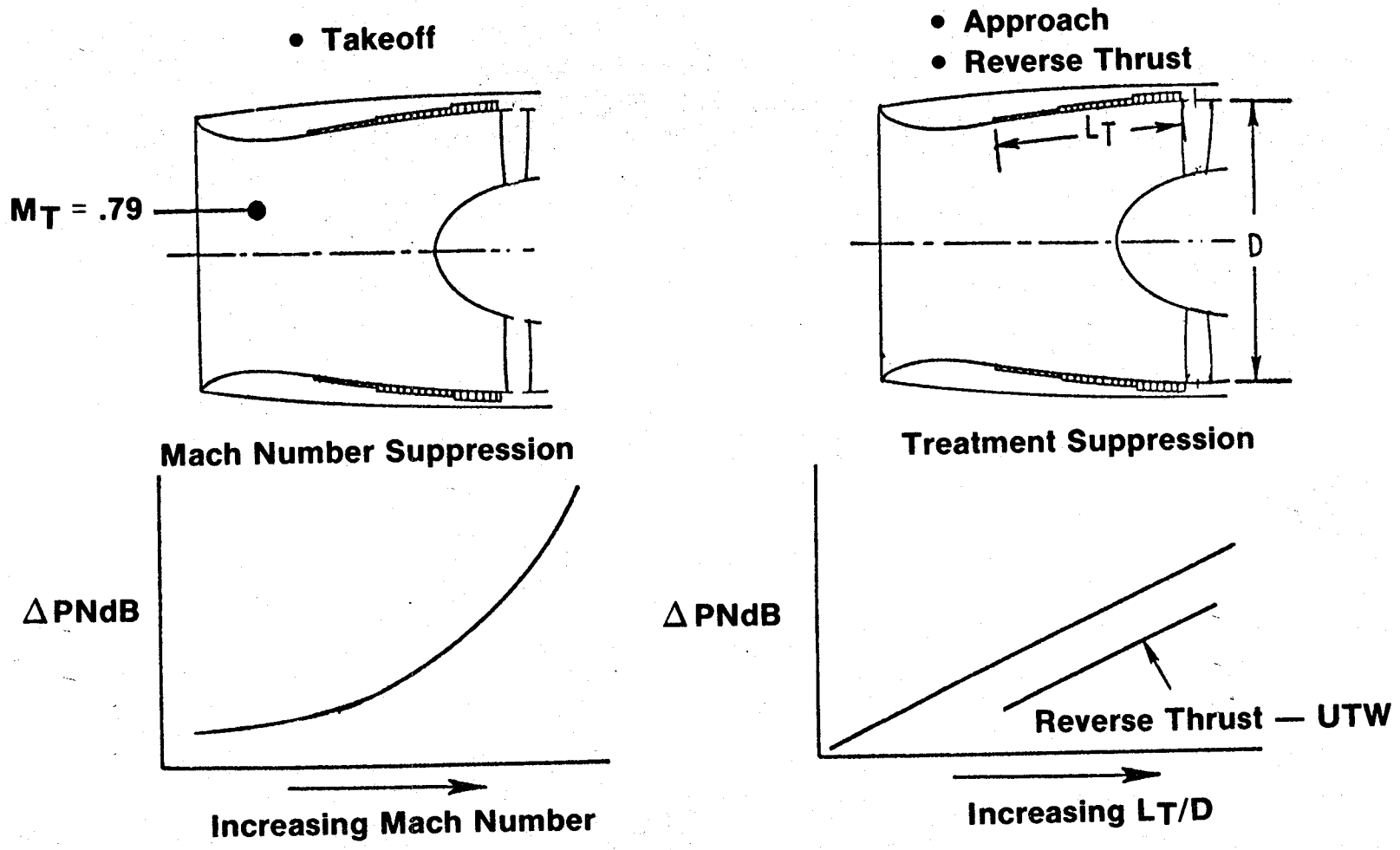
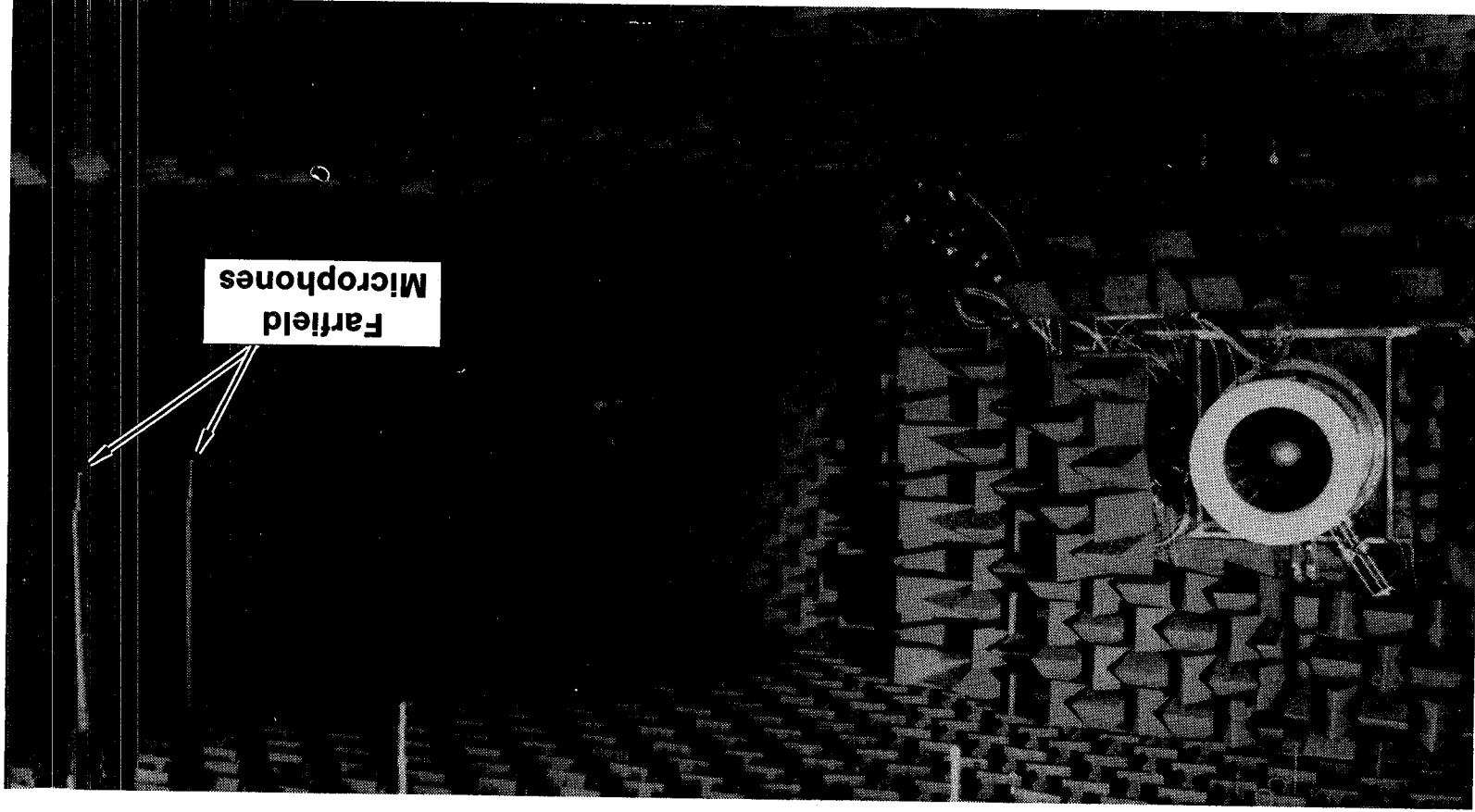Figure 107. QCSEE Inlet-Noise-Reduction Concepts.

Farfield Microphones

Figure 108. UTW QCSEE in Anechoic Chamber.

Forward Thrust

- Define unsuppressed spectrum and level
- Define suppression due to high throat Mach number
- Define suppression due to treated wall

Reverse Thrust

- Define unsuppressed spectrum and level
- Define suppression due to treated wall

Figure 109 presents the variation in inlet noise with throat Mach number and the PNL suppression that was achieved. These results indicate that the UTW takeoff suppression requirement of 12.8 PNdB could be met at an average throat Mach number of 0.79. The suppression due to high Mach number alone was about 10 PNdB with the wall treatment adding almost 3 PNdB.

In reverse thrust, the model tests indicated (as shown in Figure 110) that the objective level of suppression could be achieved; however, the unsuppressed levels were higher than expected. As will be shown later, this fact resulted in the UTW system-noise estimate in reverse thrust being revised to be above the goal of 100 PNdB.

Both inlets, as finally designed, are shown schematically in Figure 111. Both are high throat Mach number inlets designed to achieve takeoff suppression at a 0.79 throat Mach number. The treated-length-to-diameter ratio was 0.74 for both inlets. Wall treatment utilized on the inlets is shown schematically in Figure 112. The UTW utilized single-degree-of-freedom resonator treatment with a faceplate porosity of 10% and cavity depths ranging from 1.2 cm (0.5 in.) to 3.9 cm (1.5 in.). A bulk absorber type treatment was incorporated into the OTW inlet to provide wider bandwidth suppression. The bulk absorber consisted of seven compressed layers of a Kevlar material. It was a constant depth of 2.54 cm (1 in.) with porosity of 14% over the first half and 22% over the latter half. Although a scale model of the OTW fan was not tested, the inlet design was based upon General Electric experience from previous tests and consideration of the results of UTW model tests.

3.10.3 Fan Exhaust Design

As pointed out earlier in Figures 105 and 106, the engine designs incorporated both source-noise-reduction techniques and significant amounts of acoustic treatment to reduce exhaust-radiated noise. Source-noise-reduction techniques and treatment configurations were evaluated on the basis of past experience and the results of testing a low-pressure-ratio, variable-pitch, model fan (NASA Rotor 55) in the General Electric anechoic chamber. A photograph of the model as installed in the exhaust mode is shown in Figure 113. Testing evaluated such source-noise-reduction concepts as optimizing vane/blade ratio to minimize second-harmonic-tone propagation, rotor/stator spacing, and rotor/OGV treatment.

170
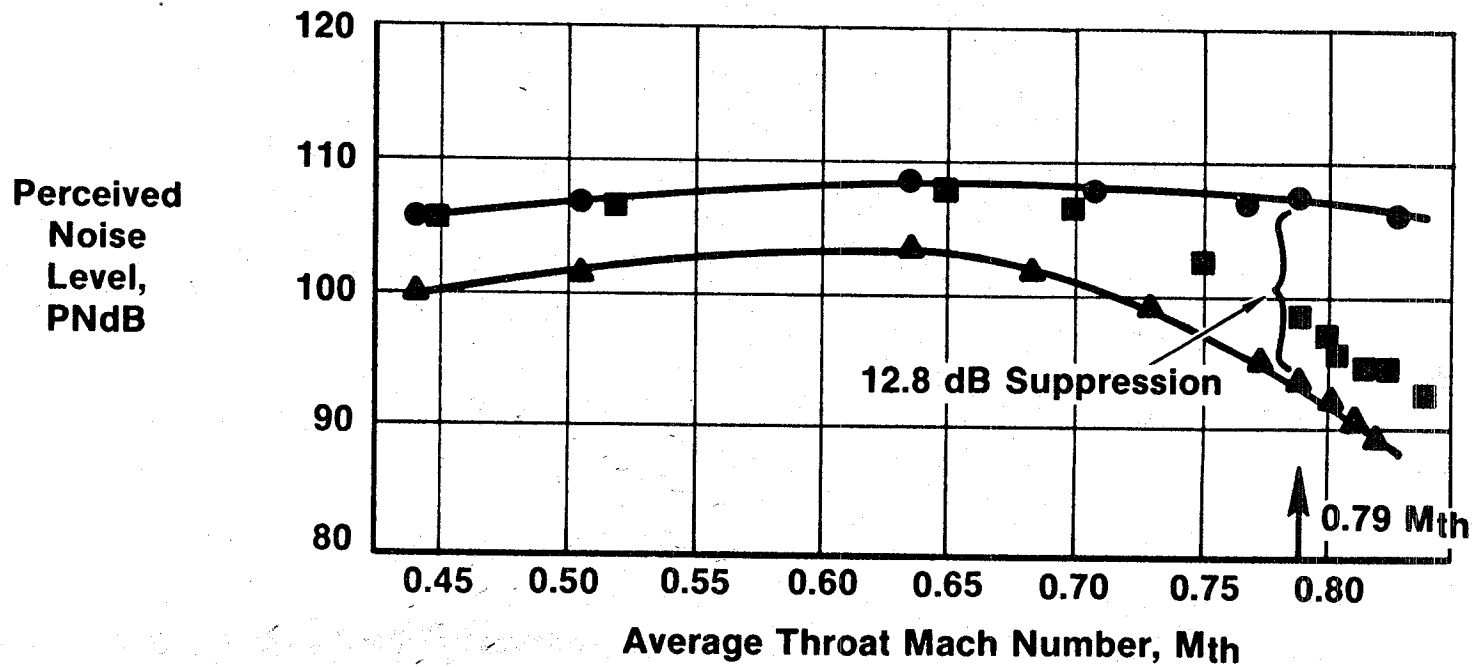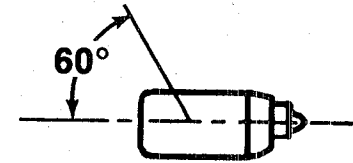
Figure 109. High Throat Mach No. Inlet Suppression, 50.8 cm (20 in.) Simulator Test.
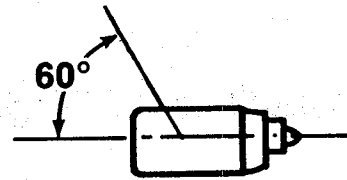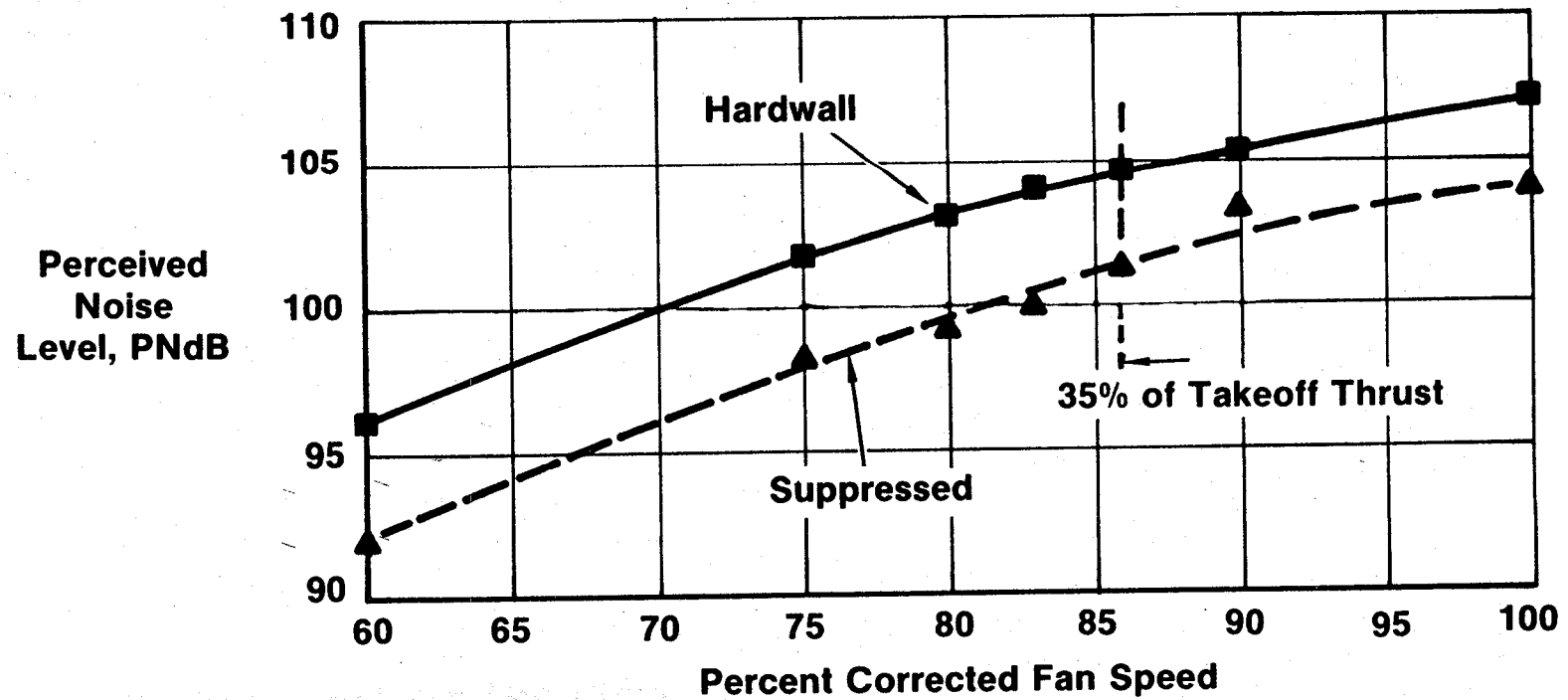
Figure 110. Reverse-Thrust Suppression, 50.8 cm (20 in.) Simulator Test.

- **0.79 Design Throat Mach Number**
- **Treated L/D = 0.74**

UTW

OTW
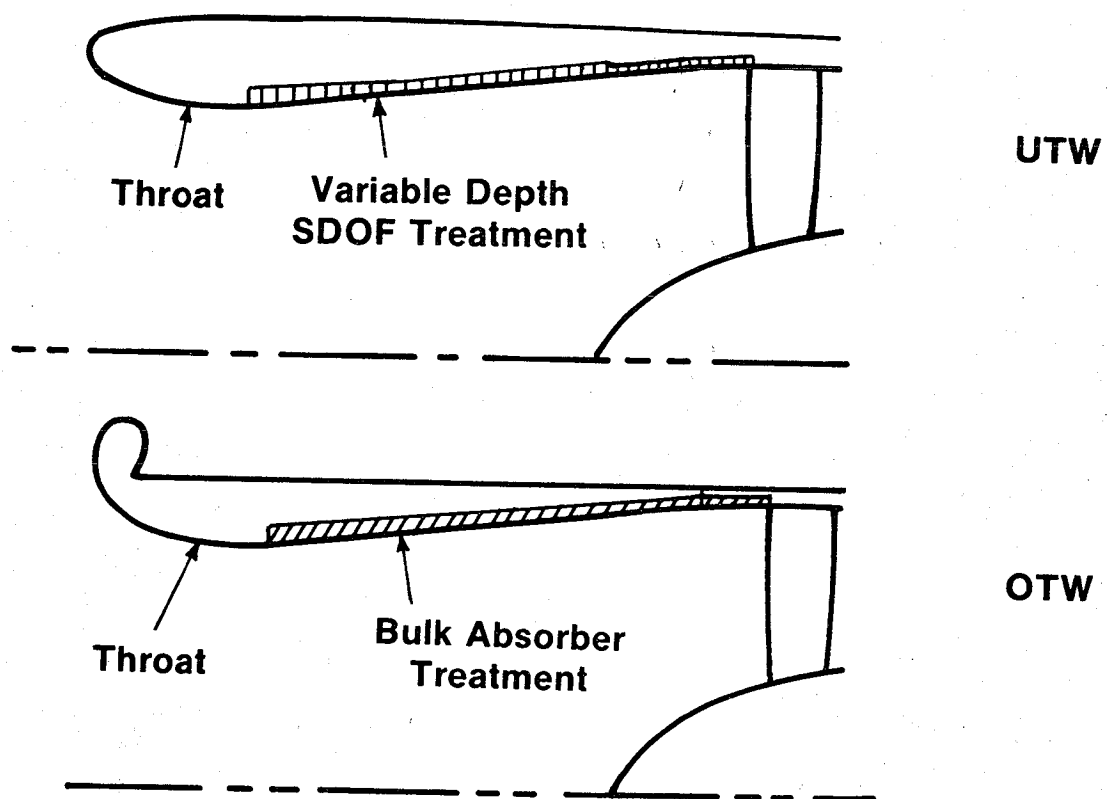
Figure 111. Inlet Acoustic Configurations.

Perforated Facesheet

Cavity
Depth

UTW (SDOF)

Facesheet Porosity_____10%
Cavity Depth_____1.2cm to 3.8cm
(0.5 in. to 1.5 in.)

Hexagonal
Honeycomb Cell

Solid Backing Sheet

Perforated Facesheet

Depth

OTW (Bulk Absorber)

Facesheet Porosity_____14 to 22%
Depth_____ 2.5 cm (1 inch)

7
Kevlar
Layers
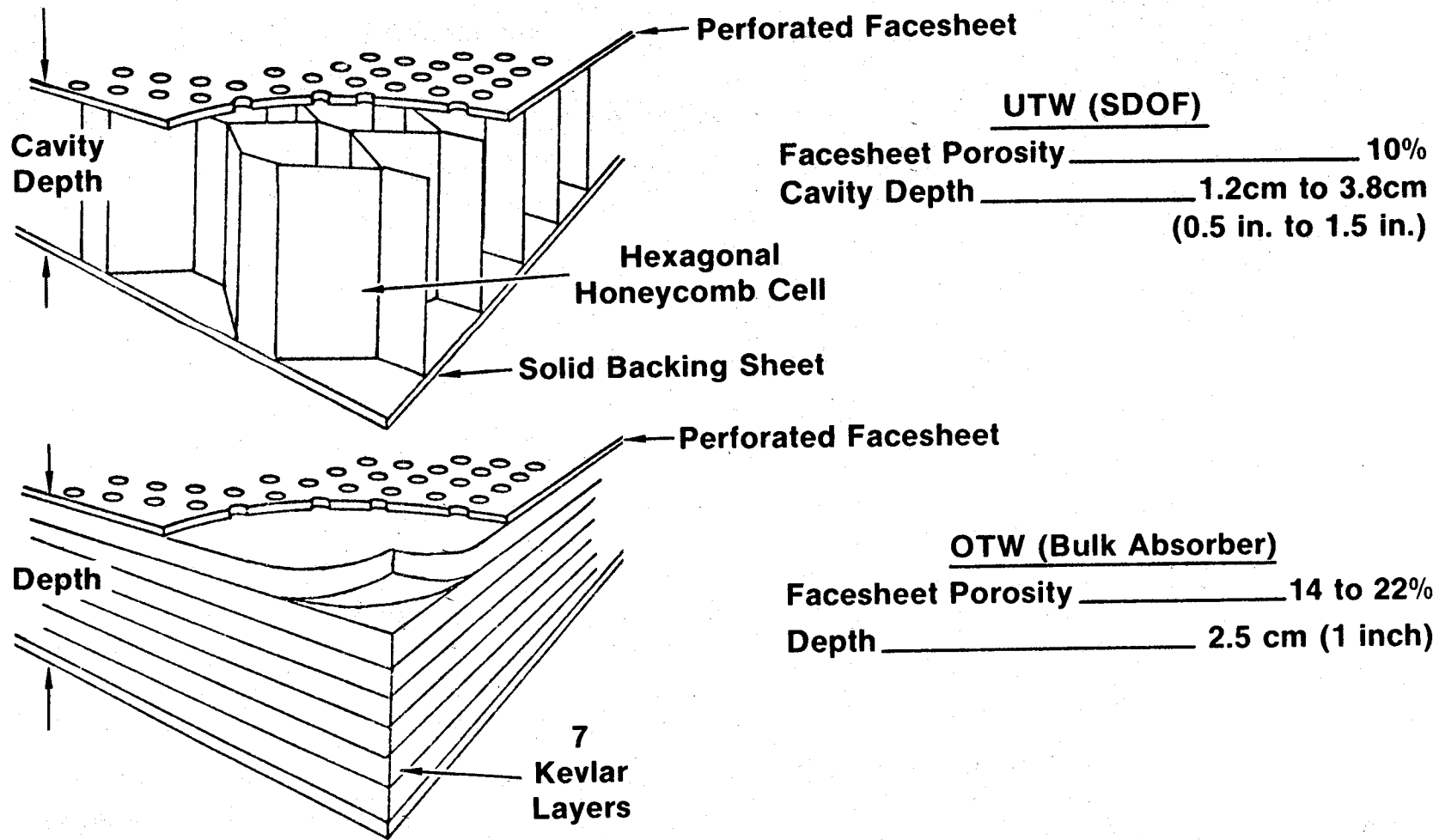
Figure 112. Inlet Acoustic Treatment.

The vane/blade ratio study was conducted at two different rotor/stator spacings. As shown in Figure 114, the data at 0.5 chord spacing indicates a second-harmonic SPL minimum at a vane/blade ratio of 1.88. At the wider spacing of 1.5 chords, the data do not show this because the rotor/stator interaction noise is masked by rotor noise caused by turbulence generated upstream of the rotor. At the close spacing, rotor/stator noise is dominant, allowing us to see the second-harmonic minimum.

A series of spacing tests from 0.5 chords to 2.0 chords was conducted. Figure 115 is a comparison between the measured levels and the sum of predicted rotor/stator interaction noise and rotor/turbulence noise at each spacing. This was done at the optimum vane/blade ratio. Excellent agreement between predicted and measured data is evident.

Tests of treatment between the rotor and OGV indicated that 4 to 5 dB suppression could be achieved at the blade-passing frequency. Accordingly, the fan frame was designed to incorporate rotor/OGV treatment.
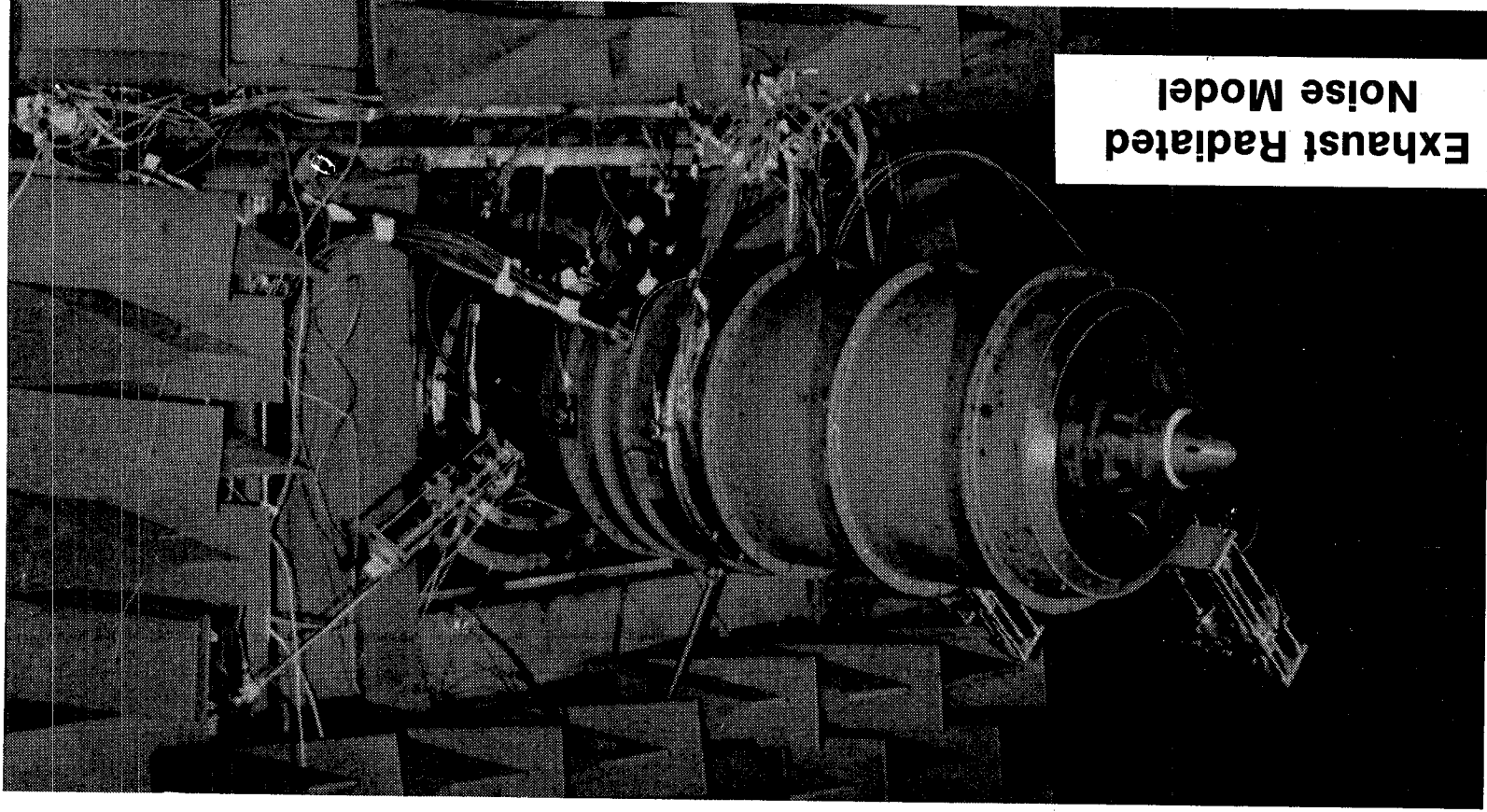
The model fan had the capability to test up to four axial sections of treatment in the exhaust mode. Various combinations of faceplate porosity, treatment depths, and axial deployment were evaluated. Suppression results from one of those configurations are represented in Figure 116. Note the axial variation in treatment depth and faceplate porosity. The results indicate that such an orientation achieves higher suppression above the peak tuning frequency than one would predict from summing the suppressions of the individual panels. On the basis of these results, design curves for the engines were changed to account for this higher level of suppression with variable-depth, variable-porosity treatment.

A schematic of the exhaust treatment design for the UTW is presented in Figure 117. OTW engine exhaust treatment was very similar. All the suppression material was the single-degree-of-freedom resonator type shown in Figure 118. Fan frame treatment between the rotor and OGV was tuned to the blade-passing frequency of each engine and had a faceplate porosity of 10%. Fan-bypass wall treatment depths varied from 1.9 cm (0.75 in.) to 5.1 cm (2.0 in.) and porosities from 15 to 22%. Splitter length of 1.02 m (40 in.) included single-degree-of-freedom treatment of 1.27 cm (0.5 in.) with a porosity of 11.5%. Although a scale-model test with treated vanes was not conducted, design studies indicated a potential for reducing high-frequency, broadband noise; thus, the pressure surface of the OGV's was treated on the full-scale engines. The resulting suppression spectrum for the UTW aft-radiated fan noise, utilizing the treatment of Figure 117, is shown in Figure 119. Such a suppression spectrum would achieve 13.4 PNdB of aft-fan-noise suppression at takeoff on the UTW.

3.10.4 Core Suppressor Design

The QCSEE core exhaust provides a rather severe problem in acoustic-suppression design. The unsuppressed source-noise spectrum has both high-frequency, broadband noise from the turbine and low-frequency, broadband noise
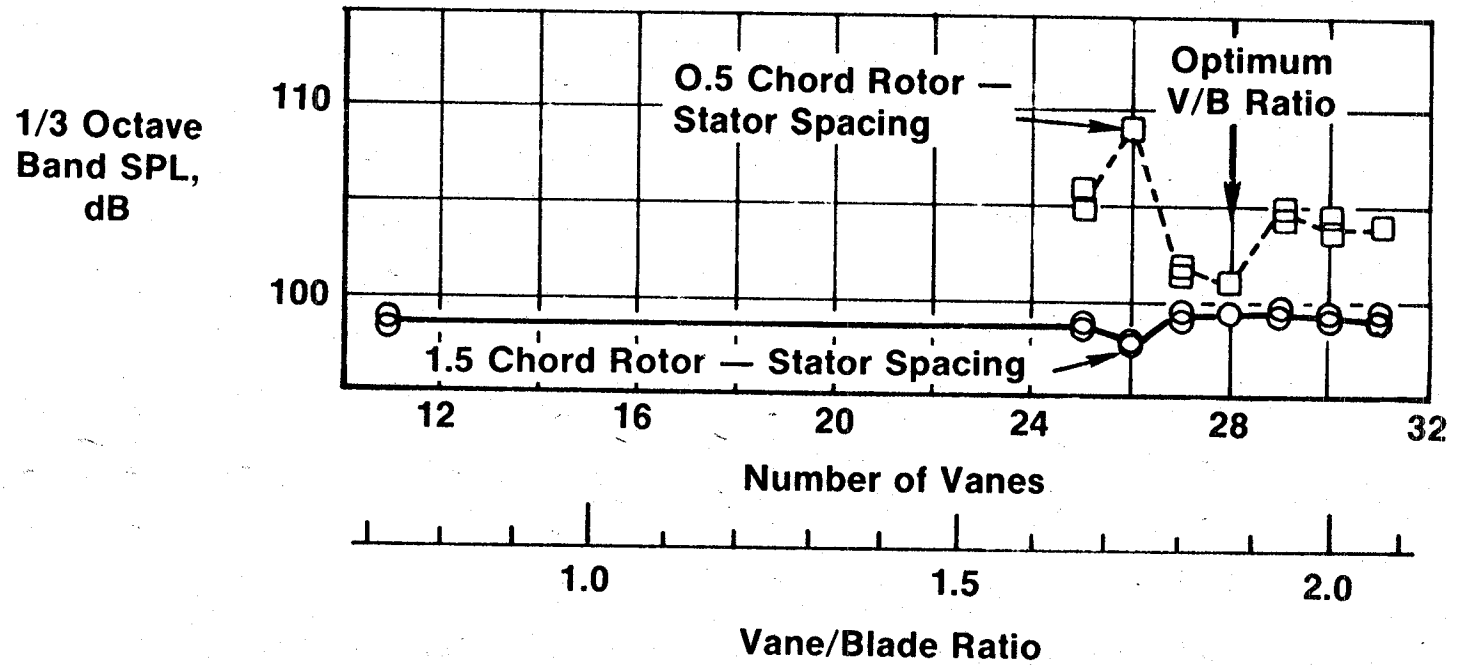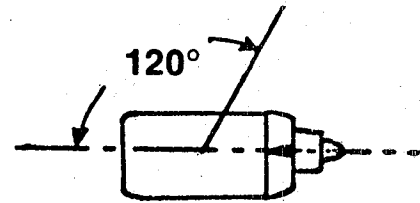
Figure 114. Effect of Vane Number on Second-Harmonic SPL.

• Low Pressure Ratio Model Fan
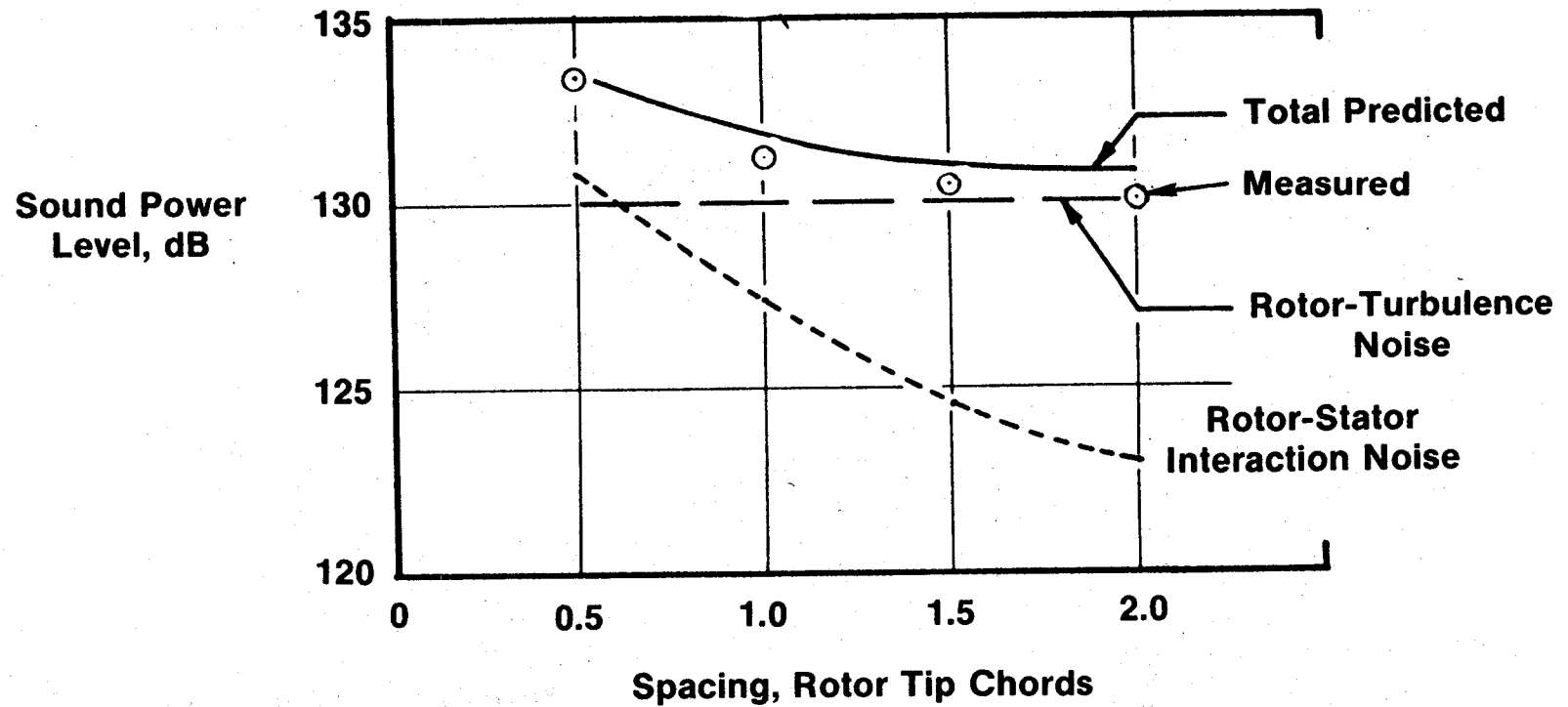
Figure 115. Summation of Rotor-Turbulence and Rotor/Stator Noise.

- **Low Pressure Ratio Fan (NASA Rotor 55)**
- **100% N/ $\sqrt{\theta}$**
- **Variable Depth, Variable Porosity**

Flow ➡

Porosity   **12%**   **12%**   **12%**   **27%**

120°
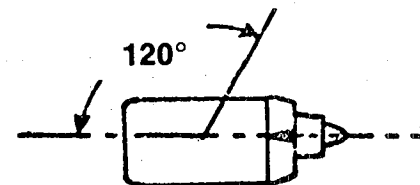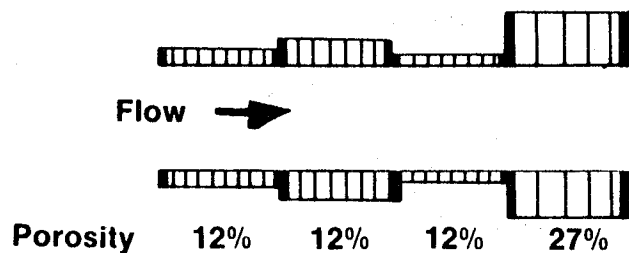
1/3 Octave Band Suppression, dB

Measured

Predicted

Frequency, Hz
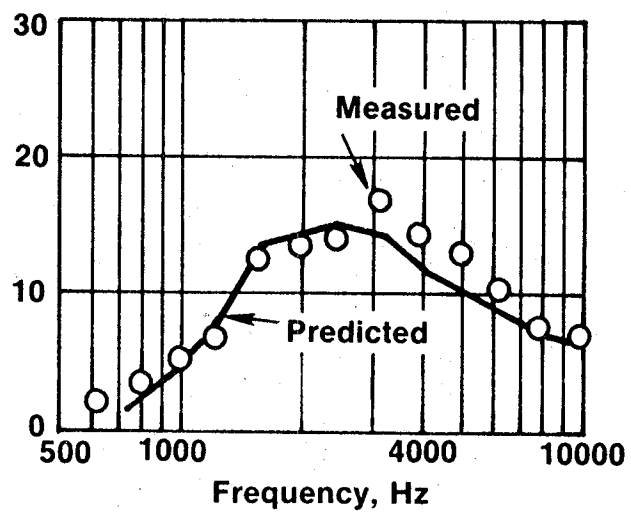
Figure 116. Scale-Model Suppression Test Results.

179

Variable Depth, Variable Porosity Treatment

Acoustic Splitter

Treated Vanes
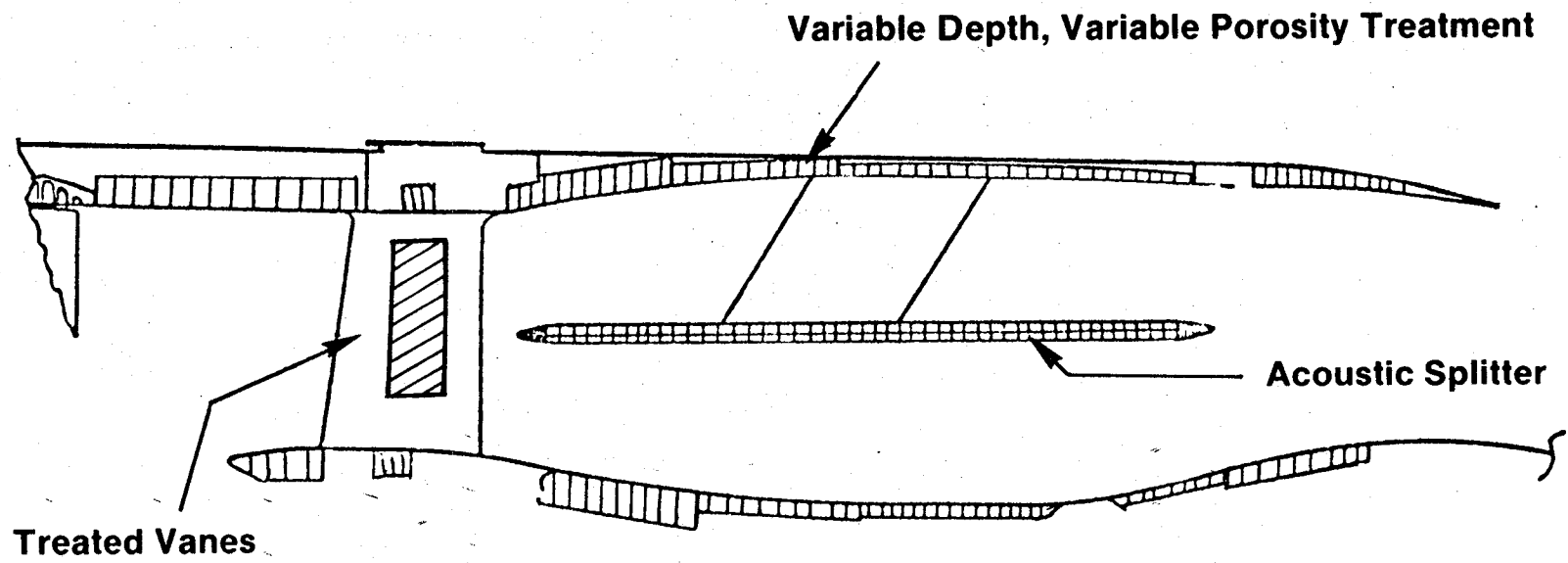
Figure 117. Fan Exhaust Treatment Configuration.

Perforated Facesheet

Cavity Depth

Solid Backing Sheet

Hexagonal Honeycomb Cell
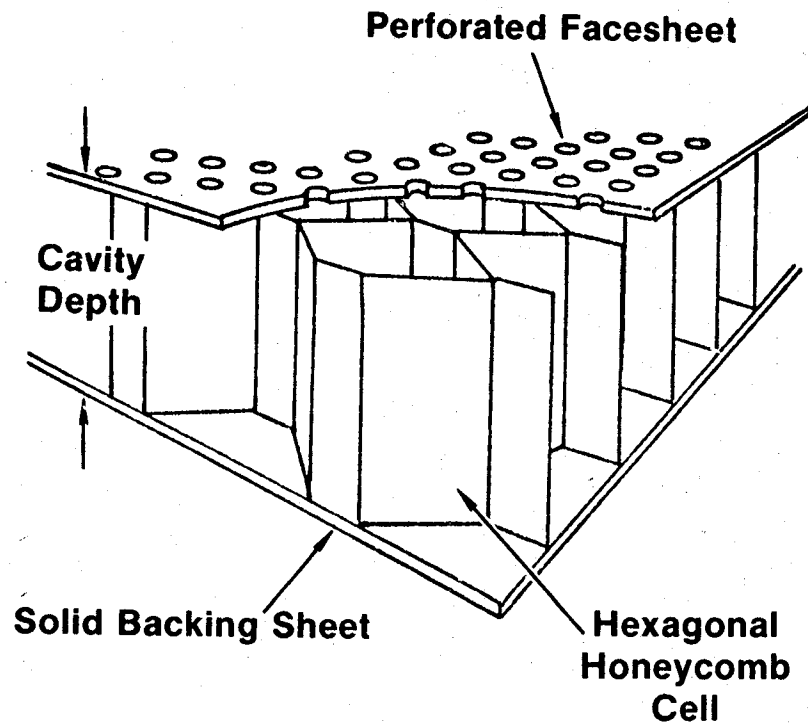
Wall Treatment

Facesheet Porosity_____10 to 22%

Cavity Depth_____ 1.9 cm to 5.1 cm

(0.75 to 2.0 in.)

Acoustic Splitter

Facesheet Porosity _____ 11.5%

Cavity Depth _____1.27 cm

(0.5 in.)

Figure 118.   Single-Degree-of-Freedom Exhaust Acoustic Treatment.

**1/3 Octave
Band Sound
Pressure Level
Suppression, dB**

**PNL Suppression
13.4 PNdB**
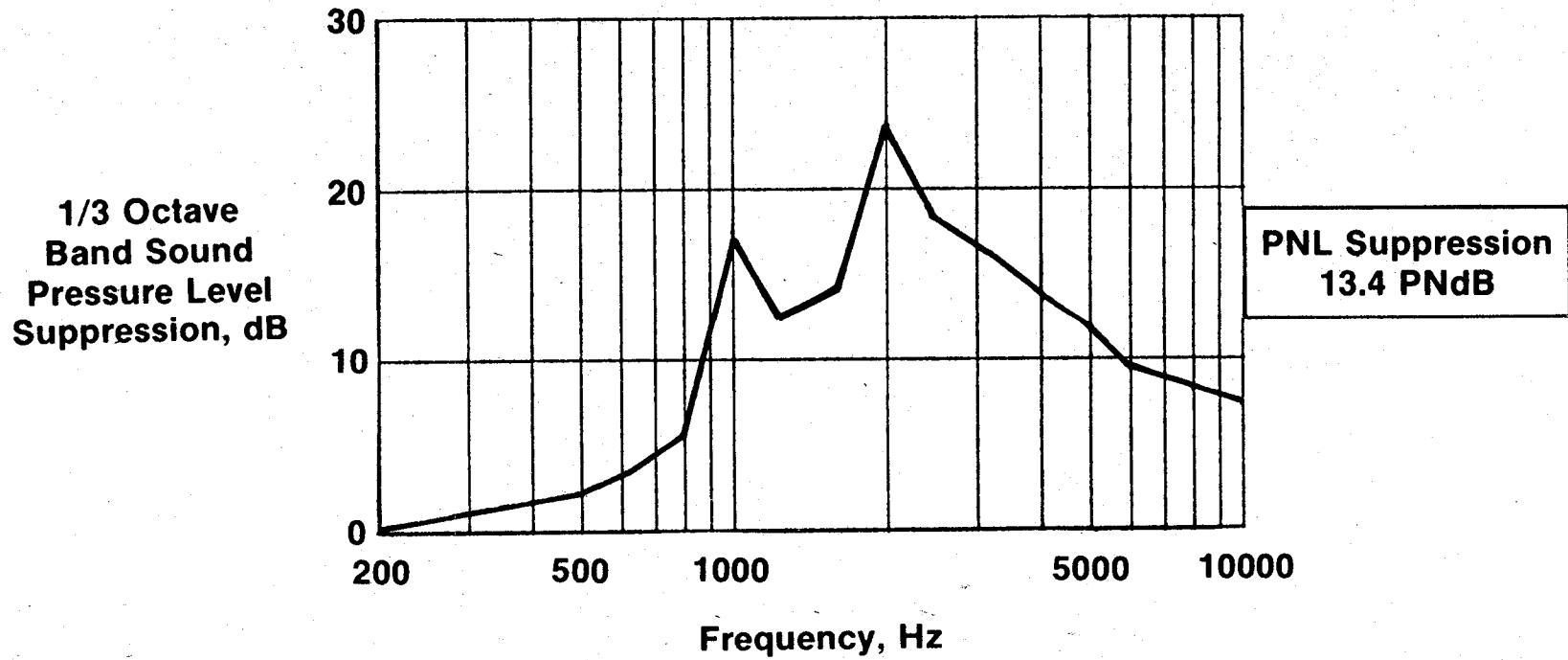
Frequency, Hz

- **Takeoff Power**
- **Max Aft Angle**

Figure 119. Predicted UTW Fan Exhaust Suppression.

from the combustor. To attain any meaningful noise reduction, the suppressor must attenuate both the high- and low-frequency noise levels. Physical constraints on the engine prevented sufficient amounts of thick (low frequency) and thin (high frequency) treatment from being installed in tandem to give adequate suppression. It was decided to adopt a new concept as shown in Figure 120 and employ a "stacked" treatment design. In this concept, the thin turbine treatment is placed along the duct walls. Thick combustor treatment is then placed behind this turbine treatment and communicated to the duct by means of tubes passing through the turbine treatment. Figure 121 shows the treated QCSEE core plug. Note the larger diameter holes which communicate to the combustor treatment.

A model of this advanced concept was built and tested in the General Electric High Temperature Duct Facility. Results from these tests are shown in Figure 122; they indicate that the stacked treatment would provide the required levels of suppression of 5.1 and 9.89 PNdB in the low- and high-frequency regimes.

3.10.5 QCSEE UTW System Noise Predictions

Since the engine noise levels were to be measured during static testing, a procedure for determining in-flight noise levels from static data was completed as a part of the design effort. This procedure includes the following:

- Jet/flap noise-calculation procedure

- Extrapolation procedures

- Corrections for engine size

- Doppler shift corrections

- Corrections for number of engines

- Dynamic effect correction

- In-flight clean-up and up-wash-angle correction

- Relative velocity correction for jet/flap noise

- Fuselage shielding and OTW shielding

- PNL to EPNL calculation

Calculated jet/flap interaction noise was used to replace the jet noise on the static engine; however, an advanced-technology allowance was assumed on jet/flap noise of 3.5 PNdB on the UTW and 2.5 PNdB on the OTW to account for anticipated reduction in jet/flap noise by the 1980's when QCSEE-powered aircraft might be flying.
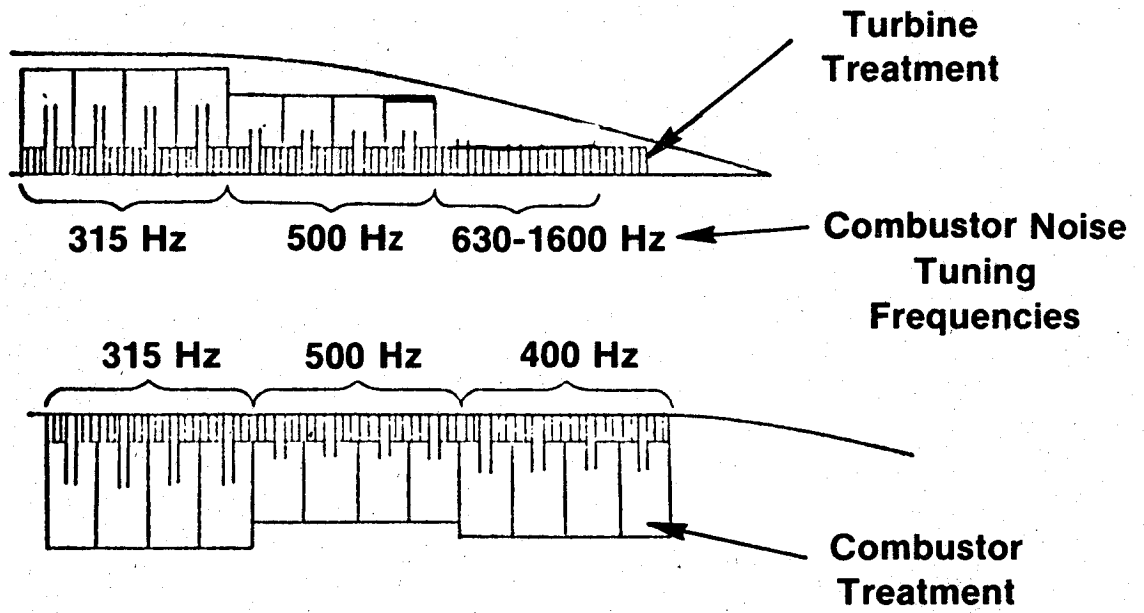
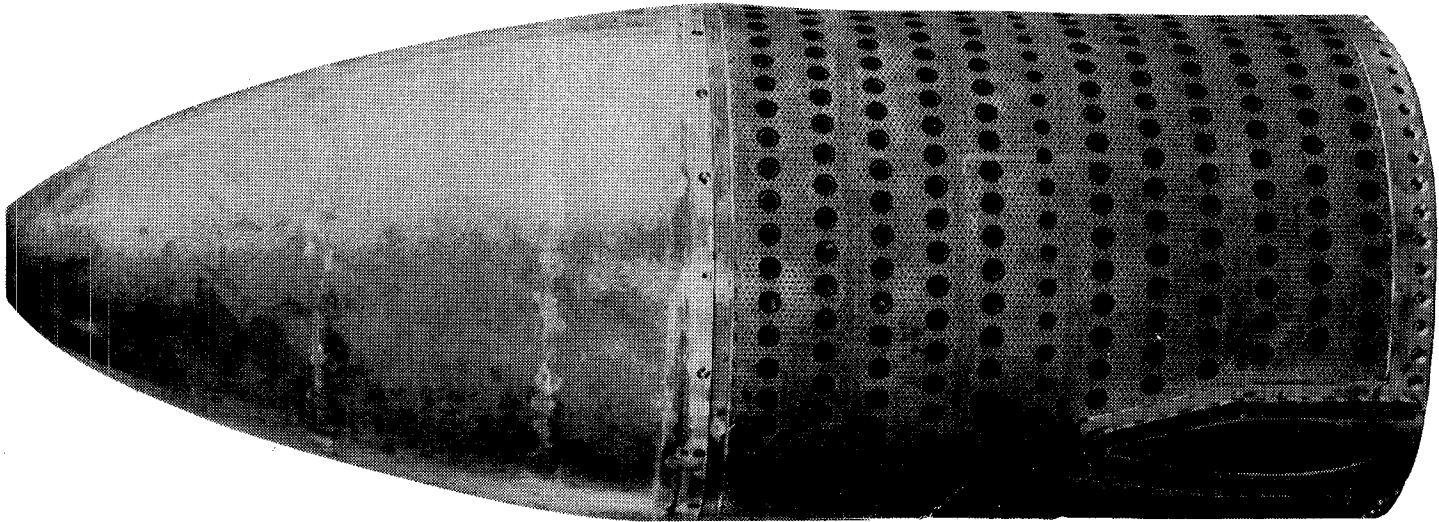Figure 120.   Core Stacked-Treatment Suppression.

Figure 121. QCSEE Core Exhaust Nozzle.

Predicted PNL Suppression
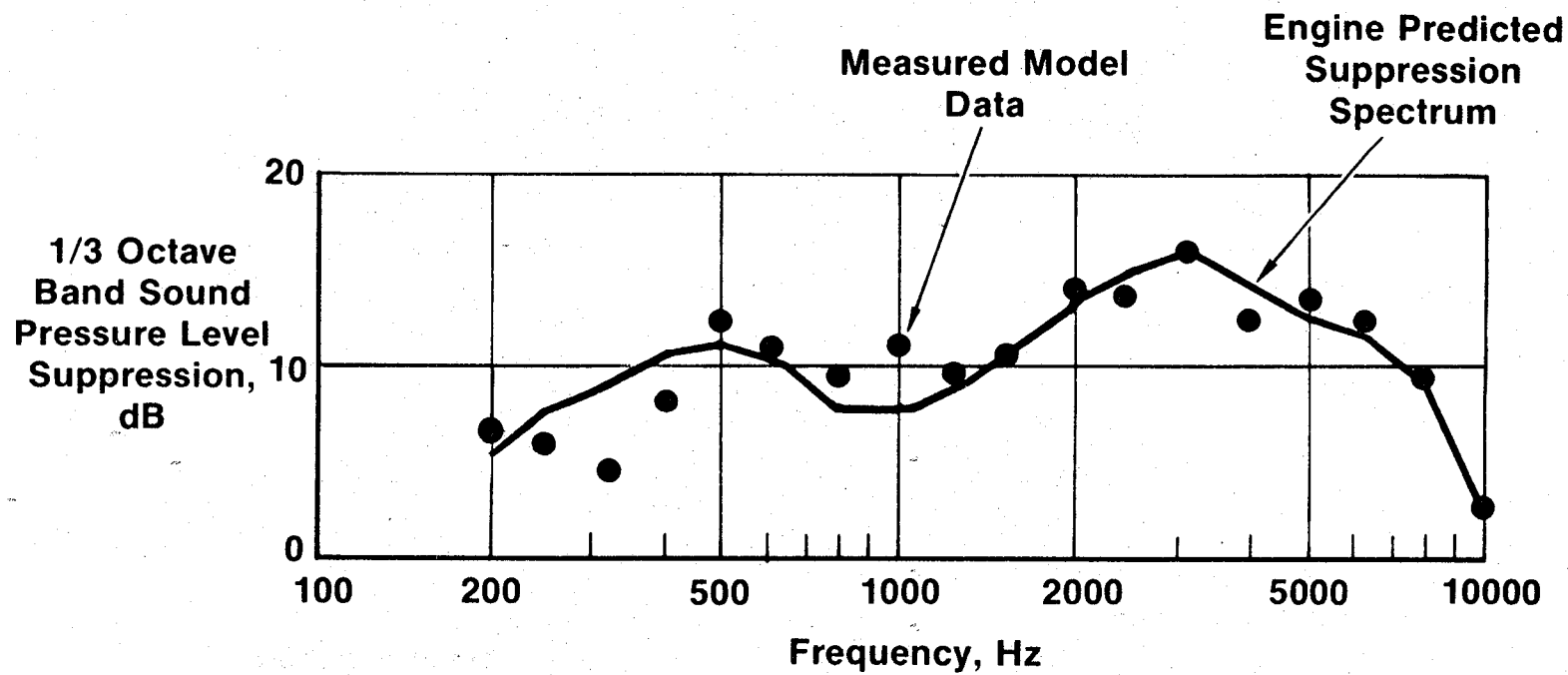Combustor___ 5.1
Turbine_____ 9.8

Figure 122.   Hot Duct Model Test Data.

System noise levels for the UTW QCSEE are presented in Figure 123 at the takeoff condition. Unsuppressed noise is dominated by the fan in both the forward and aft quadrants. The suppressed levels are balanced between fan, jet/flap, and combustor noise in the aft quadrant and dominated by jet/flap noise in the forward quadrant. The predicted EPNL for the four-engine UTW configuration at takeoff is 93.6 EPNdB compared to the goal of 95.0 EPNdB on a 152-m (500-ft) sideline.

To obtain 65% of takeoff thrust at approach, the UTW QCSEE with its variable-pitch fan may be operated at a variety of fan speed, blade-pitch angle, and fan-nozzle-area combinations. For these acoustic predictions, the fan speed was held at a takeoff speed to minimize engine-response time in the event of a waveoff during landing. Fan nozzle area was wide open to lower jet velocity, and hence jet/flap noise, and the blade-pitch angle was closed down to give the required thrust. In such a mode of operation, unsuppressed noise, Figure 124, is dominated by fan noise in both the forward and aft quadrants. Suppressed, the forward quadrant is dominated by fan noise while the aft quadrant has a balanced design with fan, combustor, and jet/flap noise about the same level. Estimated EPNL for approach is 93.3 compared to the goal of 95.0 EPNdB.

In reverse thrust, Figure 125, the UTW noise levels are dominated by the forward-quadrant fan noise both unsuppressed and suppressed. These levels, based on the 50.8-cm (20-in.) model tests, indicate that in reverse thrust the engine will be 103.9 PNdB on a 152-m (500-ft) sideline or 3.9 PNdB over the goal of 100 PNdB. It would be difficult to obtain more fan-inlet suppression without degrading the suppression at takeoff and approach and eroding the margin present at those conditions. This treated, composite-nacelle design provides the most balanced approach to meeting the three noise goals.

3.10.6 QCSEE OTW System Noise Predictions

System-noise levels for the OTW QCSEE were also predicted. At takeoff (Figure 126), unsuppressed fan noise controls forward and aft quadrants. In the suppressed configuration, fan and jet/flap noise are about the same level. The resulting system EPNL is 95.4 EPNdB, only slightly above the goal of 95. Any reduction to lower the level to 95.0 EPNdB must include jet/flap noise reduction since it is a major contributor.

At approach (Figure 127), fan suppression has lowered the dominant unsuppressed fan noise to the level of jet/flap noise. These two sources, suppressed fan and jet/flap, combine to give a predicted EPNL of 90.0 EPNdB which is well under the goal of 95.0.

For reverse-thrust operation, the OTW engine utilized a target reverser. General Electric had conducted tests on a 1/6 scale model of the OTW target thrust-reverser system. On the basis of these tests, it was realized that the jet noise levels of the target reverser were much higher than anticipated, and only a reduction in fan pressure ratio was likely to produce a significant reduction in reverse-thrust noise. With this in mind, the predicted OTW reverse-thrust noise level in Figure 128 is 106.4 PNdB or 6.4 PNdB above the goal.
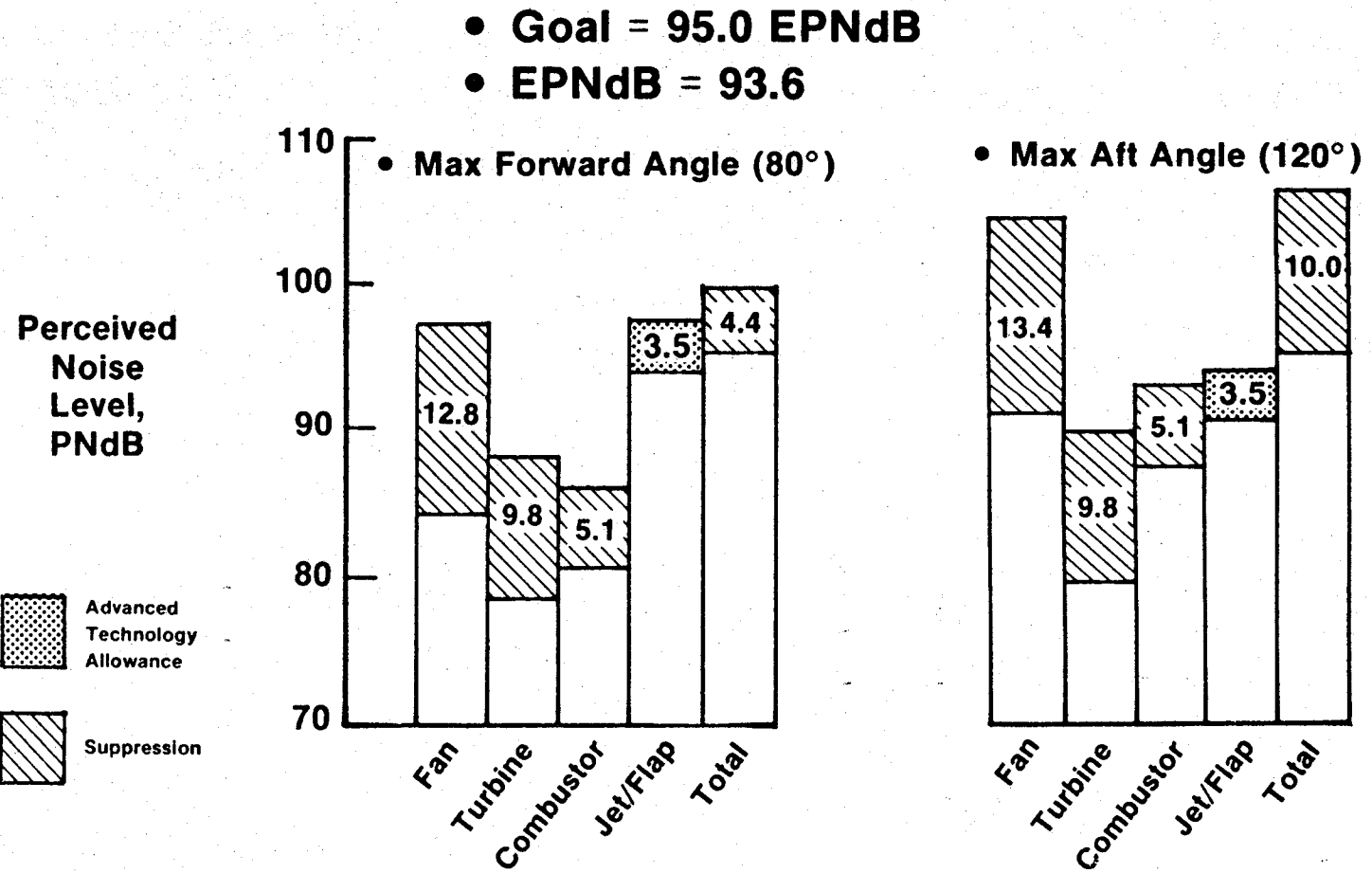
Figure 123. UTW Takeoff Noise Predictions.

- 65% of Takeoff Thrust
- Goal = 95.0 EPNdB
- EPNdB = 93.3

Perceived Noise Level, PNdB

- Max Forward Angle (60°)
- Max Aft Angle (120°)

Advanced Technology Allowance

Suppression
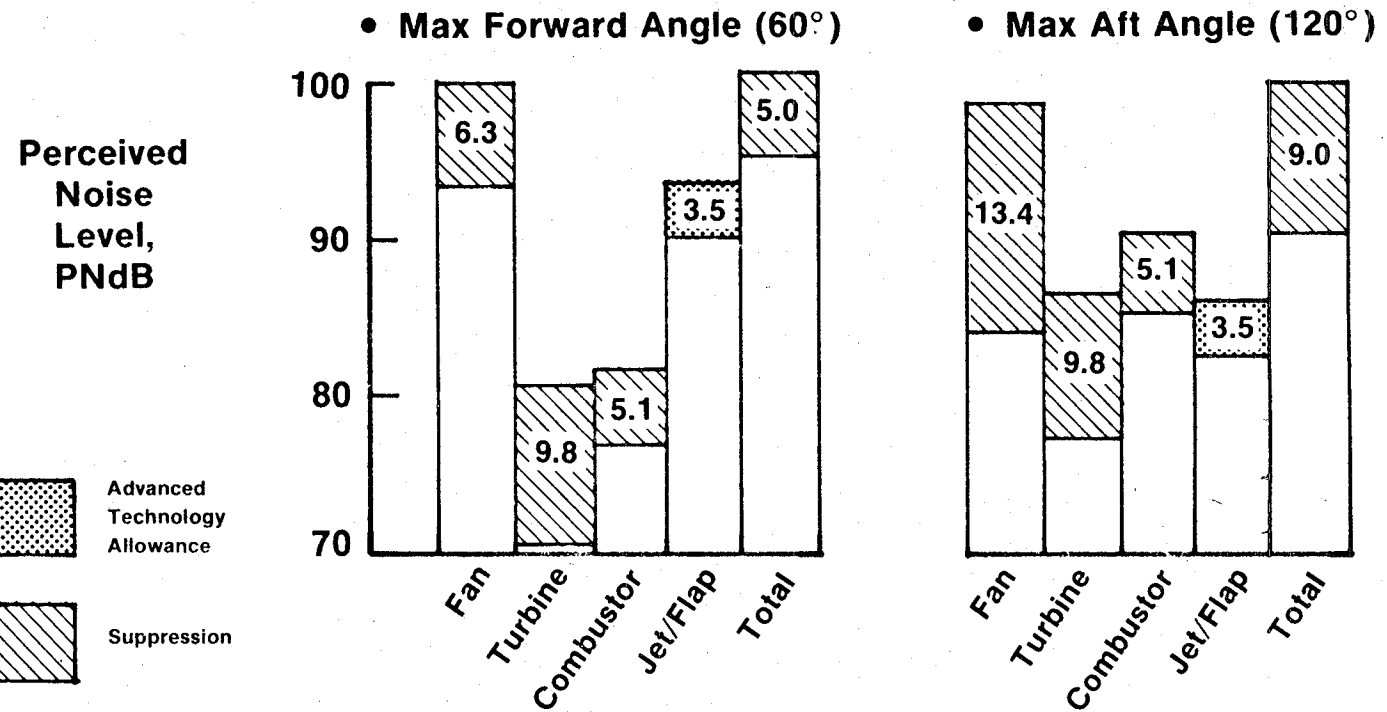
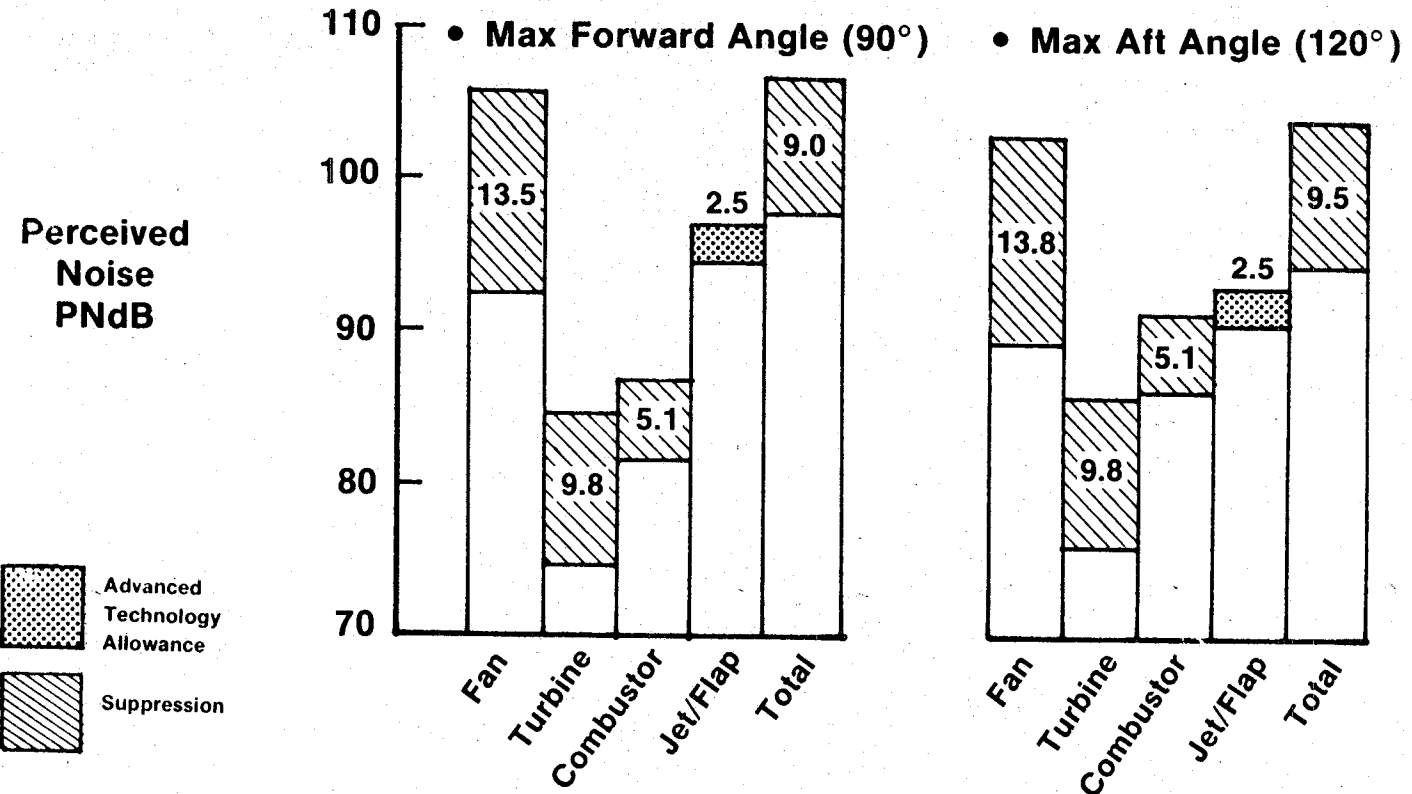Figure 124. UTW Approach Noise Predictions.

189
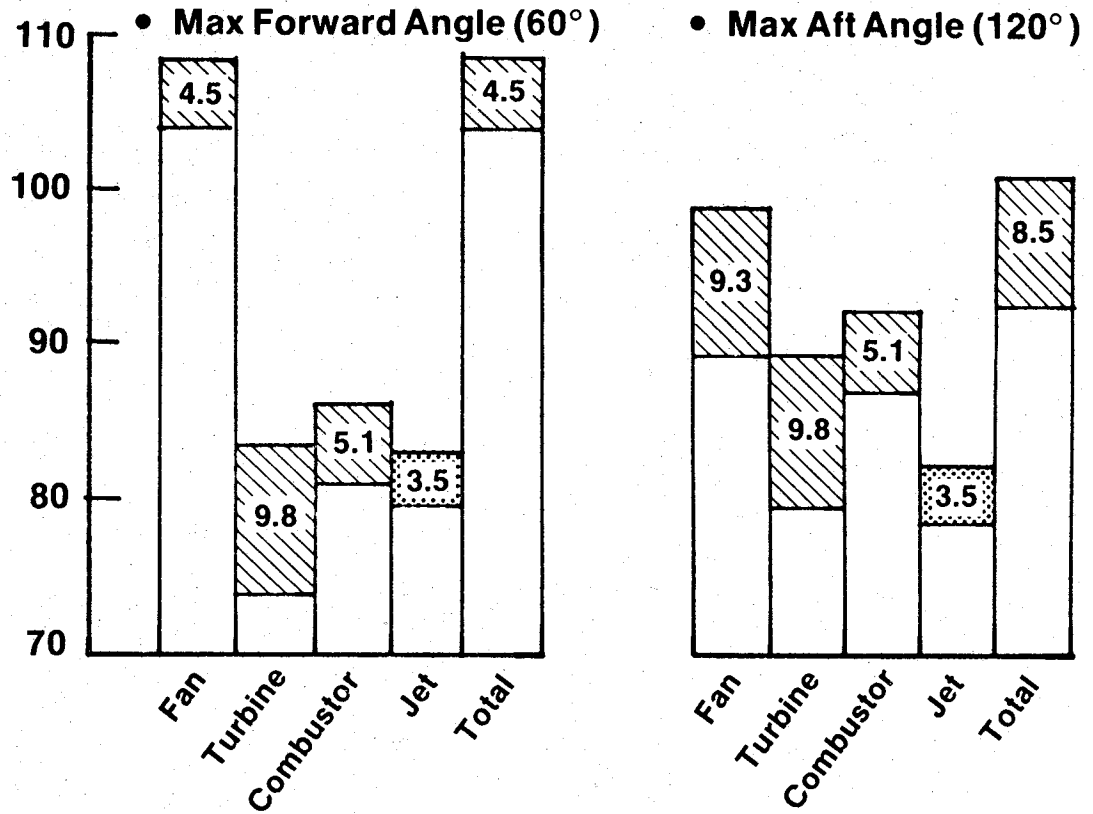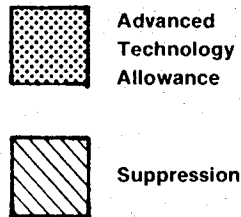
Figure 125. UTW Reverse-Thrust Noise Predictions.

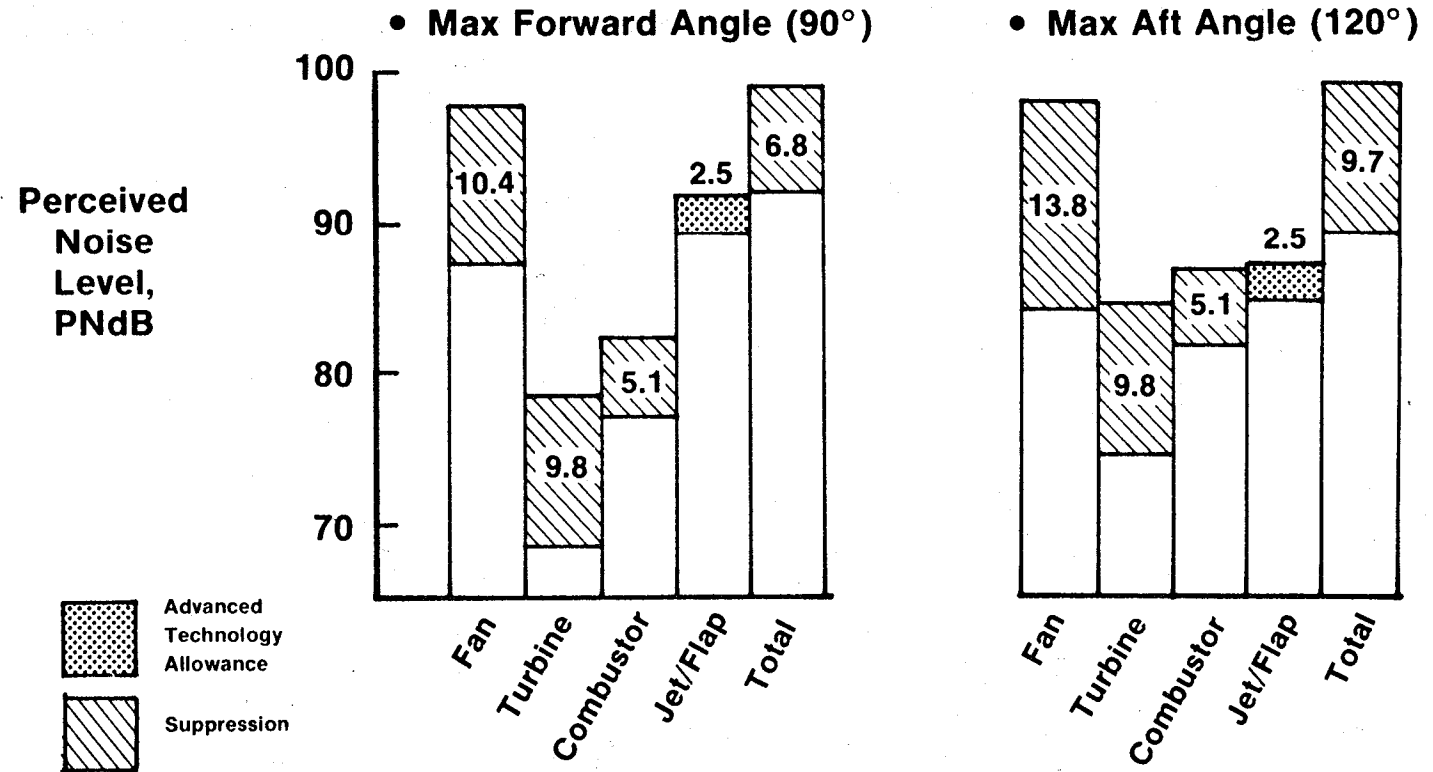Figure 126. OTW Takeoff Noise Predictions.

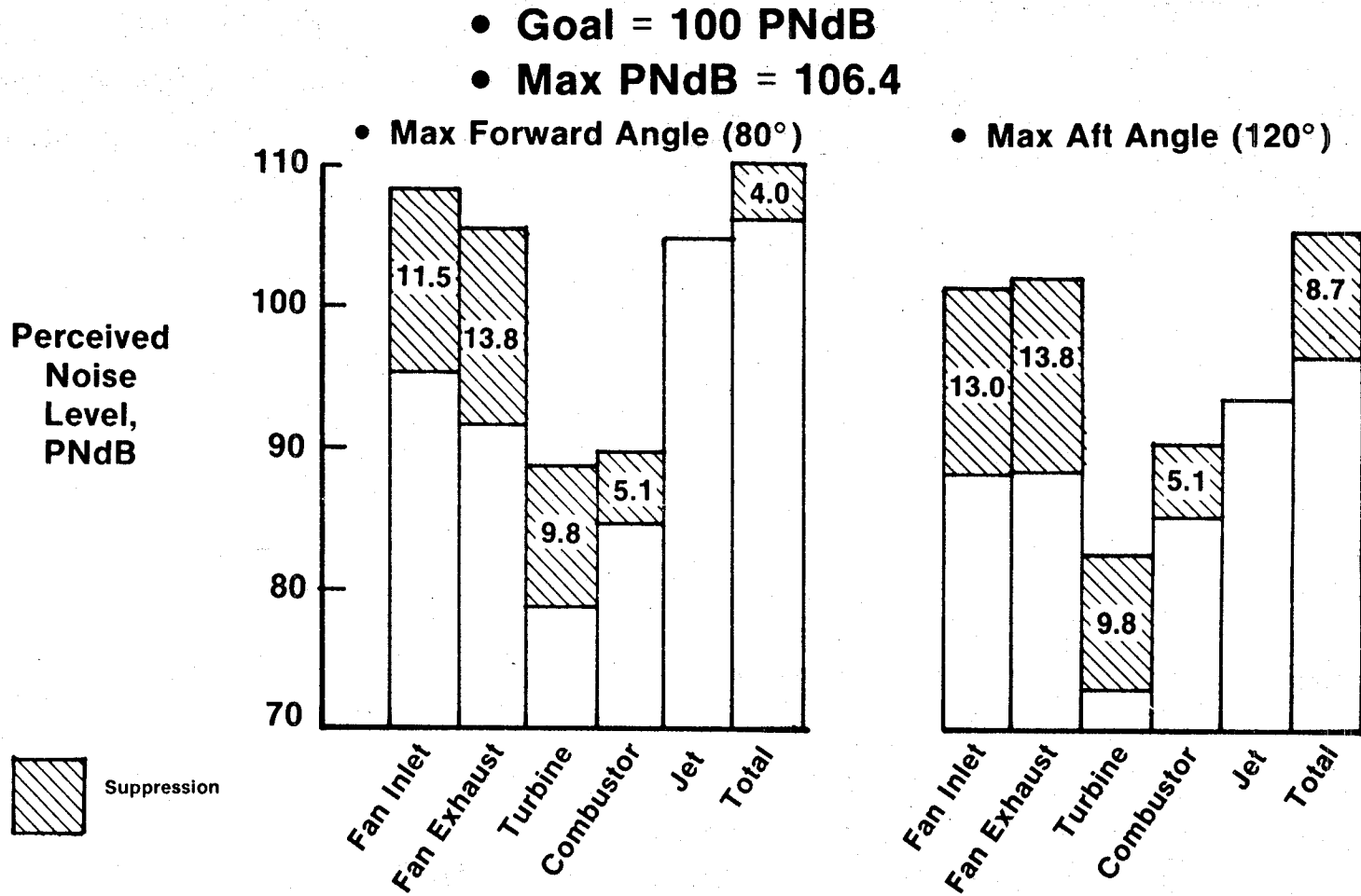Figure 127.   OTW Approach Noise Predictions.

Figure 128.   OTW Reverse-Thrust Noise Predictions.

4.0 ENGINE TEST RESULTS

This section presents and discusses the results of testing UTW and OTW propulsion systems. All testing was conducted at General Electric's Peebles, Ohio outdoor test site 4D. This site includes an overhead engine-support structure with all necessary fuel, lubrication, air, and electric facilities. An adjacent control room is linked to the Evendale computer by an automatic data-handling system using leased telephone equipment. The test site includes an acoustic field for recording far-field acoustic data over a 150° arc.

The history of UTW testing is summaried in Table XXIV. Testing was initiated on 2 September 1976 with boilerplate nacelle components and using the cam/harmonic pitch-actuation system. Mechanical and performance testing was completed except for the planned reverse-thrust test. During this phase of testing, an exhaust nozzle support-ring attachment failure occurred, allowing one nozzle flap to be drawn into the engine and causing secondary damage to the fan blades.

Damaged parts were repaired or replaced, and the engine was reinstalled in September 1977 for completion of the test program. The second installation included the ball spline pitch-actuation system and the entire composite nacelle. Planned testing, including acoustic measurements, was completed in July 1978. The engine was then refurbished and delivered to NASA for further testing at the Lewis Research Center.

The history of OTW testing is summarized in Table XXV. The entire test program was conducted on this engine between 6 April and 9 June 1977. All testing included the boilerplate nacelle and "D" shaped exhaust nozzle. The OTW engine was refurbished and delivered to NASA in July, 1977.

4.1 OVERALL ENGINE PERFORMANCE

4.1.1 UTW Performance Test

Figure 129 shows the UTW engine as it was initially tested with a bell-mouth inlet for airflow calibration and to establish uninstalled performance levels with essentially 100% ram recovery. The high throat Mach number inlet, shown in Figure 130, was then used to determine installed performance with realistic induction losses.

Measured uninstalled thrust with the bellmouth inlet is shown on Figure 131 as a function of airflow for operating lines established by four fan-exhaust-nozzle areas. Points along each operating line represent various combinations of blade angle and fan speed that can pump the indicated airflow. Thus, the curve is independent of blade angle and speed. The goal thrust level could be reached with a variety of settings of the controlled parameters.

194

Table XXIV. UTW Test History.

Boilerplate Nacelle, Cam-Harmonic Pitch Actuation

47 Hours (9/2/76 — 12/17/76)

- Mechanical and Controls Checkout
- Aero Performance Mapping — Bellmouth Inlet
- Performance Ratings — High Mach Inlet
- Reverse Thrust Test (Incomplete)

Composite Nacelle, Ball Spline Pitch Actuation

106 Hours (9/8/77 — 4/27/78, 7/13/78 — 7/21/78)

- Mechanical and Performance Checkout
- Acoustic Baseline — Bellmouth/Hardwall
- Suppressed Acoustic Test — High Mach Inlet, Treatment
- Reverse Thrust Performance and Acoustics
- Acoustic Technology and Control Tests

Table XXV. OTW Test History.

Boilerplate Nacelle

58 Hours (4/6/77 — 6/9/77)

- Mechanical and Controls Checkout
- Aero Performance Mapping — Bellmouth Inlet
- Performance Ratings — High Mach Inlet
- Reverse Thrust Performance
- Acoustic Baseline — Bellmouth, Hardwall
- Suppressed Acoustics — High Mach Inlet, Treatment
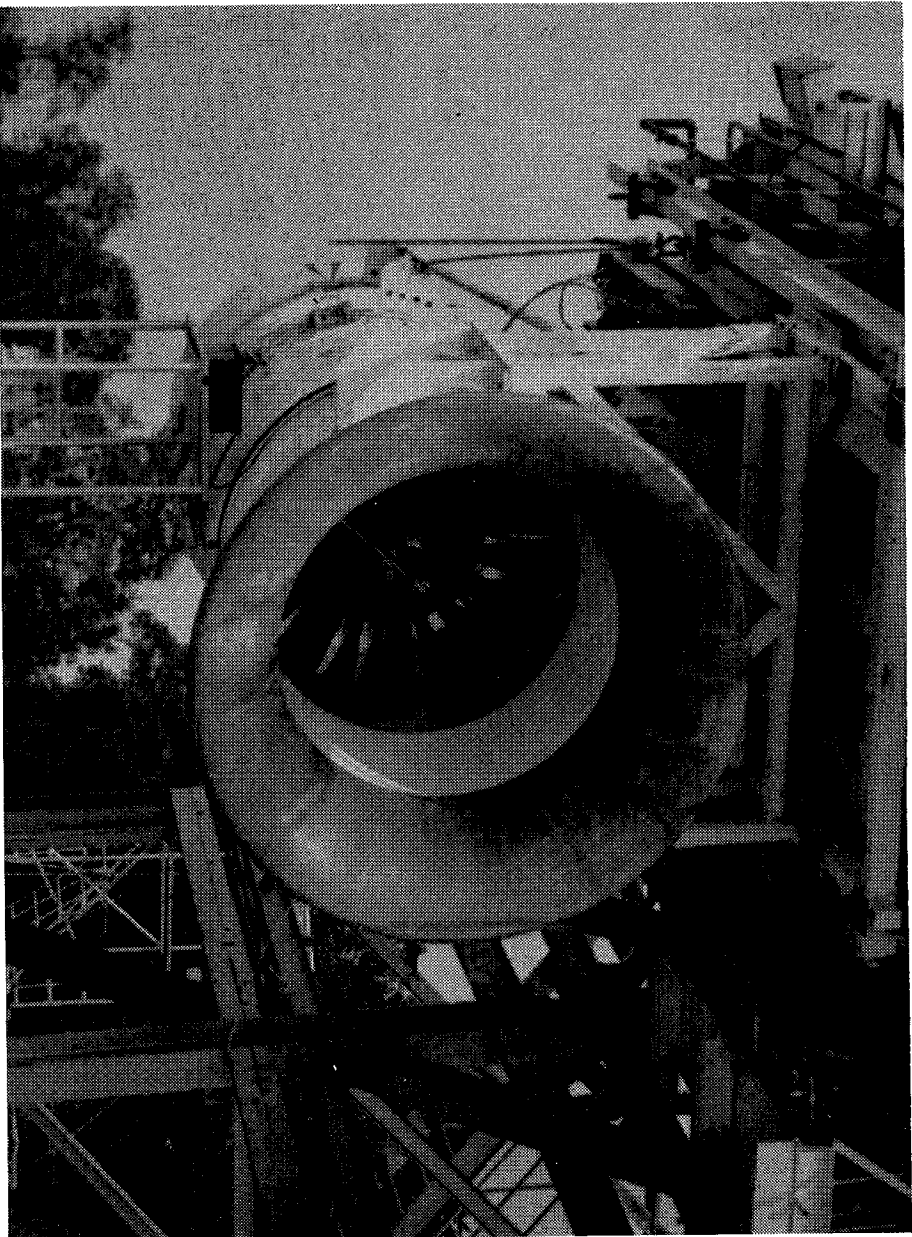- Transient Thrust Response

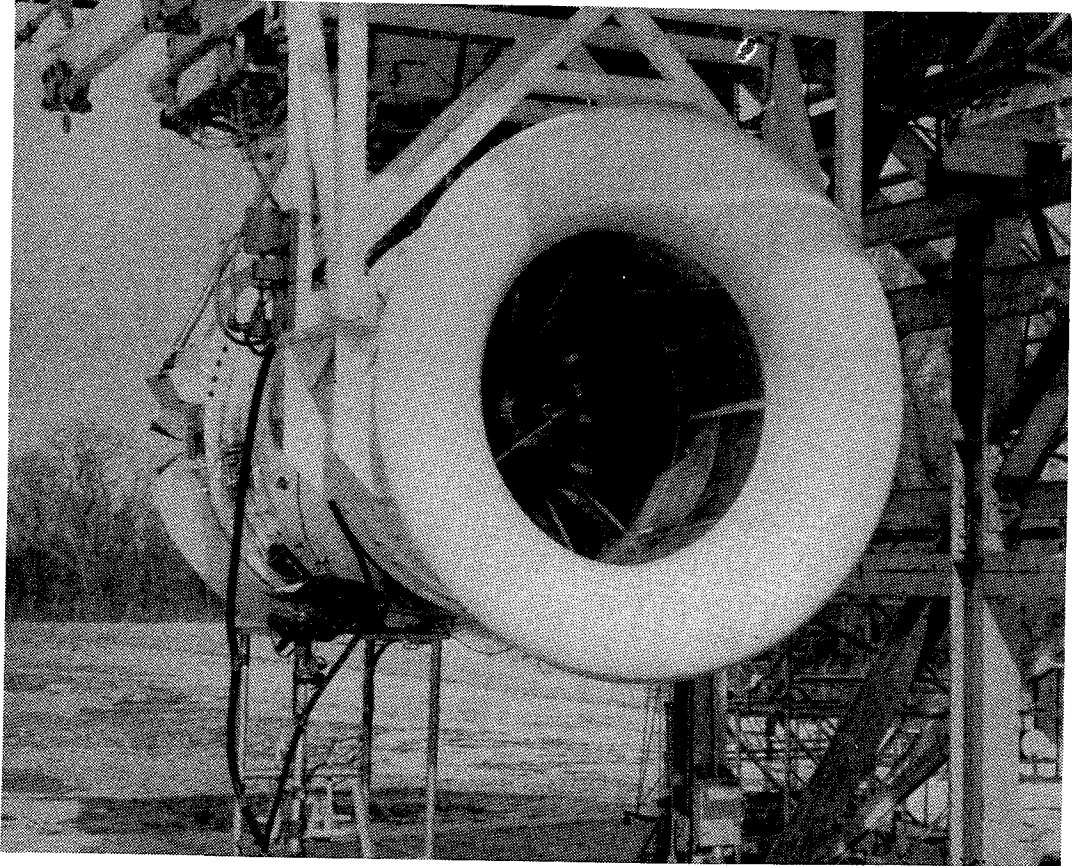Figure 129. UTW Engine with Bellmouth Inlet.

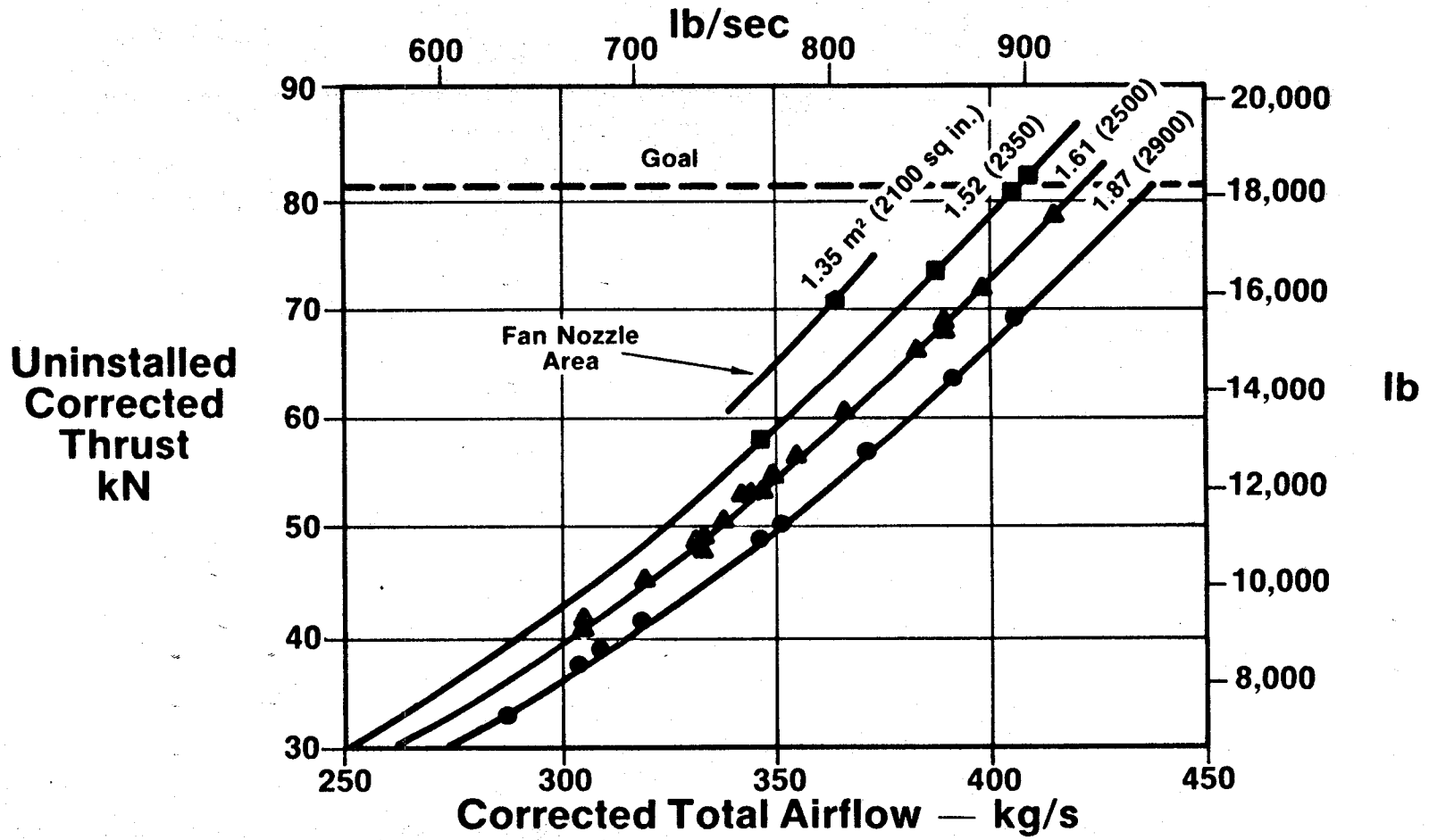Figure 130. UTW Experimental Propulsion System
Test Installation.

Figure 131. UTW Measured Thrust, Bellmouth Inlet.

Figure 132 shows the same parameters, thrust versus airflow, but at a constant 97% corrected fan speed. Curved lines represent three fan-blade angle settings. The sensitivity of thrust to blade angle is apparent in the three settings. No data points are shown, but the curve represents the best fit of all the data, crossplotted to eliminate scatter. The goal thrust was reached at this fan speed with about 4° open blade setting over a more limited range of nozzle areas.

Typical sfc buckets are shown on Figure 133, again as a function of the same three blade-angle settings. The curve shows that at an open-pitch setting of about 4°, the sfc goal can be met at rated thrust. Since acoustic data did not indicate a significant difference in noise signature over a limited range of fan-blade angles, the rating point was selected at 97% rather than 100% corrected speed and at the slightly opened pitch setting. Installed data with the high throat Mach number inlet yielded similar results but with thrust levels slightly reduced by the lower ram recovery of the flight-design inlet.

Figure 134 shows the UTW engine with the exhaust nozzle in the flared position, acting as an inlet for reverse-thrust testing. The engine was started and accelerated with the blades at the reverse setting, so no transitions were made from forward to reverse.

Figure 135 shows the reverse-thrust performance with the blades set 95° and 100° open. Blade-angle movement to these open angles indicates passage through aerodynamic stall rather than through flat pitch. This was the direction indicated by the scale-model fan test to provide the greater reverse thrust. The open 95° position is nearer to the stall line and produced a higher thrust per pound of airflow, but in both cases the turbine discharge-temperature limit was reached before the 35% reverse-thrust goal was achieved.

It was thought that the acoustic splitter might be channeling the flow in the outer annulus of the duct and increasing the pressure loss into the core, so a run was made with the splitter removed. This did increase the reverse thrust by about 2%, but again the turbine discharge limit prevented reaching the goal. Further work would be required to increase the reverse-thrust capability.

Table XXVI summarizes the UTW performance goals and the demonstrated performance levels. The engine met both the uninstalled and the installed forward-thrust and sfc goals. The reverse-thrust goal was not reached, as noted above, because operational limits were reached first; however, it did produce a potentially useful amount of reverse thrust. Aircraft studies indicated that the 27% reverse thrust achieved with the 100° open blade setting may be acceptable for stopping the airplane on a 915-m (3000-ft) runway.

lb/sec

700 750 850 900 1000

Goal

80

97% Corrected Fan Speed

Fan Nozzle Area 1.35 m² (2100 sq in.)

1.45 (2250) 1.52 (2350) 1.61 (2500) 1.71 (2650) 1.87 (2900)

Open 5°

Uninstalled Corrected Thrust kN

70

60

Nominal Pitch

lb/hr-lb

18,000

16,000

14,000

12,000

10,000

50

Closed 5°

320 340 360 380 400 420

Corrected Airflow, kg/s
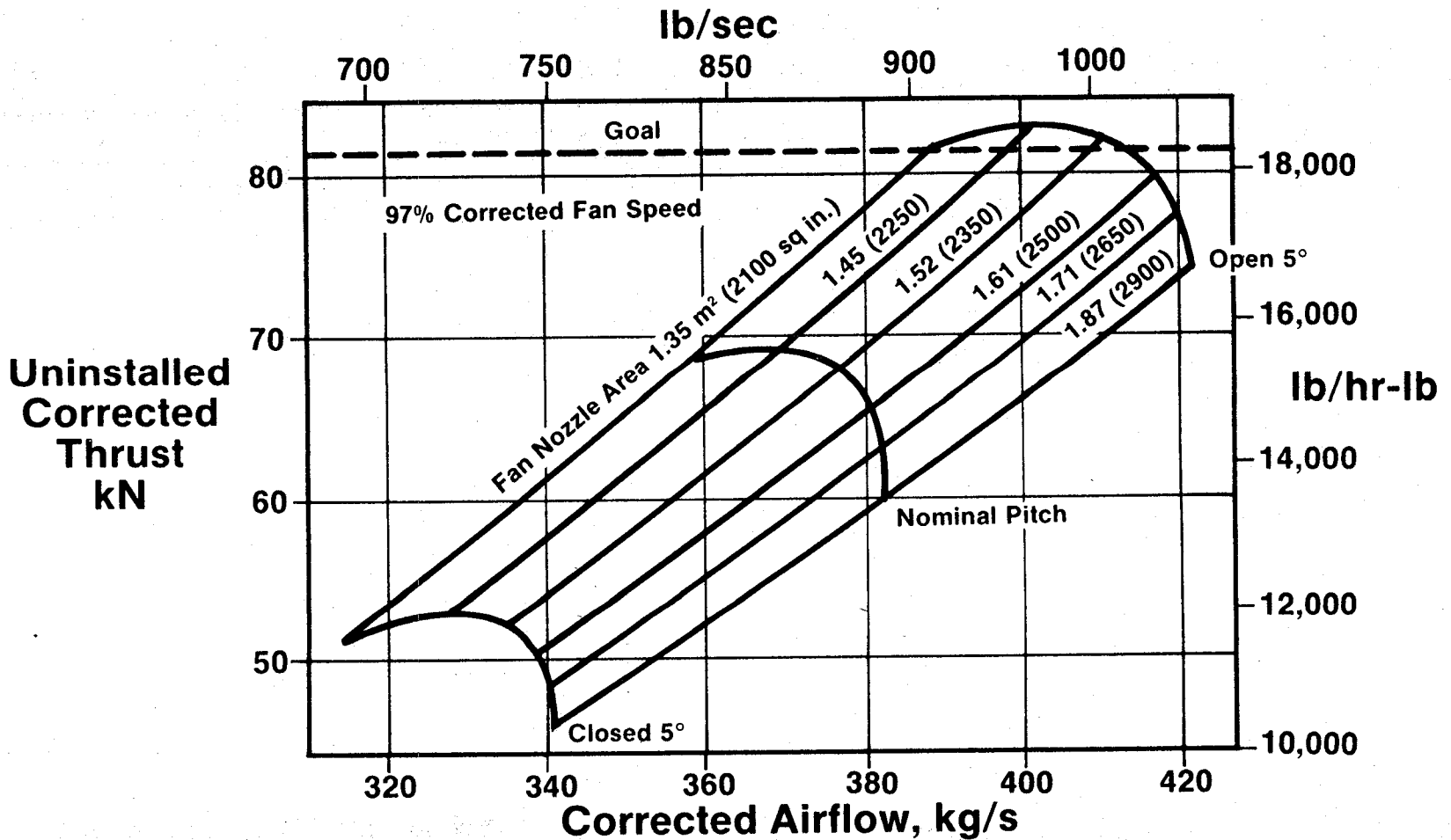
Figure 132. UTW Measured Thrust, Bellmouth Inlet, 97% Corrected Fan Speed.
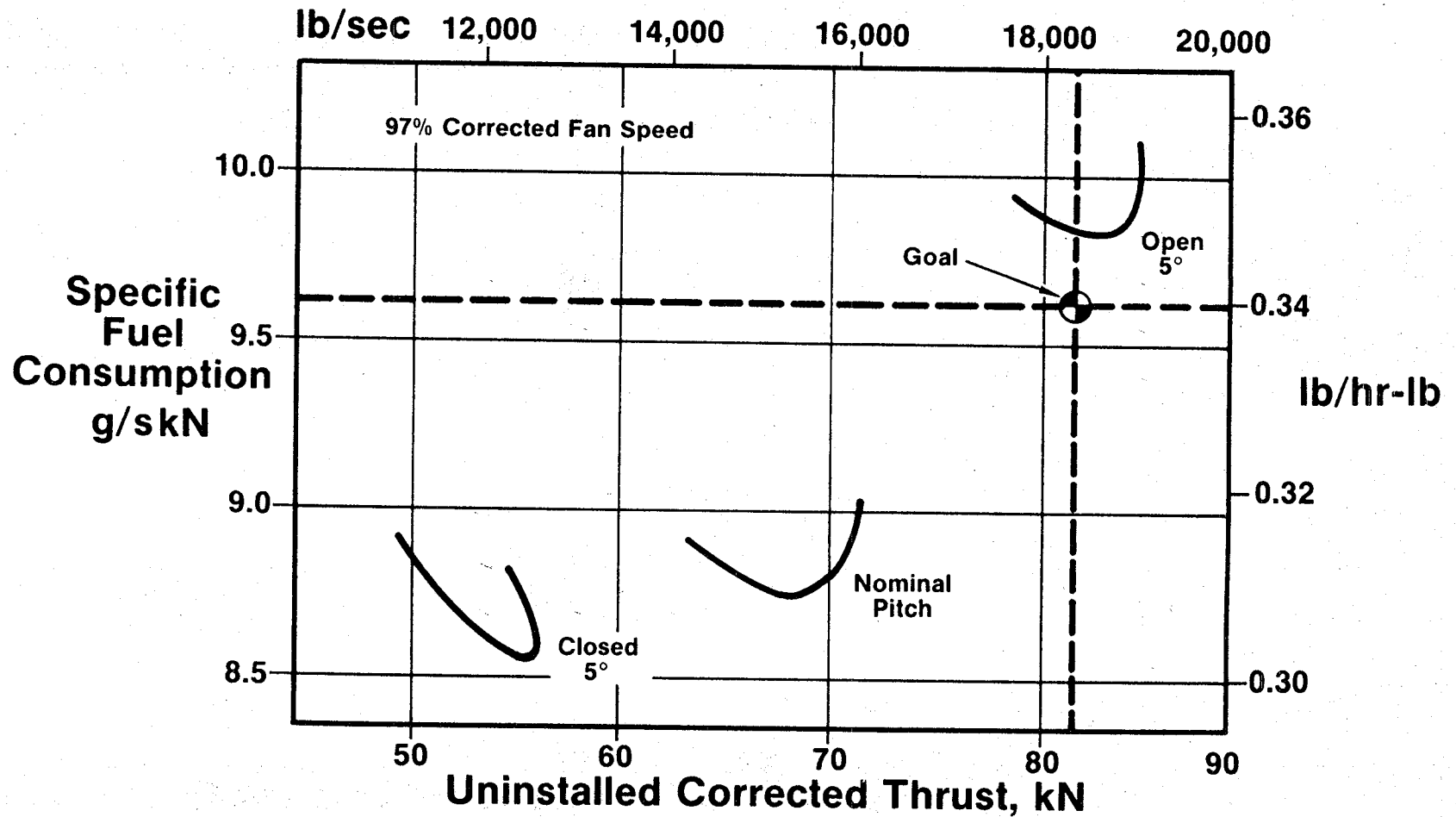
Figure 133. UTW Thrust/SFC, Bellmouth Inlet.
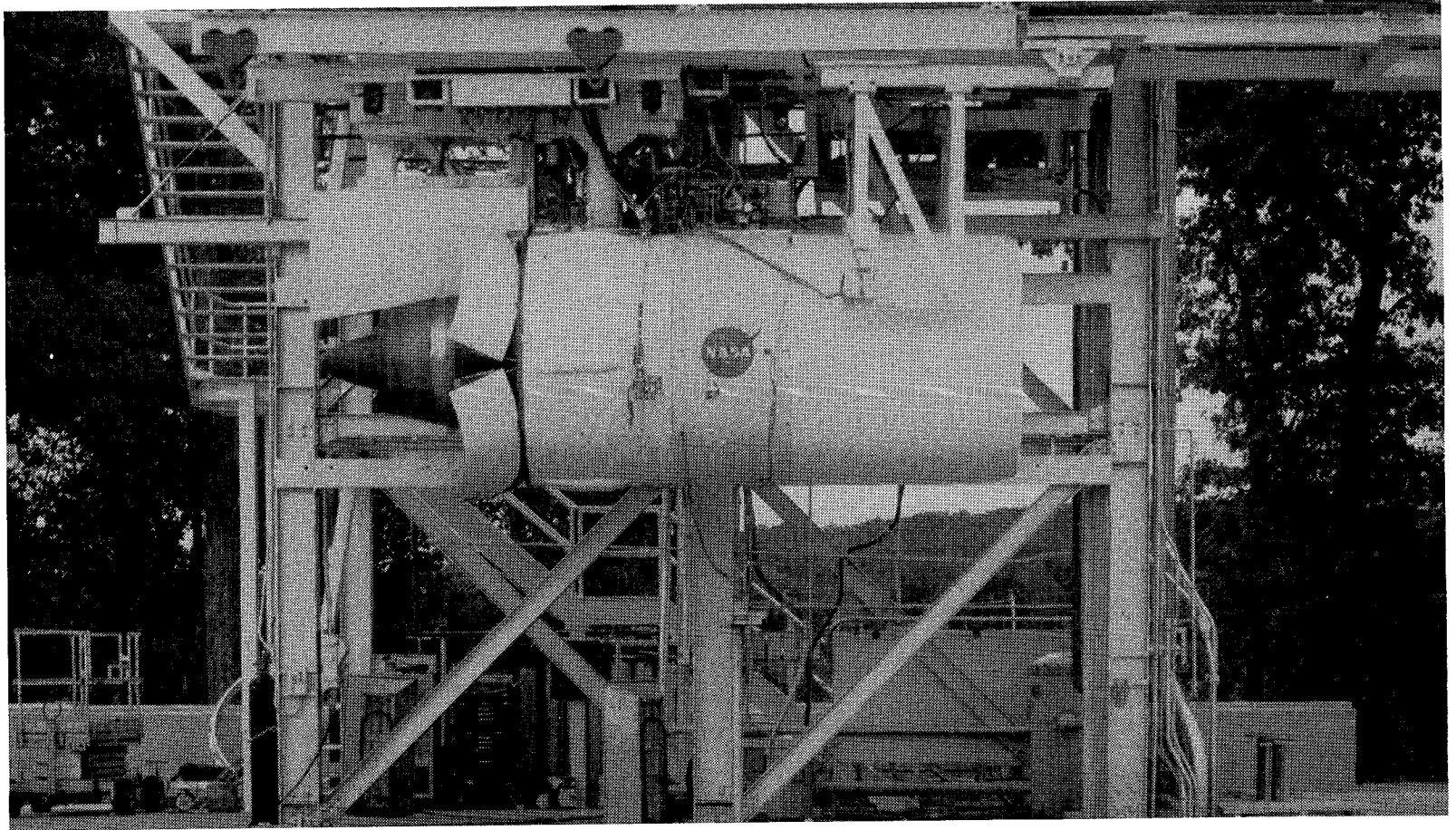
Figure 134. UTW Reverse-Thrust Test.
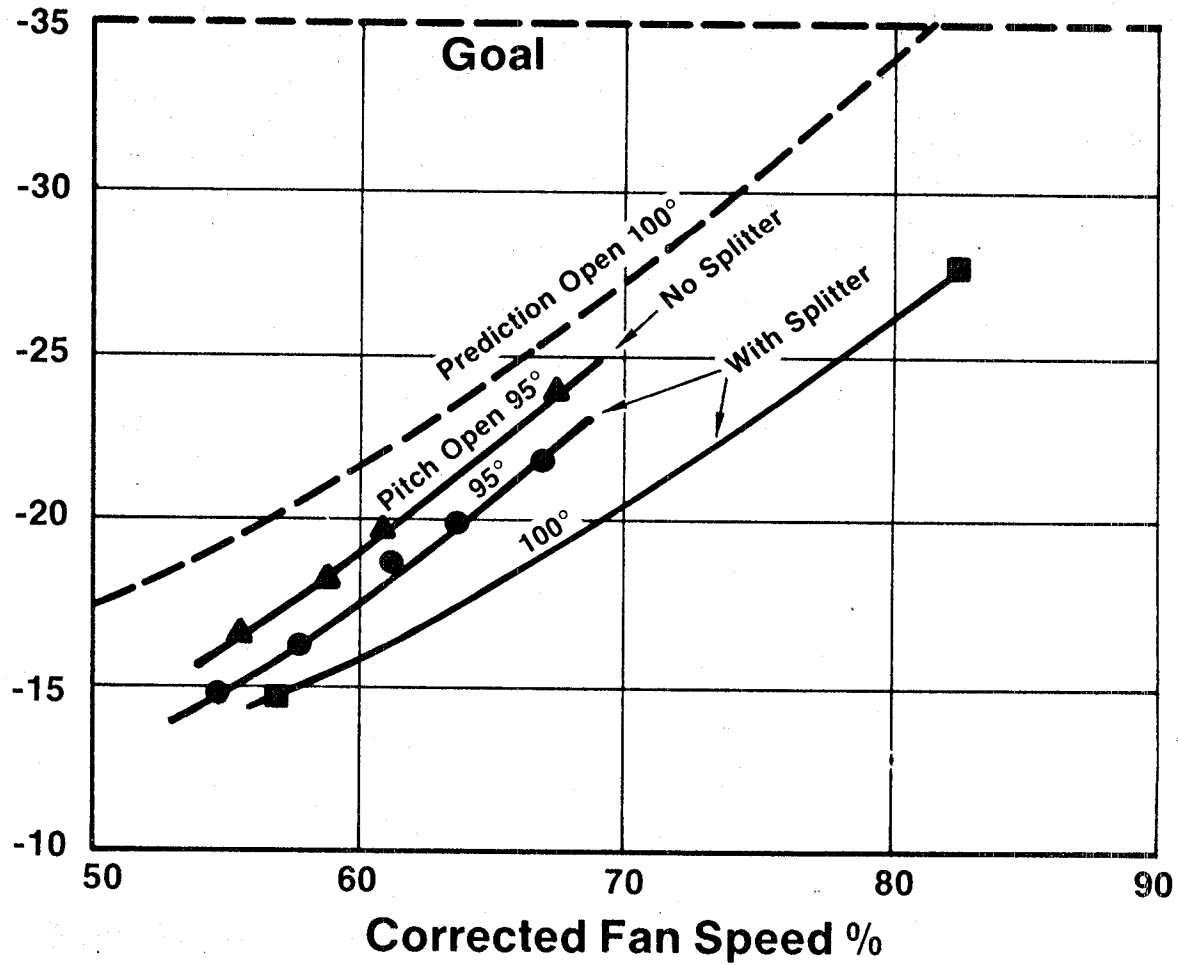
Figure 135. UTW Reverse Thrust.

Table XXVI. UTW Measured Performance, Sea Level Static, 305.5 K (90° F) Day.

	Goal	UTW Engine
Forward Mode		
• **Uninstalled Thrust kN (lb)**	81.4 (18,300)	81.4 (18,300)
• **Uninstalled SFC, g/sN (lb/hr/lb)**	0.0096 (0.34)	0.0096 (0.34)
• **Installed Thrust, kN (lb)**	77.4 (17,400)	77.4 (17,400)
• **Bypass Ratio**	11.8	11.6
• **Cycle Pressure Ratio**	13.7	15.2
Reverse Mode		
• **Installed Thrust, % Max Fwd.**	35	27

204

4.1.2 OTW Performance Test

Figure 136 shows the OTW engine which was also tested with both the bell-mouth and boilerplate high throat Mach number inlets.

Measured axial thrust values are shown on Figure 137 as a function of corrected airflow. The effect of side-door setting on exhaust-nozzle area is apparent in the three different operating lines. Data include both inlet configurations; fan inlet pressure has been corrected to sea level. Excellent agreement is shown between the two inlets.

The "D" shaped exhaust nozzle was designed to turn the exhaust down over the wing/flap surface. Since the thrust meter was capable of reading the horizontal component only, goals were based on an equivalent conical exhaust nozzle having a velocity coefficient of 0.995.

Figure 138 shows specific fuel consumption versus equivalent-conical-nozzle thrust for the same nozzle areas. The areas corresponding to 11-1/2° and 25° side-door settings are seen to meet the thrust goal and to better the sfc goal by about 3%. The 25° setting was selected for establishing the engine takeoff rating.

The exhaust nozzle was run in the inverted position so that, in the reverse-thrust configuration, the jet efflux would be directed forward and into the ground rather than into the overhead test facility and instrumentation lines. To avoid reingestion of hot exhaust gases and kicked-up debris, a long reingestion shield was used as shown in Figure 139. The effect of the shield on thrust-meter reading was first calibrated in the forward-thrust mode to establish a correction for the reverse-thrust data.

Figure 140 shows the measured axial component of reverse thrust as a function of airflow for the two blocker-door angles tested. While both angles exceeded the desired 35% reverse thrust, pressure loss in the turn was greater than expected. This caused a back pressurizing of the fan and required a greater fan speed than expected. Although the 115° blocker angle produced more turning, and more reverse thrust per pound of airflow, it also produced a higher pressure loss. Both angles required 82% corrected fan speed to reach the 35% thrust goal. The turning loss could be reduced by increasing the bypass-duct area and lowering the Mach number entering the turn. This would have a beneficial effect on reverse-thrust noise by reducing both the jet velocity and the fan speed.

The OTW engine met its uninstalled and installed forward-thrust goal and exceeded its reverse-thrust goal and sfc goal as shown in Table XXVII.

4.2 FAN AERODYNAMIC PERFORMANCE

4.2.1 UTW Fan

Full-scale fan performance was evaluated during tests of the UTW demonstrator engine. The engine, shown during build-up in Figure 141, was fully
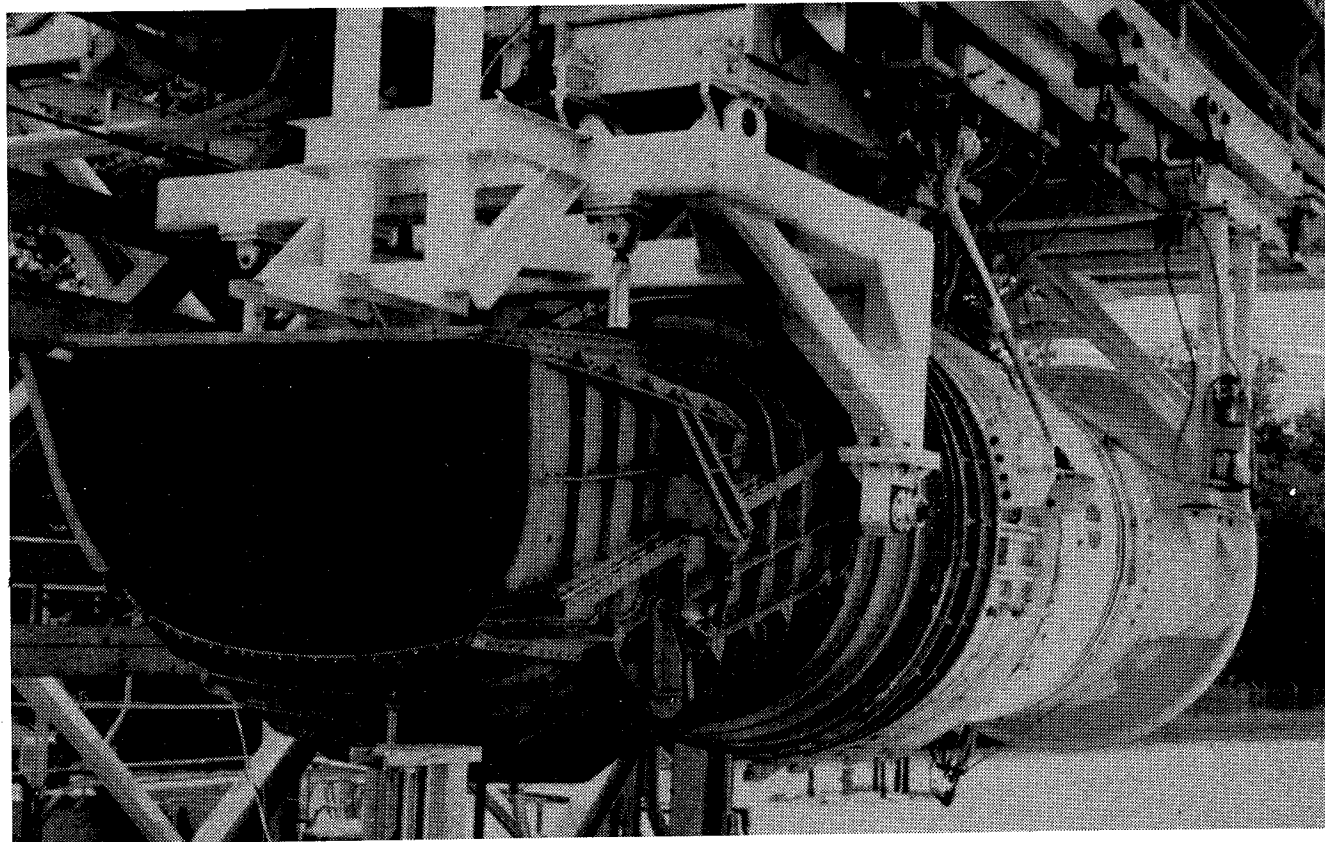
Figure 136. OTW Experimental Propulsion System Installation.
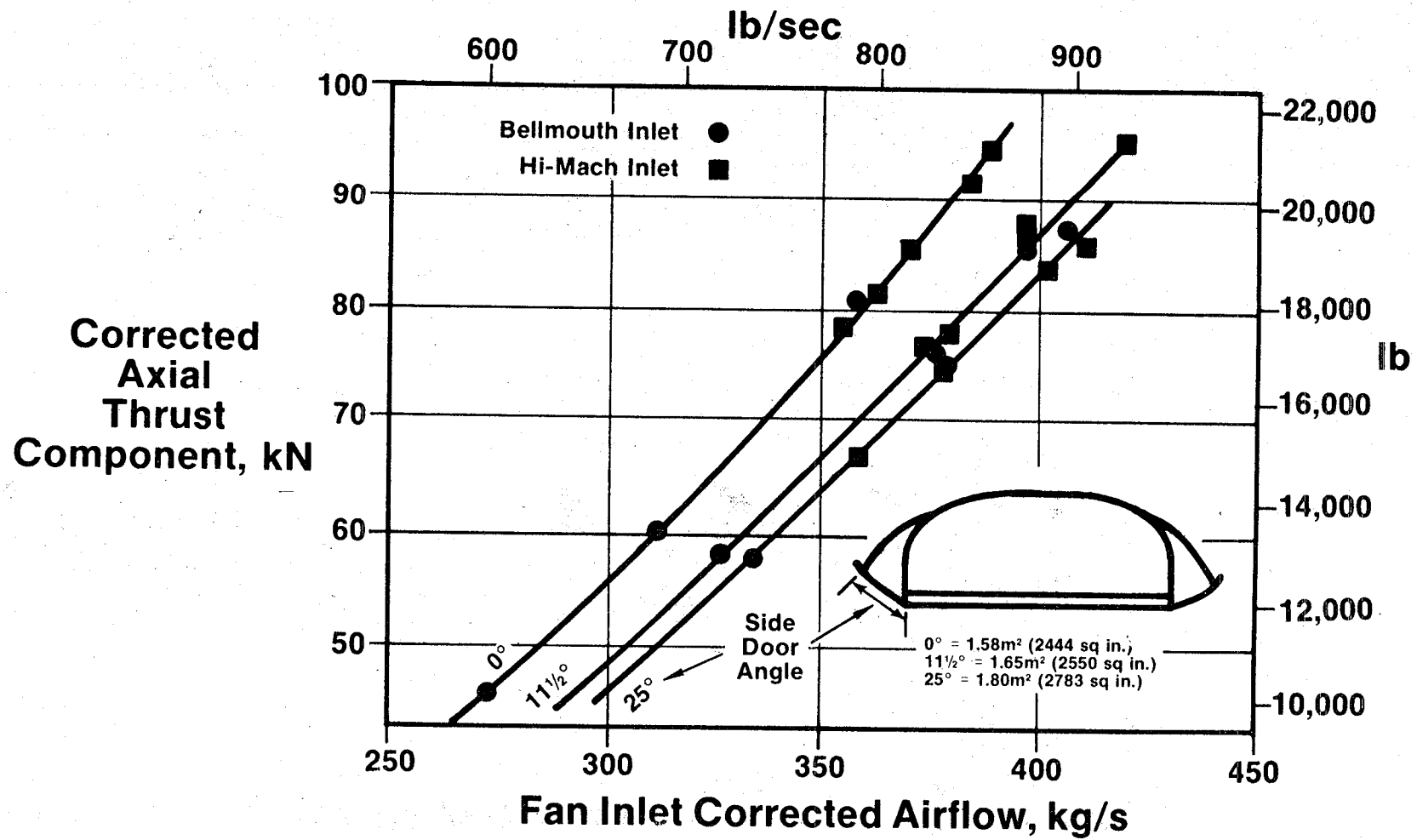
Figure 137. OTW Measured Axial Thrust, "D" Nozzle.
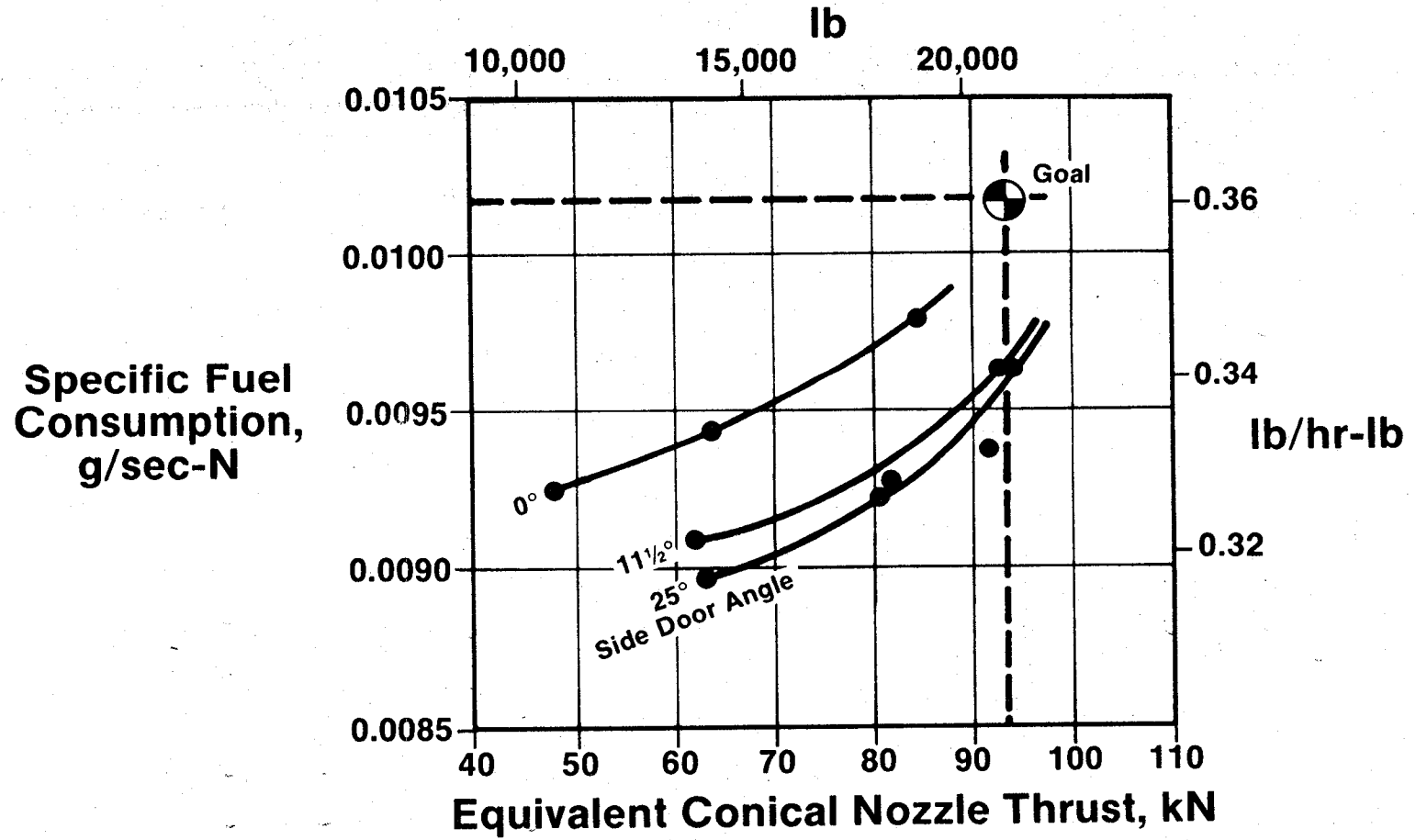
Figure 138.   Uninstalled SFC Vs. Thrust.
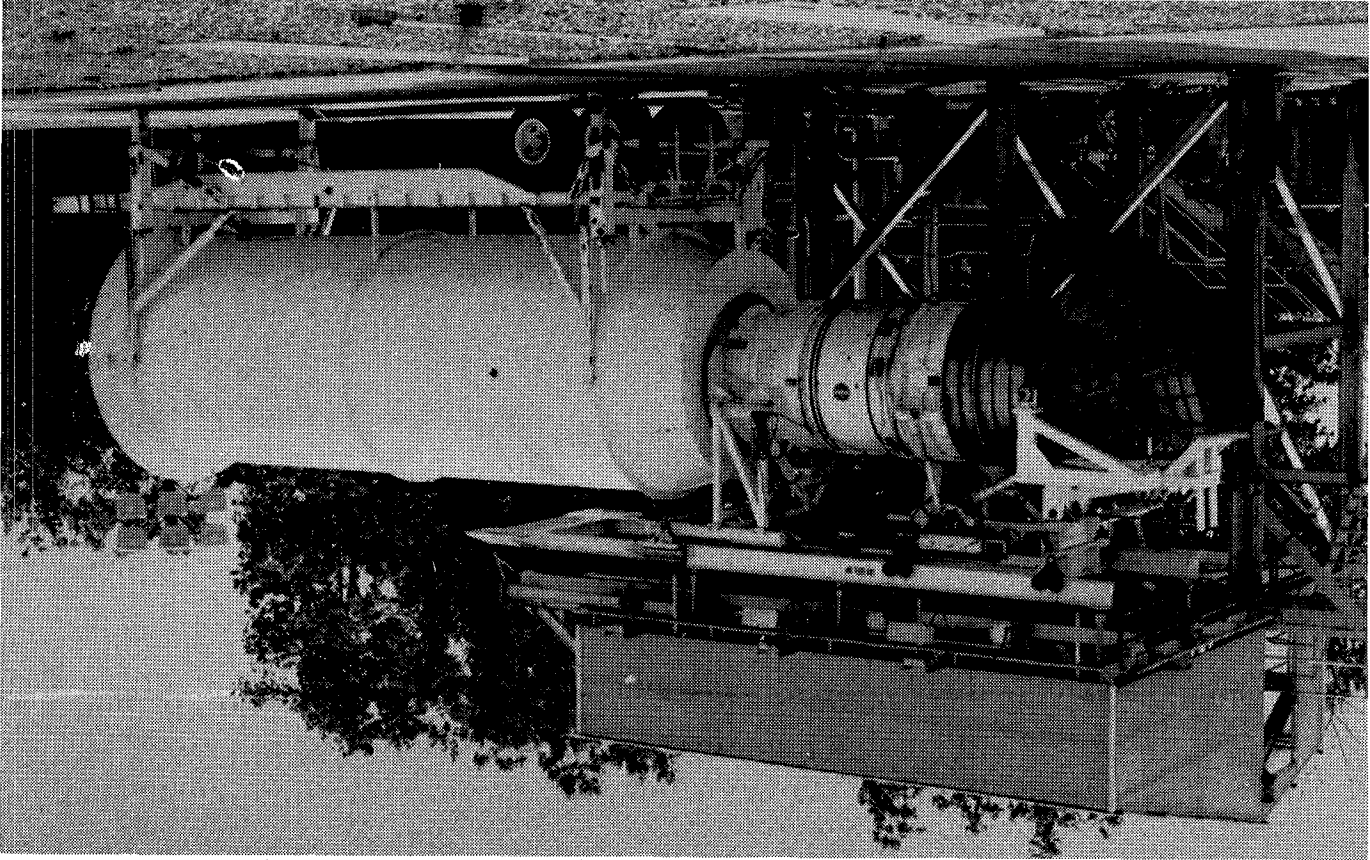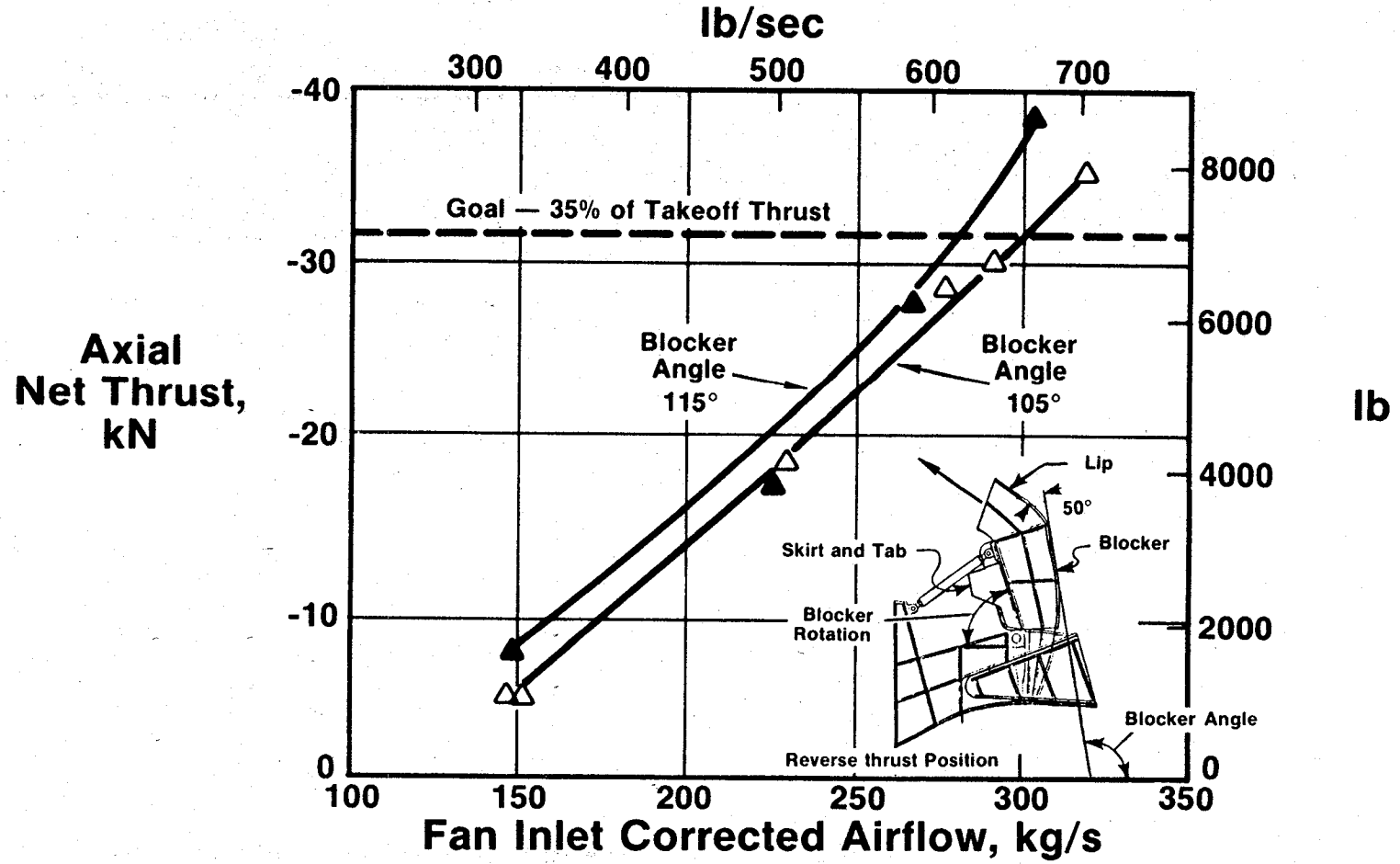
Figure 140. Reverse Thrust Vs. Airflow.

Table XXVII. OTW Measured Performance, Sea Level Static, 305.5 K (90° F) Day.

(Based on Equivalent Conical Nozzle, CV = .995)

	Goal	OTW Engine
Forward Mode		
Uninstalled Thrust, kN (lb)	93.4 (21,000)	93.4 (21,000)
Uninstalled SFC, g/sN (lb/hr/lb)	0.0102 (0.36)	0.0099 (0.35)
Installed Thrust, kN	90.3 (20,300)	90.3 (20,300)
Bypass Ratio	10.2	10.3
Cycle Pressure Ratio	15.5	17.2
Reverse Mode		
Installed Thrust, % Max Fwd.	35	35
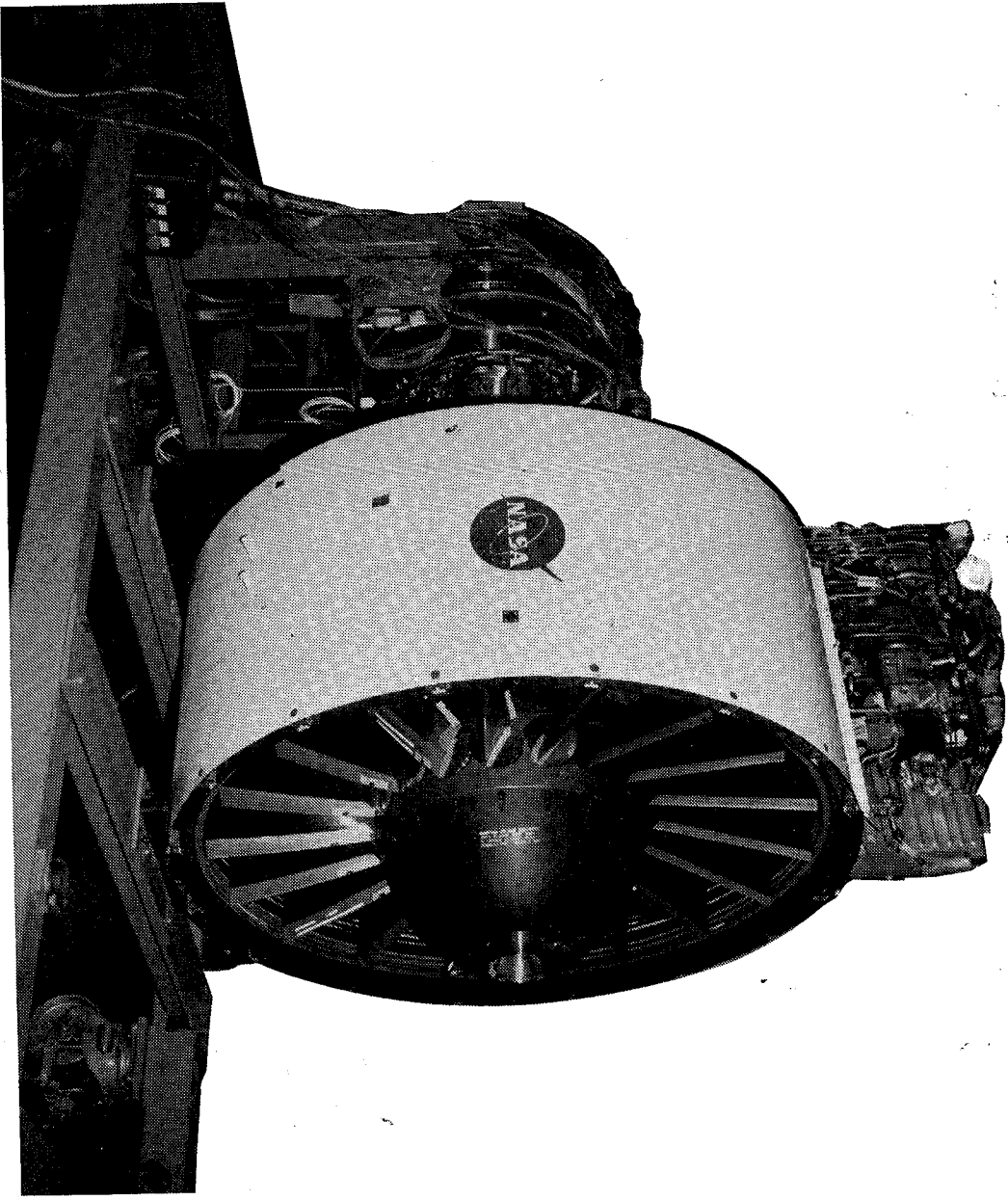
Figure 141. UTW Fan.

instrumented for performance testing, and data were recorded both in forward-and reverse-mode operation. Since all tests were conducted at sea level static inlet conditions, emphasis was placed on determining performance on lower operating lines near the takeoff power setting.

Fan bypass-stream performance in the forward mode of operation is shown in Figure 142. All data points are at the objective takeoff corrected speed, 95% of the aerodynamic design value, and are at three different rotor-pitch-angle settings. The solid speed lines in the background indicate performance measured during scale-model tests. The full-scale fan performance on the engine was very close to that expected as a result of the scale-model tests; efficiency appeared to be slightly better than in the scale model, especially with the rotor closed 5°. Full-scale fan tests confirmed that the fan take-off-flow and pressure-ratio goals could be met at 95% speed with approximately a 3° open rotor-pitch-angle setting. Similar good agreement with the scale-model-test results was obtained over the entire range of speeds and pitch angles that could be evaluated in the engine.

Full-scale fan hub performance at 95% corrected speed for the same three pitch angles is shown in Figure 143. In the engine tests, fan hub data were recorded at the inlet of the core engine rather than behind the fan inner stator, and (thus) stator exit total pressure was reduced by an estimated 1.5% transition-duct pressure loss. At the low pressure ratio of the fan hub at the takeoff condition, this duct loss reduced the efficiency by approximately seven points. The fan hub turbomachinery efficiency at takeoff pressure ratio was actually about 80% rather than being in the low 70's as shown in Figure 143 for the overall hub compression. As shown in the figure, the fan hub performance in the engine was better than in the scale-model tests, particularly at closed rotor-pitch angles, and the core engine supercharging goal was exceeded.

A limited amount of reverse-through-stall-pitch testing was conducted on the engine with the aeroperformance instrumentation installed. The results are shown in Figure 144 plotted as overall pressure ratio from atmospheric engine inlet to fan rotor exit versus total engine flow corrected by engine inlet conditions. The upper family of curves indicates reverse-mode performance predicted from the scale-model tests; the symbols indicate engine test data. Although flow at a given speed and pitch angle was within a few percent of the scale-model level, the fan overall pressure ratio was noticeably lower than expected for the engine. Since the inlet pressure was taken as atmospheric, higher flow-induction losses in the exhaust duct would have contributed to the low apparent fan pressure ratio. Limited traverse data taken in the aft engine duct during reverse-thrust operation indicated that pressure recovery was 1 to 2% lower than measured in the fan scale-model tests, and the recovery could well have been even lower than the traverse data indicated. The apparent low fan operating line could also be the result of the effective discharge area being larger in the engine than in the scale model. The blockage due to fan-exit pressure rakes was less in the engine than in the scale model, but this difference alone was not sufficient to fully account for the low operating line. A final possibility is that some
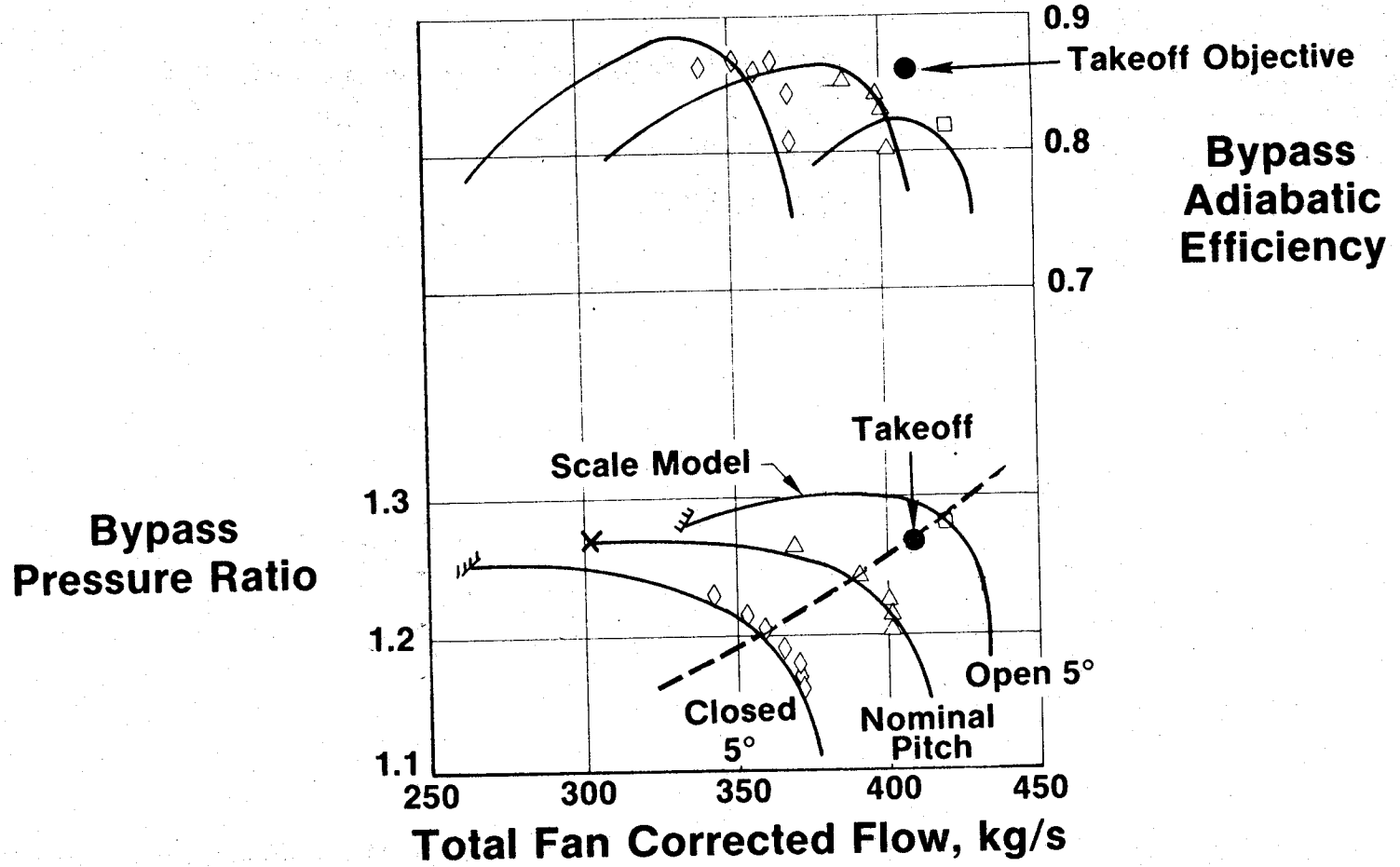
Figure 142. UTW Fan Bypass Performance at 95% Speed.
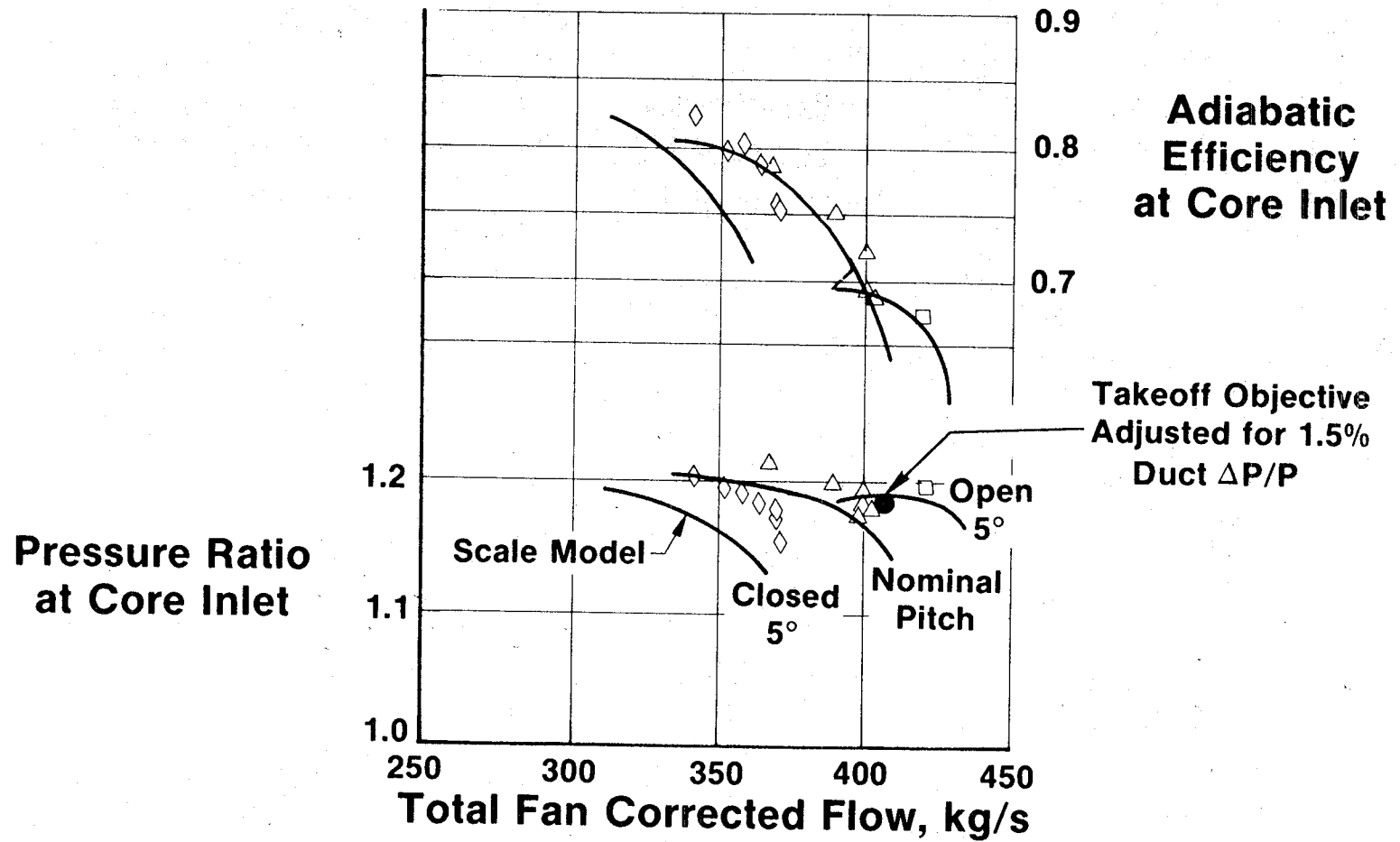
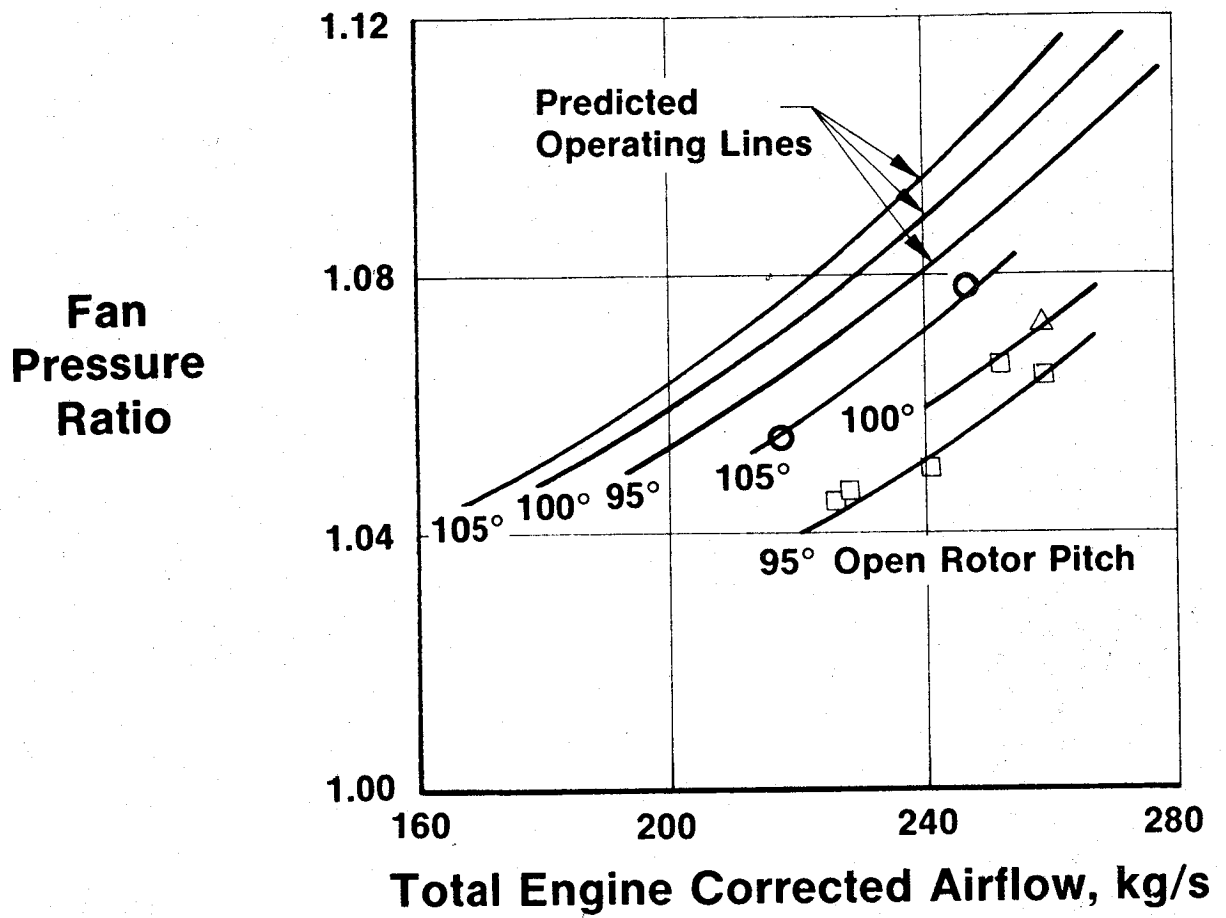Figure 143. UTW Fan Hub Performance at 95% Speed.

Figure 144.   UTW Fan Reverse-Thrust Performance.

other factor may have affected the size of the stagnant-flow region along the centerline of the engine inlet, thus altering the effective discharge area of the fan. Possible causes of this effect include differences in the ratio of core-engine flow to fan flow and differences in fan rotor hub platform shapes. Although insufficient data were recorded during engine tests to resolve this question, it is an area that deserves further testing and analysis since it directly affects the ability to predict the reverse-mode performance of this type of fan.

Although fan pumping in reverse mode was less than expected, the engine system was able to produce 27% of takeoff thrust in reverse, compared to the goal of 35%. While less than the goal, this level of reverse thrust is believed to be sufficient for many applications.

4.2.2 OTW Fan

Fan performance was evaluated during tests of the OTW engine. There was no scale-model component test conducted for the OTW fan. A photograph of the OTW engine during build-up is shown in Figure 145. A full complement of fan-performance instrumentation was installed during the engine tests.

Fan bypass-stream performance data from the engine tests are shown in Figure 146. At 100% design corrected speed, the fan exceeded flow and pressure-ratio goals by 2 to 3%. The 86.5% bypass-stream efficiency goal for the demonstrator engine was met or exceeded along an operating line through the design point. Peak fan efficiency was on a lower operating line than the lowest tested, possibly near the takeoff operating line, so the exact level of peak efficiency at high speed was not determined. No stall testing was attempted during the engine-performance runs, and no fan stalls were encountered. It was thus not possible to determine if the fan was able to meet the stall margin objectives, although 10% stall margin was demonstrated at 95% corrected speed.

Fan hub performance results are shown in Figure 147. These were based on measurements recorded at the core-engine inlet, so the design objective pressure ratio and efficiency on this performance map (indicated by the target symbols) have been lowered consistent with an estimated 1.5% transition-duct pressure loss. Hub performance results were quite encouraging in that the high level of core supercharging was achieved at 100% speed. Efficiencies at the design operating line were approximately equal to the goal (78% for the turbomachinery alone) and were significantly higher than the goal at higher operating lines.

4.2.3 CONCLUSIONS

The OTW and UTW fans both performed satisfactorily during sea level engine tests, and most of the fan aerodynamic-performance goals established for the demonstrator engine programs were met. Some further development of the UTW fan would be required to meet altitude-cruise performance goals, and
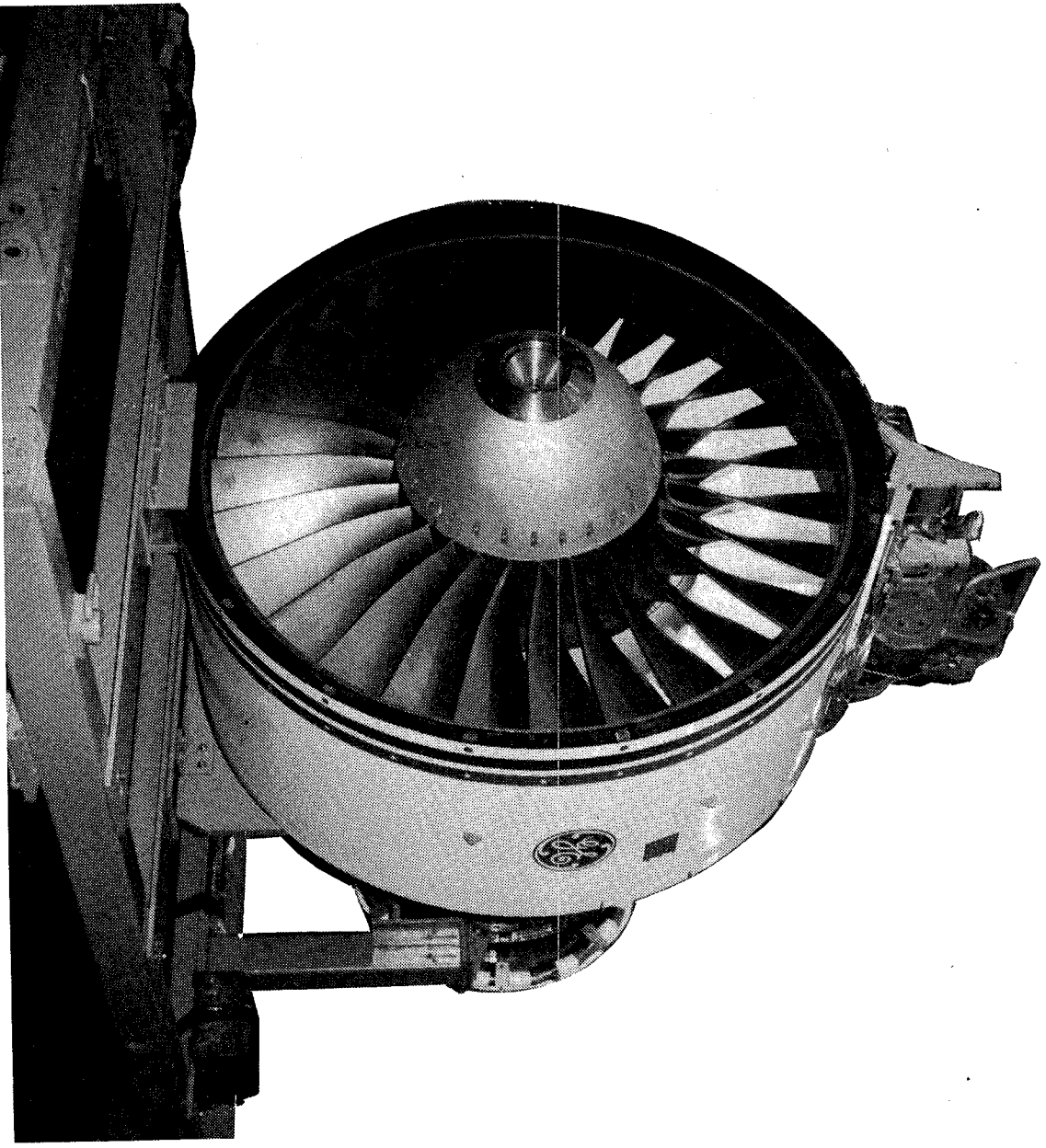
Figure 145. OTW Fan.
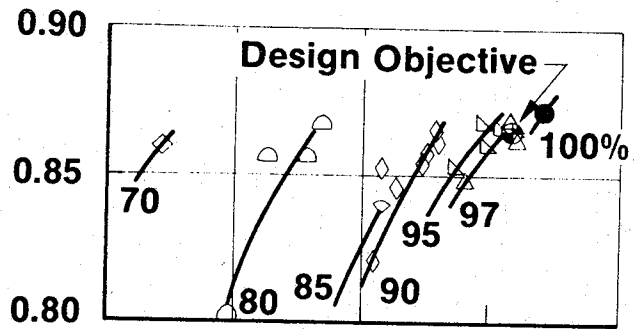
Bypass Adiabatic Efficiency
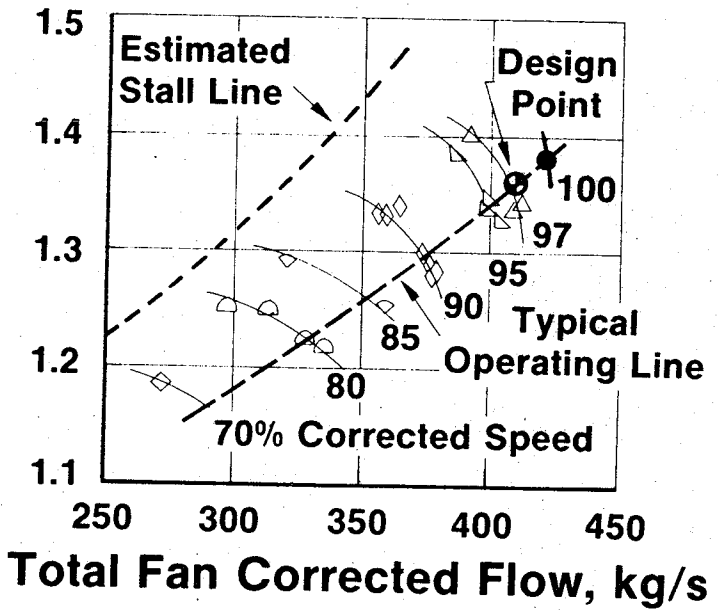
Bypass Pressure Ratio
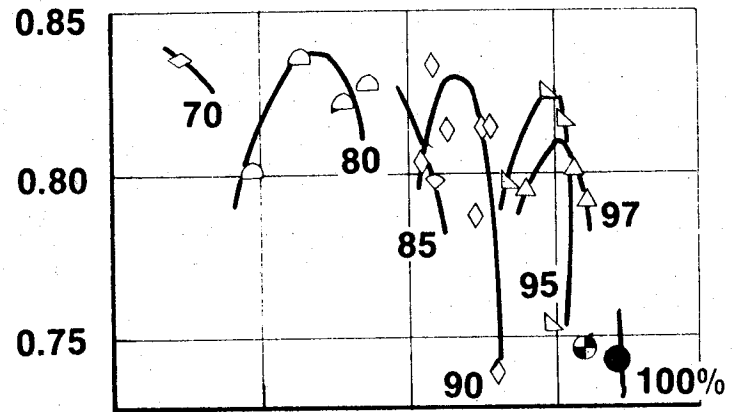
Total Fan Corrected Flow, kg/s

Figure 146. OTW Fan Bypass Performance.

Adiabatic Efficiency at Core Inlet

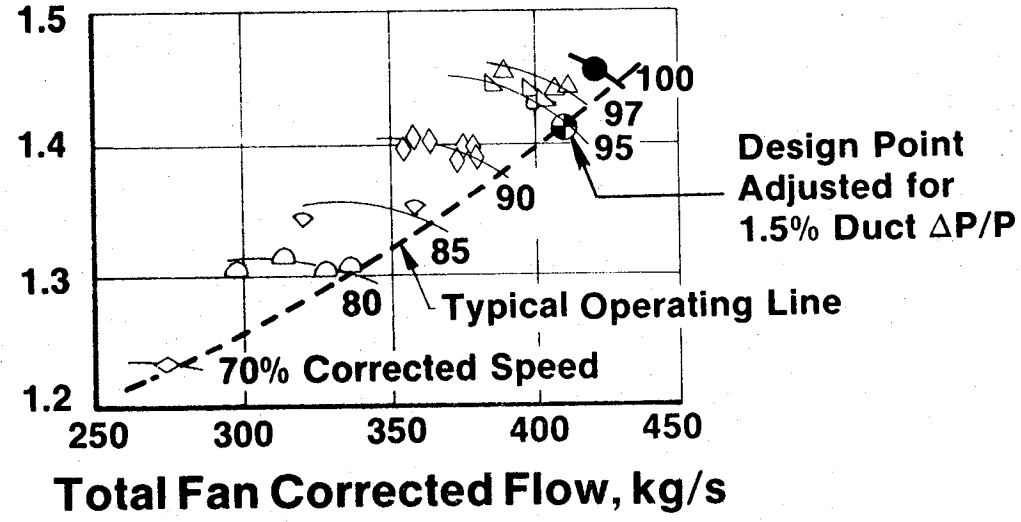**Pressure Ratio at Core Inlet**

Figure 147. OTW Fan Hub Performance.

the reduced pumping of this fan during engine reverse-mode tests needs to be understood and improved. Important advances in fan aerodynamics were demonstrated during the QCSEE program, and these advanced fan features can be used with confidence in future turbofan engines for short-haul aircraft.

4.3 MECHANICAL PERFORMANCE

4.3.1 COMPOSITE FAN BLADES

Although it was recognized that the QCSEE composite blades were not flightworthy, because of insufficient FOD resistance, they were judged to be suitable for development engine testing.

The blades performed acceptably during experimental engine test. The steady-state stress levels were low, and there were no indications of torsional instability. The only problems encountered were that the blade vibratory-stress levels exceeded scope limits at the 2 per rev/first-flex crossover, and high first-flex vibratory stresses were also noted due to crosswind and tailwind test conditions at speeds above the 2/rev crossover. It should be pointed out that the scope limits defined for the composite blade were very conservative, and no blade delamination occurred. Further, the OTW titanium blades were also excited by crosswinds and tailwinds, although they remained well within established scope limits.

4.3.2 Variable-Pitch Actuation Systems

The Hamilton Standard cam/harmonic and the General Electric ball spline systems were both engine tested. Figure 148 shows the fan rotor with the cam/harmonic system installed. Clearly visible are the nested lever arms and the spherical cam that drives the blades in unison as the cam rotates with respect to the fan disk.

The cam/harmonic system completed 47 hours of engine testing. It accurately positioned the fan blades at lower speeds, but could not move the blades against the load when operating above 85% fan speed. Since this system handled the simulated blades during whirl-rig testing, it was concluded that actual blade torques exceeded design estimates.

The ball spline system completed 106 hours of engine testing. Motor torque was increased 16% prior to engine test, and the system crisply actuated the blades at all speeds. There was an indicated 1.3° system hysteresis, based on airflow measurements, when the direction of blade movement was reversed while operating near nominal. This was again attributed to excessive actuator clearances and presented no operational problems.
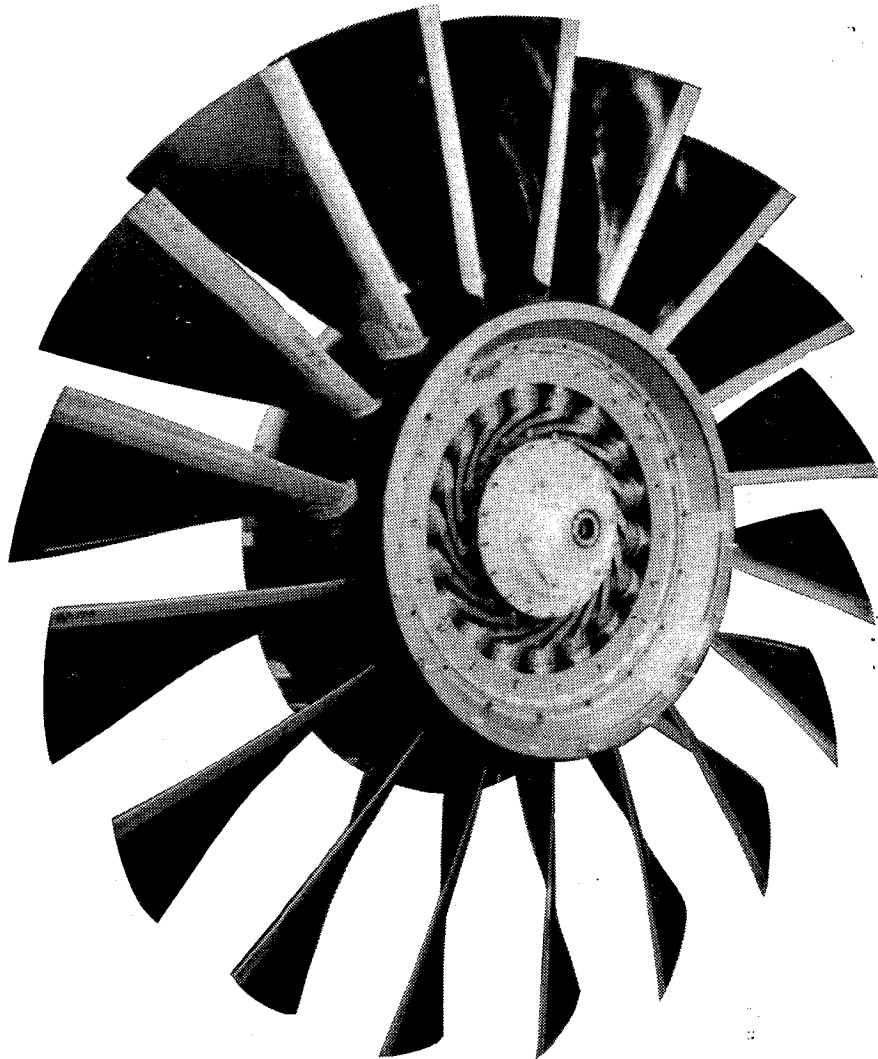
Figure 148. Fan Rotor with Cam/Harmonic System.

4.3.3 Main Reduction Gear

Figure 149 shows the UTW reduction gear, including the fan pitch-change-mechanism support, installed in the engine but with the fan shaft and ring gear removed.

There were no operational problems with either the UTW or the OTW gearsets during engine operation. The indicated reduction gear efficiency of 97.7% in the engine was somewhat lower than that experienced in the rig tests, but this is attributed at least in part to inaccuracies in the method of estimating the sources of heat rejected to the oil and oil-flow distribution from several sources within the engines. It is believed some development effort related to the placement of the oil supplied to the gears and the scavenging characteristics both within and surrounding the gearset can improve the efficiency to a value even better than that previously shown for the rig tests.

Another item of interest in the engine test was gear noise. The gear-noise level, even at meshing frequencies, appeared to be below that of the rest of the engine and indiscernible.

The UTW reduction gearset was inspected at an interim point in the engine operation. All parts passed Magnaflux satisfactorily, and tooth wear patterns were uniform. Slight corrosion was apparent on the ring gear due to inadequate removal of fingerprints, and slight evidence of bearing skidding was noted.

Neither engine was disassembled following the completion of testing; consequently, further gear inspections have not been possible. However, at this time, over 40 hours of additional testing of the OTW engine have been done at Lewis Research center with no gear problems.

4.3.4 Composite Frame

The two composite fan frames built under this program were used throughout the engine-test phase of the UTW and the OTW engines. No structural problems resulted from these tests. Both the mount region and the bypass vanes were instrumented and monitored during engine testing. The indicated stress levels were very low but were in good agreement with the analysis for the conditions run.

The main problem encountered during engine operation was oil leakage from the sump; adequate sealing of all the penetrations for lines and tubes could not be maintained. This problem was alleviated by filling the core struts and other selected areas with adhesive to provide an external seal. This was done on the test stand. Secondary FOD damage was also repairable on the stand.
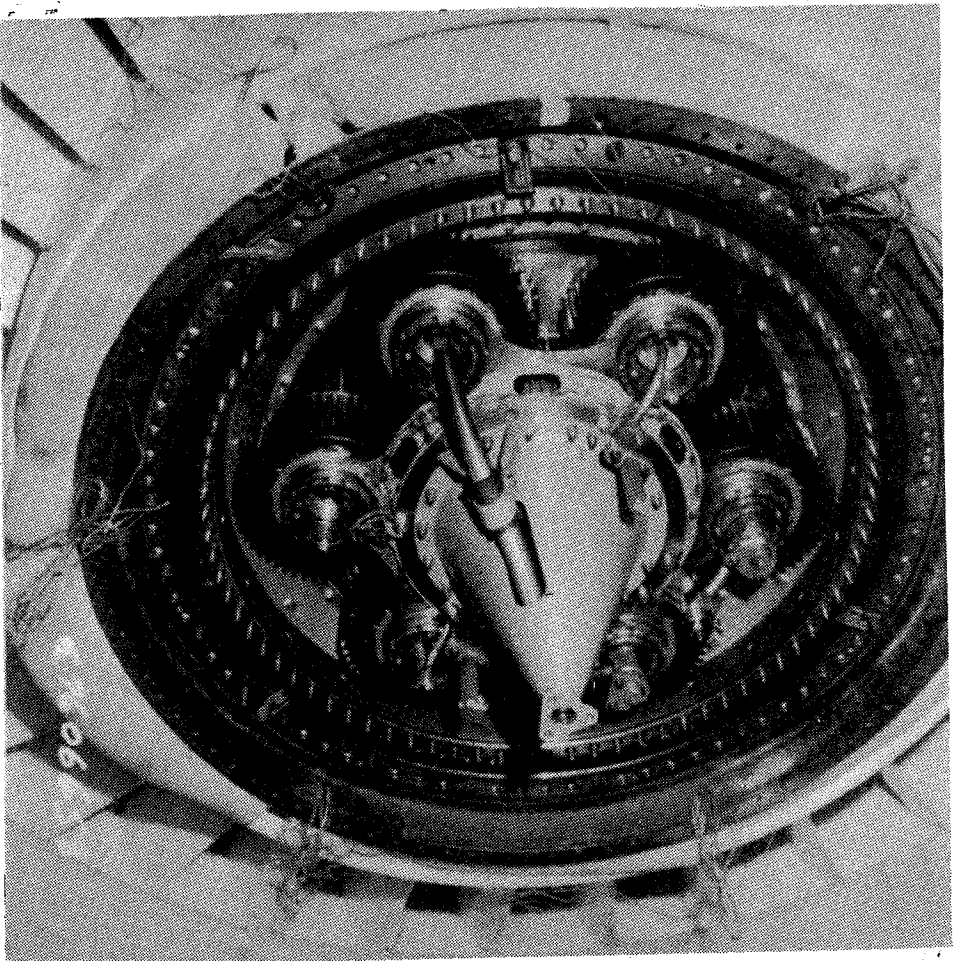
Figure 149. UTW Reduction Gear.

4.3.5 Composite Nacelle

The composite nacelle components were run on the UTW engine with the following results:

- No problems were encountered with the inlet.

- No problems were encountered with the inner core cowl.

- No problems were encountered with the outer fan cowl.

- No problems were encountered with the fan nozzle when it was installed on the composite outer cowl; however, this nozzle was also used on the boilerplate outer cowl where the hinge ring was bolted to the rear of the outer cowl rather than being bonded in. This hinge ring (due to a poorly designed bolted joint to the boilerplate outer cowl) came off during reverse-thrust testing, terminating the boilerplate nacelle tests.

- No environment degradation was noted during engine operation.

4.4 CONTROL SYSTEM TEST RESULTS

4.4.1 UTW Engine

Several control-system experiments were conducted during the overall engine test program. As noted earlier, the system is designed to hold the inlet throat Mach number constant at high power settings by variation of the fan nozzle area. Figure 150 shows the results of an inlet Mach number control experiment. The figure shows the results of a slow power increase. The control system inlet Mach number reference was set at 0.75. As the power setting was increased, the fan nozzle automatically closed to maintain the inlet Mach Number essentially constant at 0.75.

Figure 151 shows the results of a fan-speed control experiment. As noted earlier, the digital control will automatically vary fan pitch angle to hold fan speed constant. In this experiment the fan speed reference was set at 2985 rpm. As the power setting increased to demand a higher thrust level, the fan pitch automatically opened to hold the fan speed essentially constant. Actual fan-speed variation was approximately plus or minus 0.5% during the power advance. The fan pitch changed from approximately 2° closed to 3° open during the power change. The nonlinearity in pitch angle change between 85% and 90% power demand is associated with an interaction between the fan pitch and fan nozzle control systems. Between 85% and 90% power demand, the fan nozzle opened to the maximum open area, and a relatively large pitch-angle change was required to maintain fan speed. Above the 90% power setting the nozzle closed, and smaller changes in pitch angle were required to maintain control of fan speed.
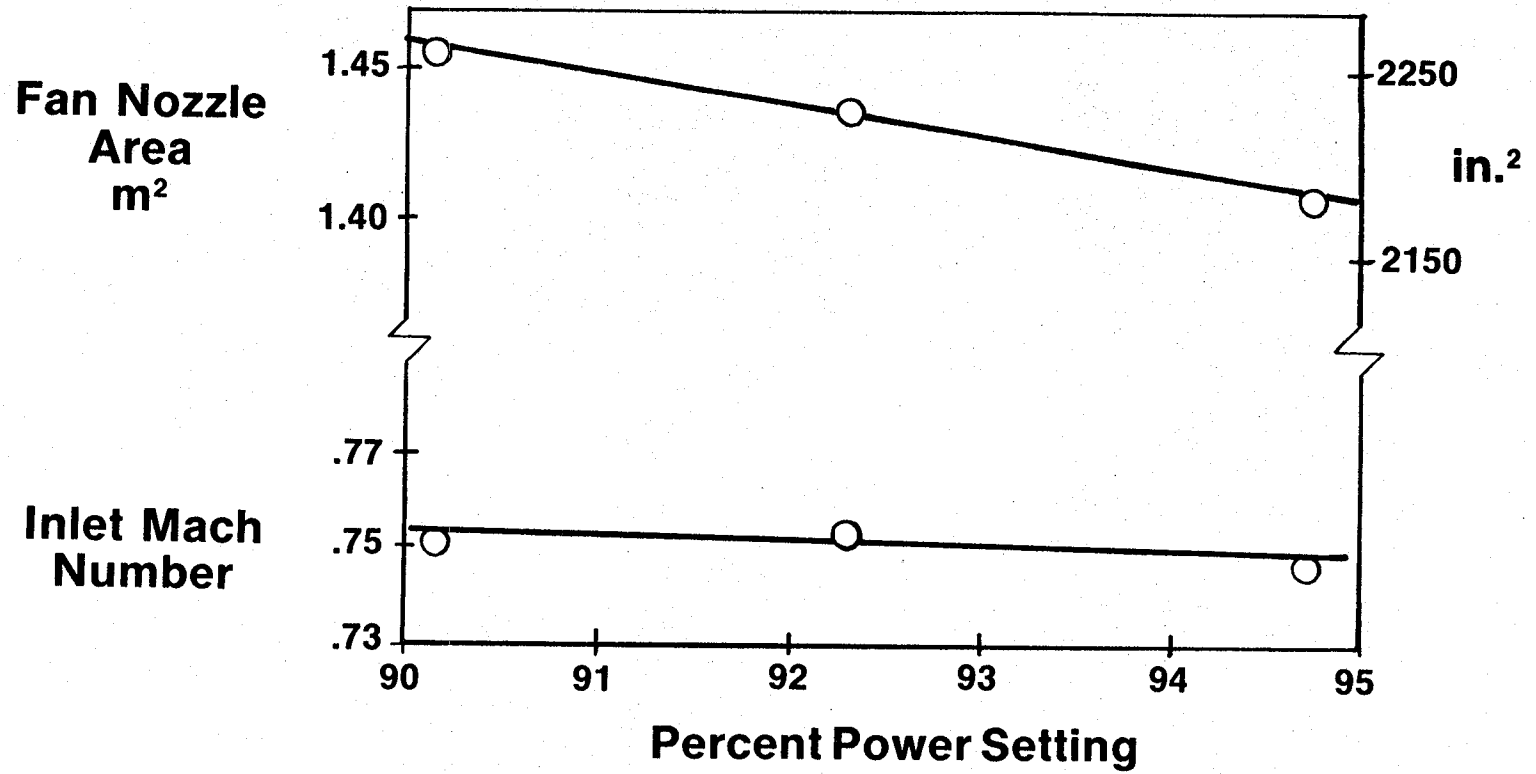
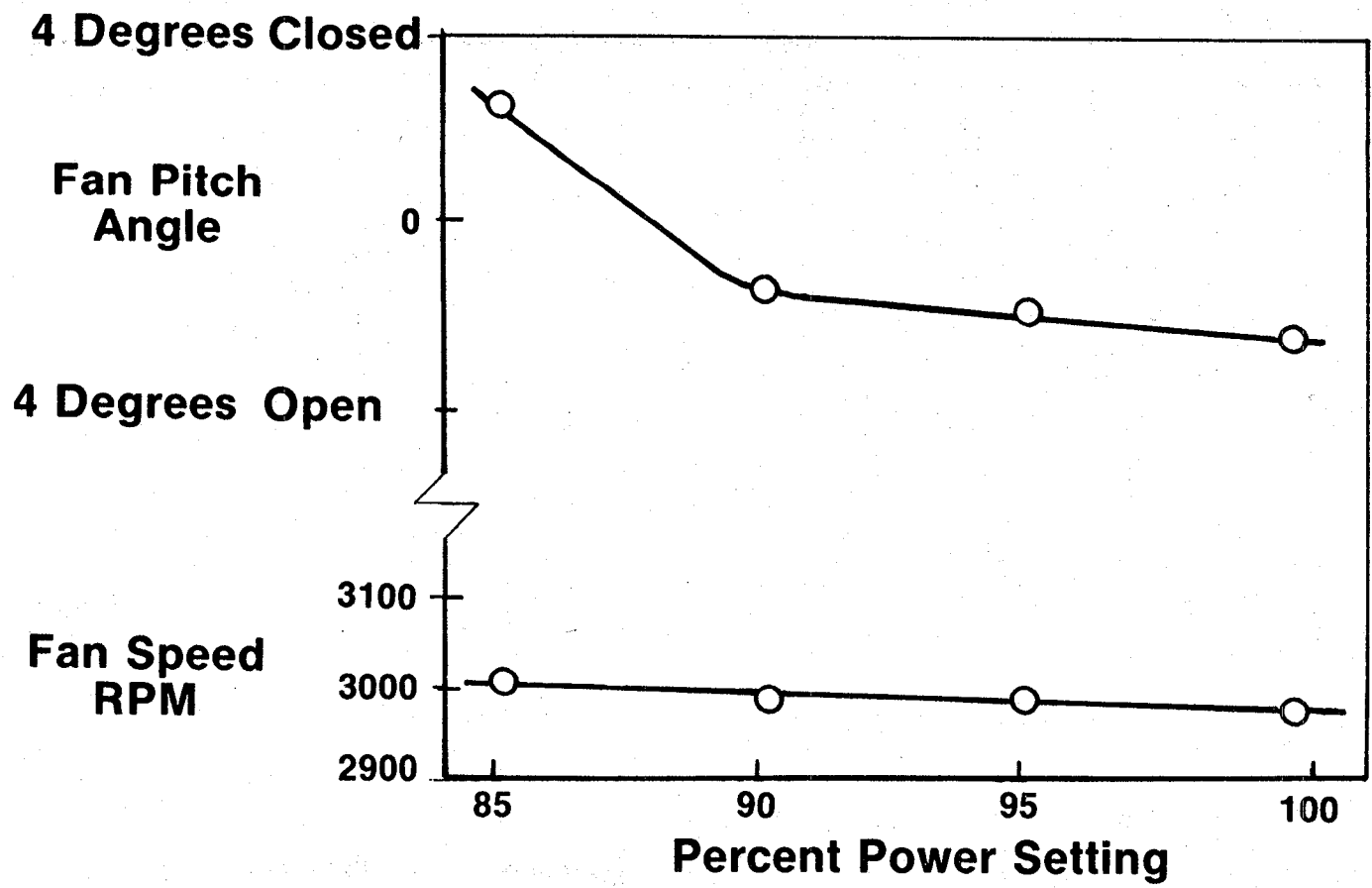Figure 150. UTW Inlet Mach Number Control.

Figure 151. UTW Fan Speed Control.

Figure 152 shows the results of another experiment on inlet Mach number control. In this experiment, the engine power demand was held constant, and the desired inlet Mach number reference was varied. As the inlet Mach number reference in the digital control was changed by an on-line adjustment, the fan nozzle opened to hold the requested inlet Mach number.

Recorded data were examined to determine the steady-state stability of the control system when it was operated with the closed-loop controls noted above. Throughout all of the closed-loop operation the steady-state stability of the controlled variables (pressure ratio, inlet Mach number, fan speed) was excellent. Table XXVIII shows typical steady-state stability results.

Sensor accuracy is an important element in the engine control system. To evaluate this element, data measured by the engine control-system sensors were compared to data measured with the experimental engine instrumentation. Table XXIX shows the results of a comparison of digital control sensors and engine instrumentation.

Summary - A multivariable digital control system was designed and engine-tested in the UTW QCSEE program. During the engine-test program, accurate and stable control was achieved in all modes of operation. Closed-loop control was demonstrated on an engine pressure-ratio/fuel-flow loop, inlet Mach number/fan-nozzle-area loop, and a fan-speed/fan-pitch loop. The digital communication link between the engine control and the engine control room was demonstrated, and accurate steady-state sensor performance was obtained.

4.4.2 OTW Engine

As noted earlier, the OTW digital control varied engine fuel flow to hold a scheduled corrected fan speed. Figure 153 shows typical engine-test data. As noted on the figure, scheduled and measured speed are nearly identical. Examination of recorded data also revealed excellent steady-state fan-speed stability.

A second primary function of the digital control was to schedule the variable compressor stators. Figure 154 shows the steady-state schedule and typical data recorded during the engine test program. It should be noted that the corrected core speed is based on a calculated compressor-inlet temperature.

One task of the propulsion control system is to prevent the engine from exceeding physical operating limits. One engine limit incorporated in the digital control memory was turbine inlet temperature. Turbine inlet temperature was calculated from fuel flow, compressor discharge pressure, and compressor discharge temperature. The calculated value of turbine inlet temperature was compared to the limit, and fuel flow was adjusted to prevent overtemperature. The OTW and UTW control incorporated this function. Figure 155 compares on-line turbine inlet temperature calculations by the

228
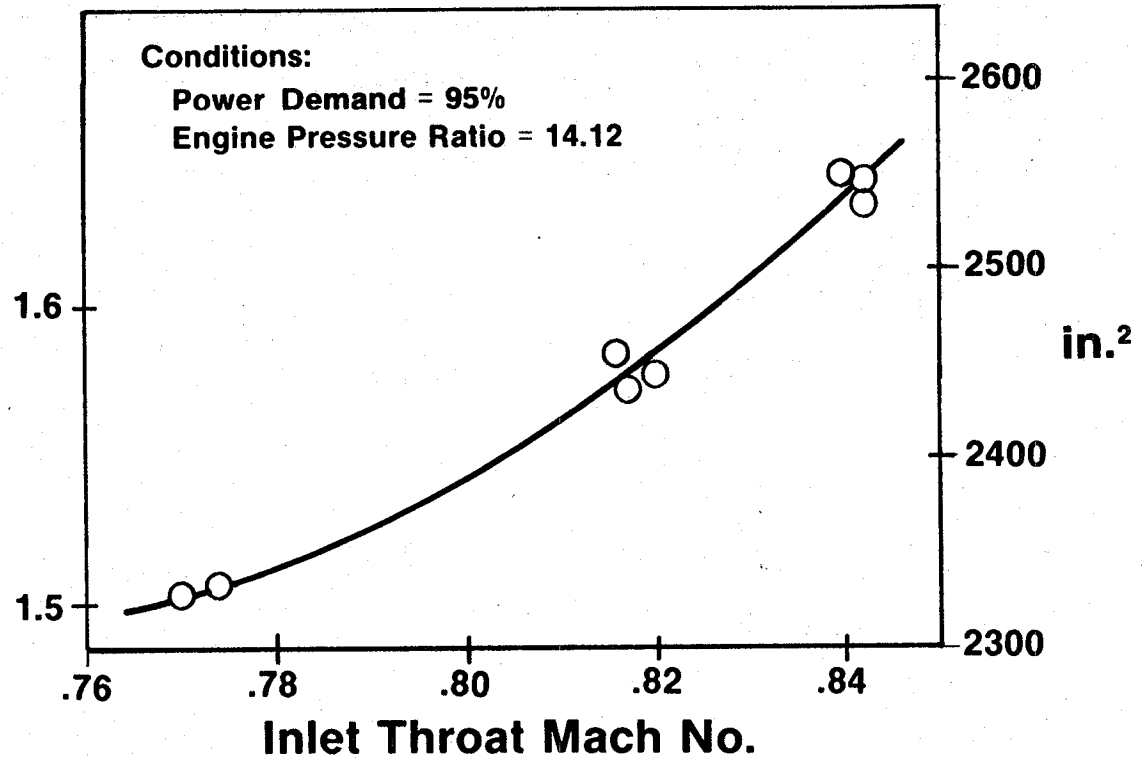
Figure 152. UTW Fan Exhaust Nozzle Tracking.

Table XXVIII. Steady-State System Stability.

	Variation
• **Pressure Ratio**	$<\pm.05$
• **Mach Number**	$\pm.005$
• **Fan Speed**	± 20 **RPM**

Table XXIX. Sensor Accuracy.

	% Variation
Fan Inlet Temperature	± 0.2
Compressor Discharge Temp.	-1.0
Compressor Discharge Pressure	$+0.4$
Fuel Flow	$+1.7$
Inlet Static Pressure	$+1.0$
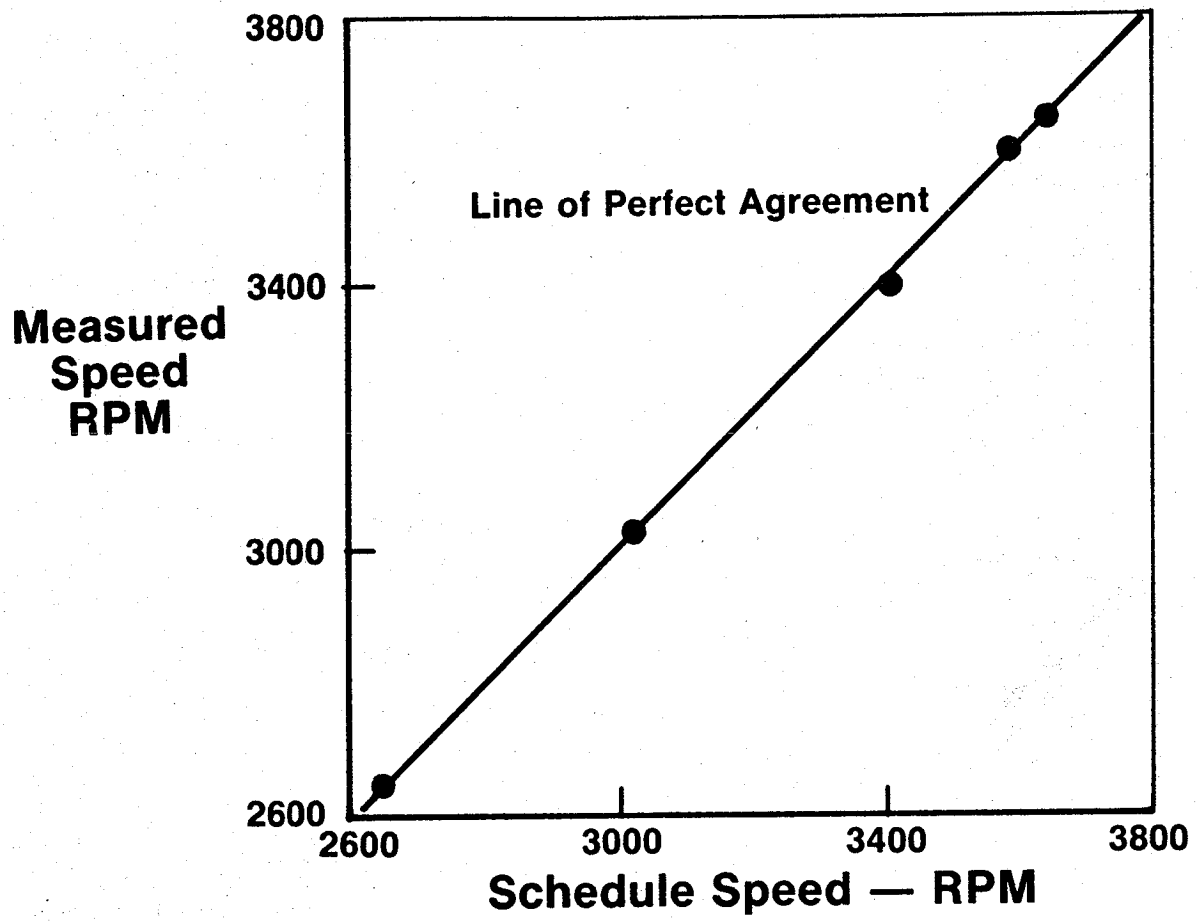
Figure 153. OTW Fan Speed Scheduling.
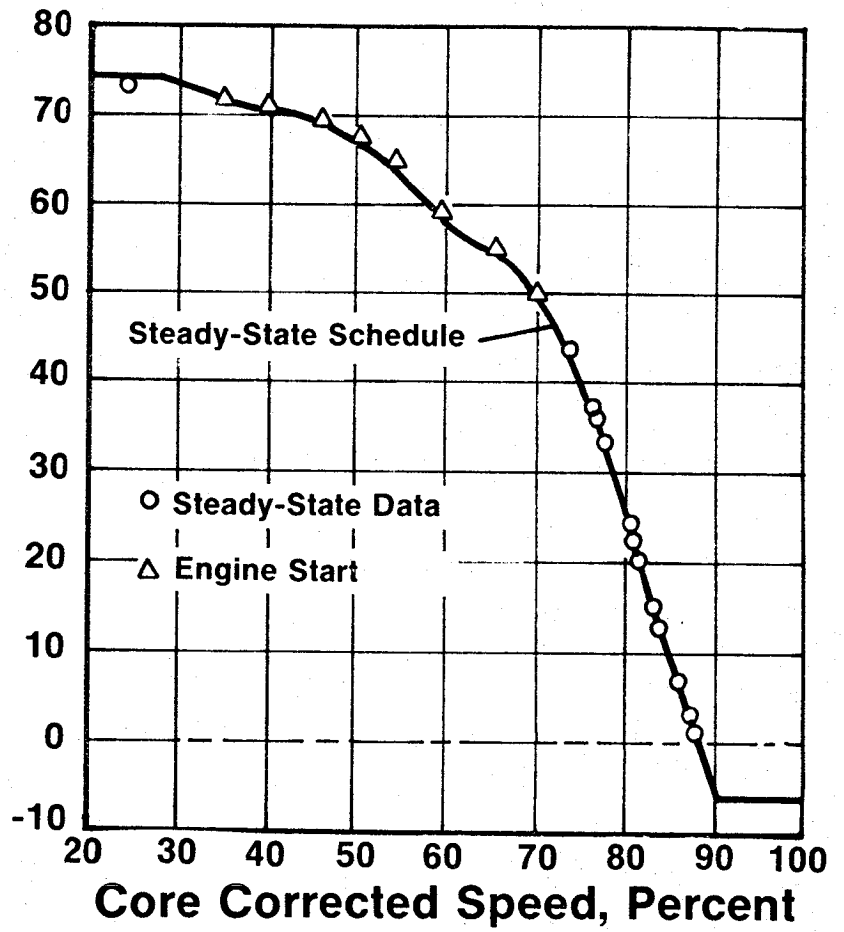
Figure 154. OTW Core Stator Control Performance.
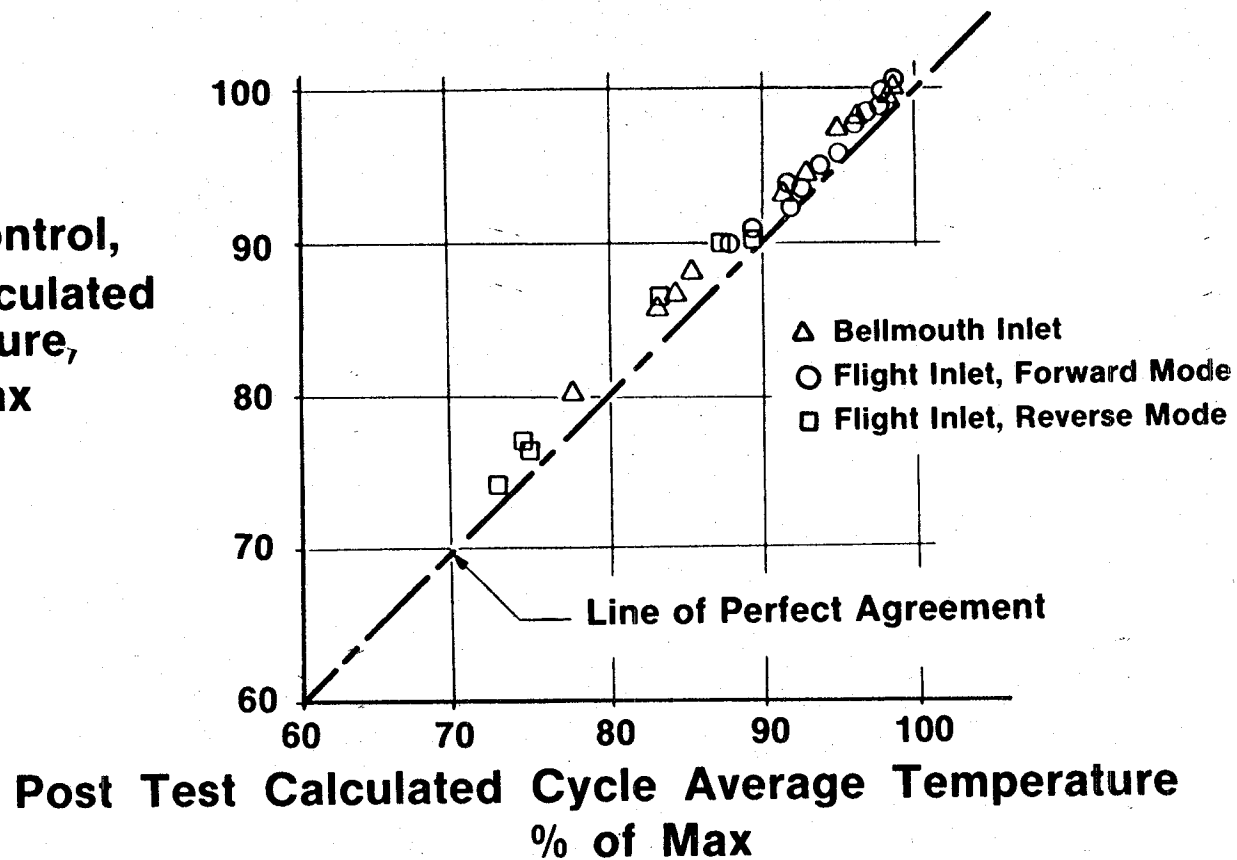
Figure 155. OTW Turbine Inlet Temperature Calculation Comparison.

digital control with posttest calculated values of turbine inlet tempera-
ture. The posttest data were calculated from cycle balance, using measured
steady-state engine data; whereas, the digital control data were continu-
ously calculated from an empirical equation in the digital control program
memory. At the higher temperature levels, where protection is required,
the digital control data agree with the posttest data within approximately
1.5%. Examination of recorded data showed that most of this error was
associated with an error in fuel-flow measurement. With further develop-
ment of the fuel-flow sensor an on-line, accurately calculated, turbine-
inlet temperature could be implemented in a flight application.

During the engine test program, the engine was operated on the calcu-
lated turbine temperature limit. The limit level could be varied through an
on-line adjustment. Engine operation on the limit was stable.

During the engine start cycle, the control system schedules engine
acceleration fuel flow to prevent compressor stall. As noted earlier, the
digital control incorporated the acceleration schedule in a series of poly-
nomial equations. Figure 156 shows a typical start on the OTW engine with
the full authority digital control. In this figure, the engine is being
motored at core speed of 4000 rpm, at zero time, on the air starter. At
approximately 1 second the combustor ignitor is energized, and the fuel stop
cock is opened. An engine light is achieved in approximately 2 seconds as
indicated by the rise in turbine discharge temperature. Over the next 25
seconds, the engine accelerates to idle speed. Through this period, the
digital control is calculating and implementing the acceleration fuel-flow
limit.

As noted earlier, the QCSEE's were required to have rapid thrust-
response capability. Figure 157 shows the thrust-reponse requirement and
the results of one transient-response experiment. The test results were
obtained with a 25° core stator reset. As indicated on the figure, the
experimental engine met the thrust-response requirement.

Summary - A full-authority, engine-mounted, digital control was designed
and tested on the OTW QCSEE. During the engine-test program, the digital
control functioned to provide reliable engine starting; it scheduled fan
speed and core stator angle accurately. System stability was excellent from
idle to full power. The calculated turbine inlet temperature concept was
evaluated, and the control system manipulated the engine variables to demon-
strate the transient-response requirement.

4.5 ACOUSTIC TEST RESULTS

The QCSEE acoustic-test program was conducted to measure the system-noise
levels of the UTW and OTW engines and to evaluate the component-technology
features on both engines. Both forward- and reverse-thrust noise levels were
measured with the engine alone, i.e., without a wing-flap system in place.
Where possible the component source levels and suppression have been assessed,
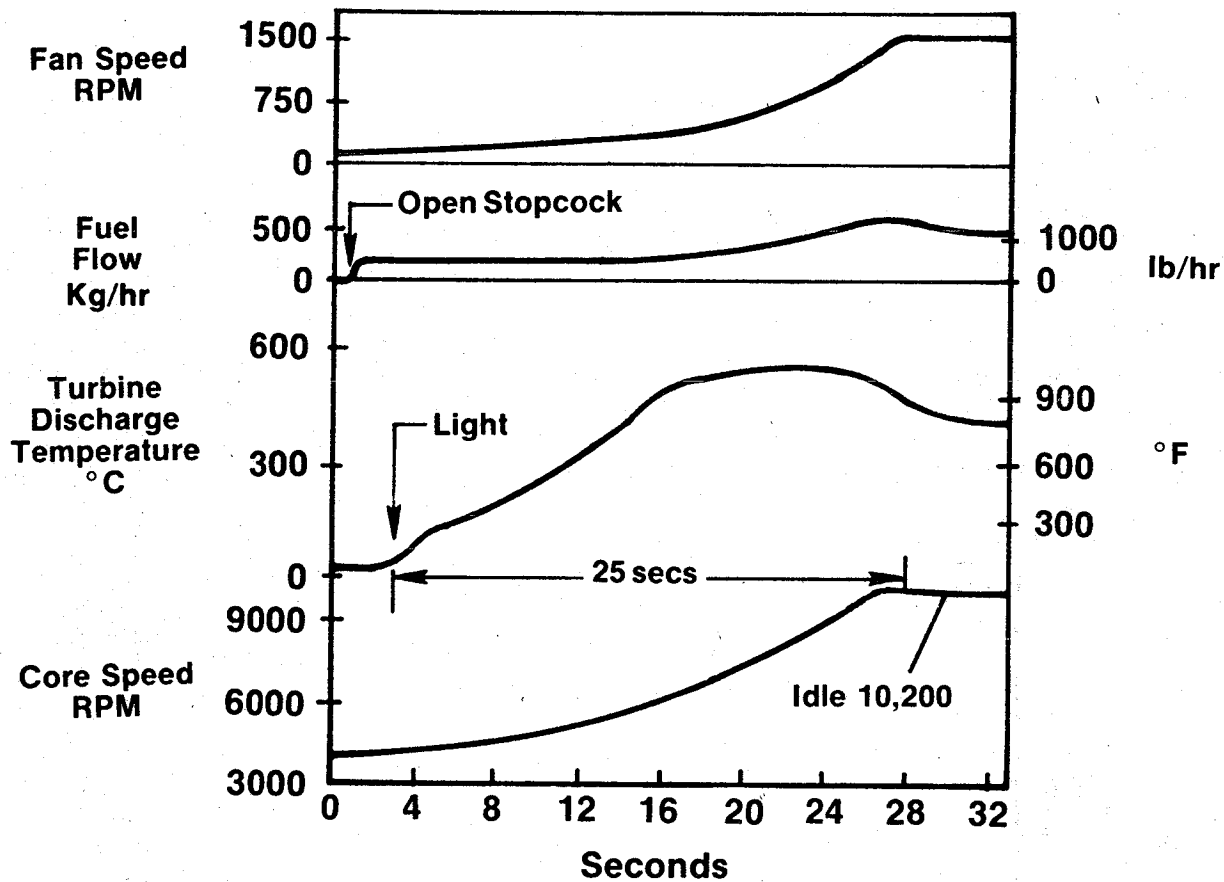but in some cases the noise reduction achieved by the total system will be
presented.

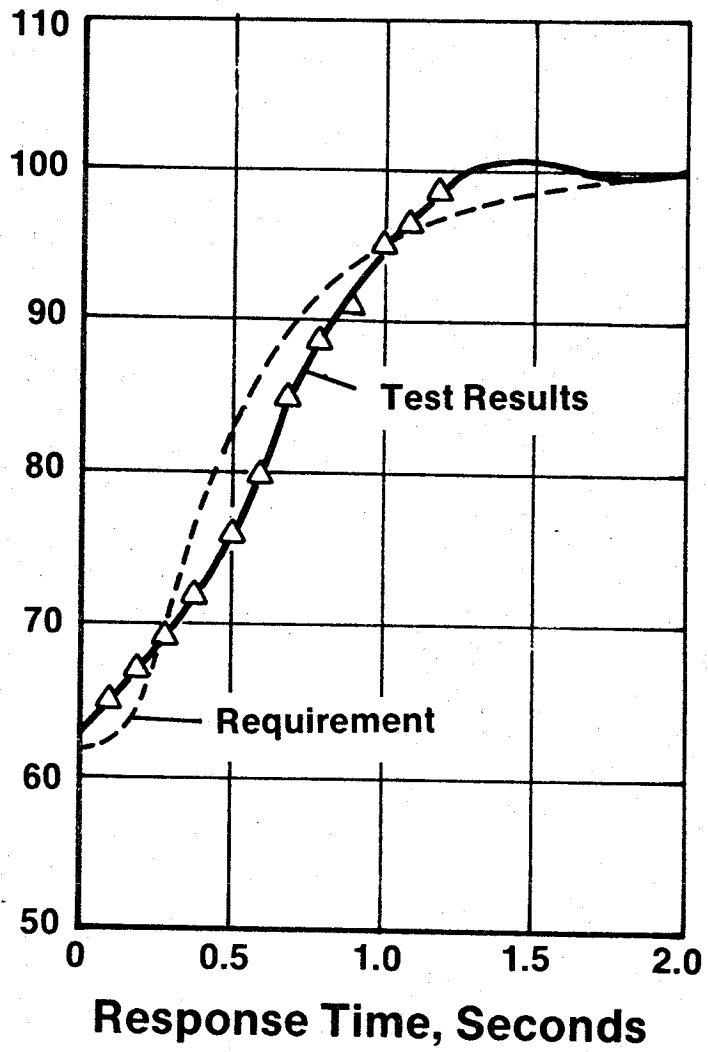Figure 156. OTW Typical Engine Start.

Figure 157. OTW Thrust Response.

The UTW acoustic test program was carried out with the composite nacelle mounted as shown in Figure 158 on the acoustic test pad. The engine center-line was 3.96 m (13 ft) from the ground. Since data were taken without the wing-flap system in place, the noise produced by the jet-flap interaction source had to be calculated and added to the measured engine-noise level in order to calculate the aircraft system noise for comparison to the program noise goals.

4.5.1 Test Configuration and Measurements

The five test configurations shown in Figure 159 permitted evaluation of the basic UTW engine noise levels as well as assessment of the major noise components. The baseline configuration was untreated with the exception of the fan frame between the rotor and OGV's, treatment on the OGV's, and in the core compressor inlet. Configuration No. 2 was the same as the baseline with the exception that the vanes were taped to determine the effect of this treatment. Both of these configurations were run with an untreated bellmouth inlet, and the resulting data were used to define the baseline system and fan-component-noise levels. The fully suppressed nacelle was run both in forward and in reverse thrust. Configurations 4 and 5 were tested with the fan-exhaust splitter and the core suppressor removed, respectively, to determine the impact of these two suppression elements. All configurations were oper-ated over a range of engine conditions including speed variation, blade angle setting, and nozzle area.

All noise testing was done on the acoustic pad at the Peebles test facility. The ground surface shown in Figure 160 is concrete, but most of the testing was carried out with a gravel field surface. Noise measure-ment instrumentation locations, shown in Figure 161, consisted of a far-field microphone arc at 46.5 m (152.4 ft) with microphones on 12.2-m (40-ft) towers, every 10°. The acoustic directional array, which was used at six angles to separate engine sources and aid in component-suppression evalua-tion, is a highly directional receiver mounted on a movable cart. Internal engine instrumentation was also used and consisted of sound-separation probes and wall pressure transducers in the fan inlet and fan exhaust ducts.

4.5.2 UTW Results

Prior to test, the major noise-component spectra were estimated using calculation procedures for the jet noise, combustion noise, and turbine noise and scaling fan-noise spectra from previously measured fixed-pitch-fan noise data. Fan pressure ratio and tip speed were the primary scaling parameters used to obtain estimates of both inlet-radiated and exhaust-radiated fan noise. Each of these component spectra are plotted in Figures 162 and 163 at the maximum forward and aft angles of noise radiation for the takeoff power setting of the UTW engine. The heavy line on each plot is the logarithmic sum of these individual spectra and is an estimate of the measured baseline engine spectra at 46.3-m (152-ft) radius. The symbols on Figure 162
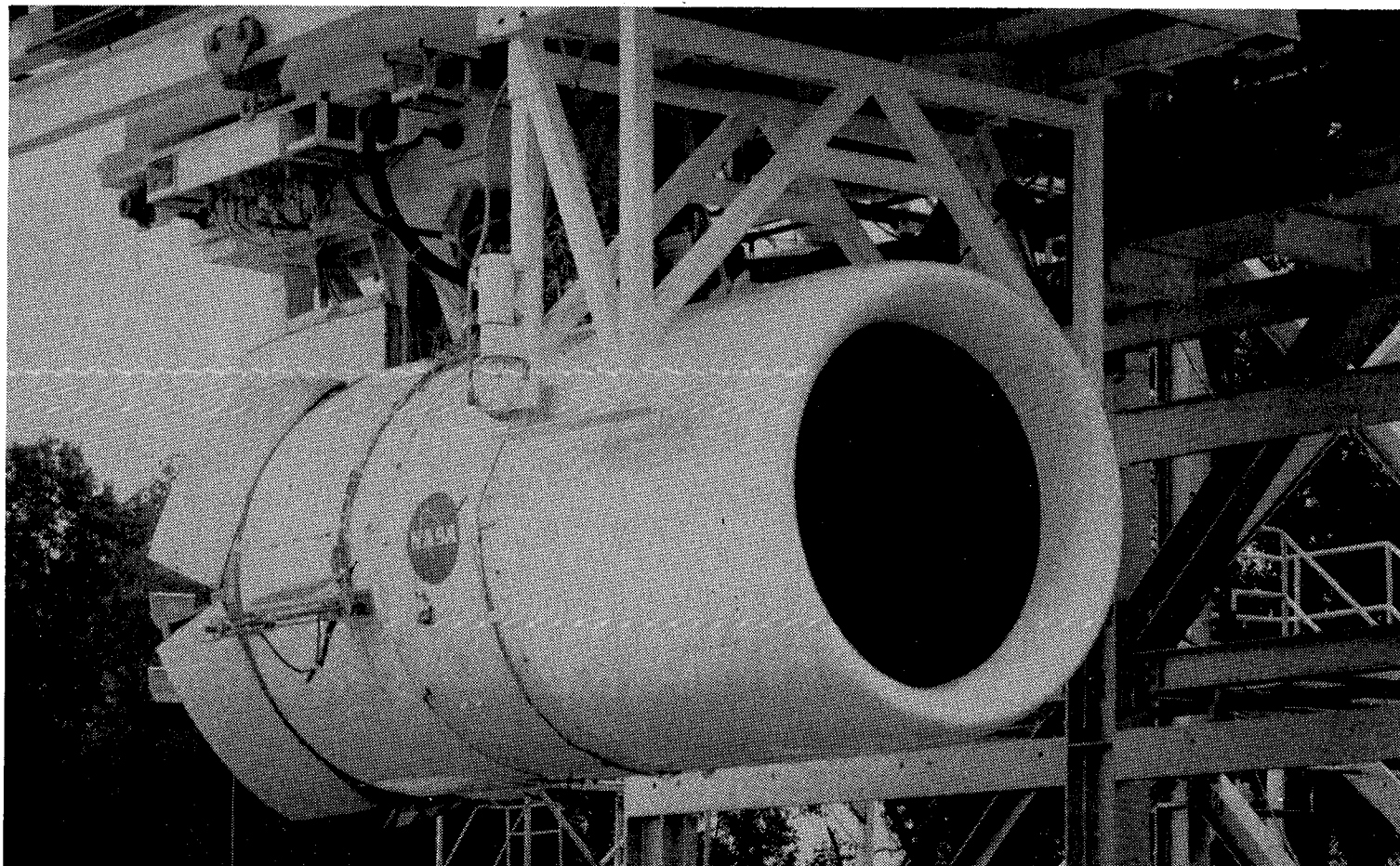
Figure 158. UTW QCSEE.
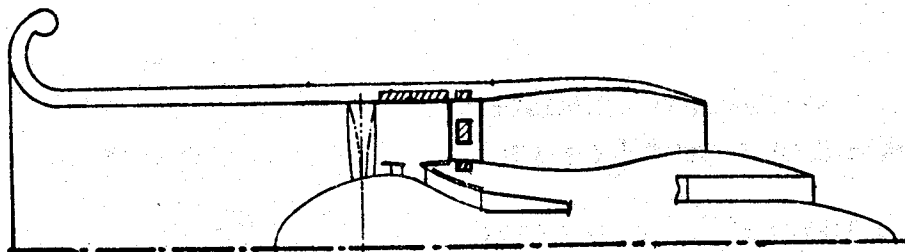
1. Baseline (Untreated Except for Treated Frame and Vane)

2. Baseline with Untreated Vanes
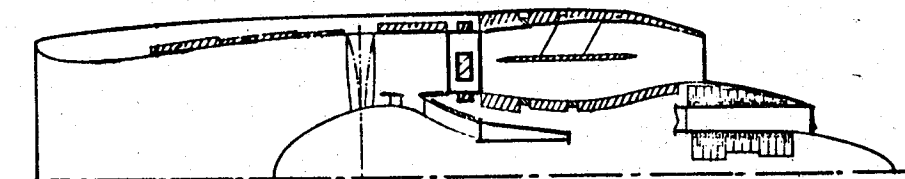
3. Fully Suppressed (Forward and Reverse Thrust)
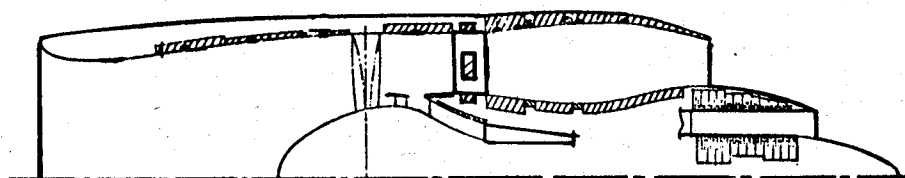
4. Without Fan Exhaust Splitter
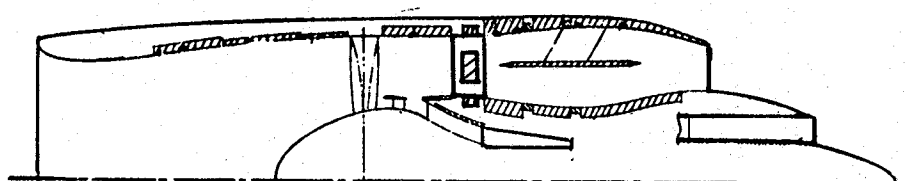
5. Without Core Treatment

Figure 159.   UTW Acoustic Test Configurations.
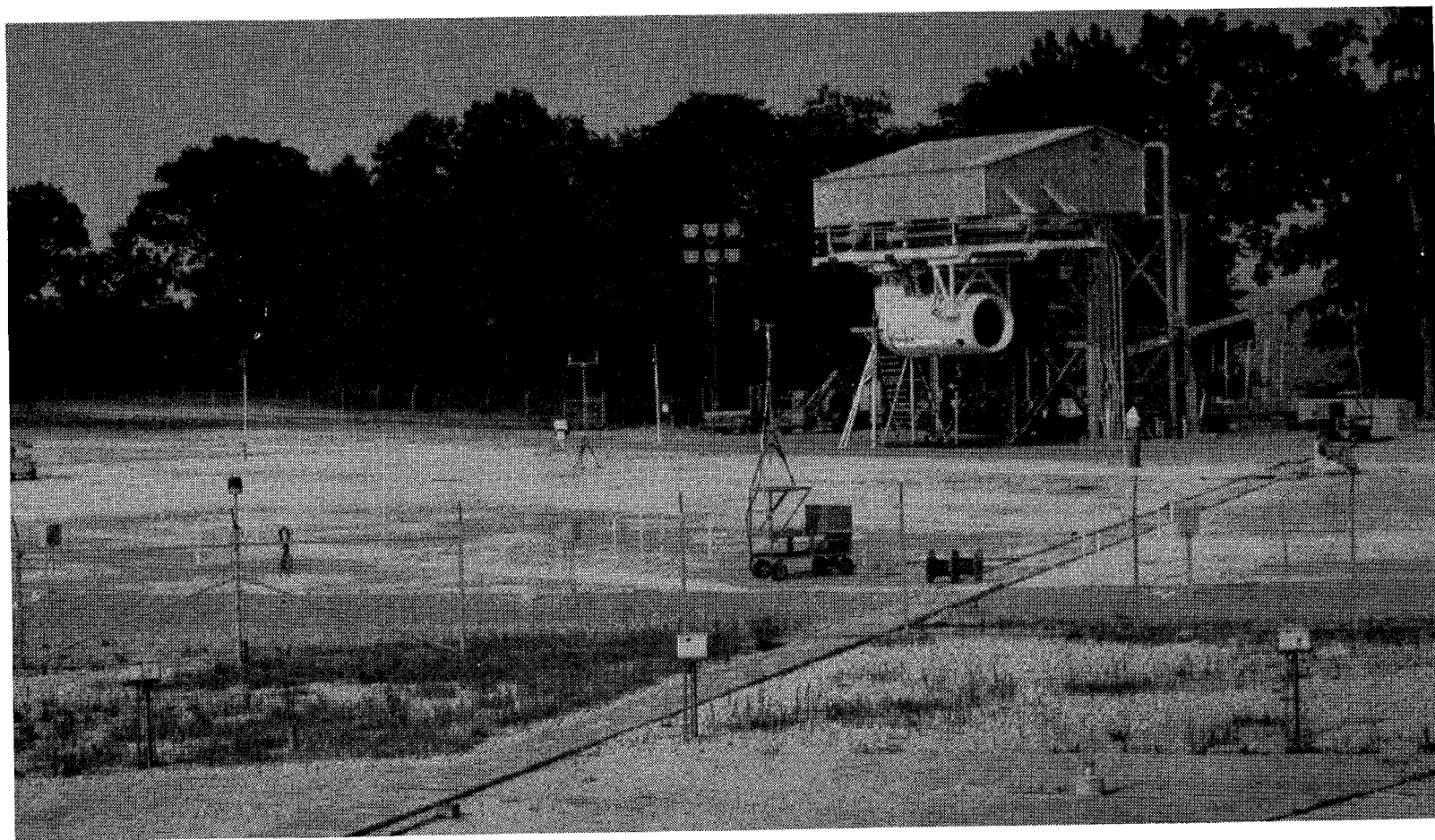
Figure 160. Acoustic Test Site.
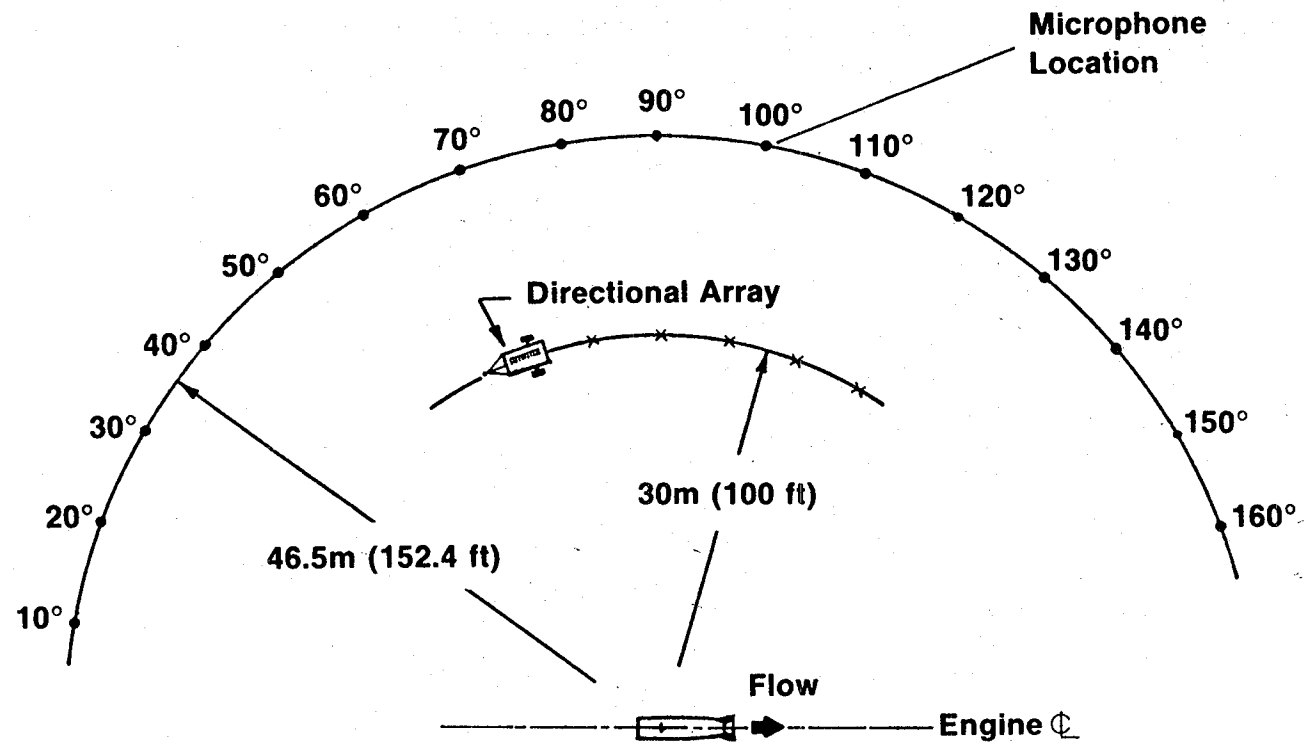
Figure 161. Peebles Acoustic Test Sound Field.
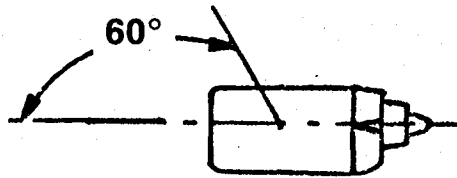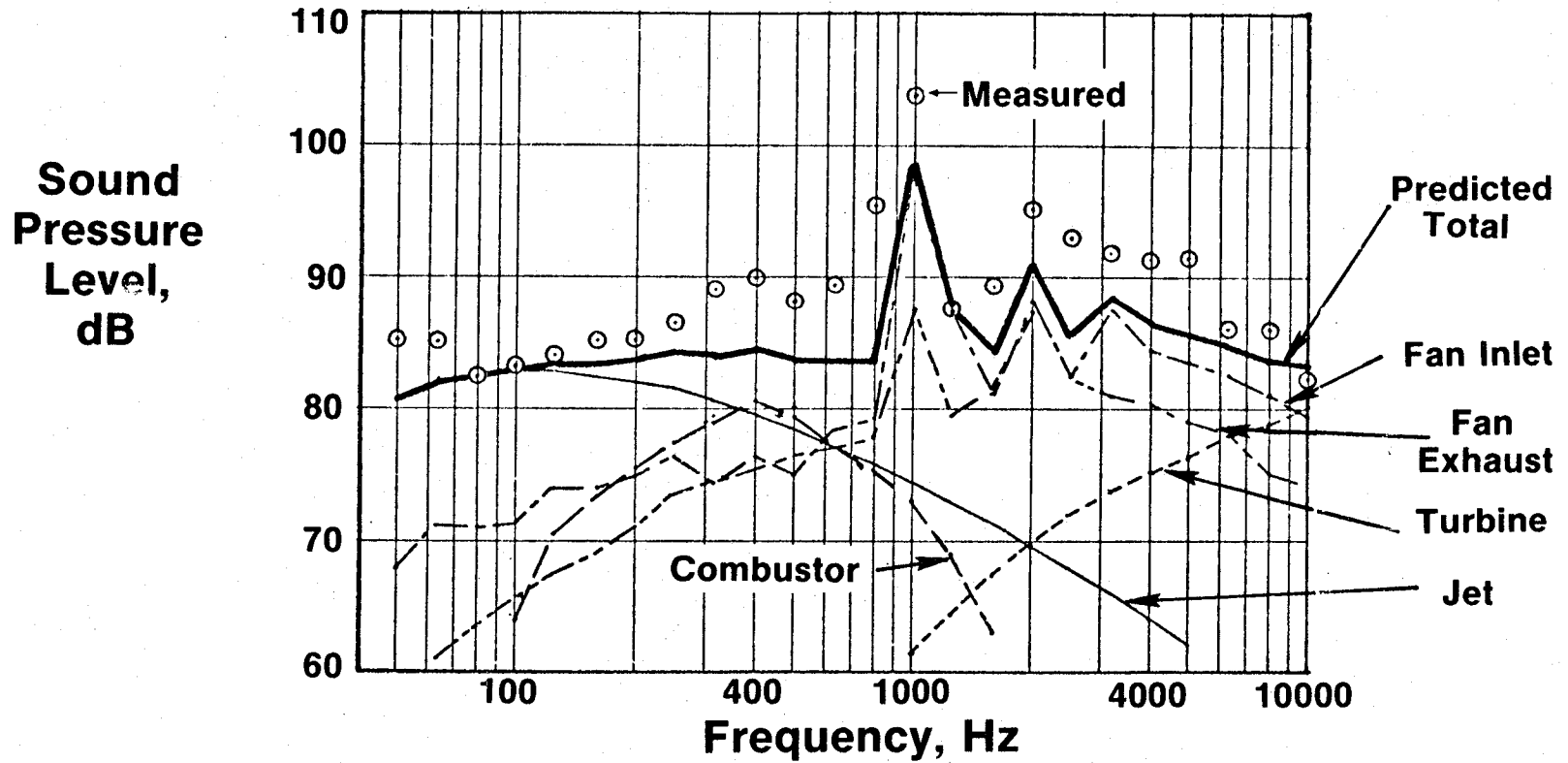
Figure 162. UTW Inlet-Radiated Baseline Noise.
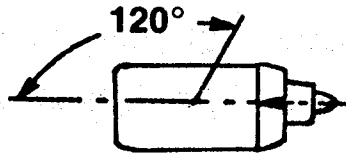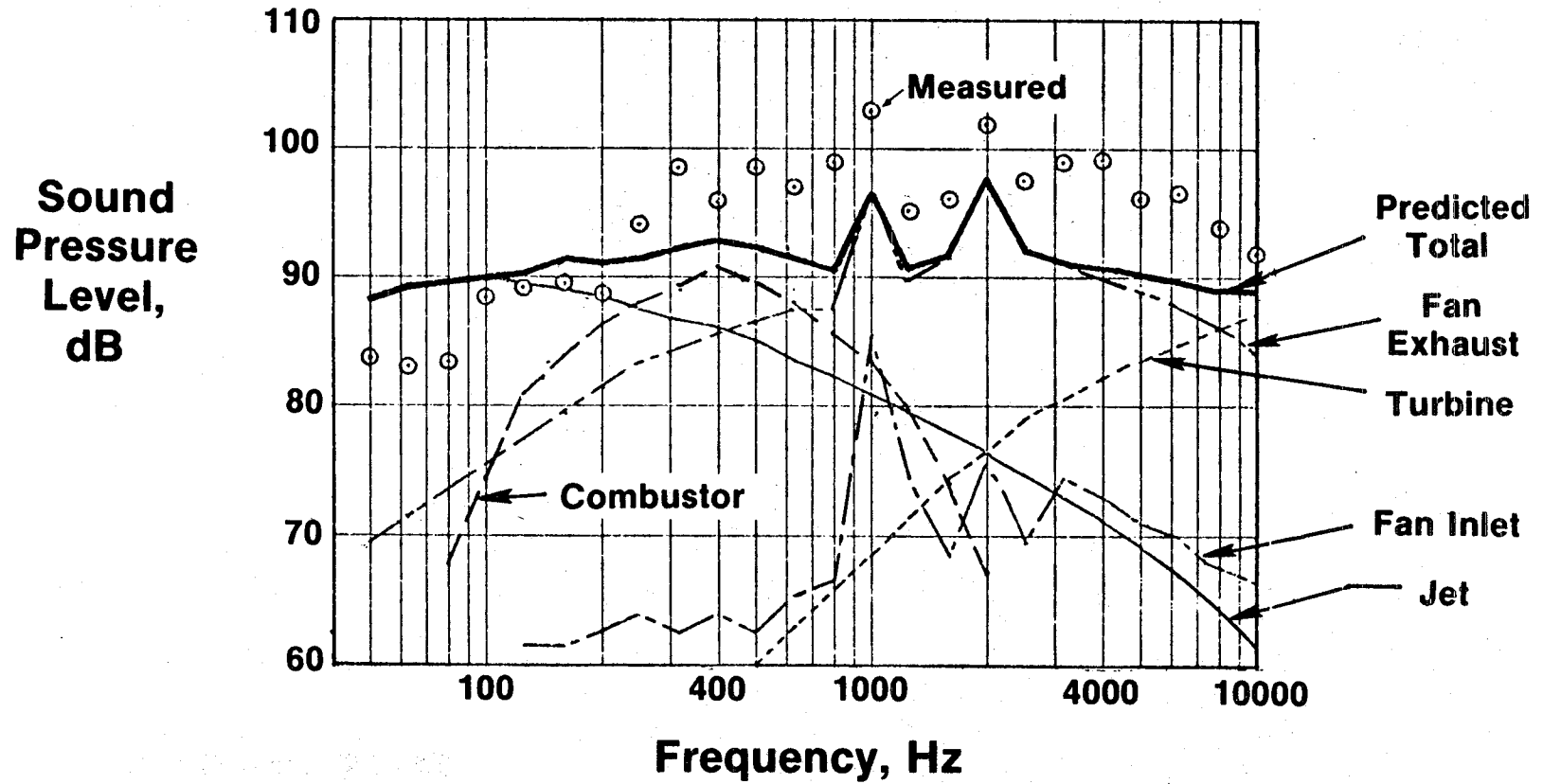
Figure 163. UTW Exhaust-Radiated Baseline Noise.

and 163 are the measured data from the baseline test. In general, the measured levels are on the order of 5 dB higher than expected over the entire high-frequency spectrum. Since the system noise above 800 Hz is controlled by fan noise, it appears that the estimates based on the fixed-pitch-fan data cannot be used to reliably predict variable-pitch-fan designs; i.e., solidity, blade number, and perhaps the vane-frame design are probably causing this divergence, and the exact cause needs to be the focus of additional investigation.

One of the potential advantages of a variable-pitch fan was thought to be the capability to minimize noise by continuously optimizing blade incidence angle and loading over the fan-speed range. Data shown in Figure 164, taken at forward and aft max angles, takeoff and approach thrusts, show no tendency to identify a minimum noise point. These data represent a range of incidence angles and loading large enough to reveal any acoustic advantages which might be present. Fan-source mechanisms are many and varied for the static test case. For example, one of the major noise-source mechanisms statically is known to be the interaction of the rotor with inlet turbulence. This source appears to be made up of both a dipole source and a quadrapole source; one varies with blade loading, and one is independent of loading. If, for this fan design, the dipole, rotor/turbulence interaction source controls, then no change with blade angle would occur. In flight, however, the ingested turbulence is no longer affected by the contraction ratio of the static inlet, and this rotor-turbulence interaction noise is reduced. Therefore in the flight case the effect of blade angle may be important.

The inlet design, which has been described previously, is shown in Figure 165 in cross section. The treatment begins 11.2 cm (4.4 in.) downstream of the high Mach number throat and is designed to produce 12.8 PNdB suppression at takeoff and 6.3 PNdB suppression at approach, both at the maximum forward-radiation angle on a 152-m (500-ft) sideline.

The suppression results of this inlet design are shown in Figure 166; the sideline PNL has been plotted as a function of throat Mach number for the baseline test and the fully suppressed configuration. (The baseline data taken with the cylindrical inlet is plotted at equivalent fan rpm points since, of course, the inlet Mach numbers are quite low.) Several sets of data with different blade angle settings make up the fully suppressed line. The indicated suppression at a throat M_n of 0.79 is only 9 PNdB and is changing very slowly with increasing throat M_n. This trend is contrary to the scale-model results, but additional analysis with the directional array revealed the problem. Separating the measured spectrum into noise emanating from the inlet and noise reaching the forward quadrant, but radiated from the fan exhaust, produced the dotted and dashed curves of this figure. It is obvious that the aft-radiated noise, which is increasing with engine speed (and M_{th}), is a "floor" to the inlet-noise reduction. The indicated suppression (baseline to "inlet noise") is now seen to be 14.5 PNdB at the design Mach number.
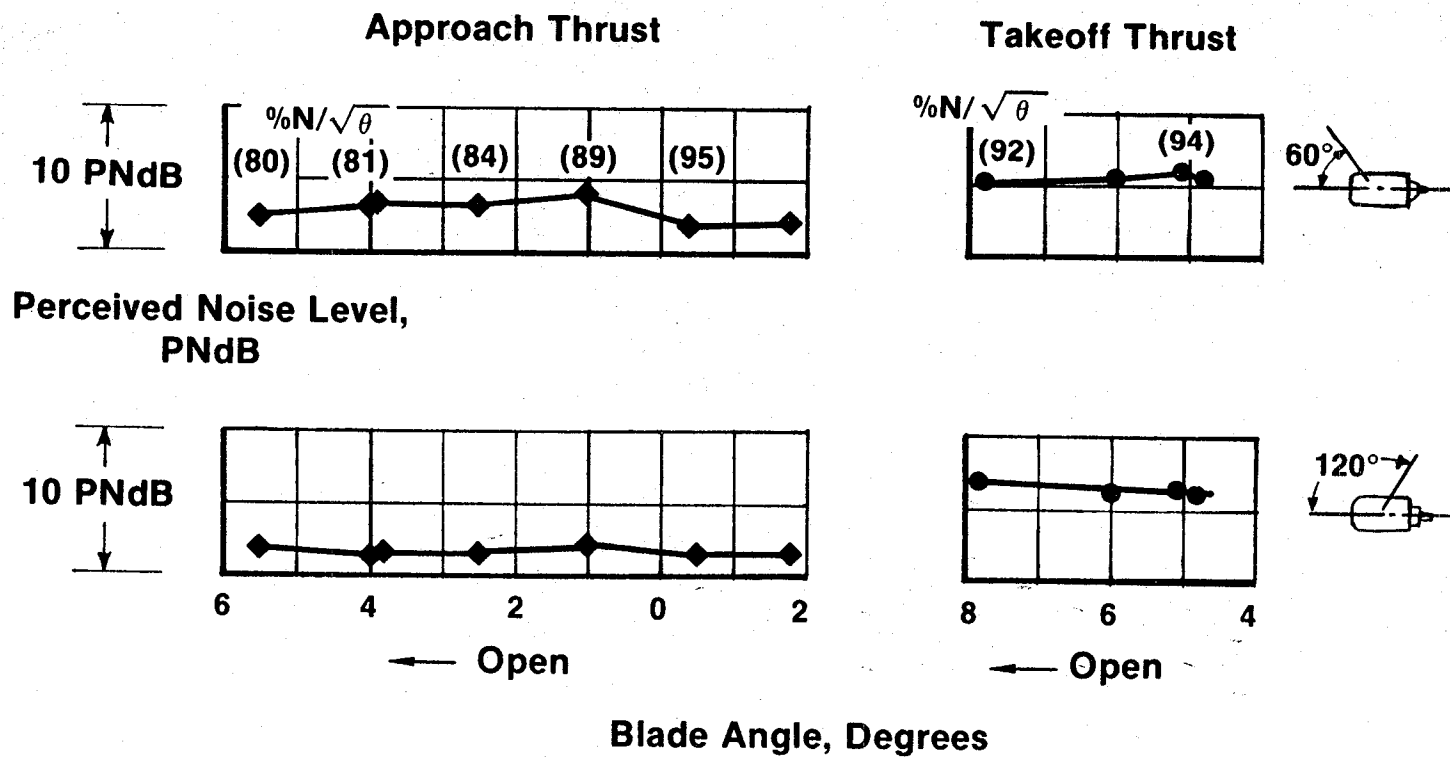
Figure 164. Variation of PNL with Blade Angle.

Throat　　　　**SDOF Treatment**
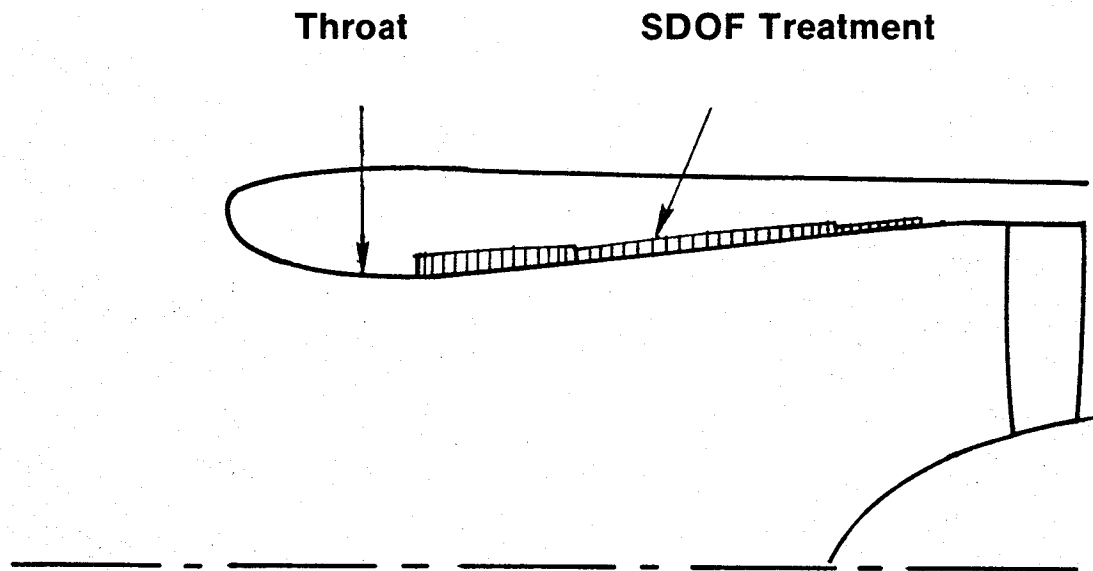
PNL Suppression Prediction

Takeoff	12.8 PNdB
Approach	6.3 PNdB

Figure 165. UTW Inlet Configuration.

Blade Angle

X 3.3° Open
△ 4.7° Open
O 5.0° Open
□ 8.0° Open

Baseline (Hardwall Bellmouth)

Fully Suppressed High Mach Inlet

Exhaust Radiated Noise

Inlet Radiated Noise

10 PNdB

Throat Mach Number

.5   .6   .7   .8   .9
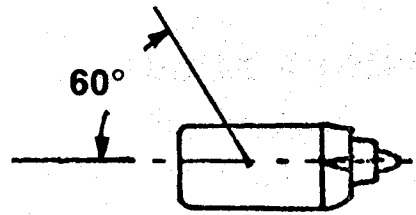
Figure 166. Effect of Inlet Throat Mach Number on PNL.

The aft treatment design is shown in Figure 167 with the predicted system suppression values at takeoff and approach. Due to the large bypass ratio and fan diameter, the fan exhaust passage height is 50.8 cm (20 inches). The desired fan exhaust suppression required the use of a splitter in this large duct. The splitter was removable, and the exhaust suppression was measured with and without the splitter in place. The measured system suppression as a function of engine thrust at the maximum aft-radiation angle is plotted in Figure 168 and shows a value of 8.0 PNdB, roughly constant over the engine power-setting range. The suppression spectra, for the splitter-out case shown in Figure 169 at takeoff and approach, are in good agreement with the prediction but miss the predicted suppression by 2 dB in one critical band (2000 Hz). This results in PNL reduction short of the prediction by about 1.5 PNdB. With the exhaust splitter in place, peak SPL suppression of almost 15 dB was measured at the 120° far-field position, and this is shown in Figure 170. In general, the suppression did not meet expectations at the second-harmonic frequency at approach nor at the fundamental and second-harmonic frequencies at takeoff. There appears to be a flanking transmission path which prevents the full suppression from being measured, and this is the subject of additional data analysis.

Taping the treatment in the vanes provided an opportunity to evaluate the suppression potential of treatment in this location. Total treated area is small, about 0.67 m^2 (7.2 ft^2), and because of treatment-thickness limitations the design frequency was high (about 4 kHz). The measured suppression spectrum (Figure 171) in the aft quadrant shows about 2 dB over a broad frequency range; this could be very beneficial to engine systems with marginal or inadequate suppression.

The core suppressor for the QCSEE was designed to suppress both high-frequency, turbine-generated noise and low-frequency, combustor-generated noise. Since both of these components are marginal in terms of contribution to the total system noise, it was recognized in the beginning of the program that it would be extremely difficult to measure the unsuppressed and suppressed levels of these components. If the fan exhaust suppression levels are achieved, however, this core 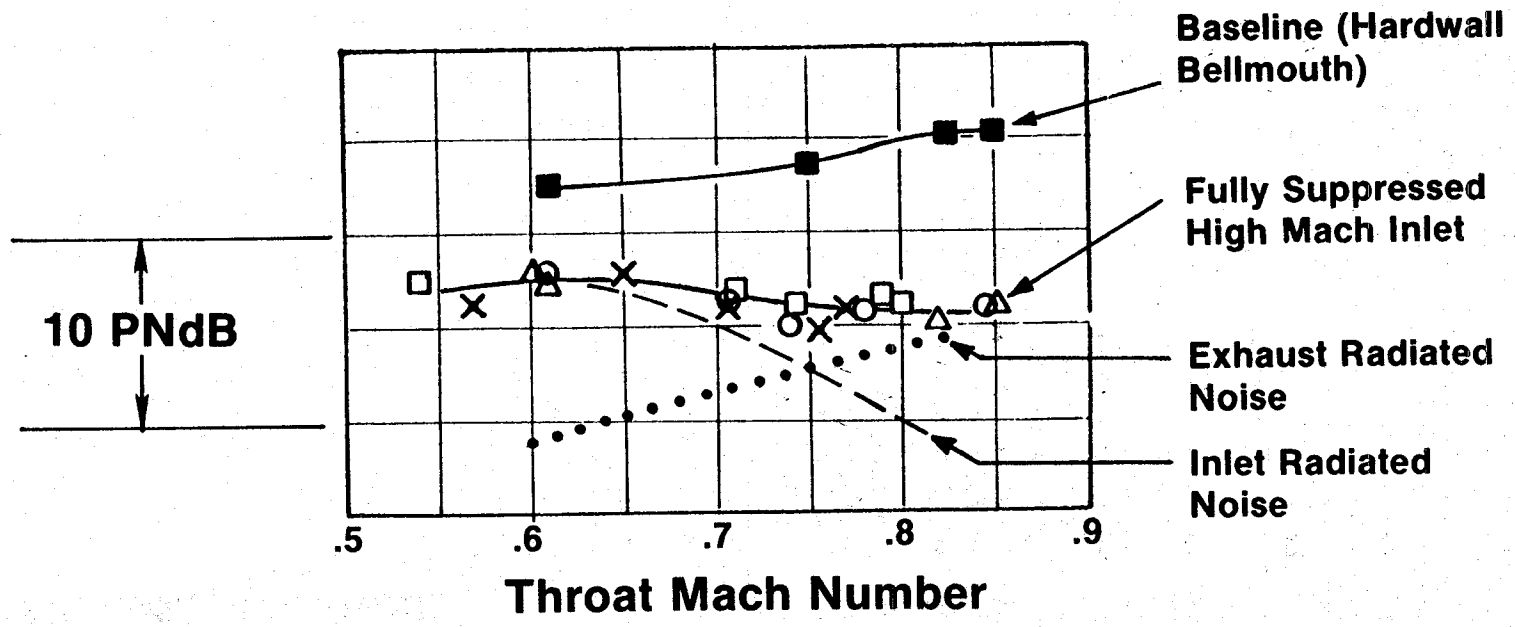noise must be reduced to meet the system goals. The difficulty in measurement of the core suppression has been compounded by the fan-source-noise increase (5 dB) which results in aft fan noise levels high enough to completely mask the high-frequency core suppression. In a similar fashion, low-frequency jet noise masks the low-frequency suppression of the combustor noise. The comparison of the measured and predicted core suppression in Figure 172, therefore, reflects the measurement difficulties just described rather than poor performance of the core suppression. Additional engine testing is required to confirm the good performance of the core suppressor indicated from the component test.

Reverse-thrust noise testing of the UTW engine was done with two blade angles over a range of reverse thrust. The measured max PNL values, shown in Figure 173, occurred at an angle of 70° on a 152-m (500-ft) sideline and were substantially above the noise goal of 100 PNdB for 35% reverse thrust. Maximum reverse thrust achieved was 27%, and at this thrust level the 152-m

- **Predicted Exhaust Suppression**
  - **Takeoff   9.2 PNdB**
  - **Approach   9.6 PNdB**
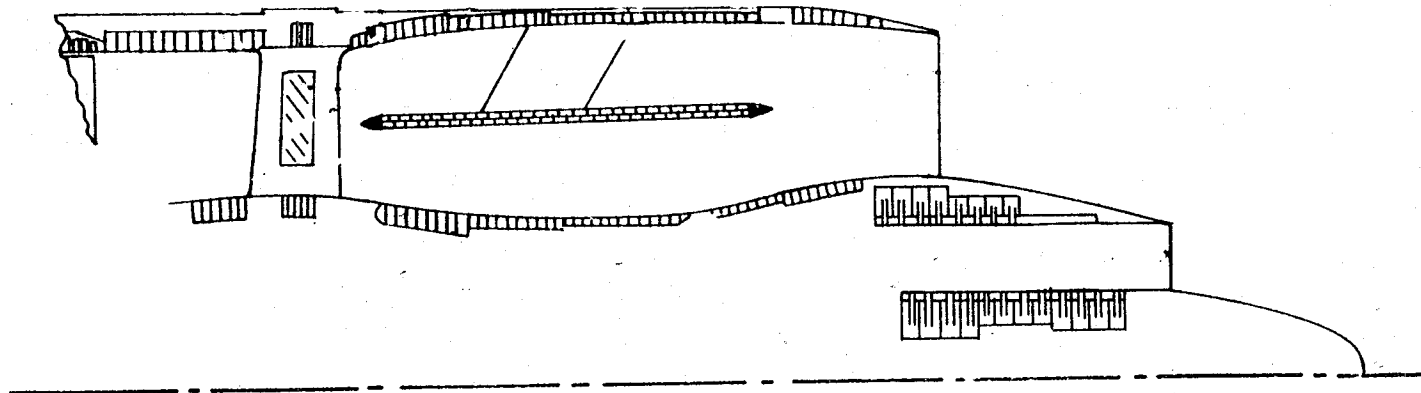
Figure 167.   UTW Exhaust Treatment Configuration.
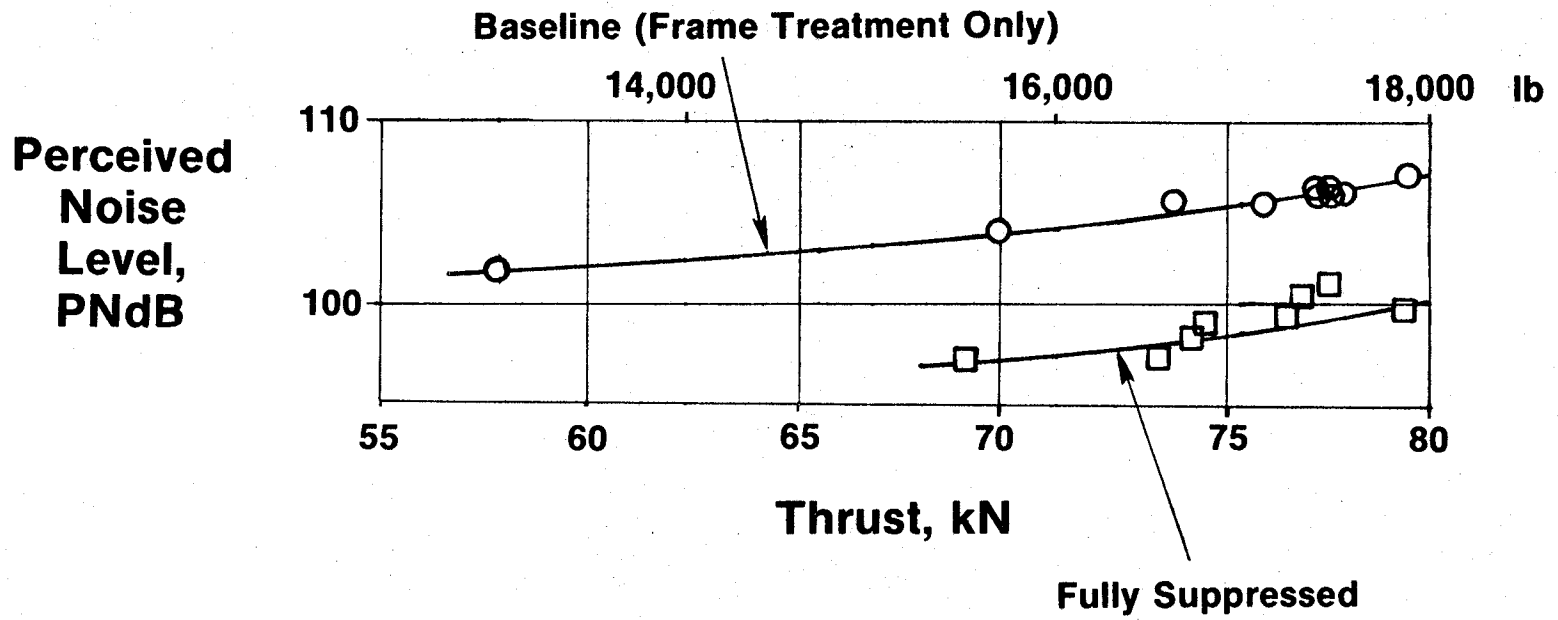
Figure 168. Exhaust-Quadrant PNL Variation with Thrust.

● Wall Treatment Only

120°
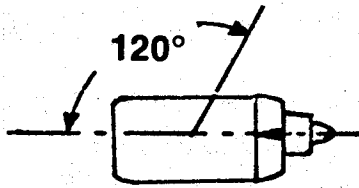
**1/3 OBSPL
Suppression,
Δ dB**

	Δ PNdB	
	Approach	Takeoff
Measured	4.4	4.0
Predicted	5.8	5.4

Approach

Predicted

Measured

Takeoff

Predicted

Measured

Frequency, Hz
100 200 400 800 1600 3150 6300 12500
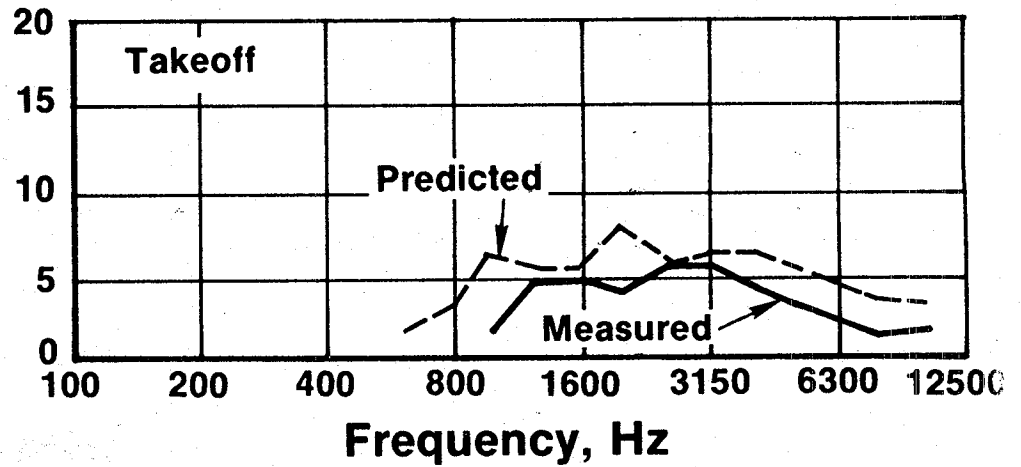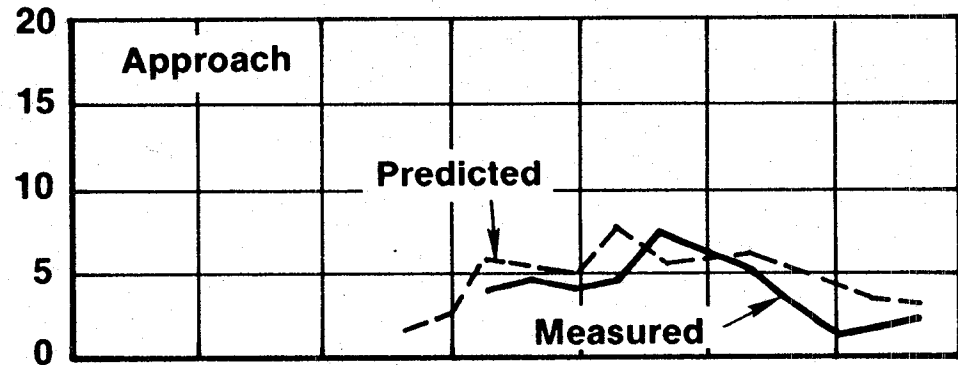
Figure 169. Exhaust-Quadrant System Suppression Spectra, Wall Treatment Only.

120°

1/3 Octave Band SPL Suppression, dB

• With Splitter

Approach

Predicted

Measured

20
15
10
5
0

Takeoff

Predicted

Measured

20
15
10
5
0

100   200   400   800   1600   3150   6300   12500

Frequency, Hz
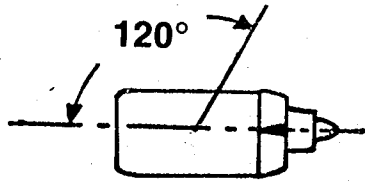
	Δ PNdB	
	Approach	Takeoff
Measured	8.0	7.5
Predicted	9.6	9.2
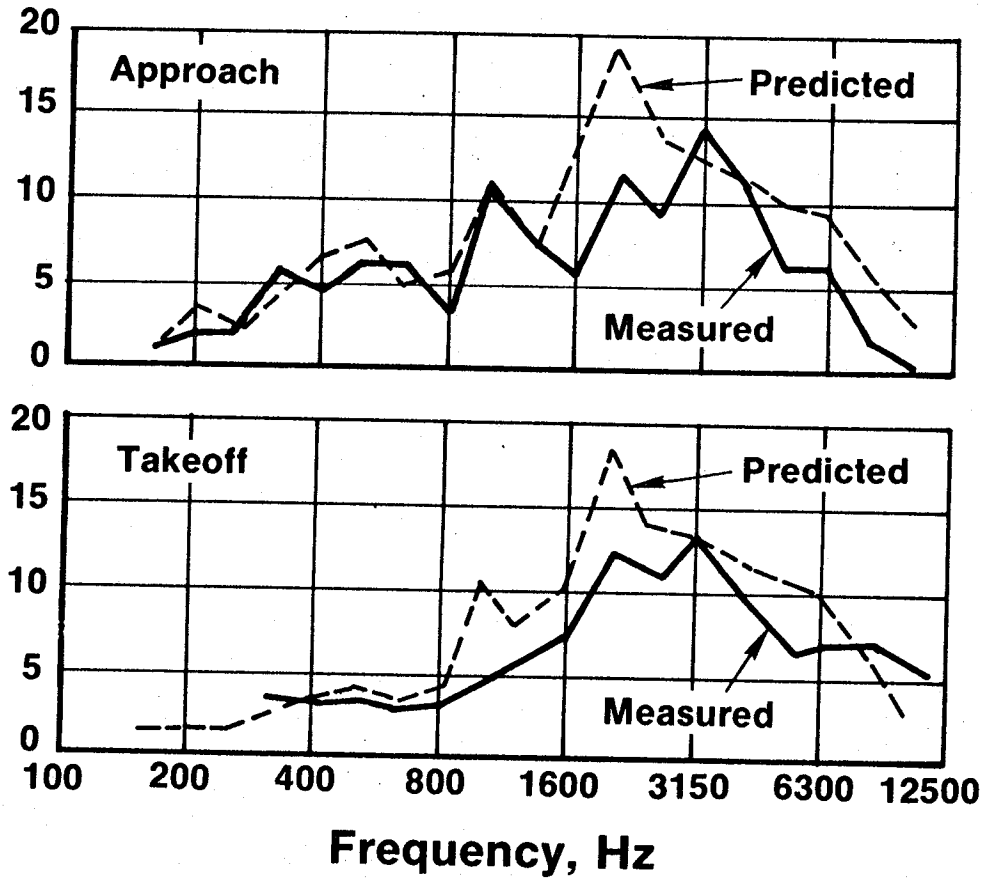
Figure 170.   Exhaust-Quadrant System Suppression Spectra, with Splitter.

Vane Treatment

120°
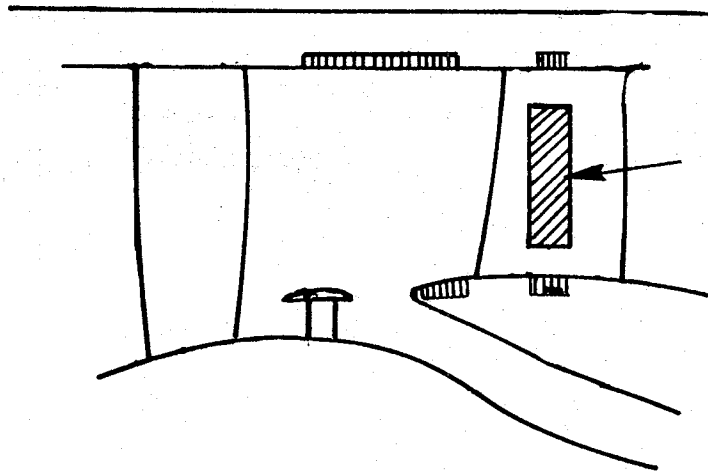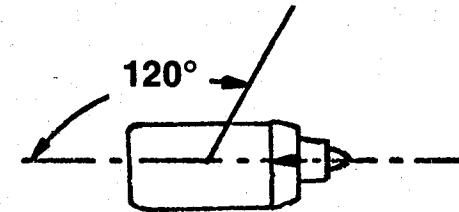
1/3 Octave Band Sound Pressure Level Suppression, dB

Frequency, KHz
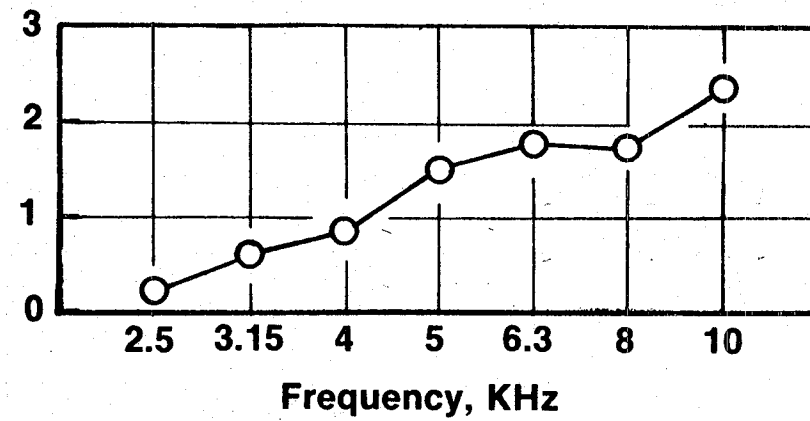
Figure 171. Treated-Vane Suppression.

1/3 Octave Band SPL Suppression, dB

Frequency, Hz
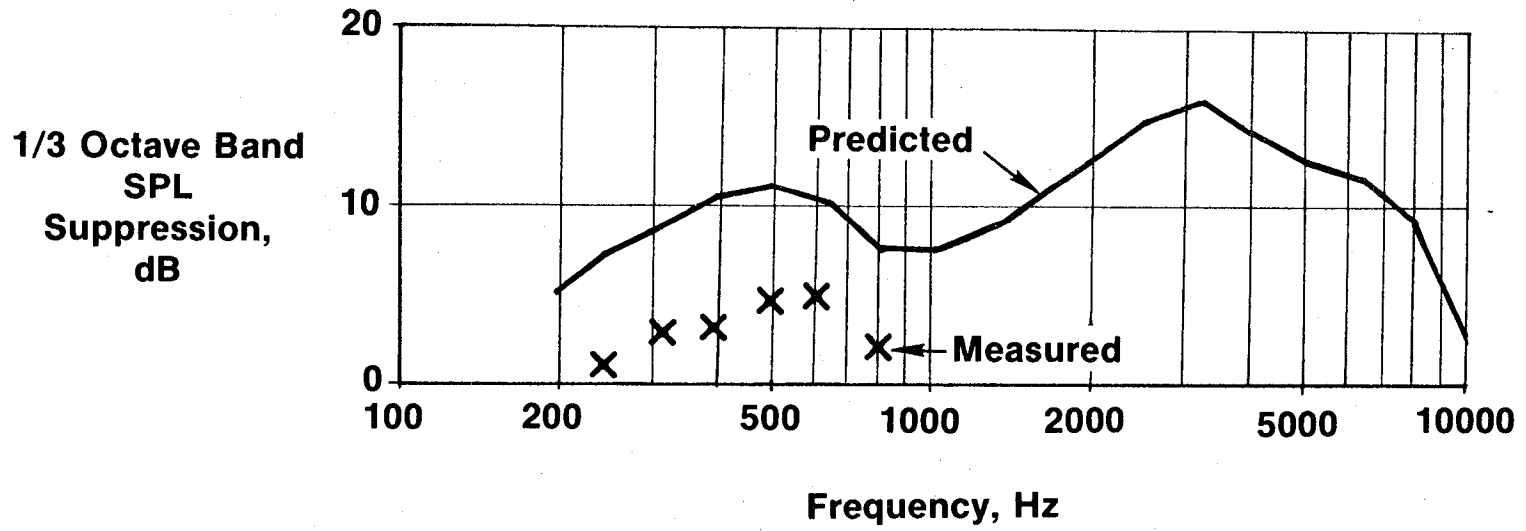
Figure 172. Core Suppression from Far-Field Measurements, Approach Thrust.

152m (500 ft) Sideline Fully Suppressed
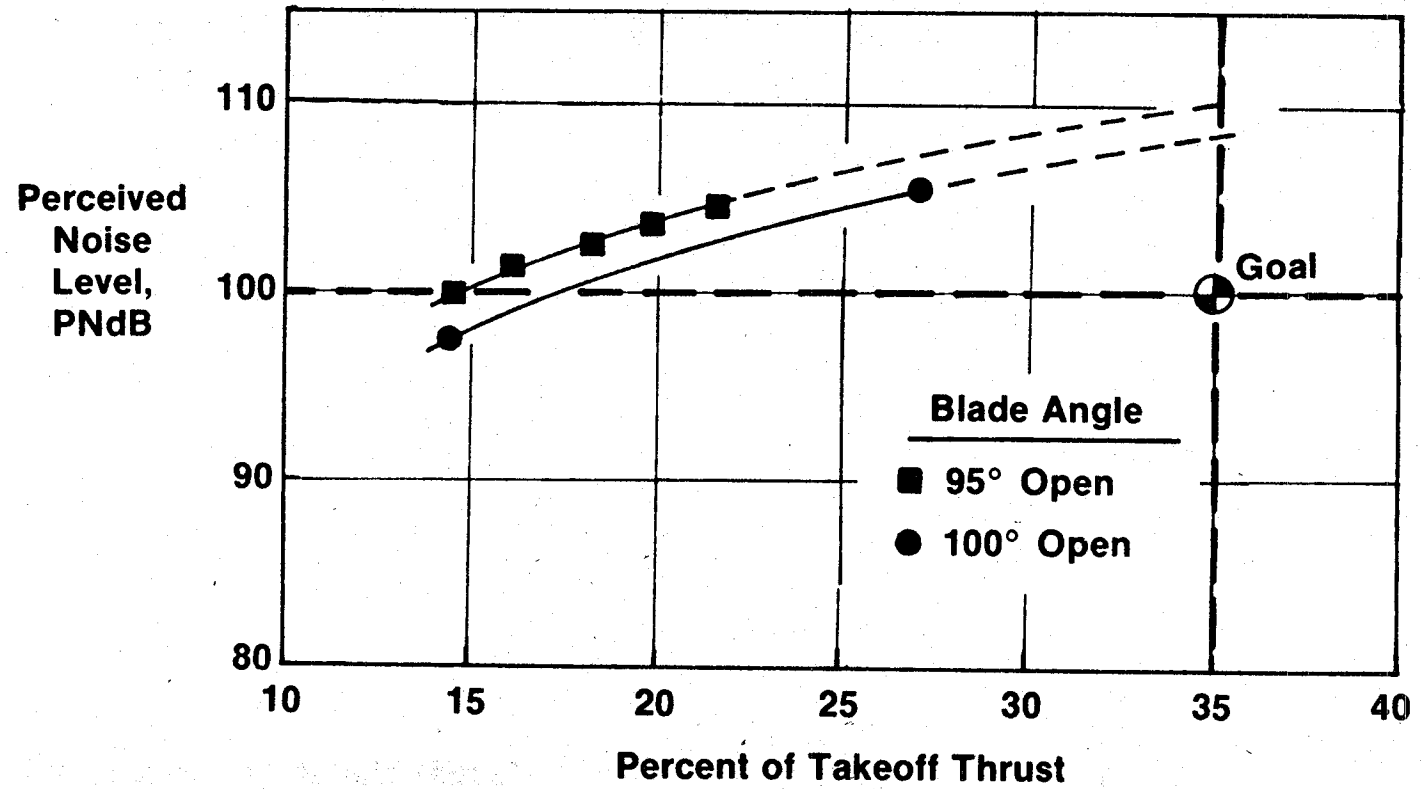
Figure 173. Variation of Peak PNL with Percent Reverse Thrust.

(500-ft) sideline noise is 106 PNdB. Although higher than the goal, this measured reverse-thrust engine-noise level is consistent with the scale-model fan data and collectively provides a good data base for future reverse-pitch-fan noise predictions.

The UTW engine noise summary in Table XXX shows that the aft-radiated engine noise is 9 PNdB higher than the calculated jet-flap component and makes a major contribution to the system EPNL at takeoff. The noise goal was exceeded by 2.2 EPNdB primarily as a result of the unexpected increase in aft fan-source noise. At approach the forward-radiated fan noise is slightly higher than expected due to low approach suppression, but the system noise misses the goal of 95 EPNdB by only 0.7 EPNdB.

4.5.3 OTW Results

The OTW engine was tested in an inverted mode (Figure 174) to permit the deployment of the thrust reverser. Acoustic testing was conducted with five configurations (Figure 175), starting with a baseline which was untreated except for treatment in the frame area and on the vanes. Three forward-thrust configurations were used to determine system-noise levels and to evaluate component suppression. The hybrid inlet was evaluated without treatment in order to determine the acceleration-suppression alone, and a more moderate suppression approach was evaluated by removing the aft fan duct splitter and the core suppressor. The reverse-thrust noise was measured with the fully suppressed nacelle.

The agreement of the measured inlet-radiated baseline levels with the predicted spectrum was excellent as seen in Figure 176. All the major features of the dominant fan-inlet noise are seen to be accurately predicted. The aft-radiated noise shown in Figure 177 was correctly predicted at blade-passing frequency, but SPL's at the second harmonic and above are substantially below predictions. The only factor that appears to explain this over-prediction at high frequency is a very effective suppression characteristic for the frame and vane treatment which was not separately evaluated during the program.

The hybrid inlet for the OTW engine, shown in Figure 178, was constructed with a bulk absorber material for the treated area. A Kevlar felt covered with a perforated plate was used. This very effective treatment was used to improve the approach suppression with the hybrid inlet; 13.5 PNdB suppression was anticipated at the takeoff power setting.

The takeoff suppression spectrum, shown in Figure 179, exceeded the goal slightly, reaching 14 PNdB at the maximum forward angle and suppressing the inlet noise down to the jet-noise floor up to 2500 Hz. Peak suppression at blade-passing frequency was almost 20 dB. The suppression was entirely due to the acceleration effect since the untreated inlet was identical to the treated. At approach, Figure 180, the inlet suppression with the bulk absorber is improved over that achieved with the resonator treatment, but the OTW inlet did not achieve the predicted suppression. The difficulty

256

Table XXX. UTW Composite Nacelle System Noise.

	Forward Quadrant		Aft Quadrant	
	Engine	Jet/Flap	Engine	Jet/Flap
Takeoff				
PNL	91.7	94.6	99.0	90.0
Quadrant Total PNL	97.0		99.9	
System EPNL	97.2			
Approach				
PNL	96.7	89.8	95.6	82.7
Quadrant Total PNL	97.9		96.0	
System EPNL	95.7			
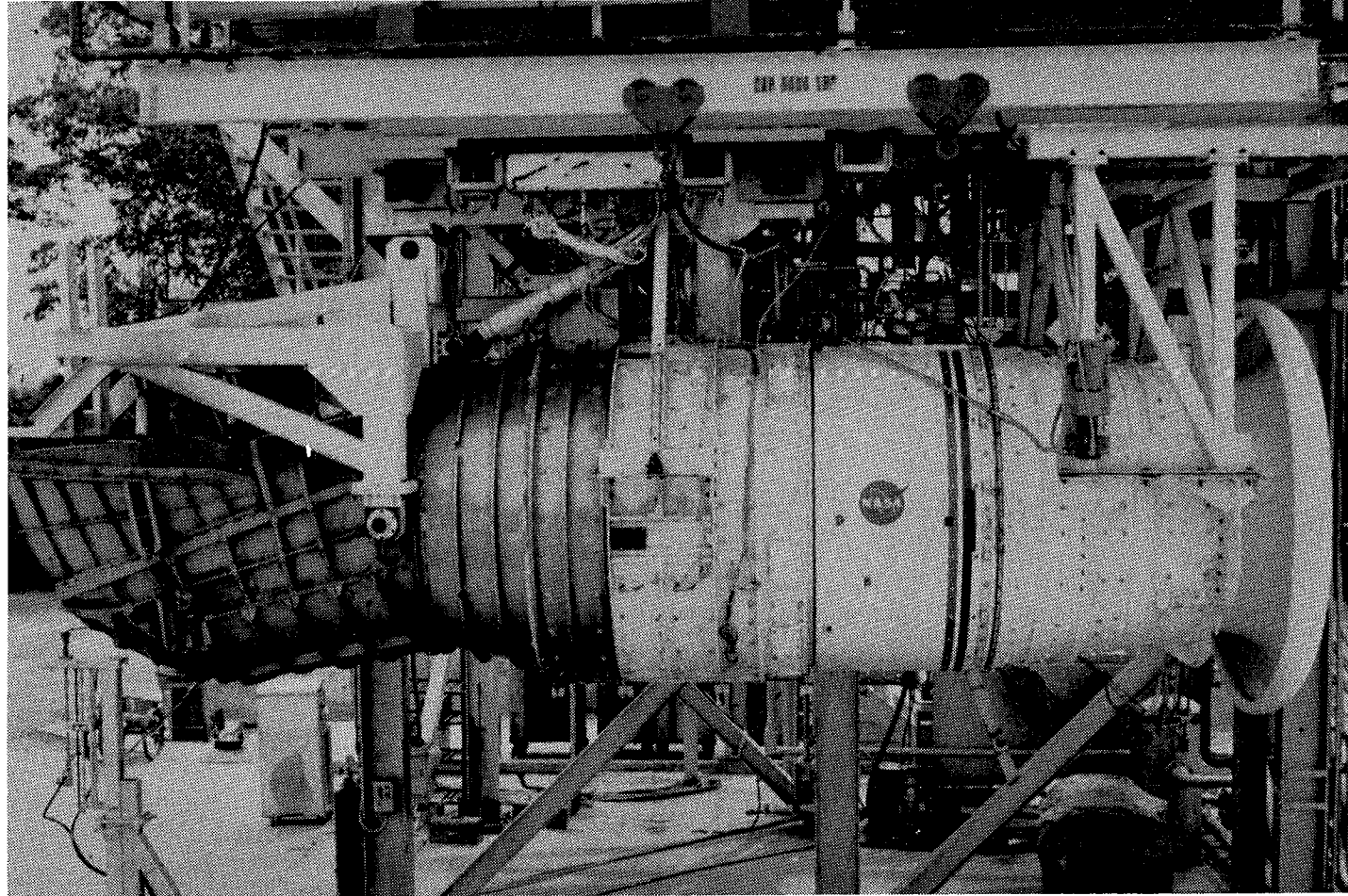
Figure 174. OTW QCSEE.
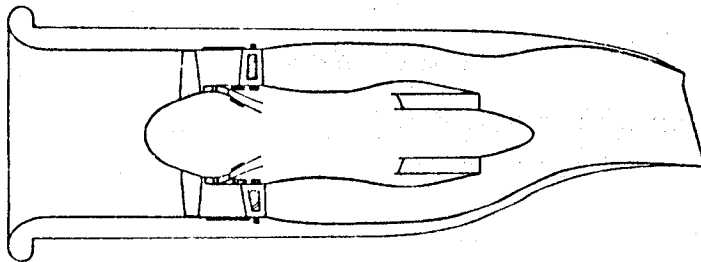
Baseline

   1. **Untreated Except for Frame and Vane Treatment**
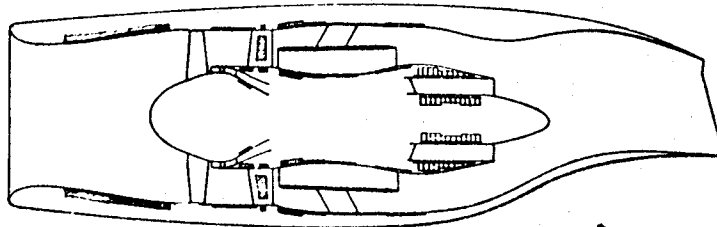
Suppressed Engine-Forward Thrust

   2. **Fully Suppressed**
   3. **Untreated High Mach Inlet**
   4. **Untreated Core and Splitter Removed**
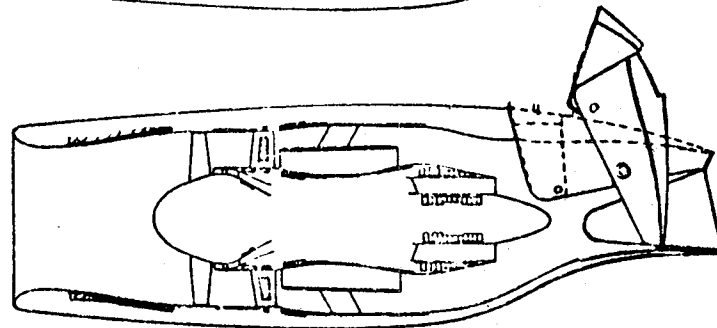
Suppressed Engine-Reverse Thrust

   5. **Fully Suppressed**

Figure 175.   OTW Acoustic Test Configurations.
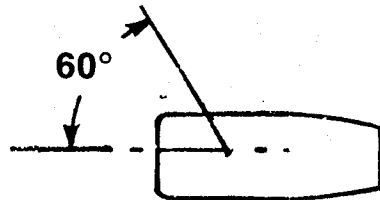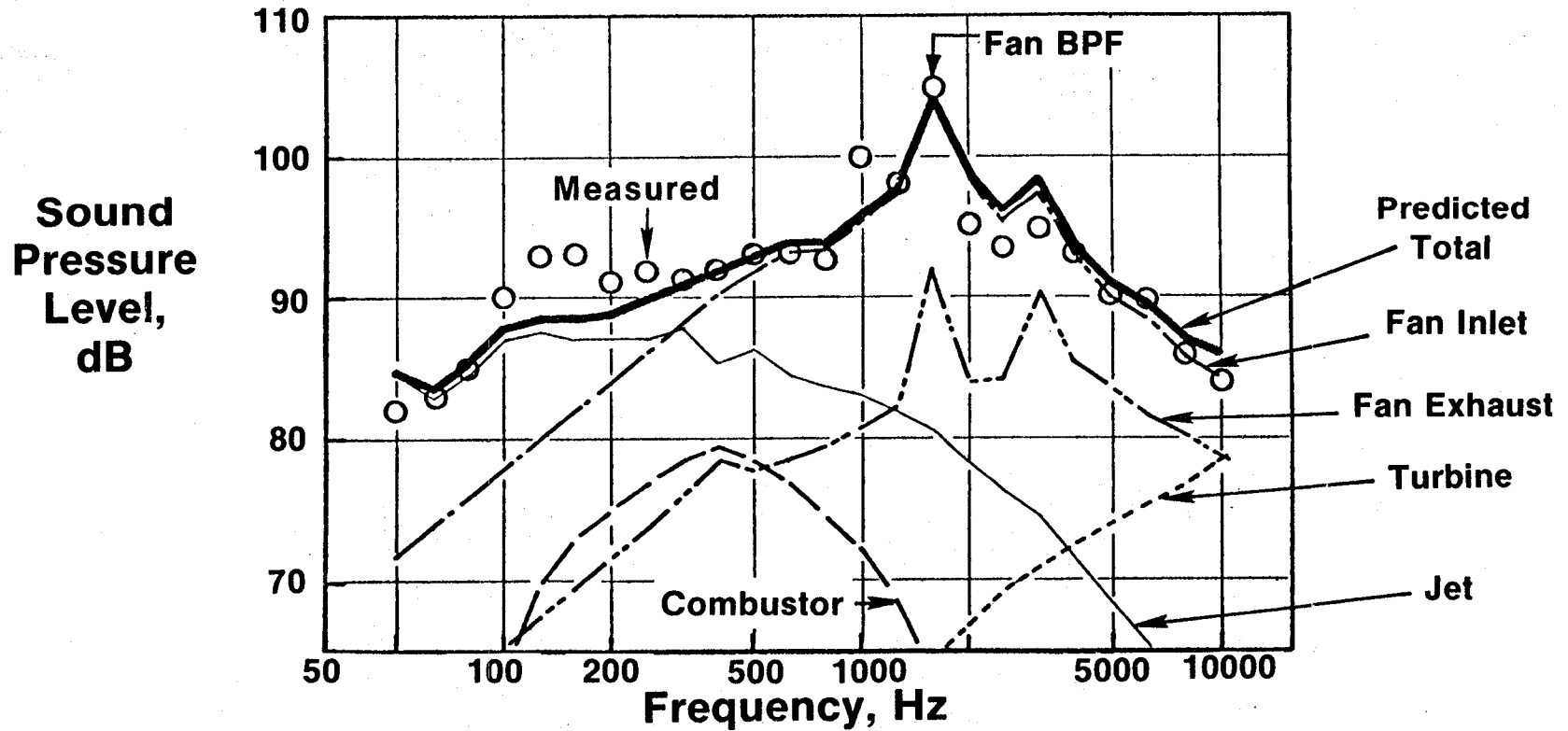
Figure 176. OTW Inlet-Radiated Baseline Noise.
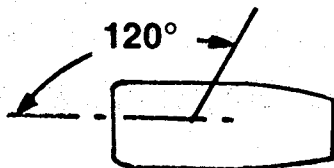
Figure 177. OTW Exhaust-Radiated Baseline Noise.

Throat

Bulk Absorber
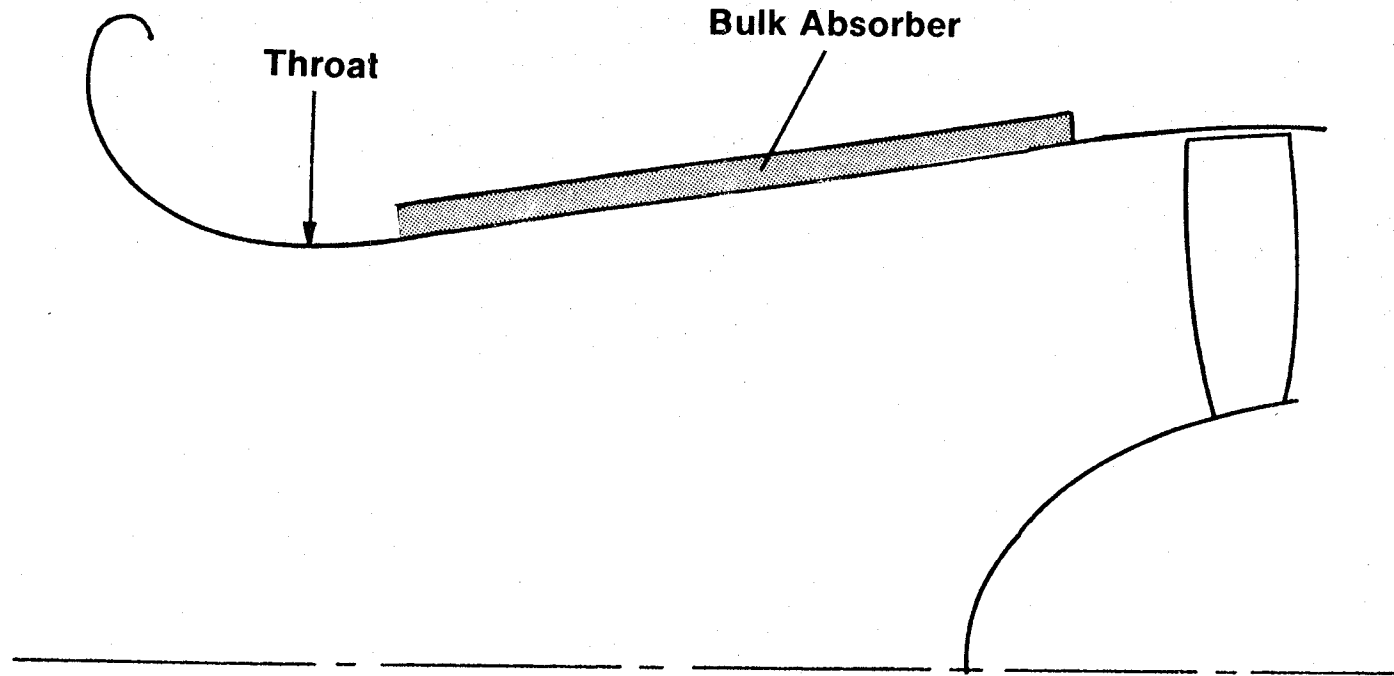
PNL Suppression Predicted

Takeoff   13.5 PNdB

Approach   10.4 PNdB

Figure 178. OTW Inlet Configuration.

Figure 179. OTW Inlet-Radiated Noise at Takeoff.

152m (500 ft) Sideline

○ Bellmouth
◇ Untreated High Mach Inlet
□ Treated High Mach Inlet

60°
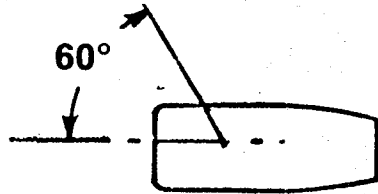
Sound
Pressure
Level,
dB

PNL Suppression	
Predicted	Measured
10.4	7.5

Estimated Jet

Frequency, Hz
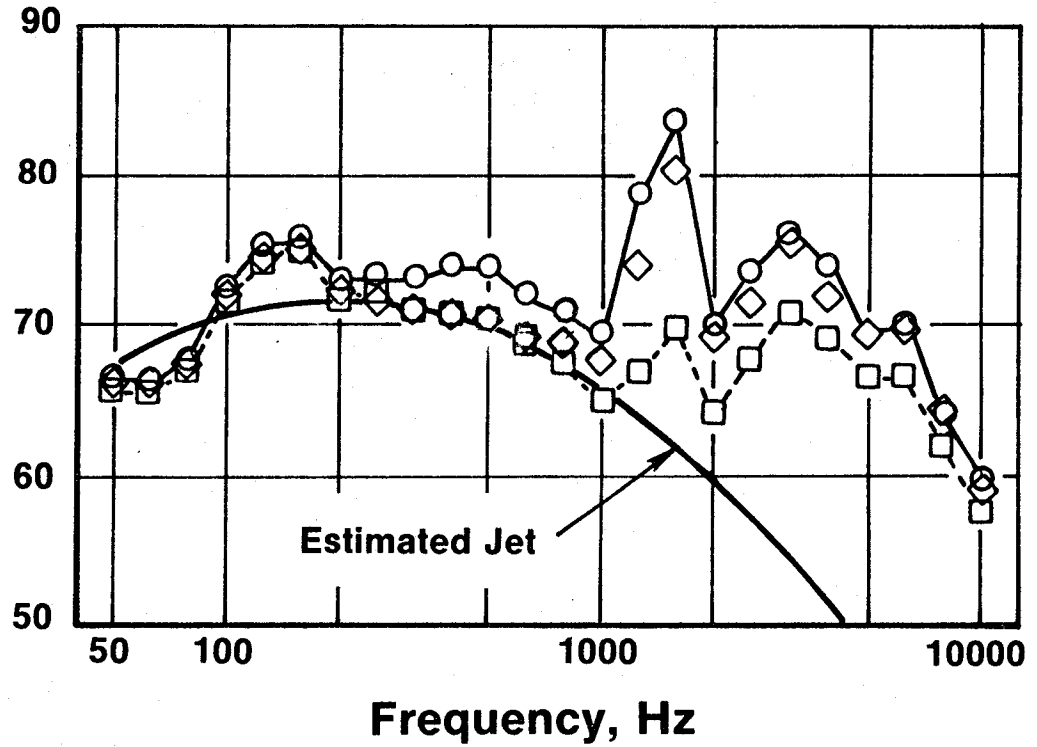
Figure 180.   OTW Inlet-Radiated Noise at Approach.

in this design is not the performance of the bulk absorber as a treatment but that the requirement for a high-porosity, perforated face sheet in the presence of high subsonic wall Mach numbers tends to generate high-frequency broadband noise that reduces the effective suppression bandwidth. In spite of this, 7.5 PNdB of inlet suppression with only wall treatment is good suppression performance.

The measured system exhaust suppression is shown in Figure 181 by comparing the baseline and the fully suppressed configurations. The suppressed spectrum, which will be shown later, is controlled by jet noise - making the measurement of aft suppression very difficult. Less than 5 PNdB of system suppression is shown here, and it increases to only 6 PNdB when the calculated jet noise is removed. The four shaded symbols are reduced by removing the calculated jet noise. In Figure 182 the plot of the suppressed and unsuppressed spectra shows two reasons for the low measured suppression. First, the second-harmonic source level being lower than predicted leaves very little tone suppression available. Second, the suppression above 2500 Hz is effectively zero, and this is the apparent result of a "floor-noise source" which prevents the suppression from being detected in the far-field measurements. This floor source is apparently boundary-layer noise generated in the exhaust duct and common nozzle from the high-velocity airflow over perforated surfaces. Although the wall Mach numbers were kept as low as possible, the calculated levels from flow noise are very close to the measured spectrum levels above 2500 Hz. The lack of high-frequency suppression is evident in Figure 183, a comparison of the measured and predicted suppression spectra at takeoff. The "missing second harmonic" in the source spectra produces the discrepancy at 3150 Hz.

The OTW reverse-thrust test was conducted with the exhaust deflected downward and forward, with impingement on the concrete pad, as shown in Figure 184. Scale-model testing prior to the engine test indicated that the flow-over-the-ground-plane source would not be a major factor in the engine reverse-thrust noise measurements. Of greater importance were parameters such as lip angle, lip length, and distance of blocker from nozzle exit plane. The full-scale engine design incorporated these scale-model results to the fullest extent possible consistent with thrust-reverser performance and mechanical design. But it was expected, based on the scale-model program, that the engine levels would exceed the noise goal by about 6 PNdB. This prediction was confirmed by the engine data shown in Figure 185. Based on the scale-model tests, lower noise levels could have been achieved with larger nozzle-to-blocker spacing and increased reverser lip length, but these "noise improvements" could not be incorporated in the current engine design because of mechanical-design requirements for deployment and stowage.

In summary, the calculated system levels shown in Table XXXI for the OTW were within 2.2 EPNdB of meeting the system noise goal at takeoff and were lower by 0.4 EPNdB than the noise goal at approach.
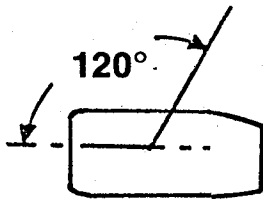
- **152m (500 ft) Sideline**
- **Flagged Symbols Corrected for Jet Noise**

○ **Baseline**
□ **Fully Suppressed**

120°

Perceived Noise Level, PNdB

Baseline

Fully Suppressed

Percent Corrected Fan Speed
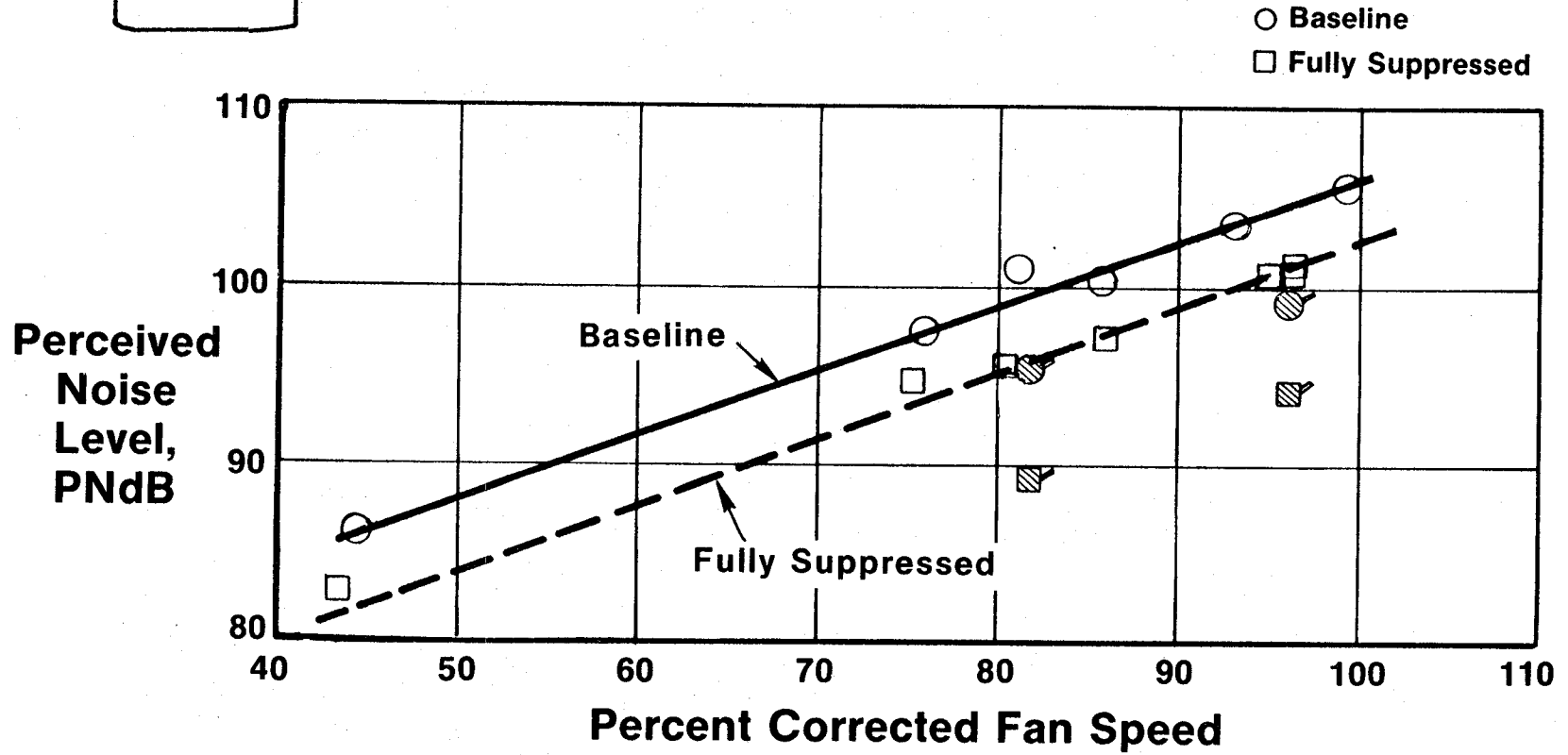
Figure 181. Measured Exhaust PNL.
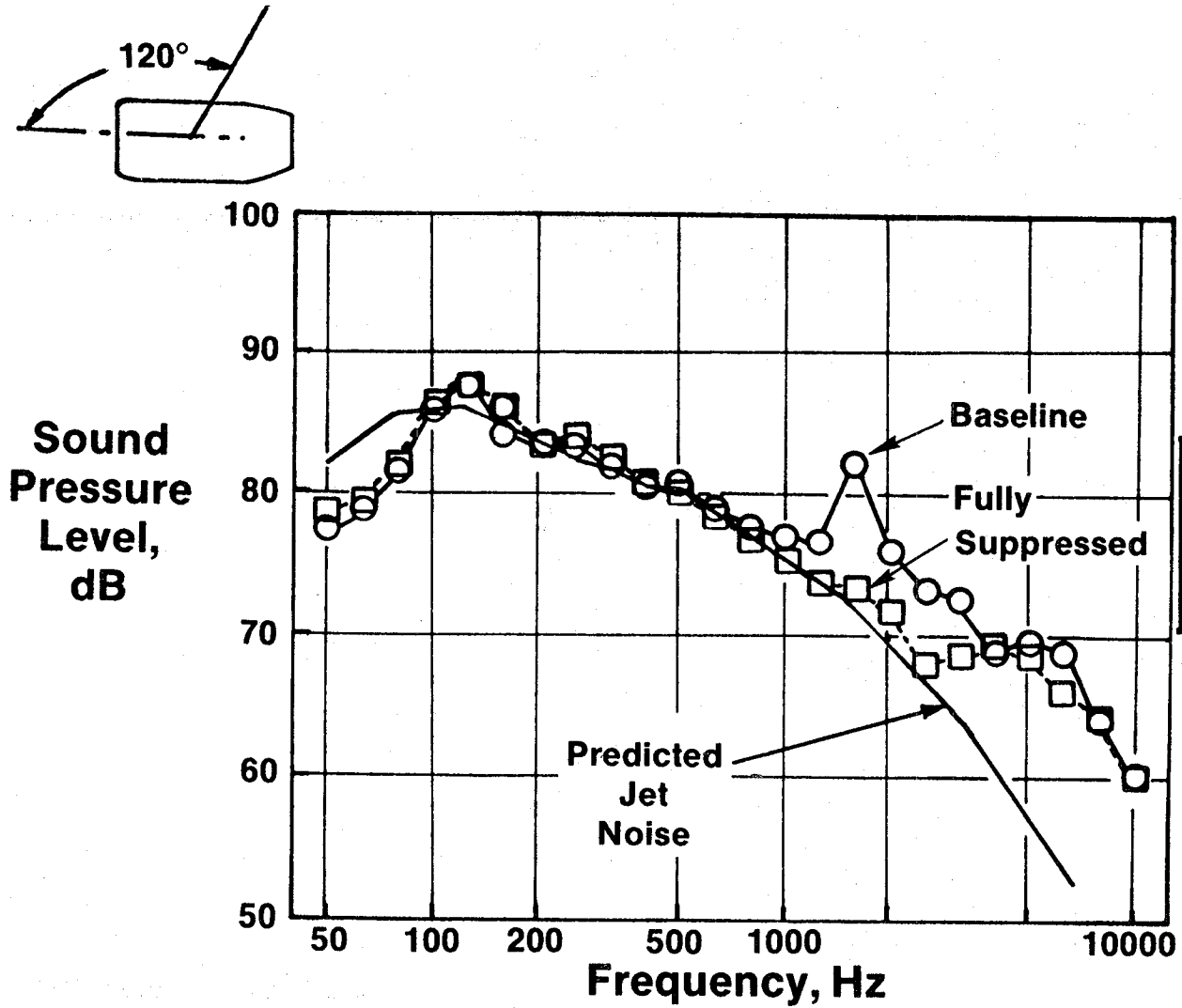
Figure 182. OTW Exhaust-Radiated Noise at Takeoff.
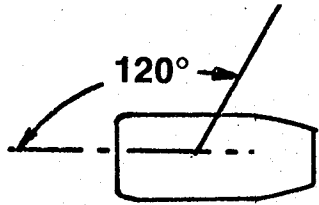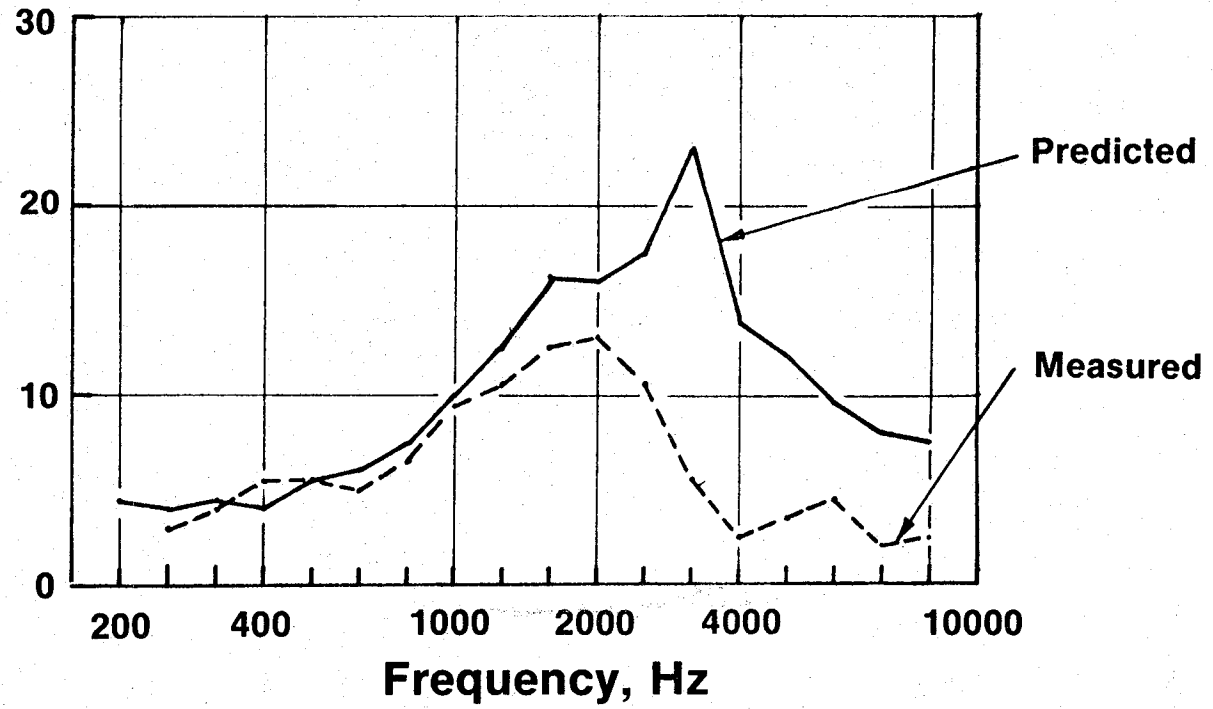
Figure 183. OTW Exhaust Suppression at Takeoff.
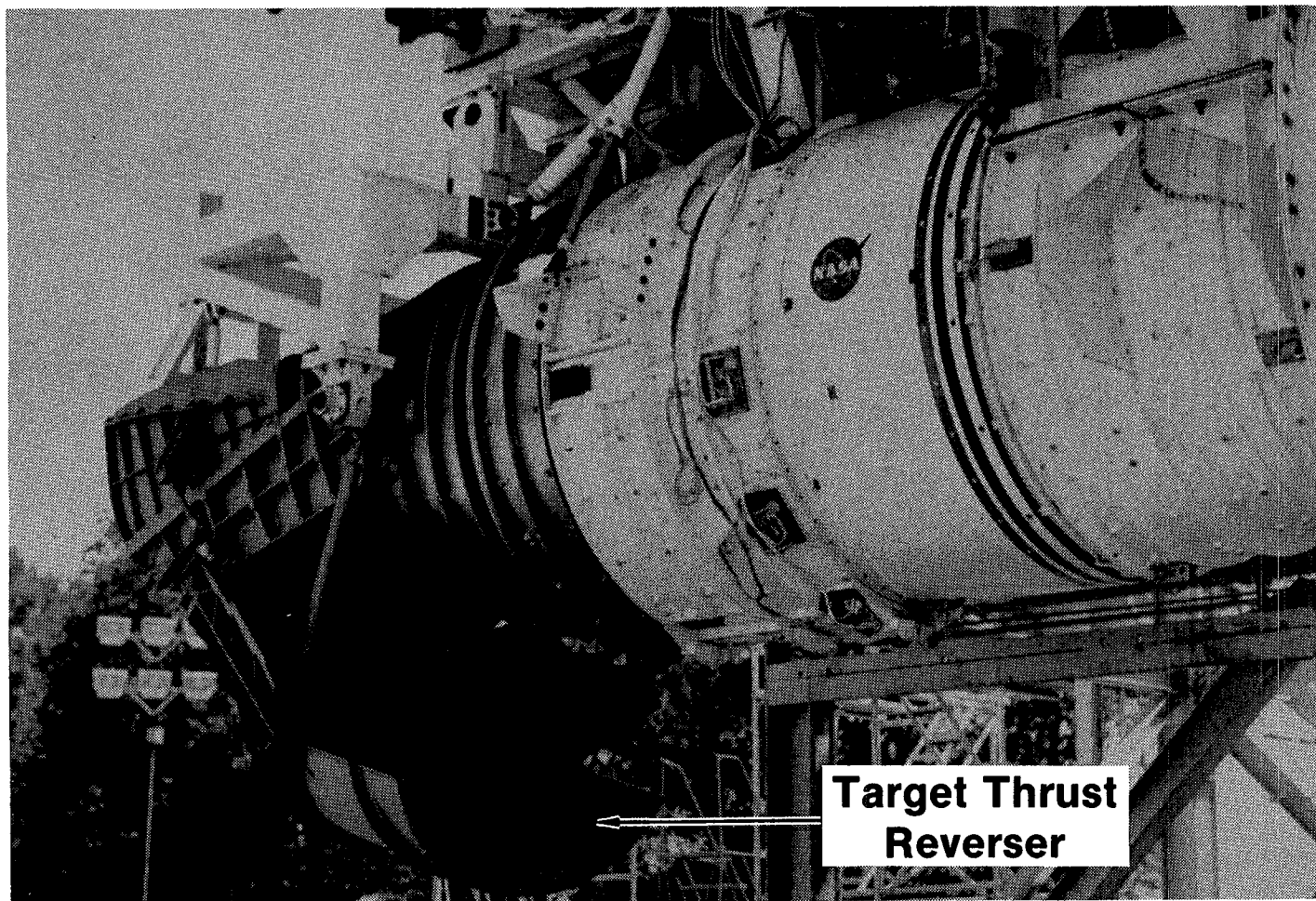
Target Thrust Reverser

Figure 184.   OTW QCSEE with Thrust Reverser Deployed.

152m (500 ft) Sideline
Fully Suppressed
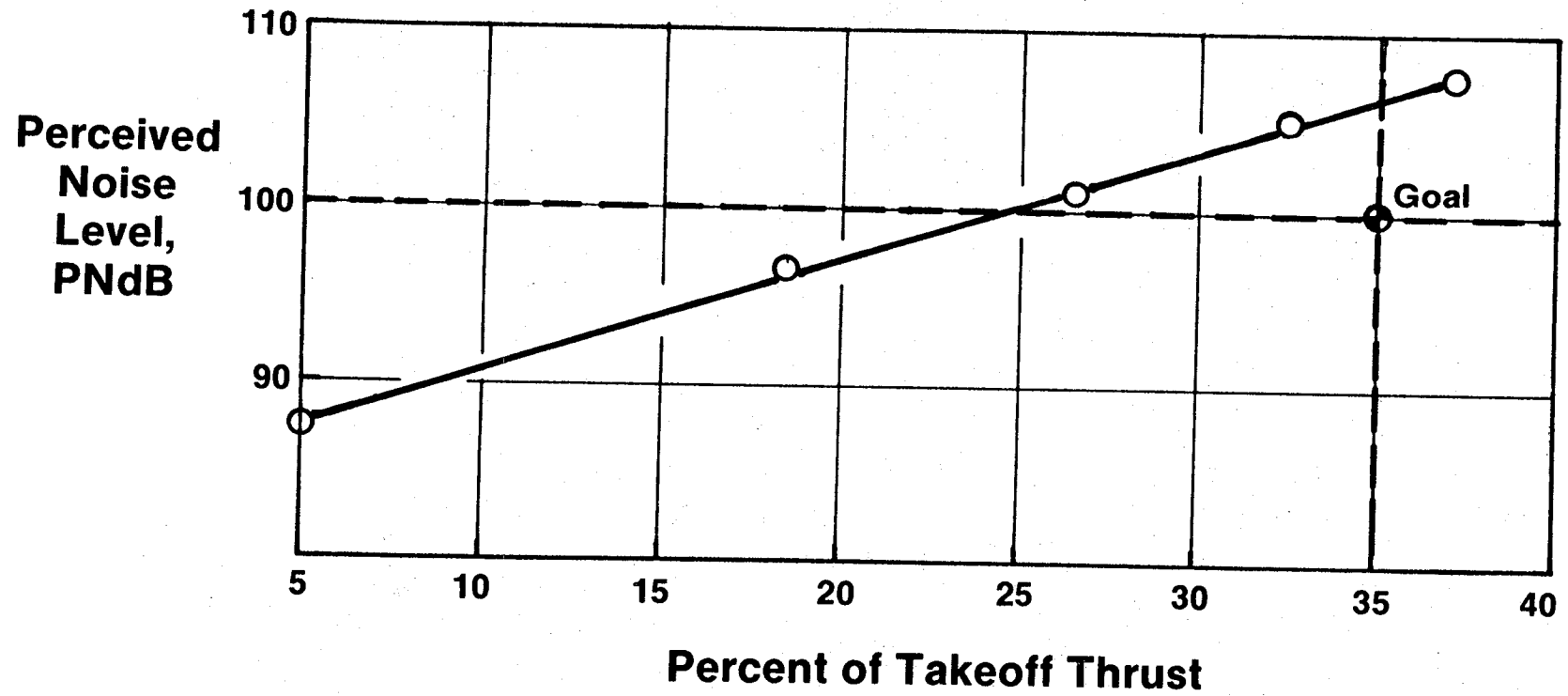
Figure 185. OTW Reverse-Thrust System Noise.

Table XXXI. OTW Boilerplate Nacelle System Noise.

	Forward Quadrant		Aft Quadrant	
	Engine	Jet/Flap	Engine	Jet/Flap
Takeoff				
PNL	94.8	95.8	96.8	93.2
Quadrant Total PNL	99.0		99.1	
System EPNL		97.2		
Approach				
PNL	95.4	89.9	90.8	87.2
Quadrant Total PNL	97.1		93.1	
System EPNL		94.6		

4.5.4 Summary

Using the measured engine-noise levels from the program and calculated flap noise, contours have been calculated both for UTW- and for OTW-powered aircraft. The takeoff and approach flight paths are shown in Figure 186 for a 66,700-kg (147,000-lb) TOGW aircraft, along with 90, 95, and 100 EPNdB contours. To provide some perspective of how small these noise contours are, the 95 EPNdB contour areas are listed in Table XXXII and compared to similar areas of two typical narrowbody jets and a widebody aircraft. The contour area for the widebody is one-fouth to one-tenth of the narrowbody contour while the QCSEE-powered aircraft give another step reduction of one-tenth, producing 95 EPNdB contours of less than 1.295 km^2 (1/2 mi^2).

In summary, the noise goals for the QCSEE progam were very challenging, representing a noise-reduction-technology step of about 10 EPNdB. Although many of the low-noise characteristics of the engines resulted from the basic cycle design, several unique noise-reduction concepts have been demonstrated which are applicable to many engines, and these represent an improvement in low-noise technology. The most difficult aspect of the QCSEE noise goal was to achieve simultaneous success with the prediction and suppression of several major noise-source components. Simultaneous success was necessary since all of these sources were contributors to the suppressed-engine perceived noise levels; therefore, missing even one of the component levels jeopardized achievement of the noise goals. As a result of this aspect of the program, the following list of accomplishments can be placed in perspective.

- Takeoff and approach system levels for both engines were within 2 EPNdB of the 152-m (500-ft) sideline goal of 95 EPNdB.

- The baseline system noise measurements met or were lower than the predictions on the OTW engine. Baseline levels on the UTW engine were higher than anticipated, but the program has provided a large data base for understanding and predicting variable-pitch-fan noise.

- The hybrid inlet was successful at takeoff power settings, achieving 14 to 15 PNdB suppression at the maximum forward angle. This represents three times the suppression achieved in the past without the use of splitters or variable inlet geometry. Up to 7.5 PNdB suppression was measured at approach power; this is an improvement over previous designs.

- Aft fan suppression of 2 dB was demonstrated for treated vanes. This is a significant suppression for a very modest amount of treated area.

- Aft fan-duct suppression was as predicted where flanking noise-transmission paths and/or "floor noise sources" didn't prevent accurate measurement.

272
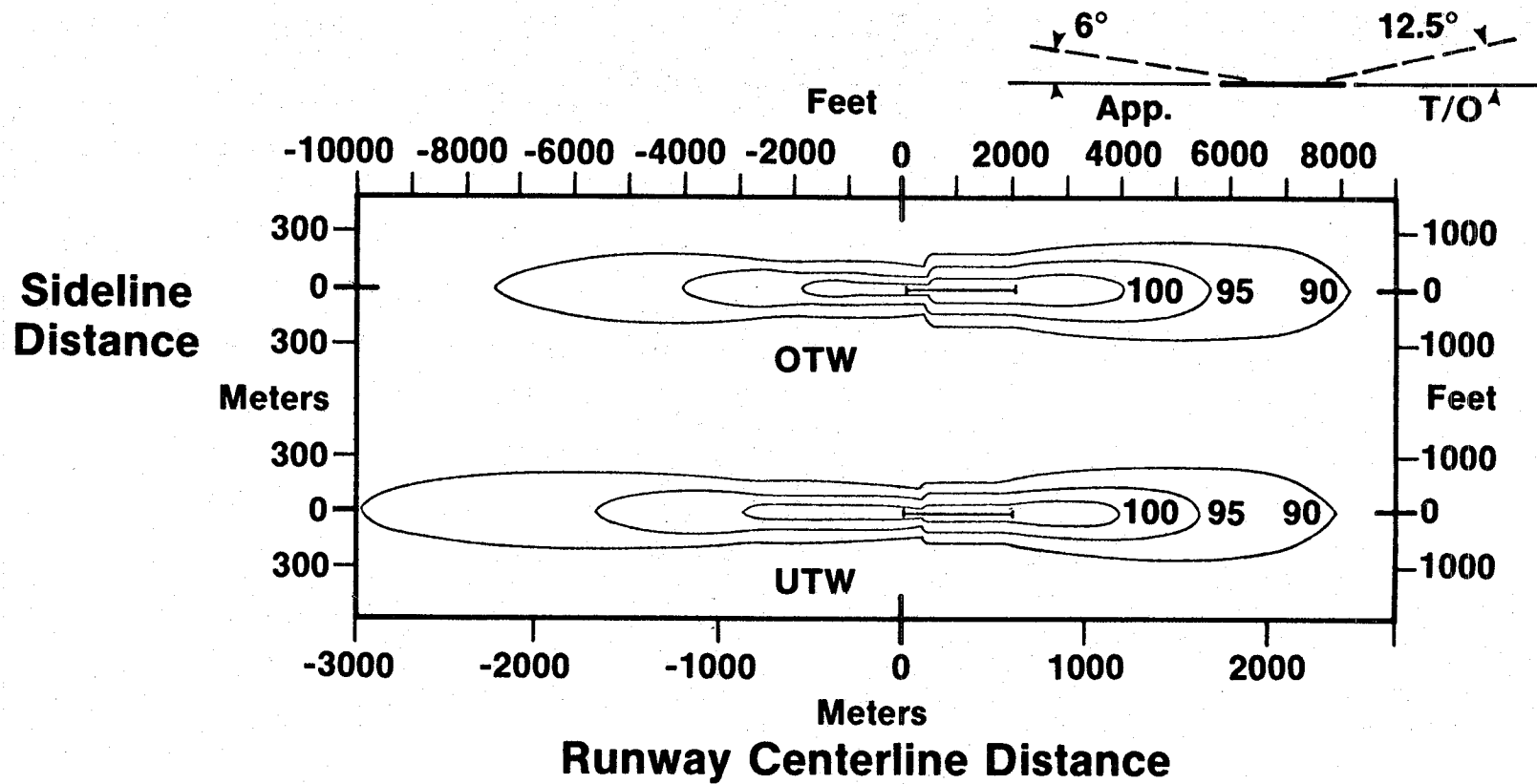
Figure 186. QCSEE Approach and Takeoff EPNdB Contours.

Table XXXII. Comparison of Footprint Areas: QCSEE to Typical
Current Aircraft.

Aircraft	TOGW		95 EPNL Contour Area	
	kg	(lb)	Sq km	Sq mi
707 (Jet)	146,000	(322,000)	66.5	25.66
DC-9 (Fanjet)	44,500	(98,000)	31.8	12.25
DC-10-30 (Fanjet)	252,000	(555,000)	9.4	3.57
QCSEE — UTW	66,700	(147,000)	1.0	0.38
QCSEE — OTW	66,700	(147,000)	0.8	0.32

- The suppression of the unique core-nozzle suppressor, designed to attenuate both high-frequency turbine noise and low-frequency combustor noise, was not completely measured due to the masking effects of jet noise and duct-flow noise.

- The reverse-thrust noise produced by both the UTW reverse-pitch fan and the OTW reverser was higher than predicted, but again the data available from engine and scale-model programs provide the basis for more accurate prediction models.

Finally, from the acoustic technology standpoint, in almost every case where component acoustic objectives were not completely met the data and understanding of the limiting problems are available and will ensure the improvement of similar designs in the future.

4.6 MEASURED PROPULSION SYSTEM WEIGHT

The weight of each of the advanced components was measured during assembly of the engines. However, the UTW and OTW experimental engines contained a number of differences, from ultimate flight configurations, that affected system weight. These included the following items.

In the interest of reducing program cost, a number of material substitutions and fabrication shortcuts were made in the experimental hardware. An example is the use of titanium blades in place of composites in the OTW fan.

Boilerplate nacelle components were built to allow the use of interchangeable acoustic treatment and hard-wall panels. The nacelle hardware was designed for use on both engines, with some compromise in flowpath and length for the OTW engine.

Both engines were heavily instrumented for experimental testing. A photograph of the UTW engine nearing completion of assembly is shown in Figure 187. The weight of wires, tubes, connectors, rake mounting pads, and slip-ring supporting structure totaled several hundred pounds in each engine.

Finally, the engines were designed to meet noise objectives with a 610-m (2000-ft) runway. As a result of the airline operational scenario and the aircraft company design studies, it was determined that a 915-m (3000-ft) runway would be a better compromise between aircraft economics and ability to operate from small airports. This would be reflected in a reduced takeoff power setting for the flight engines, reducing noise and allowing the acoustic splitter and core exhaust nozzle treatment to be eliminated with significant weight savings.

Because of these differences between the experimental and flight-engine configurations, it was necessary to modify the actual hardware weight results to reflect the equivalent weight of flight engines.
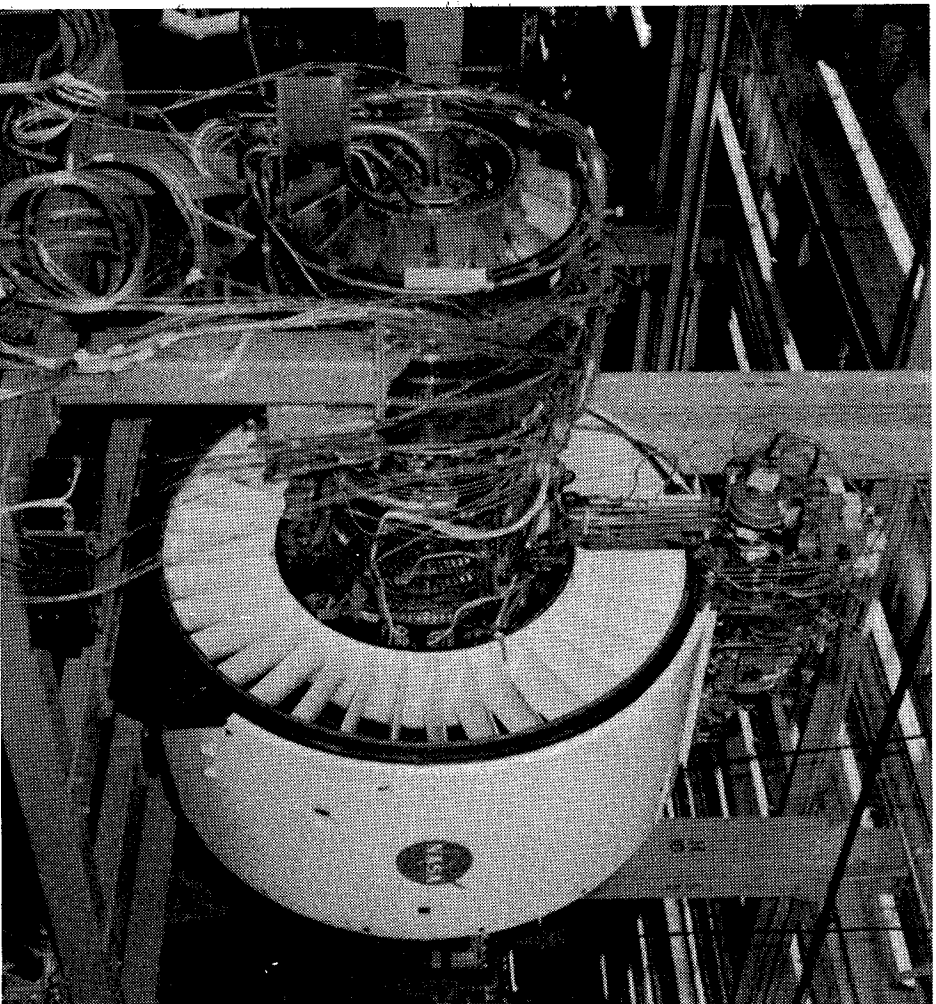
Figure 187. UTW Engine Assembly.

4.6.1 UTW System

Table XXXIII shows the weight breakdown of the UTW experimental engine and the projected weight of a UTW flight configuration. Some of the significant differences are as follows:

The F101 core was designed for a supersonic flight envelope and provided excess inlet-temperature capability. The use of more titanium in the compressor and freedom to redesign the turbine frame would save weight as shown.

The fan rotor utilized a steel shaft, and the reduction gear a steel star carrier, for cost saving. Substitution of titanium would save weight.

The composite fan frame included many shortcuts in fabrication technique, material thicknesses, potting and sealing compounds, additional instrumentation, and service lines. A detailed analysis of the measured frame weight showed that a substantial weight saving from the experimental hardware is possible, even after adding a metal sump liner to the flight frame.

Differences in the smaller components are primarily a result of using special-purpose parts in place of off-the-shelf components.

Total projected weight of the flight engine is 1436 kg (3166 lb) compared to the actual 1693 kg (3732 lb) weight of the experimental engine.

Table XXXIV shows a similar comparison of the nacelle components. The major differences here are results of eliminating the acoustic splitter and core nozzle treatment. In addition a number of metal inserts for instrumentation rakes and struts could be eliminated. The core cowl could be made in two pieces instead of four if a larger autoclave were available. The equivalent flight weight of the composite nacelle is 466 kg (1028 lb) which, added to the engine weight, results in a total propulsion system weight of 1902 kg (4194 lb).

4.6.2 OTW System

Table XXXV shows the OTW engine weight breakdown. Differences between the experimental and flight-weight numbers are much like those of the UTW engine with one major exception: the titanium fan blades and resulting heavier disk are reflected in a much greater saving in fan-rotor weight in the flight configuration.

The OTW nacelle weight is shown on Table XXXVI for the flight engine since only boilerplate components were built for this engine. The projected flight propulsion system weight is 1980 kg (4364 lb).

Table XXXIII. UTW Engine Weight.

	Experimental		Flight	
	(kg)	(lb)	(kg)	(lb)
Modified F101 Core & LPT Turbine	663	1461	622	1372
Fan Rotor	217	478	192	423
Reduction Gear	93	204	86	190
Composite Fan Frame	318	702	215	474
Brgs., Drives & Lube Components	275	607	201	444
Fuel System	32	70	20	45
Electrical System	26	58	15	33
VP Mechanism (Ball Spline)	69	152	62	137
Piping, Wiring and Misc.	36	80	22	48
Total Engine	1693	3732	1436	3166

Table XXXIV. UTW Nacelle Weight.

	Experimental		Flight	
	(kg)	(lb)	(kg)	(lb)
Composite Inlet	242	533	150	330
Composite Fan Duct	125	275	91	201
Composite Flare Nozzle	41	90	30	67
Composite Core Cowl	69	153	41	91
Core Exhaust Nozzle	93	206	64	142
Lube & Hydraulic System	161	354	78	172
Instrumentation (Approximately)	227	500	11	25
Total Nacelle	958	2111	466	1028
Engine			1436	3166
Propulsion System			1902	4194

Table XXXV. OTW Engine Weight.

	Experimental (kg)	(lb)	Flight (kg)	(lb)
Modified F101 Core & LP Turbine	663	1461	622	1372
Fan Rotor	364	802	173	382
Reduction Gear	90	198	83	184
Composite Fan Frame	312	687	208	459
Brgs., Drives & Lube Components	275	607	189	417
Fuel System	34	74	20	44
Electrical System	26	58	15	33
Piping, Wiring and Misc.	36	80	20	43
Total Engine	1799	3967	1331	2934

Table XXXVI. OTW Nacelle Weight.

	Experimental	Flight (kg)	(lb)
Composite Inlet		150	330
Composite Fan Duct		117	259
Composite Core Cowl	Boilerplate	40	88
Core Exhaust Nozzle		38	84
Aft Nacelle		113	250
"D" Nozzle/Thrust Reverser		121	266
Lube & Hydraulic System		64	140
Instrumentation		6	13
Total Nacelle		649	1430
Engine		1331	2934
Propulsion System		1980	4364

4.7 THRUST-TO-WEIGHT RATIO ASSESSMENT

Thrust-to-weight ratio was evaluated on both an uninstalled and an installed basis. Table XXXVII shows both goal and projected values. The goals were set on the basis of conceptual design studies at the outset of the program. The projected numbers have been adjusted to take into account the results of actual design and testing experience. This experience has caused a small reduction in our expectations, but the absolute levels are still relatively high, and the reductions are within the scatter range of such predictions.

To place these installed values in their proper context, the experimental engine cycles were selected for acoustic and other considerations rather than to optimize weight. Large, high-bypass engines generally suffer heavy installation penalties. These penalties have been largely offset by the lightweight integrated QCSEE nacelle components, with the result that both propulsion systems exhibit attractive installed thrust-to-weight characteristics that are comparable with the best current CTOL propulsion systems.

Table XXXVII. Thrust-to-Weight Assessment.

	UTW		OTW	
	N/kg	lb/lb	N/kg	lb/lb
Uninstalled				
• **Goal**	60.8	(6.2)	72.6	(7.4)
• **Projected**	56.7	(5.78)	70.2	(7.16)
Installed				
• **Goal**	42.2	(4.3)	46.1	(4.7)
• **Projected**	40.7	(4.15)	45.6	(4.65)

282

5.0 CONCLUSIONS

A number of significant conclusions can be drawn from the results of the QCSEE design and development effort. Some of these conclusions apply only to short-haul engines, but many are of a general nature applicable to other types of advanced propulsion systems.

5.1 ENGINE PERFORMANCE

Since both engines met the forward-performance goals, there should be no reluctance to apply very high bypass cycles in cases where the aircraft thrust requirements can be matched. Since these cycles have very low fan pressure ratio and high thrust lapse, they are most applicable to powered-lift aircraft.

Because of the use of the F101 core engine without boost stages, both engines exhibited low cycle pressure ratios. As a result, cruise sfc was not as attractive as it could be if an advanced-design, higher-pressure-ratio core were used. Therefore, particularly in view of the current energy situation and rising fuel cost, product versions of the engines should incorporate higher-pressure-ratio cores.

Although the UTW engine failed to meet the 35% reverse-thrust goal, it did produce 27% reverse thrust; this might be sufficient to stop an aircraft on a 915-m (3000-ft) runway. Furthermore, additional development testing could result in higher levels of reverse thrust. It may be concluded that the variable-pitch fan concept can be developed to provide effective thrust reversal.

While the OTW engine exceeded the 35% reverse-thrust goal, it did so with higher than expected pressure losses. Reverse-thrust noise could be reduced by redesigning the aft nacelle flowpath.

5.2 FAN PERFORMANCE

The OTW and UTW fans both performed satisfactorily during sea level static engine tests, and most of the fan aeroperformance goals established for the experimental engine programs were met. Some futher development of the UTW fan is required to meet altitude-cruise performance goals, and the reduced pumping of this fan during engine reverse-mode tests needs to be understood and improved. Important advances in fan aerodynamic technology were demonstrated during the QCSEE program, and these advanced fan features can be used with confidence in future turbofan engines for short-haul aircraft.

5.3 COMPOSITE FAN BLADES

It was concluded that some form of lightweight blade must be developed to make variable-pitch fans practical. Because of lack of FOD resistance during bird ingestion, the QCSEE composite blade is acceptable only for experimental ground test. Subsequent developments of other programs have identified candidate materials that could possibly solve this problem; however, none of this work has been completed to date. Some of these material candidates are:

- Stitched or multidirectional-weave polymerics

- Superhybrid

- Boron aluminum

- Hollow titanium

5.4 VARIABLE-PITCH SYSTEMS

Both variable-pitch systems, the harmonic drive and the ball spline, demonstrated concept feasibility during whirl-rig and engine testing. Either system could be developed for operational use.

Actual blade-turning moments exceeded the anticipated (calculated) values; therefore, either system must be sized for somewhat higher torque capacity than originally specified.

5.5 MAIN REDUCTION GEAR

The QCSEE main reduction gear transmitted up to 12.7 MW (17,000 hp) for many hours without incident - a significant accomplishment for a lightweight gear system.

Total time on the UTW gear is approximately 202 hours: test rig, 49 hours; engine, 153 hours.

Total time on the OTW gear is approximately 135 hours: test rig, 36 hours; engine (GE), 58 hours; engine (NASA), 41 hours.

Although this is hardly sufficient operating experience on which to ensure the achievement of the 36,000 hours life and 6,000 hours time before overhaul (TBO) objectives, the feasibility of a geared fan drive has been satisfactorily demonstrated; with the benefit of further development effort, acceptable reduction-gear performance and life for operational engines can be expected.

5.6 COMPOSITE FRAME

Based on the information generated by the QCSEE program, the following conclusions have been reached concerning the use of graphite/epoxy for engine frames.

- Composite construction shows promise for application to major frames. It has been shown that these frames can take advantage of the unique characteristics of composites.

- The static tests of the frame verified the analysis, and engine tests were in reasonable agreement.

- As the frame was actually built, it was difficult to fabricate. The need for better part tooling and better assembly tooling was apparent. In the future it should be more efficient to use fewer individual pieces by more piece integration in the as-molded condition.

- The sump area was difficult to seal against oil leakage. The use of a metal sump liner would help.

5.7 COMPOSITE NACELLE

The following conclusions have been reached concerning the use of advanced composite materials in engine nacelle hardware.

- The program demonstrated the ability to design stiff, light, thin, nacelle structures utilizing composite materials.

- Basic, low-temperature, nacelle structures can be easily fabricated using state-of-the-art techniques.

- The PMR/graphite inner cowl provided a successful demonstration of a new, high-temperature, composite system.

5.8 DIGITAL CONTROL

During the NASA/GE QCSEE program, two engine-mounted digital controls were designed, fabricated, and tested on the two experimental engines. Throughout the engine-test program, approximately 200 hours of operation, the digital controls scheduled the engine variables and maintained engine operation within all safety limits. Several experiments were performed during the engine-test program to evaluate the control system capability with respect to control-system requirement. Nearly all requirements were met satisfactorily. Table XXXVIII compares primary control system requirements with engine-test

results. As a result of this successful development program, the digital control technology base has been expanded and will hasten the application of digital controls on future propulsion systems.

5.9 LOW-EMISSION COMBUSTOR

The double-annular combustor was successfully developed to meet the EPA 1979 emissions standards for class T2 engines within the very limited space available in the F101 combustor envelope. The principles used are directly applicable to other engines and should be considered depending upon the specific emissions requirements.

5.10 ACOUSTICS

Although the 95 EPNdB sideline-noise goal was not reached by either engine, both demonstrated within about 2 dB of the goal. This is considered to be an outstanding accomplishment in light of the severity of the goal. Both engines demonstrated 95 EPNdB contour areas of less than 1.295 km^2 (1/2 mi^2). This would confine the noise nuisance to the airport proper and alleviate the community noise problems.

Some of the noise-reduction features (such as the low-tip-speed, low-pressure-ratio fans) are most applicable to short-haul engines. However, if community noise becomes a sufficiently powerful driver, these features could be used in CTOL aircraft by oversizing the engines and accepting a weight penalty.

5.11 WEIGHT

The projected thrust-to-weight ratio of UTW and OTW flight engines are comparable on an installed basis with the best current CTOL propulsion systems. Therefore, it can be concluded that it is feasible to produce economically competitive, powered-lift aircraft systems meeting demanding noise and pollution requirements.

Table XXXVIII. Control System Summary and Conclusions.

Requirements	Results	
	UTW	OTW
● Set Percent Rated Thrust	✓	✓
● Maintain Engine Safety Limits	✓	✓
● Reduce Pilot Workload	✓	✓
● Control Inlet Mach Number	✓	N/A
● Rapid Thrust Response	Partial	✓
● Failure Detection and Corrective Action	N/A	Partial
● Engine Condition Monitoring	✓	✓
● Interface with Aircraft Digital Computer	✓	✓

6.0 RECOMMENDATIONS

The following recommendations for future development action are made considering those items excluded from, or not completed under, the QCSEE program. The intent of each is to bring the new technology elements a step closer to utilization. A number of these recommendations are included in the test program being conducted at the NASA Lewis Research Center. However, all are included below for completness.

Overall Engines

- Conduct additional UTW reverse-thrust testing with instrumentation to determine the cause of lower-than-predicted reverse thrust.

- Conduct transient UTW thrust-reversal testing.

Composite Fan Blades

- Pursue the development of alternate lightweight blade approaches to provide a flightworthy design. This is essential to the operational use of a variable-pitch fan and applicable to many other fixed-pitch fan engines.

Variable-Pitch Actuation Systems - If interest in variable-pitch fans remains high enough to warrant further development of the UTW fan, the following modifications in the variable-pitch actuation systems are suggested:

- The cam/harmonic system could be modified to increase torque capacity by 40% to ensure moving the blades at all fan speeds. This would entail increasing the size of the hydraulic motor in the beta regulator, modifying the core cowl to accept the longer regulator, and procuring a higher-torque-rated flexible cable. The stronger cable would also be stiffer and might present an installation problem.

- The running hysteresis of the ball spline system could probably be improved by rebuilding the ball spline and ball screw using larger diameter balls to reduce clearance.

Main Reduction Gear

- Conduct extended reduction gear endurance testing using the available back-to-back rig and QCSEE hardware. Early testing should include further optimization of the lube supply and scavenge system to attempt to reduce churning and further improve gear efficiency.

Composite Frame and Nacelle

- Static load test the OTW composite fan frame to destruction to determine if it meets design load objectives.

- The composite core cowl was cooled by shop air and an insulation blanket throughout UTW engine testing. Full verification of this design would include the design and testing of a flight-type heat shield and the use of fan-discharge air for cooling.

Digital Control

- Conduct UTW transient testing with electrical gain adjustment of the pitch-control system.

- Reprogram and test the OTW FICA system.

Low-Emissions Combustor

- Conduct engine testing of a double-annular combustor to develop pattern factor and profile.

Acoustics

- Verify wing/flap interaction-noise assumptions.

- Evaluate boundary-layer noise effect as a noise floor for aft fan-duct suppression.

- Evaluate "D" nozzle acoustic characteristics more fully by using acoustic probes correlated with far-field microphones. Include hard-wall core nozzle testing. Alternately, test with conical nozzles to separate core- and fan-noise sources.

- Conduct additional UTW acoustic tests to:

  a. Verify wing/flap interaction-noise assumptions.

  b. Utilizing acoustic probes, determine precise causes of higher than predicted fan source noise for both forward and reverse thrust.

  c. Evaluate suppression of the core nozzle by use of probes and/or coherence measurements.

7.0 RELATED REPORTS

1. Main Reduction Gears Test Program Final Report, 3/77, CR134669.

2. QCSEE Preliminary Analysis and Design Report, Vol. I, 10/74, CR134838.

3. QCSEE Preliminary Analysis and Design Report, Vol. II, 10/74, CR134839.

4. UTW Engine Composite Fan Blade Design, 5/75, CR134840.

5. Aerodynamic and Preliminary Mechanical Design of the QCSEE OTW Fan, 9/75, CR134841.

6. UTW Fan Preliminary Design, 2/75, CR134842.

7. UTW Engine Composite Fan Blade Preliminary Design Test Report, 9/75, CR134846.

8. Under the Wing (UTW) Final Design Report, 6/77, CR134847.

9. Over the Wing (OTW) Final Design Report, 6/77, CR134848.

10. Demonstration of Short Haul Aircraft Aft Noise Reduction Techniques on a 20 inch (50.8 cm) Diameter Fan, Vol. I, 4/75, CR134849.

11. Demonstration of Short Haul Aircraft Aft Noise Reduction Techniques on a 20 inch (50.8 cm) Diameter Fan, Vol. II, 4/75, CR134850.

12. Demonstration of Short Haul Aircraft Noise Reduction Techniques on a 20 inch (50.8 cm) Diameter Fan, Vol. III, 4/75, CR134851.

13. Hamilton Standard Cam/Harmonic Variable Pitch Fan Actuation System Detailed Design Report, 3/76, CR134852.

14. Aerodynamic Characteristics of 30.5 cm Diameter Inlets, 8/75, CR134866.

15. Test Results From a 14 cm Inlet for a Variable Pitch Fan Thrust Reverser, 12/75, CR134867.

16. Preliminary UTW Flight Propulsion System Analysis Report, 2/76, CR134868.

17. Main Reduction Gears Detailed Design Final Report, 3/75, CR134872.

18. Ball Spline Pitch Change Mechanism Design Report, 3/77, CR134873.

19. Main Reduction Gears Bearing Development Program, 4/76, CR134890.

20. Acoustic Analysis of Aft Noise Reduction Techniques Measured on a Subsonic Tip Speed 50.8 cm (20 inch) Diameter Fan, 1/77, CR134891.

21. UTW Engine Simulation Results, 8/77, CR134914.

22. Aerodynamic and Mechanical Design of the QCSEE Over the Wing Fan, 4/76, CR134915.

23. Clean Combustor Test Report, 10/75, CR134916.

24. UTW Digital Control System Design Report, 1/78, CR134920.

25. UTW Boilerplate Nacelle and Core Exhaust Nozzle Design Report, 10/76, CR135008.

26. Aerodynamic and Mechanical Design of the QCSEE Under the Wing Fan, 3/77, CR135009.

27. Composite Fan Frame Subsystem Test Report, 9/77, CR135010.

28. Aerodynamic and Aeromechanical Performance of a 50.8 cm (20 inch) Diameter 1.34 Pressure Ratio Variable Pitch Fan with Core Flow, 8/77, CR135017.

29. UTW Engine Composite Fan Blade Final Design Test Report, 2/77, CR135046.

30. OTW Engine Simulation Results, 10/78, CR135049.

31. UTW Composite Nacelle Subsystem Test Report, 7/77, CR135075.

32. Acoustic Performance of a 50.8 cm (20 inch) Variable Pitch Fan and Inlet, Vol. I, 11/78, CR135117.

33. Acoustic Performance of a 50.8 cm (20 inch) Variable Pitch Fan and Inlet, Vol. II, 11/78, CR135118.

34. Whirl Test of Cam/Harmonic Pitch Change Actuation System, 10/78, CR135140.

35. Core Engine Noise Measurements, 12/77, CR135160.

36. OTW Boilerplate Nacelle Design Report, 5/77, CR135168.

37. UTW Engine Boilerplate Nacelle Test Report, Vol. I Summary, 12/77, CR135249.

38. UTW Engine Boilerplate Nacelle Test Report, Vol. II Aerodynamic Performance, 12/77, CR135250.

39. UTW Engine Boilerplate Nacelle Test Report, Vol. III Mechanical Performance, 12/77, CR135251.

40. Acoustic and Aerodynamic Tests on a Scale Model OTW Thrust Reverser and Forward Thrust Nozzle, 1/78, CR135254.

41. Acoustic Treatment Design and Development, 11/78, CR135266.

42. Under the Wing (UTW) Engine Acoustic Design, 1/78, CR135267.

43. Over the Wing (OTW) Engine Acoustic Design, 6/78, CR135268.

44. Composite Frame Design, 9/78, CR135278.

45. PMR Core Cowl Design Report, 7/78, CR135279.

46. Preliminary OTW Flight Propulsion System Analysis Report, 6/77, CR135296.

47. OTW Propulsion System Test Report, Vol. I Summary, 1/78, CR135323.

48. OTW Propulsion System Test Report, Vol. II Aerodynamics and Performance, 7/78, CR135324.

49. OTW Propulsion System Test Report, Vol. III Mechanical Performance, 2/78, CR135325.

50. OTW Propulsion System Test Report, Vol. IV Acoustic Performance, 5/79, CR135326.

51. OTW Digital Control System Design Report, 11/78, CR135337.

52. UTW Composite Nacelle Design Report, 8/78, CR135352.

53. Ball Spline Pitch Change Mechanism Whirligig Test Report, 10/78, CR135354.

54. UTW Engine Composite Nacelle Test Report, Vol. I Summary, Mechanical and Aerodynamic Performance, 5/79, CR159471.

55. UTW Engine Composite Nacelle Test Report, Vol. II Acoustic Performance, Pending, CR159472.

56. Clean Combustor Development Report, Pending, CR159483.

AiResearch Division
Garret Corporation
F.B. Wallace
P.O. Box 5217
Phoenix, Arizona 85010

American Airlines
Maintenance and Engineering Center
K. Grayson
Tulsa, Oklahoma 74151

Andrews Air Force Base
Lt. Col. G. Strand
AFSC Headquarters
Washington, D.C. 20334

AVCO/Lycoming
S. Deckert
550 S. Main Street
Stratford, Connecticut 06497

The Boeing Company
H. Higgins
P.O. Box 3999
Seattle, Washington 98124

The Boeing Company
Wichita Division
D. Torkelson
Wichita, Kansas 67210

Bolt, Beranek and Newman, Inc.
R. Hayden
50 Moulton Street
Cambridge, Massachusetts 02138

Curtiss-Wright Corporation
Power Systems Division
W. Johnson
One Passaic Street
Wood Ridge, New Jersey 07075

Department of Transportation
NASA/DOT Joint Office of Noise
   Abatement
C. Foster
Office of Secretary
Washington, D. C. 20590

Detroit Diesel Allison Division
   of General Motors
F. Walters
Suite 312
333 West First Street
Dayton, Ohio 45402

Douglas Aircraft Company
L. Malthan
3855 Lakewood Boulevard
Long Beach, California 90801

Environment Protection Agency
J. Schettino
1835 "K" Street, NW
Washington, D.C. 20460

Federal Aviation Administration
Noise Abatement Division
J. Woodall
Washington, D.C. 20590

General Dynamics Convair Division
G. Nicoloff
San Diego, California 92112

Grumman Aerospace Corporation
C. Hoeltzer
South Oyster Bay Road
Bethpage, New York 11714

Hamilton Standard
Division of United Aircraft
A. Jackson
Windsor Locks, Connecticut 06096

Lockheed Aircraft Corporation
T. Higgins
Burbank, California 91503

Lockheed Georgia Company
H.S. Sweet
Marietta, Georgia 30060

NASA Installations

NASA Headquarters
N.F. Rekos
Washington, D.C. 20546

NASA-Ames Research Center
L. Roberts
Moffett Field, California 94035

NASA-Flight Research Center
D.R. Scott
Edwards, California 93523

NASA-Langley Research Center
R. Kuhn
Hampton, Virginia 23665

NASA-Lewis Research Center
21000 Brookpark Road
Cleveland, Ohio 44135

M.A. Beheim
D.N. Bowditch
L.J. Chelko
C.C. Ciepluch
E.W. Conrad
A. Ginsburg
M.J. Hartmann
R.H. Kemp
Lewis Library
R.W. Luidens
D.L. Nored
Report Control Office
L.W. Schopen
R.W. Schroeder
M.F. Valerino

NASA/Air Force Liaison
Wright-Patterson Air Force Base
Dayton, Ohio 45433

L. Obery
C. Simpson
Col. C.E. Painter
G.K. Richey
G.P. Peterson

Pratt & Whitney Aircraft
Division of United Aircraft Corp.
J. Chew
20800 Center Ridge Road
Rocky River, Ohio 44116

Rohr Corporation
F. Hom
Box 878
Foot and H Street
Chula Vista, California 92012

Wyle Laboratories
L. Sutherland
128 Maryland Street
El Segundo, California 90245

Rockwell International
Los Angeles Division
Attn: D. Schlundt
International Airport
Los Angeles, California 90009

End of Document